Protein-Lipid Interactions -Biophysical characterization of the interactions between proteins andlipid bilayers.

Vad, Brian

Publication date:
2009

Document Version
Publisher's PDF, also known as Version of record

Protein-Lipid Interactions –

Biophysical characterization of the interactions between proteins and lipid bilayers.

PhD thesis Brian Stougaard Vad

Department of life science

Aalborg University – 2009

Aalborg University

Department of life sciences

Sohngaardsholmsvej 49

DK-9000 Aalborg

Thesis Title:

Protein lipid interactions - Biophysical characterization of the interactions between proteins and lipid bilayers.

Author

Brian Stougaard Vad

Thesis period

1st August 2005 to 6th of January 2009

Supervisors

Daniel Otzen, Interdisciplinary Nanoscience Center (iNANO), Department of Molecular Biology, University of Aarhus, Gustav Wieds Vej 10C, DENMARK

Ole Mouritsen, Center for Biomembrane Physics, Department of Physics and Chemistry, University of Southern Denmark, Campusvej 55, DK-5230 Odense M, Denmark

Number of pages

183

PhD School

The international Doctoral school of technology and Science.

PhD Programme

Biotechnology, Chemistry and environmental engineering.

Preface

The general theme of this thesis has been the interactions between proteins and lipids. This has been done both by looking at the inner membrane protein DsbB but also the single alpha helix peptides Novicidin and Pardaxin and the β-sheet peptide SerAdan. We have investigated the folding and lipid insertion of these proteins with the aim of seeing how this affects the secondary structure and activity of the proteins but also the changes that the proteins induce in the lipids.

The thesis has been submitted to the faculty of science and engineering at Aalborg University, Denmark as a part of the requirement for obtaining the PhD degree. It is divided into 3 parts. The First part is an introduction to the Anti microbial peptides, bacterial and model membranes leading over to a summarizing discussion of the Peptides Novicidin, Pardaxin and SerAdan which all display membrane perturbing features. The Second part is a report on the dynamic AFM measurements performed on the inner membrane protein DsbB. The report includes an introduction to DsbB, Dynamic AFM, the motivation for the initiation of the study and the results we obtained plus a discussion of these results. The Third part contains the three articles which that have been published or are ready to be published in peer reviewed international papers based on part of the work done in this thesis.

The work of this PhD study has been carried out in the lab of Professor Dr Daniel E. Otzen (Interdisciplinary Nanoscience Center (iNANO), Centre for Insoluble Protein Structures, Department of Molecular Biology, University of Aarhus, Aarhus C, Denmark) and also in the lab of professor Ole Mouritsen (MEMPHYS - Center for Biomembrane Physics Department of Physics and Chemistry, University of Southern Denmark, Odense M, Denmark) where most of the atomic force microscopy experiments were conducted. The PhD study was funded by BioNET, a Danish research network for experimental and theoretical biophysics. The center is supported by the VILLUM KANN RASMUSSEN FOUNDATION and constitutes a nation-wide collaborative effort involving the biophysics groups at the University of Copenhagen, the University of Southern Denmark, and the University of Aalborg

Finally I would like to acknowledge the following persons:

I would like to thank Novozymes for supplying Novicidin and D-Novicidin and elaborating on the minimal inhibitory concentrations of these, and Jan Mondrup Pedersen (Interdisciplinary Nanoscience Center, iNANO) for synthesizing Novicidin and the acyl/dansyl derivatives.

Thanks to Daniel Otzen for inspiring supervision and for always being a pillar of knowledge, when things got confusing.

Thanks to my supervisor Ole Mouritsen and the entire Memphys group at SDU for supervision and sharing their unrivaled expertise in the field Membrane Biophysics.

Loads of thanks to the protein biophysics group, for keeping science fun, helping with stimulating scientific discussions and for sharing their expertise in different fields.

Finally I would like to thank my wife and daughter for countless moments of laughter and joy even when things were not all that funny.

Aalborg University, January 2009

_____

Papers

1 **Divorcing folding from function: How acylation affects the membrane-perturbing properties of an anti-microbial peptide**: Brian Vad, Line Aagot Thomsen, Jan Mondrup Pedersen, Troels Skrydstrup, Kresten Bertelsen, Niels Chr. Nielsen, Zuzana Valnickova, Jan J. Enghild and Daniel E. Otzen *to be submitted.*

2 **The anti microbial peptide Pardaxin displays a charge dependent orientation in lipid bilayers**: Brian Vad, Kresten Berthelsen, Charlotte Hau Johansen, Jan Mondrup Pedersen and Daniel E. Otzen *to be submitted.*

3 **Kinetic partitioning between aggregation and vesicle permeabilization by modified ADan**: Lise W Nesgaard; Brian S Vad; Gunna Christiansen; Daniel E. Otzen Biochim Biophys Acta. 2009 Jan; 1794(1):84-93. Epub 2008 Oct 15

Summary

The main theme of this thesis is the study of protein lipid membrane interactions. This may be divided into two subcategories. Firstly, the mode of interaction and degree of membrane perturbation by 3 peptides with very different origins and structure/charge properties, namely SerAdan, Pardaxin and Novicidin. Secondly, an attempt to characterize the mechanical stability of the inner membrane DsbB the amphipatic environment in which in it is situated be it lipids or detergents.

SerAdan Adan is derived from the Adan peptide but is designed not to be oxidized by replacing the Cysteins at position 5 and 22 with the amino acid Serine [1]. SerAdan is produced in humans due to a decamer duplication of the Bri gene which produces a prepro protein that after furin cleavage results in the 36 AA peptide SerAdan. There have been some studies on the disruption of neuronal cells but none that have looked into the specific mode of interaction of SerAdan with membranes. We did a study of the interaction of SerAdan with model lipid membrane and have shown that SerAdan has a very pronounced membrane perturbing effect which is comparable to that of Anti microbial peptides, being active at 1/500 molar ratios. The binding and the subsequent perturbation of lipid vesicles was linked to the surface charge of the vesicles as we could observe a higher degree of perturbation with anionic vesicles and we could completely prevent binding by the addition of high concentrations of Sodium Chloride. Interestingly the membrane perturbing effect of SerAdan was found to very time dependent. The time dependence of membrane could be linked to the time profile for fibril formation by SerAdan with the prefibrillar species being the membrane active component.

Pardaxin is a 33 amino acid residue peptide derived from the red sea mose´s sole *Pardachirus Marmoratusa*, a fish which secretes it as a milky substance from the base of its dorsal and anal fins. It uses it as a mode of defense against sharks as it very irritating to sharks gills and locks the jaws presumably due to calcium release in the muscle tissue. There have been a lot of studies on the mode of interaction of Pardaxin both with live cells and with model membranes and this has been shown that the orientation Pardaxin in membranes is influenced by the length of lipid acyl chain. We wanted to investigate whether Pardaxin would also be dependent on the charge interactions between Pardaxin and membranes. Pardaxin and lipid charge interactions have been looked at previously but with inconclusive results due to limitations in the methods used. We decided to combine three different methods in order to shed more light on these interactions, namely a vesicle disruption assay, carbon abundance NMR and a visualization technique combining Laser confocal scanning microscopy and Giant unilamellar vesicles. We showed with the vesicle disruption assay that there is a pH/charge dependent of disruption of vesicles with respect to the time profile and possibly the mode of action. The Abundance carbon NMR showed an increased degree of order in the acyl chain of zwitterionic lipids upon addition of Pardaxin. In the presence of anionic lipids we only observed an increase in the disorder of the lipid headgroup upon binding of Pardaxin showing that there was clear dependence of lipid

charge in the orientation of Pardaxin in lipid membranes. By LSCM it was unequivocally demonstrated that the presence of negative charged lipids changes the mode of action from pore formation to total vesicle disruption.

The AMP Novicidin is a variant of the 18-residue Novispirin, which in turn is derived from the N-terminal region of the cathelicidin peptide SMAP-29 from sheep. We had demonstrated in a previous study on the parental peptide Novispirin that it did not fold into an alpha helix upon adsorption and disruption of zwitterionic vesicles and found this to be the case for Novicidin as well. There is only one reported study of Novicidin at present, which does not look into the mode of interaction with this protein. In order to further investigate the link between folding and membrane permeabilization, we have studied the effect of acylating the N-terminus of the antimicrobial peptide Novicidin with C8, C12 and C16 chains. Acylation was chosen because an earlier study with the AMP Magainin showed that acylation changes the secondary structure of the peptide in solution. The Acylation of Novicidin increased the ability to form α-helical structure in the presence of zwitterionic vesicles but actually reduced the ability to permeabilize these vesicles as well as intact *E. coli* cells, even at concentrations sufficiently low to prevent formation of peptide micelles. Surprisingly, this decrease in permeabilising ability is not so marked in mixed vesicles containing 20% anionic lipids, confirmed by microscopy studies that show wt-Novicidin's and acylated versions preference for vesicles containing 20% anionic lipids among populations of different vesicles. Stopped flow fluorescence measurements of Novicidin labeled with the environmental sensitive probe dansyl indicated that Novicidin binds to zwitterionic vesicles in a more peripheral manner which was more effective at disrupting the membrane integrity. Our data suggest that induction of α-helical structure, rather than facilitating membrane disruption, may inhibit it. They also reveal multiple modes of interaction between AMPs and simple model membranes, hinting that interactions may be even more varied in the complex environment of live bacterial membranes.

The second part of the study was trying to make a systematic study of the mechanical stability of a membrane protein and trying to link this to the properties of either the membrane or the detergent in which it was situated. The parameters we intended to vary in order to understand their influence were key lipid/detergent components like the acyl chain length, degree of saturation, the headgroup charge and geometry. The model protein which we chose for our studies is the inner membrane protein DsbB from *E. coli*. DsbB is a 176–residue protein which consists of 4 transmembrane helices and 2 large cytoplasmic loops. We established the procedure for routinely incorporating DsbB in lipid vesicles without losing its activity and to a great extend retaining its secondary structure. We were also able to covalently link detergent-solubilized DsbB onto a mica substrate. Dynamic AFM was measured on DsbB in detergent and in lipids with two different modes of binding to the cantilever either unspecific binding to a silicium nitrate cantilever or thiol gold bond between a free cystein and a gold covered cantilever. Preliminary measurements leading to ~1800 dynamic force spectra for each of the four different setups were performed. A program was made for semiautomatic analysis of the force spectra

was run on the data sets which yielded somewhere between 2 and 8% spectra containing force peak events. Less than 0.25 % of the spectra contained spectra with unfolding lengths corresponding to that of the full length protein. The lack of sufficient data meant that no conclusions with regards to the mechanical stability of the structural elements cold be drawn on the basis of this work, but it forms a platform on which to continue further investigations in this area.

Resume

Hovedtemaet i denne afhandling har været studiet af protein lipid interaktioner. Under dette hovedtema er afhandlingen delt op i to underafsnit. Først er der interaktionsmåde og grad af membranpertubering af 3 peptider med meget forskelligt ophav og struktur/ladnings egenskaber, SerAdan, Pardaxin og Novicidin. Den anden del af afhandlingen beskriver et forsøg på at karakterisere den mekaniske stabilitet af det indre membranprotein DsbB opløst enten i lipider eller i detergent.

SerAdan stammer fra Adan peptidet, men er designet til ikke at blive oxideret ved at erstatte cysteinerne i position 5 og 22 med aminosyren Serine.[1][1][1] SerAdan bliver produceret i mennesker på grund af en decamer kopiering af Bri genet som producerer et præpro protein som efter Furin kløvning resulterer i det 36 aminosyre lange peptid SerAdan. Der er lavet studier af den neuron ødelæggende effect af SerAdan, men der ikke nogen studier der specifikt har kigget på den måde som SerAdan interagerer med lipidmembraner. Vi har foretaget et studie af SerAdans interaktion med model lipid membraner og vist at SerAdan har en udpræget membran pertuberende effekt som er sammenlignelig med den der observeres for antimikrobielle peptider altså aktivitet ved 1/500 i molært ratio. Bindingen og den efterfølgende pertubering af lipid vesikler er forbundet med ladningen af de anvendte lipider. Der var en markant højere pertubering af anioniske vesikler og denne binding kunne forhindres fuldstændigt ved tilsætning af høje koncentrationer af natriumklorid. Den membran pertuberende effekt af SerAdan viste sig at være meget afhængig af tidsfaktoren. Denne tidsafhængighed kunne kædes sammen med tidsprofilen for SerAdans fibril dannelse hvor den præfibrillede specie var den membran aktive komponent.

Pardaxin er et peotide bestående af 33 aminosyrer og stammer fra røde havs flynderen *Pardachirus Marmoratusa*, en fisk som sekreterer en hvid mælket substans fra kirtler som befinder sig ved roden af dens finner. Dette sekret bliver brugt som et forsvar imod hajer som finder det meget irriterende, da det angriber dens gæller og får dens kæbemuskler til at låse sandsynligvis på grund af frigivelse af calcium i muskelvævet. Der har været en del studier der har kigget på måden hvorpå Pardaxin interagerer både med levende celler men også med model lipid membraner, hvilket har vist at orienteringen af Pardaxin i membraner er påvirket af længden af lipid acyl kæden. Vi ønskede at undersøge hvorvidt interaktionen mellem Pardaxin og lipid membraner også var påvirket at ladningen af lipid hovedgruppen. Pardaxin og lipid ladnings interaktioner er blevet undersøgt før, men resultaterne har været inkonklusive på grund af begrænsninger i målemetoden. Vi besluttede at kombinere tre forskellige metoder til at undersøge disse interaktioner nemlig et vesikel ødelæggelses assay, Carbon abundance NMR og en visualiseringsteknik der kombinerer Laser confocal scanningsmikroskopi og gigantiske unilaminære vesikler. Med vesikel ødelæggelses assayet viste vi at der var pH/ladnings betinget ødelæggelse af vesikler både med hensyn til tidsprofilen og virkemåden. NMR forsøgene viste

en højere grad af orden i acylkæden af zwitterioniske lipider ved tilsættelse af Pardaxin. I tilstedeværelse af anioniske lipider kunne der kun observeres en højere grad af uorden i lipid hovedgruppen ved binding af Pardaxin. Dette indikerer en klar indvirkning af lipid hovedgruppens ladning på orientering af Pardaxin i lipidmembraner. Med Laser confocal scanningsmikroskopi var det muligt utvetydigt at vise at tilstedeværelsen af anioniske lipider ændrede pardaxins virkemåde fra poredannelse til vesikel ødelæggelse.

Det antimikrobielle peptid Novicidin er en variant af det 18 aminosyre lange peptid Novispirin som stammer fra den N-terminale ende af cathelicidin peptidet SMAP-29. Vi har demonstreret i et tidligere studie af Novispirin, at det ikke folder til en α-helix ved adsorbtion og pertubering af zwitterioniske vesikler og fandt at dette også var tilfældet for Novicidin. Der er på nuværende tidspunkt kun publiseret et studie af Novicidin og dette kigger ikke på virkemåden af Novicidin. For bedre at kunne undersøge forbindelsen imellem proteinfoldning og membran permeabilisering har vi acyleret N-terminus af Novicidin med C8, C12 og C16 kæder. Acylering blev valgt fordi tidligere studier med AMPét Magainin har vist at acylering ændrede peptidets struktur i opløsning. Acyleringen af Novicidin forøgede evnen til at danne α-helix i tilstedeværelsen af zwitterioniske vesikler, men kontrært til dette sænkede det peptidets evne til at permeabilisere både vesikler og intakte *E. coli* celler. Dette fænoment blev observeret langt under de koncentrationer som ville give anledning til formation af peptidmiceller. Overraskende var denne sænkning af permebiliseringsevnen ikke så udpræget ved anioniske vesikler. Dette blev bekræftiget ved mikroskopistudier, hvor vi viste at i en blanding af anioniske og zwitterioniske vesikler var der en klar præference for anioniske vesikler også selvom Novicidin var acyleret. Stopped flow fluorescence målinger af lablet Novicidin med den miljøsensitive probe Dansyl indikerede at Novicidin binder mere perifært til zwitterioniske vesikler, hvilket var mere membrane pertuberende end bindingen der blev observeret med anioniske vesikler. Vores data indikerer at induktionen af α-helix inhiberer membran permeabilisering snarer end fremme den. Dataene afslører forskellige grader af interaktion mellem AMPér og simple lipidmembraner hvilket kan tolkes som at interaktionerne muligvis er endnu mere kompleks i bakterielle membraner.

Den anden del af afhandlingen er et systematisk forsøg på at karakterisere den mekaniske stabilitet af et membranprotein og prøve at forbinde det til egenskaber af den lipidmembran eller detergent hvori det befinder sig. De parametre vi varierede var kerne egenskaber for lipid/detergenter såsom acylkæde længde, mætningsgrad og hovedgruppeladning og geometri. Modelproteinet som vi valgte til vores studie er det indre membran DsbB fra E. Coli, som er et 176 aminosyre protein som består af 4 transmembrane helixer og to store cytoplasmiske løkker. Vi etablerede en procedure til inkorporering af DsbB i lipid vesikler uden at miste dets aktivitet og i høj grad også beholde dets sekundære struktur. Vi var også i stand til covalent at binde detergent opløst DsbB på et mica substrat. Dynamisk AFM blev målt på DsbB i detergent og lipid med to forskellige bindingsmåder til cantileveren enten uspecifik binding til en silicium nitratcantilever eller kovalent binding med et thiolbinding til en guldcantilever. Foreløbige

målinger førte til 1800 unikke kraft spektra for hver af de 4 forsøgsopstillinger. Der blev lavet et databehandlingsprogram for at gøre analysen semiautomatisk og hvert datasæt resulterede imellem 2-8 % spektra indeholdende kraft spektra. Mindre end 0,25 % af spektra indeholdt spektra med udfoldningslængder der svarede til den fulde længde af proteinet. Den utilstrækkelige datamængde betyder, at der ikke kunne drages nogen endelige konklusioner vedrørende den mekaniske stabilitet af strukturelle elementer på baggrund af arbejdet i denne afhandling, men udgør en platform fra hvilken vi vil foretage yderligere undersøgelser.

Abbreviations:

2D: Two dimensional
^{o}C: Degrees Celsius
AFM: Atomic Force Microscopy
AMP: Anti microbial Peptide
ATP: AdenosinTriPhosphat
Au: Arbitrary units
CCD: Charge Coupled Device
CD: Circular Dichroism
CMC: Critical Micelle Concentration
Cys: Cystein
CHAPS: 3-[(3-Cholamidopropyl)dimethylammonio]-1-propanesulfonate
DsbB: Disulfide bond protein B
DCD-1: Dermaceptin 1
DDM: Dodecyl maltoside
DNA: Deoxyribonucleic acid
DPC: Dodecylphosphocholine
DMSO: Dimethyl Sulphooxide
DOPC: Dioleyl Phosphocholine
DOPG: Dioleyl phosphatidylglycerol
EDTA: ethylenediaminetetraacetic acid
HIV: Human immunodeficiency virus
IPTG: Isopropyl β-D-1-thiogalactopyranoside,
E. coli: Escherichia coli
EYL: Egg yolk lipid extract
KDa: KiloDalton
KDO: 2-keto-3-deoxyoctonoic acid
LB: Luria-Bertani Broth
LD50: 50% lethal dose
LSCM: Laser scanning confocal microscope
LPS: Lipopolysaccharides
LUV: Large Unilamellar Vesicles
MD: Molecular Dynamics.
MIC: Miniamal Inhibitory concentration
MLV: Multilamenar vesicles
NaCl: Sodium Chloride
NMR: Nuclear Magnetic resonance
Nc: Novicidin wt
NcC8: Novicidin with a 8 carbon acyl chain

NcC12: Novicidin with a 12 carbon acyl chain
NcC16: Novicidin with a 16 carbon acyl chain
Nm: Nanometers
OG: Octylglucoside
PC: PhosphoCholine
PE: phosphatidylethanolamine
PG: phosphatidylglycerol
pN: pico Newton
PS: Phosphotidyl Serine
QCM: Quartz Crystal Microbalance
RNA: Ribonucleic acid
R_h: mean radius
SDS: Sodium dodecyl sulfate
SM: SpingeoMyelin
SUV: Smal unilamellar vesicles
TM: TransMembrane
Wt: Wildtype

Contents

Part III : Papers

Part I

Studies on protein - lipid interactions using Novicidin and Pardaxin and the SerAdan as model proteins.

1 Introduction to lipids

Introduction

This introduction is meant a general overview over the very diverse field of antimicrobial peptides and what are the features that distinguish them from other proteins in terms of their structure, interactions with membranes and internal cell components. There is also an introductory part on lipids, including their location but also how they influence the structure and qualities of naturally occurring membranes. Furthermore, this part also emphasis on how lipids are used in model systems when we try to make sensible emulations of in vivo systems.

1 Introduction to Lipids – The fats of life

Lipids are the main constituent of biological membranes. Lipid layers have many features such as controllable flexibility and water impermeability. The membranes serve not only as barriers towards the extracellular space but also for internal compartmentalization [2, 3] and additionally they can be used as energy storage [4]. The lipid molecules are a highly varied group and more than a thousand different lipids have been isolated from a single cell [5]. The composition of lipid membranes varies greatly from species to species but in multi cellular organism there is also some variances between different tissues [6, 7]. This chapter will focus on naturally occurring membranes and the model membrane systems that are used to emulate these. Given the rich complexity of the lipid family I will in this thesis only focus on the general membrane compositions of mammalian and bacterial cells as these the most relevant for this study

1.1 The Mammalian cell

The most commonly used example of the membrane from Mammalian cells is those of the red blood cells which largely consist of lipids. The distribution of lipids between the two leaflets of these membranes is asymmetric [8, 9]. The leaflet facing the cytoplasm consist primarily of the amino phospholipids phosphatidyl Serine (PS) [10] and phosphatidylethanolamine (PE) [11] The outer leaflet consist mostly of the phosphocholines, phosphatidyl choline (PC) [12] and spingeomyelin [13]. This asymmetric distribution of phosphocholines and amino phospholipids is mainly regulated by an ATP dependent aminophospholipid translocase [14, 15] but it has also been shown that the leaflet asymmetry is aided by a subset of proteins that are characterized by a few transmembrane helices. When the asymmetry is lost it is often a sign of significant cell genesis events and for example the exposure of PS in the outer leaflet will trigger coagulation cascades and cell scavenging processes [16-18]. It should also be noted that PS has been shown

1 Introduction to lipids

to be present on the surface of cancerous and other pathological cells [19]. From species to species there is interestingly a larger difference in the PC-SM distribution of the outer leaflet (see table 1.1) of red blood cells. This presumably means that there is a large difference in how these cells interact with membrane active peptides as increasing amounts of SM will result in a more rigid membrane.

Table 1.1: The total lipid content of the red blood cells from different species. The Choline phospholipids are primarily found in the outer leaflet while the amino phospholipids are found in the inner leaflet.

Organism	PC	SM	Total choline phospholipids	PE	PS	Total amino phospholipids	Others
Rat	47.5	12.8	60.3	21.5	10.8	32.3	7.4
Rabbit	33.9	19.0	52.9	31.9	12.2	44.1	2.0
Human	34.7	20.1	54.8	28.0	14.3	42.3	2.9
Pig	23.3	26.5	49.8	29.7	17.8	47.5	2.7
Sheep	-	51.0	51.0	26.2	14.1	40.3	8.7

1.2 The Bacterial membrane

With regards to the buildup of the membrane wall bacteria are divided into two subgroups known Gram Positive and Gram negative bacteria. The gram positive bacteria are the simpler of the two with only one membrane bilayer (see figure 1.1) and it includes many well-known genera such as Bacillus, Listeria, Staphylococcus, Streptococcus, Enterococcus, and Clostridium. The membrane of gram positive bacteria is stabilized by a peptide-glycan-techtoic acid network which stains positive for the Gram staining, hence the name. The phospholipids make up 80 % of the cytoplasmic membrane and they consist primarily of PG but also the amino acyl derivatives of these making it very negatively charged. There is a greater divergence in the phospholipid make up of different species within the Gram positive group compared to the gram Negative.

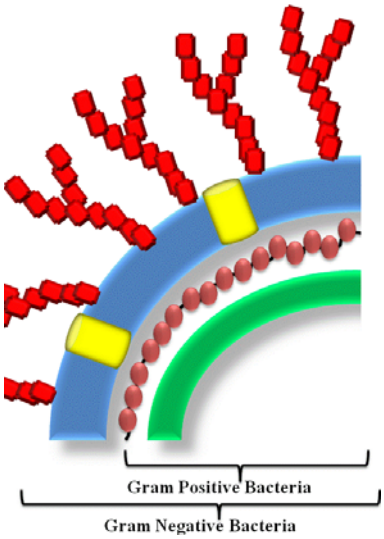

Figure 1.1: A schematic view of the membrane architecture of gram negative and gram positive bacteria. In the outer membrane (blue) specific for gram positive bacteria we have the asymmetric LPS network indicated in red and porins shown in yellow. In magenta colors we can see the peptido glycan layer which is found either in the periplasmic space of gram positive or the outer layer gram negative bacteria. The peptido glycan layer helps to stabilize the inner or cytoplasmic membrane shown in green.

The architecture of the gram negative bacteria differ a lot from the gram positive with an additional outer membrane composed primarily of PE combined with a negatively charged lipid polysaccharide moiety protruding from it. The LPS Layer plays a stabilizing part in the outer

1 Introduction to lipids

membrane of but also works as an endotoxin, and induces a strong response from normal animal immune system[20]. The gram negative bacteria also have the stabilizing peptido glycan layer in between the outer membrane and the cytoplasmic membrane. The Cytoplasmic membrane consists primarily of PE and also some PG making it negatively charged[21].

Table 1.2: The phospholipid contents of different Gram negative and Gram positive bacteria. The lipids have been divided into those that constitute the Outer Membrane [11] and those that make the Cytoplasmic Membrane [22]

Bacteria species		PG	DPG	L-lysyl PG	PE	Others
Gram-negative						
Erwinia carotovora	OIM	14	8	0	78	0
Eschericha coli	OM	3	6	0	91	0
	CM	6	12	0	82	0
Salmonella typhimurium	OM	17	2	0	81	0
	CM	33	7	0	6	0
Pseudomonas cepacia	OM	13	0	0	87	0
	CM	18	0	0	82	0
Gram positive						
Bacillus megaterium	CM	40	5	15	40	0
Bacillus subtilis	CM	29	47	7	10	6
Micrococcus luteus	CM	26	67	0	0	7
Staphylococcus aureus	CM	57	5	38	0	Trace

1.3 Model Membranes

With this enormous complexity and huge diversity of lipids not only between species but also in different membranes in one cell it is clear that for understanding the key parameters in the protein lipid interactions we are tempted simplify our experimental conditions. First off we can define the curvature of the membranes we look at by preparing our membranes by different techniques. It is possible producing vesicles ranging from 30 to 200000 nm, we can produce uniformly flat bilayers and even single bilayer leaflets if it is desired, examples of this the can be seen in figure 1.2. Normally we limit the experiments to certain essential lipid headgroups namely phosphatidylcholine (PC), phosphatidylserine (PS), phosphatidylglycerol (PG) and phosphatidylethanolamine (PE). By mixing these lipids in ratios that are comparable to those in natural membranes we have an easy way of testing for example species specificity of a membrane active protein. One can also look at the effects of different acyl chain lengths and different degrees of saturation to see how if the protein lipid interaction is dependent on the lipid packing. Finally people have also looked at the effects of adding Lippopolysaccharides and cholesterol which are very specific for gram positive bacteria and eukaryotic cells respectively.

1 Introduction to lipids

In the following section we will go through the physiochemical properties of these compounds. In thesis we have limited ourselves to two lipids namely DOPC and DOPG which we have mixed in different ratios. The rationale for choosing these two lipids is to make the simplest emulators of mammalian and bacterial cells when the primary focus is the charge interactions. The pure DOPC is used as an emulator of the zwitterionic bacterial membranes and when DOPG is included it is to reproduce the negative charge of bacterial cells. When the Di oleic moiety is chosen as the lipid acyl group the reason is twofold, one is that we are above the phase transition when working at ambient temperatures. The second reason is that this will result in perfect mixing of the two lipids and one does not have to take into account the formation of negatively charged islet in the membrane.

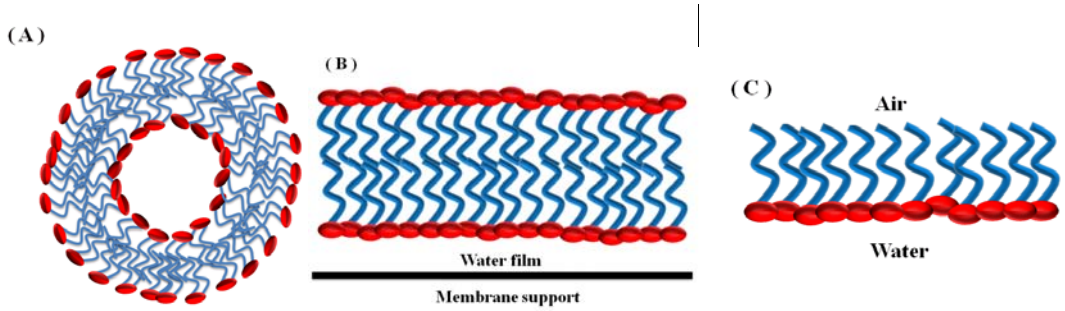

Figure 1.2: It is possible prepare vesicles (A) with different techniques such as sonication, extrusion and electroporation which will result in vesicles with approximate sizes of 30nm, 200 nm and 30 μM respectively. It is possible to collapse vesicles on a substrate giving a uniformly flat bilayer (B) or even producing a single bilayer leaflet (C) by spreading an oil emersion on an air water interface.

1.4 Model Membrane Preparation

Prior to preparation of membranes usually the lipids that are to be used will be used are dissolved in an organic solvent. This is both for reducing possible hydrolysis and especially when dealing with saturated lipids but also because some lipids will not mix homogeneously when dissolved in an aqua's phase. Usually chloroform is used because of its low vapor pressure and contrary to for example methanol it does not form hydrogen bonds with the polar head groups making it easier to evaporate. When preparing vesicles one should make sure that the lipids are above the phase transition temperature both while preparing but also after as this is essential for vesicle size distribution[23].

1.4.1 Multi laminar vesicles

This type of vesicles is the easiest to produce but the sizes of the vesicles will vary greatly and like the name implies they will consist of multiple layers of vesicles. This might cause problems with absorption in spectroscopic experiment. These types of vesicles are the starting material for some of the other vesicle types. MLV´s are made by drying out a thin film of the lipids usually in a glass container to avoid leakage of pollutants from the container into the sample. The film is

1 Introduction to lipids

the hydrated and with agitation the lipid films will be sheared off into large disk or myelin structures. The exposed hydrophobic edges will then try to reseal resulting in the formation of vesicles. Additional agitation by shaking, swirling or vortexing will produce a heterogeneous solution of MLV´s that will make the suspension milky white.

1.4.2 Small unilamellar vesicles

This group of vesicles is the smallest vesicles that can be produced, due to limitations induced by the curvature stress of the membranes. Because of the inherent frustration in this type of vesicles a lot of energy has to be put into the formation of them so sonication is usually the preferred technique. The use of sonication for lipid sample preparation was reported as early as 1967 [24] and is hence one of the first mechanical formation of vesicles. One advantage of this technique is that due to local heating high energy output the samples need not be heated above the phase transition temperature. The starting material is MLV´s prepared as was described above. There is then two ways of preparing the samples either by insertion of a tip sonicator into the sample or by emerging the sample in a bath sonicator, the rod sonicator is the most commonly used of the two. The outcome is a homogeneous group of unilamellar vesicles with a diameter below 40 nm which means the solution is essentially clear. These SUV´s are usually meta stable, the high energy curvature will by relaxed by fusing of vesicles into 60 to 80 nm vesicles over a matter of days[25].

1.4.3 Large unilamellar vesicles

Large unilamellar liposomes refer to vesicles that are larger than a 100 nm and consist of only a single bilayer membrane. They have the advantage of having less curvature pressure than the SUV´s and still being able to give reasonably low noise levels in spectroscopic experiments. Usually these are prepared by extrusion where a lipid solution by application of pressure is forced through a polycarbonate filter with predefined pores sizes or removal of detergents from lipid detergent mixture. The extrusion method gives the best vesicles with regards to the homogeneity of the size distribution. Again the starting material is MLV´s which are then put through 10-15 cycles of freeze thawing. This is done to make the MLV´s unilamellar as contrary to LUV´s they will break up during the freeze thaw process [26]. After this step the vesicles can be extruded but the technique will work best within the size range 100 – 500 nm. Usually the vesicles will end being slightly bigger than the pore size as the lipids change their morphology, to an extended shape allowing them to squeeze through the pores. Shear stress within the pore will then break the vesicles into smaller vesicles that fit the interior of the pore. This means the vesicle size is determined not only by the pore geometry, but also by the velocity of the suspension through the pore, the number of extrusion cycles and the mechanical properties of the bilayer membrane[27]. When preparing LMV´s by the detergent depletion method we start by mixing the lipid of choice in the form of MLV´s with detergent in a detergent/lipid molar ratio of 2/10 taking into account that the final detergent concentration should be above the CMC. This will dissolve the MLV´s and produce a homogeneous solution of mixed micelles. The following

1 Introduction to lipids

detergent depletion can be achieved by either dilution[28], dialysis, size filtration or adsorption. The size and homogeneity of the vesicles produce will greatly depend on the detergents and the rate of detergent removal but in general the faster the detergent removal, the smaller the vesicle size. The reason for this is that residual detergent in slow removal will increase the vesicle size and heterogeneity.[29] For an overview of the different vesicle sizes obtained using different detergents and detergent removal methods see table 1.3.

Table 1.3: The size distribution of vesicles as function of detergent and the detergent removal rate.

Detergent	Phospholipid	Vesicle diameter [Å]	Detergent removal
CHAPS	EYL	2900	Very slow (dialysis)
OG	EYL	2400	Very slow
CHAPS	EYL	2080	Slow (gel chromatography)
Triton X-100	EYL-EPA	1500	Slow (adsorbent beads)
GCh	EYL	1300/380	Fast(dilution): gel state/liquid crystalline state
C12 E8	EYL	600	Medium(adsorbent beads)
OG	EYL	610	Fast (dilution)
C12 E8	EYL	560	Fast (adsorption)
OG	EYL	300	Extremely fast (dilution)
SCh	EYL	300	Medium (gel chromatography)

1.4.4 Giant Unilamellar vesicles

Giant Unilamellar vesicles are vesicles with diameters between 5 – 200 μm [30] which gives them two very clear advantages their sizes are comparable to those for naturally occurring cells and it is possible to visualize them with normal light microscopy. There are three main methods for the formation of GUV´s, gentle hydration, Solvent evaporation and electroformation which all start out with an organic solvent suspension of lipids. In the gentle hydration method the lipids are deposited on either a glass[31] or Teflon slide[32] and allowed to hydrate for up to 36 hours. After this time a white "cloud" will rise from the deposited and with some agitation this can be solubilized. This method will give a rise to a slightly heterogeneous solution with up to 15 μm vesicles there will however be a tendency to some degree multi laminarity with this method[33]. The second method is solvent evaporation in an aqueous solution originally described by Mosho and coworkers[34]. The clear benefit of this method compared to the gentle hydration is that it takes much less time as GUV´s can be prepared within 2 min the drawback is the possible organic solvent residues that will be present in your sample. It works by putting an organic solvent solution of lipids in a glass flask, adding appropriate amounts of Millipore water and then evaporating the organic solvent by reduced pressure. This will result in an opalescent

1 Introduction to lipids

fluid that contains GUV´s with a diameter of up to 50 µm, but again with some degree multi laminarity.

The final method is the one described by Angelova and Dimitrov in 1986[35] using an oscillating electrical field to mediate the formation of vesicles. A lipid solution in chloroform is spread out on two platinum wires in a Teflon chamber. The organic solvent is then evaporated by pressure reduction for a few hours. The buffer of choice is then added (max 10 mM) and a low frequency AC field of 10 hertz is then applied for a couple of hours. This will result in GUV´s that are more or less bound to the platinum wires, depending on the lipid, which can be solubilized by gentle pipetting. This method is more time consuming than the solvent evaporation method but this is compensating by a higher degree of homogeneity of the samples with a size distribution between 30 – 60 µm in diameter and also a reduced occurrence of multi laminarity.

1.4.5 Supported Bilayers

The planar supported lipid bilayers are interesting as cell membrane mimickers and have been used for a wide variety of techniques such as Confocal laser microscopy[36], QCM [37], Atomic force microscopy [38] and Surface Plasmon resonance [39]. The method of choice is spreading small vesicles on a hydrophilic support. This method was originally pioneered by McConnell et al [40] and is now routinely used for creating supported lipid bilayers which allows for free diffusion and rotation of lipid molecules. The substrate used is for deposition is most commonly freshly cleaved mica [41] or silica where an aqueous solution of lipids is deposited for roughly 30 minutes and subsequently washed with buffer to remove any additional layers of lipid. An important factor is also the presence of calcium ions which greatly facilitates the formation of SLB. There are several suggested pathways for going from vesicles to an adsorbed lipid bilayer, the spontaneous rupture of vesicles due to vesicle deformation as they adsorb, the fusing of neighboring adsorbed vesicle, edges of already formed bilayers causing rupture of adsorbed vesicles and a critical coverage of the surface that starts a cascade rupturing event.

1.5 Physiochemical properties of lipids

Lipids can generally by subdivided into three mayor groups: glycerolbased lipids, cholesterol and ceramide based sphingiolipid. The subgroup of the glycerol based lipids are composed of two subgroups where is referred to as glycosylglycerides and the other more commonly known is the phospholipids. The phosphor lipids are composed of a glycerol backbone onto which there are two acyl chains attached at the sn1 and sn2 position at the sn3 in the Para position there is phosphate group that has been esterified to simple organic molecule containing a carbohydrate group. The acyl chains are often referred to as the tail and the molecule attached to the phosphate

1 Introduction to lipids

group as the "headgroups". The tail is the hydrophobic part of the lipids and the headgroup is the hydrophilic part. The length of the acyl chains vary in natural lipids between C14 and C18. Most phophatidylcholines have a Cis unsaturated fatty acid acyl chain making them fluid at room temperature.

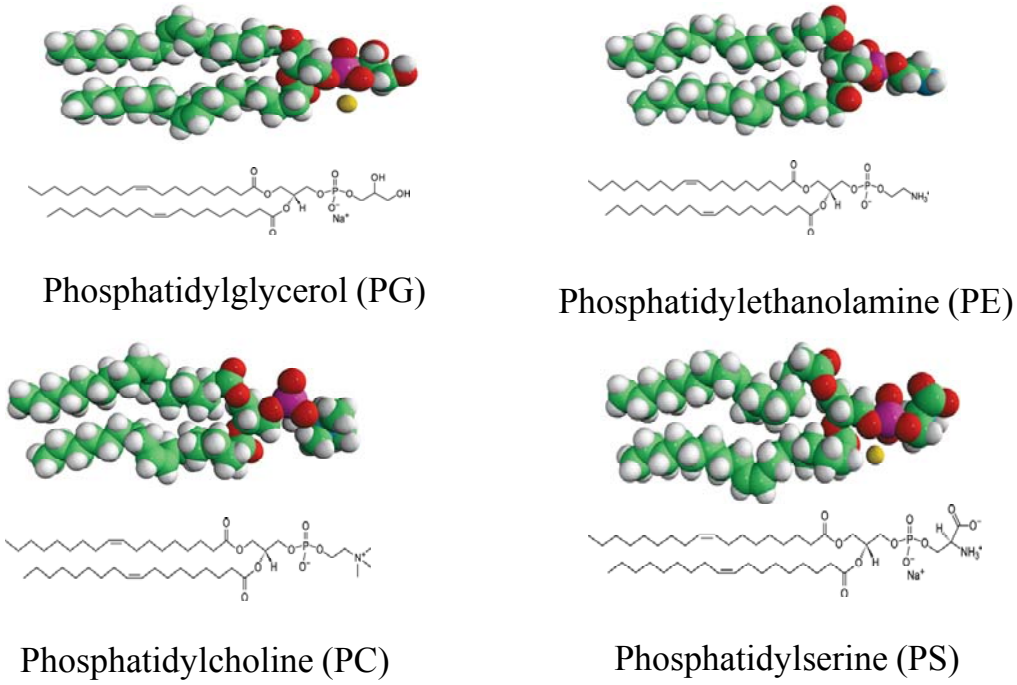

Figure 1.3: In this figure we see the four different headgroups of the most commonly used glycerol based lipids for preparation of model membranes, phosphatidylcholine (PC), phosphatidylserine (PS), phosphatidylglycerol (PG) and phosphatidylethanolamine (PE). In the three dimensional representation the carbon groups are shown in green, hydrogen white, oxygen red, phosphate purple and Nitrogen in blue. They are all shown with di-oleic acid as the acyl moiety for ease of comparison.

As mentioned previously there are several naturally occurring headgroups like choline, ethanolamine, serine and glycine which all have different properties (see figure 1.3).

The choline glycerophospholipids (PC) have a pKa value of around 13.9 and produces a polar head group with a strong zwitterionic character over the entire pH range. In animal cells, the fatty acid from the sn1-position is frequently 16:0 and that from the 2-position is 18:1 or 18:2 but in rare instances choline glycerophospholipids with a higher degree of unsaturation is found. The head group and of phosphatidyl cholines have roughly the same dimensions as the tail giving it a cylindrical shape in a lipid bilayer with tails facing each other and the headgroups facing the aqua's environment.

Ethanolamine glycerophospholipids (PE) are zwitterionic over the pH range of 2-7 and is in the anionic form in the pH range 7-10. The smaller size of the ethanolamine head group gives it a

1 Introduction to lipids

conical shape that imposes a curvature stress which is utilized by cells for budding, fusion and fission [42, 43]. While ethanolamine glycerophospholipids only occurs in small amounts in mammalian and plant cells it is the major constituent of Bacterial membranes. The pattern of fatty acid distribution in ethanolamine phospholipids generally shows a higher degree of unsaturation than what is found in choline phospholipids.

The phosphatidyl glycerol's (PG) have a second glycerol attached to the phosphate at the sn3 position. The phosphate group has a pKa of ~ 1 giving it a net charge of -1 at physiological pH conditions. This lipid occurs widely but very low amounts are found in animal tissues (mainly in mitochondria), in plants it forms 20 to 30 % of total phospholipids (mainly in the chloroplast). In bacteria it is the second most abundant lipid, for example *Escherichia coli*, has up to 20% phosphatidylglycerol in its membranes while phosphatidyl ethanolamine makes up much of the rest (see table 1.2).

Serine glycerophospholipids (PS) are the only lipids in animal cells that contain an amino acid. It possesses three ionizable groups: a diester phosphoric acid, an amino group and a carboxyl. The pKa of the carboxyl group of PS is around 3.6 and the pKa of its amino group is around 9.8 Thus at pH 7, the phosphate and the carboxyl functions are in anionic form and the amino group is positively charged which means that it is zwitterionic but will have a net negative charge. The head group shape of PS is similar to that of PC and will also spontaneously form vesicles in an aqueous solution.

Cholesterol is not really a lipid but rather a waxy alcohol that is found in the plasma membrane of all animals where it greatly modulates the membrane properties. It consists of a bulky steroid group and a hydrocarbon tail. The hydroxyl group on cholesterol interacts with the phosphate head of the membrane, and the bulky steroid and the hydrocarbon chain is embedded in the membrane. Cholesterol is minimally soluble in water but does not form vesicles in the absence of lipids. When as can be seen from the structure Cholesterol (see figure 1.4) is uncharged which means that it does not play a role with regards to electrostatic mediated interactions of membrane active proteins.

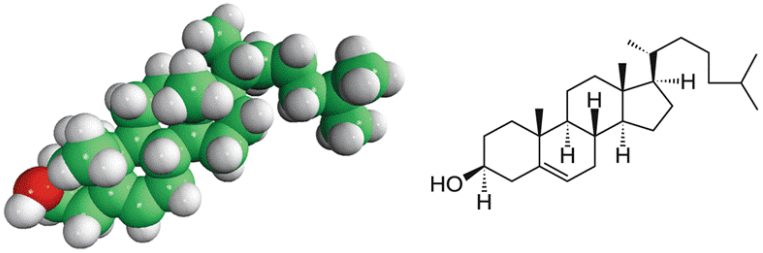

Figure 1.4: The three dimensional structure (left) and the Fisher projection of Cholesterol derived from sheep's wool. It consists of a sterol head group with an OH group shown in red and a C6 acyl chain with the carbon groups shown in green.

1 Introduction to lipids

LPS typically consist of a hydrophobic domain known as lipid A (or endotoxin), a nonrepeating "core" oligosaccharide, and a distal polysaccharide (or O-antigen) (see figure 1.5) and is the largest of the lipid molecules that we know with a MW of around 10 KDa. The lipid A part contains the hydrophobic, membrane-anchoring region of LPS that allows it to pack together with the other lipids in outer membrane forming the characteristic outer layer of gram negative bacteria seen in figure 1.1. Lipid A consists of a phosphorylated N-acetylglucosamine [44] dimer with 6 or 7 fatty acids (FA) attached. Usually 6 FA are found and they are all saturated. Some FA is attached directly to the NAG dimer and others are esterified to the 3-hydroxy fatty acids that are characteristically present. The structure of Lipid A is highly conserved among Gram-negative bacteria. The Core polysaccharide is attached to the 6 position of one NAG. Two unusual sugars are usually present, heptose and 2-keto-3-deoxyoctonoic acid (KDO) The KDO is unique and invariably present in LPS and so has been an indicator in assays for LPS.

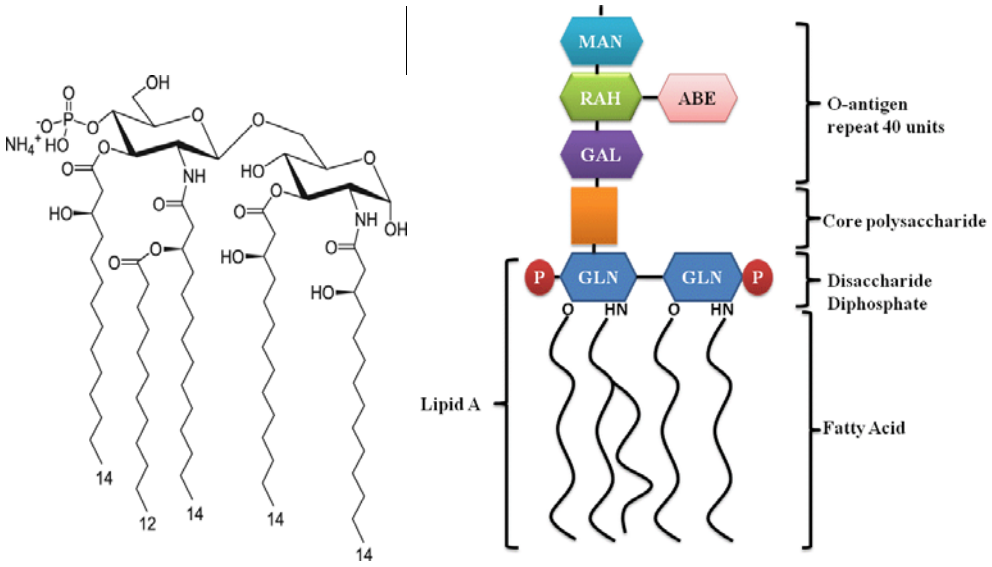

Figure 1.5: To the left is the fisher projection of a lipid A moiety and on the right the schematic structure of LPS with the O Antigen at the outer end, the core polysaccharide in the middle and at last the membrane bound Lipid A.

With minor variations, the core polysaccharide is common to all members of a bacterial genus, but it is structurally distinct in other genera of Gram-negative bacteria. The O antigen or O side chain is attached to the core polysaccharide. It consists of repeating oligosaccharide subunits made up of 3 - 5 sugars. The individual chains vary in length ranging up to 40 repeat units. The O polysaccharide is much longer than the core polysaccharide and it maintains the hydrophilic domain of the LPS molecule. A major antigenic determinant (antibody-combining site) of the Gram-negative cell wall resides in the O polysaccharide. Great variation occurs in the composition of the sugars in the O side chain between species and even strains of Gram-negative bacteria. At least 20 different sugars are known to occur and many of these sugars are unique

dideoxyhexoses, which only occur in Gram-negative cell walls. Variations in sugar content of the O polysaccharide contribute to the wide variety of antigenic types of *Salmonella* and *E. coli* and presumably other strains of Gram-negative species. Particular sugars in the structure, especially the terminal ones, confer immunological specificity of the O antigen, in addition to "smoothness" (colony morphology) of the strain. Loss of the O specific region by mutation results in the strain becoming a "rough" (colony morphology) or R strain. The overall net charge of LPS is negative due to the phosphate and ethanol amine groups found at the core region. This charge addition may facilitate some protein lipid interactions but the mesh of the outer polysaccharide will to some degree counter this effect by simple steric hindrance [45-47].

1.6 The properties and forces governing lipid bilayers.

1.6.1 The membrane pressure profile

As mentioned previously the cell uses the phospholipids as a way of compartmentalizing different components primarily because it is their inherent nature to form two dimensional bilayers in aqueous environments with physiological pH and ionic strength. Some lipids however do form nonlamellar structures but they can also be used by cells for mediating specific events that involve changing the morphology of the membrane. This feature of spontaneous curvature is intimately linked to the lateral surface pressure of the membrane. There are several forces involved in the modulation of the lateral surface. The most prominent of these are the electrostatic interactions between the hydrated headgroups, there is the restriction of contacts at the top of the

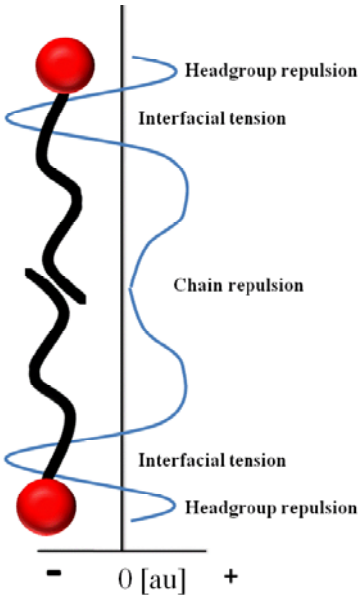

Figure 1.6: Lateral pressure profile of a cross section of a lipid membrane with the different forces responsible.

acyl chains caused by the hydrophobic effect, hydrophobic interactions between the acyl chain and then there is steric repulsion headgroups and acyl chains. Because these forces are restricted to defined zones, the pressure can be up to several hundred atmospheres.

For an overview of the lateral pressure through the membrane see figure 1.6. The lateral pressure profile can also be influenced by several external factors like the temperature, ionic strength and small molecules partitioning into the membrane. The lateral pressure profile plays an important

1 Introduction to lipids

role not only in the lipid – lipid interactions but also the protein- lipid interactions and one must assume that these are very stringently controlled by the cells.

1.6.2 Membrane Electrostatics

The surface electrostatics play an important part of the assembly of the lipid membranes hence also in lipid protein interactions. The association of cationic proteins to anionic lipids is a very well studied phenomenon and is naturally driven by the positive electrostatic interactions. It has been shown that a cell can have anionic patches on the membrane driving the proteins to a specific location on the cell and the proteins can also have different modes of interaction depending on the charge density. Cationic lipids have also been found and studies show that they associate with anionic lipids and subsequently regulate peripheral lipid - protein interactions and also lipid – small molecule interactions. The size of these membrane domains can vary from several molecules up to several microns and have life spans that range the microsecond scale up to hours. Especially in the longer lasting domains the constituents may be changing all the time much as we imagine it for a micelle. A way for the cell to manipulate the membrane to form these domains of specific charge densities can be by phase separation.

1.6.3 Membrane Phases

The naturally occurring bilayer forming lipids can exist in several different phases which are defined by the diffusion rate of the individual lipids and the acyl chain order parameter. For example lipid bilayers combined with different amounts of cholesterol will show three distinct phases, liquid disordered, liquid ordered and solid gel. The liquid disordered phase is characterized by a low degree of acyl chain order and a fast diffusion rate while the liquid ordered phase also has a fast diffusion rate but the acyl chain order is also very high. The third and final phase is the solid gel which as the name indicates has a very slow diffusion rate and is bestowed with a high degree of acyl chain order [48]. See figure 1.7.

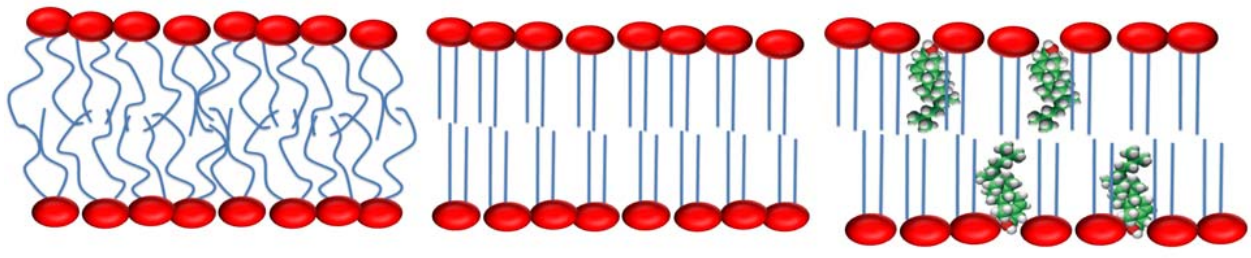

Figure 1.7 : The three most relevant phases for biological membranes - the liquid disordered (left), the gel phase (middle) and the liquid ordered [1]. The liquid disordered is characterized by low degree of acyl chain order and a fast diffusion rate, the gel phase very slow diffusion rate and a high degree of acyl chain order and the liquid ordered

1 Introduction to lipids

phase by fast diffusion rates and high acyl chain order. The latter is often induced by the presence of cholesterol molecules shown in light green.

1.6.4 Membrane Thickness

The thickness of the membrane is off course also a very important parameter since this is a key determining factor in how membrane active proteins interact with the lipid bilayer. The thickness is given by the length of the acyl chains with an increase in chain length we naturally see an increase in the bilayer thickness but also an increasing degree of saturation will thicken the bilayer. There are also physical parameters that will influence the bilayer for example the degree of hydration and temperature. A decrease in hydration will make the lipid head groups come together forcing the acyl chains to stretch out while an increase in temperature will make them contract. The latter is especially apparent around the phase transition temperature were you can observe large changes in bilayer thickness. But small membrane associating molecules can also change membrane also greatly affect bilayer thickness. The most well known example is cholesterol which increases the acyl chain order and hence membrane thickness. The hydrophobic sterol structure of cholesterol which has a natural affinity for the solid gel phase as this gives a closer hydrophobic packing. And yet the stiff and bulky structure of it would fit better in the liquid disordered phase which means the bilayer becomes “frustrated”. This is resolved by the induction of the third phase liquid ordered which stretches the acyl chains thickening the membrane. It should also be noted that unsaturated lipids greatly reduces this ordering and rigidifying effect of cholesterol.

1.6.5 Membrane Dynamics

The bilayer itself is by no means a static entity as there is a continuous movement of the individual lipids. There are several ways in which the lipids can move from the minute movements around the carbon bonds to larger scale movement such as rotation, lateral diffusion, protrusion from the bilayer and flip flopping from either side of the membrane leaflets see figure 1.8.

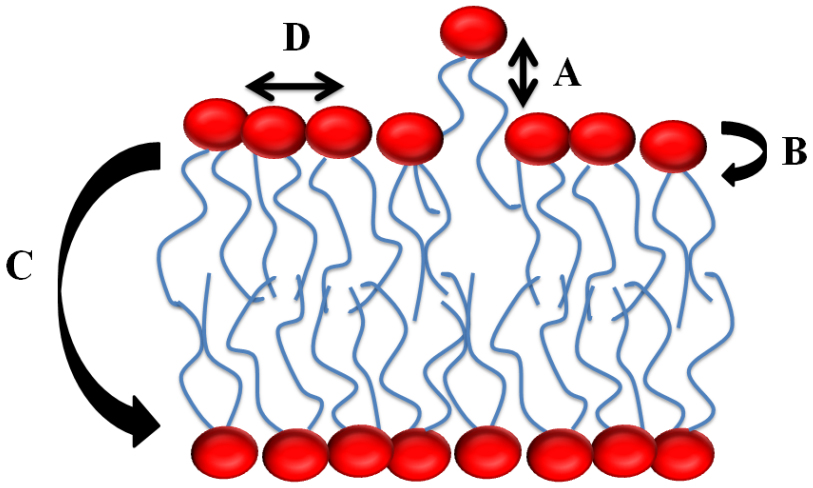

1 Introduction to lipids

Figure 1.8: Schematic overview of a lipid membrane and the different modes of movement that the phospholipids undergo in the membrane. Movements are indicated by arrows showing protrusion from the bilayer (A), rotation around its own axis (B), flip-flopping from either side of the membrane (C) and lateral diffusion (D).

The timescale of these movements, range from picoseconds to hours, with a natural correlation between the scale of movement and time course. To illustrate this we can see in figure 1.9 how the different parts of lipid are at fixed positions but are given as bell shaped distributions with regard to their position relative to the bilayer center. This movement is something which is naturally also very dependent of the temperature of the system; with a decrease in temperature we observe an increase in the timescale. In the in vivo situation there are also other factors to take in to account, you can have different phases in which the movement is restricted to and you also have obstacles in the form of different membrane components that are immobilized for example by binding to the cytoskeleton. This will also affects the mobility of membrane proteins as they swim through this sea of lipids.

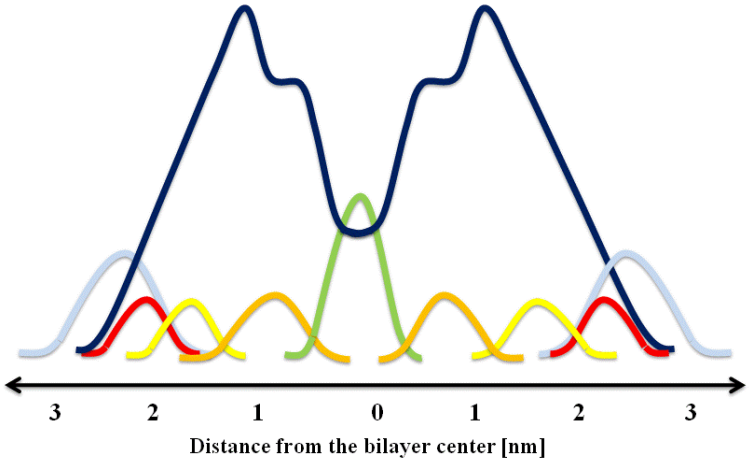

Figure 1.9: The Trans bilayer density map of a DOPC bilayer which has been obtained x-ray and neutron scattering. The curves show the probability of finding the different segments of the lipid molecules. Starting from the center of the bilayer we find the terminal CH3 in green, the CH2 in dark blue, the carbon double bond in orange, the COO group in yellow, Glycerol in red and bound water in light blue.

2 The Role of Antimicrobial Peptides

2 The role of Anti Microbial Peptides

There are many classes of anti microbial peptides all of which have been divided into subgroups on the basis of their amino acid composition and their secondary structure. Here we will introduce the largest and most well known of these with regards to their general features and how they work as. For a full list of these see table 2.1.

Table 2.1: The table includes the five most well established groups of antimicrobial peptides with examples of proteins belonging to these subgroups.

Classes of antimicrobial peptides				
Anionic peptides	**Cationic peptides enriched for specific amino acids**	**Linear cationic α-helical peptides**	**Anionic and cationic peptides that contain disulphide bonds**	**Anionic and cationic peptide fragments of larger proteins**
Maximin H5 from amphibians	Proline containing peptides from honeybees	Cecropins, andropin ceratoxin and melittin from insects	Peptides with 1 disulphide bond include brevinins	Lactoferricin from lactoferrin
Small anionic peptides rich in glutamic and aspartic acids from sheep, cattle and humans	Proline and phenylalanine containing peptides including prophenin from pigs	Cecropin p1 from Ascaris nematodes	Peptides with 2 disulphide bonds include protegrin from pigs and tychpesins from horseshoecrab.	Casocidin I from human casein.
Dermicidin from humans	Glycin containing peptides including hymenoptaecin from honeybees	Pleurocidin from the winter flounder	Insect defensins	Antimicrobial domains from bovine α-lactaalbumin, Human hameoglubin, lysozyme and ovaalbumin
	Tryptophan containing peptides including indolicidin from cattle	Seminalplasmin, BMAP, SMAP, PMAP from cattle, sheep and pigs	Peptides with >3 disulphide bonds include drosomycin from fruitflies and plant antifungal defensins	
	Small histidine rich salivary polypeptides including histatins from humans and other higher primates	CAP 18 from rabbits	A- defensins from humans, rabbits and rats. B-defensins from humans, cattle, mice, rats, pigs, goats and poultry	
	Glycine and Proline rich peptides include holotricin from beetles.	LL37 from humans	Plectasin derived from a fungi	

2.1 Cationic peptides enriched in specific amino acids

The cationic peptides that are enriched in specific amino acid contain more than forty members. The amino acid in which they are enriched is greatly depending on the organism from which they are isolated. The largest subgroup of these peptides; the Proline- and glycine-rich, are mostly from insects and active against Gram-negative bacteria. Their mode of action is not fully elucidated but most like involves translocation without cell lysis. Another subgroup is the cystein enriched peptides which should not be mistaken for the defensin AMP family which represent the most diverse AMP family among arthropods. In mammals these AMP´s are usually enriched

in histidine and tend to be specific towards fungi e.g. Histatin found in Human saliva translocates the outer membrane of bacterial cells and is then targeted to the mitochondrion [22, 49, 50]. Also two tryptophan enriched peptides have been isolated from porcine. Both display a surprisingly broad specificity ranging from bacteria to fungi and even the enveloped HIV virus [51-53].

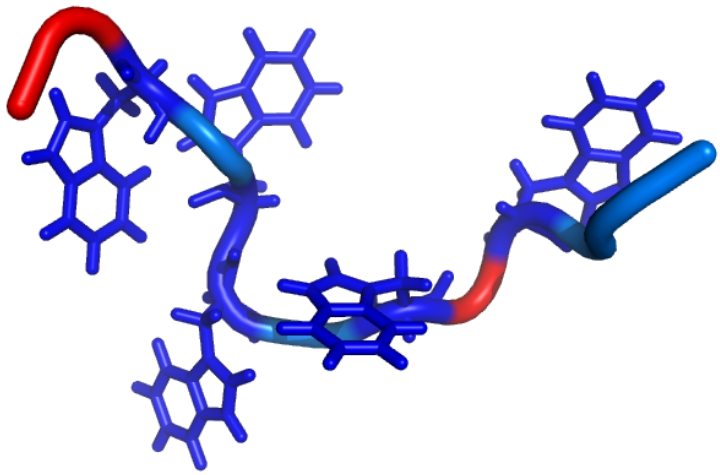

Figure 2.1: cartoon structure of indolicidin with the Tryptophans shown as blue sticks and the positively charged residues shown in red.

2.1.1 Example: Indolicidin

Indolicidin is cationic antimicrobial that was purified from the cytoplasmic granules of bovine neutrophils [53]. It consists of only 13 amino acids and out of these 5 are tryptophan's making it a member of the AMP group that is enriched in is enriched specific amino acids. This makes it the naturally occurring protein with the highest known percentage of tryptophans ranking in at 39 % but it is also the smallest known AMP. Indolicidin also contains three prolines, which are known to reduce the flexibility around the peptide backbone, giving it a distinct structure that is very different from the well known alpha helix and beta sheet structures in solution. Hancock et al showed that the circular dichroism spectra changed from unstructured to a poly – L – Proline II helical structure upon adsorption to POPC/POPG vesicles. This was complemented by the NMR structure of the peptide bound to zwitterionic dodecylphosphocholine (see figure 2.1) and the anionic detergent sodium dodecyle sulfate [54]. In both of these the structure is very well defined but represented a unique membrane-associated peptide structure. The complexes with DPC and SDS had a central hydrophobic core composed of Proline and tryptophan, which was bracketed by positively charged regions near the peptide termini. The tryptophan side chains, with one exception, folded flat against the peptide backbone, thus giving the molecule a wedge shape. It was established that the preferred location of Indolicidin in DPC micelles and lipid bilayers, using spin-label probes, was at the membrane interface. Indolicidin has a broad

2 The Role of Antimicrobial Peptides

spectrum of antimicrobial activity against Gram-positive and Gram-negative bacteria where it has been shown to have a Minimal Inhibitory Concentrations (MIC) between 0.5 and 64 μg/ml but it is also active against protozoa[55], fungi [56] and the enveloped virus HIV-1[57]. The mode of action seems to be bilayer disruption as it has been shown to cause cytoplasmic release of E-coli within minutes and also facilitate an increase in the transmembrane current of planar lipid bilayers[58].

2.2 Linear cationic helical peptides

The largest and most diverse group of the antimicrobial peptides known so far is the linear cationic helical peptides where more than 300 different peptides have been found. These peptides are usually short meaning less than 40 amino acid residues, lack cystein residues and can sometimes have a kink or a hinge region in the middle [59]. They are active against a wide range of pathogens, including Gram-positive and Gram-negative bacteria, fungi and protozoa. In aqueous solution most of them are unstructured but upon adsorption to a lipid membrane or in the presence of alcohols or detergents they are converted into an α-helical structure [60].

The mode of action by which this group of amps work, is to target the bacterial plasma membrane and permeabilized it in a concentration dependent manner. This is done in a variety of ways, including barrel-stave model [61], carpet model [62], and torroidal model [63]. In the barrel stave model the peptides reach the membrane either as monomer or oligomer and subsequently assemble on the surface, finally transversing the membrane by pore formation. This mode of action is mostly driven by the hydrophobic interactions with the acyl chains and is therefore less specific towards membranes of different lipid compositions. A minimum of 22 amino acids is necessary to transverse the bacterial membrane for an α-helical peptide. In the carpet model the positively charged peptides cover the membrane in carpet like fashion until they reach a concentration where they permeate the cell by disrupting cell curvature. As opposed to the barrel stave model, the peptide does not need to assume a specific structure and the peptides are always in contact with the lipid headgroups at the interface with the acyl chains. This mode of action is more sensitive to the lipid headgroup charge, explaining why it is more specific towards the negatively charged surface of bacteria. The torroidal pore model is a mixture between the carpet model and the barrel stave model. Defined pores are formed as in the barrel stave model but the peptides lie in the lipid headgroup-acyl chain interface. This is possible because the peptides induce a sharp bending of the lipids so that the lipid headgroups can line the interior of the pore.

There are several parameters that are important for how linear cationic AMP´s interact with membranes and what their mode action is. There is a substantial amount of evidence that not

2 The Role of Antimicrobial Peptides

only the net charge of the peptide that determines the specificity but also how this charge is distributed along the peptide chain [64, 65]. Anti microbial peptides with an evenly charge distribution along the peptide seem to have a higher affinity towards bacterial membranes rather than mammalian. On the other hand the peptides that have a low net charge or were the charge is unevenly distributed there is a lack of specificity and you can observe toxicity to bacterial, mammalian and fungal cells. Another factor is the propensity for helix formation as most of the linear cationic have a charge distribution that makes them amphipatic upon folding into a helical coil. This diversion of hydrophobicity and charge permits stronger interaction with the cell membrane as the peptide can bury itself in the interface between the lipid headgroup and the acyl chain. Another factor is the self association of AMP´s which is usually driven by either an N- or C terminus or by specific amino acids in the peptide sequence. This can allow for the formation of helical bundles that can initiate a strong hydrophobic interaction with zwitterionic membranes. An example of how peptide association can influence the selectivity of AMPs is the two AMPs Dermaseptin B and Dermaseptin S [11, 66] which differs in only a single amino acid and has the same amount of helix content in solution. But their degree of association is very different; Dermaseptin B oligomerises and permeates both zwitterionic and anionic membranes in contrast to the monomeric Dermaseptin S which only permeates anionic vesicles. A way to manipulate these self association properties is to attach a multimer forming moiety in the form of an acyl chain to the peptide. This way modulating the mode of action has been observed in vivo e.g. with the lipopeptide antibiotic polymyxin B [67].

Another measure for the peptide amhipacity is the hydrophobic moment [68] which is the dependence of the hydrophobic moment per residue on the mean residue hydrophobicity. There is a tendency for peptides with a high hydrophobic moment and moderate hydrophobicity to be the most membrane lytic [12, 69]. However, there are some drawbacks to this measure which makes it difficult to make absolute correlations between hydrophobic moment and activity. One is that often the AMPs have the charged residues unevenly distributed and the other is that it is assumed in the calculation of the hydrophobic moment that the helix is ideal with 100 % helicity. The calculation of hydrophobic moment allows intelligent mutations when it is desired to modulate the activity of AMP´s.

Hydrophobic interactions play an important role in the partitioning of the amps into the membrane bilayer. There are two things that must be taken into account with regards to peptide hydrophobicity for amps to be useful in the host immune response system. One is that the peptide has to be soluble so that it can be stored for some period of time and not to self aggregate to a great extent but also to allow transport to the target cell. On the other hand the hydrophobicity has to be high enough to make it energetically favorable to interact with the hydrophobic region of the membrane and increase the permeability.

2 The Role of Antimicrobial Peptides

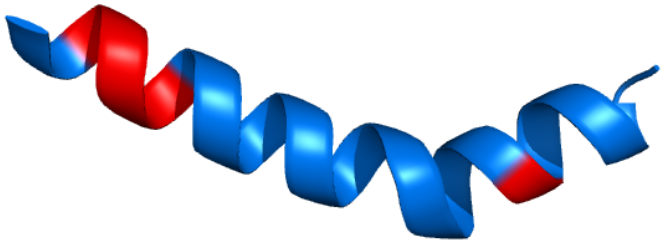

Figure 2.2: Cartoon figure AMP Melittin showing the kinked α-helical structure with negatively charged residues shown in red.

2.2.1 Example: Melitinin

Melitinin was one of the first AMP´s that was described in 1972 [70] and it is also one of the most well studied AMP there is. Melitinin is the principal component of the venom of the European Honey bee *Apis mellifera* as it constitutes more than fifty percent of the dry weight of the bee venom. Mellitin induces membrane permeabilization and lysis of both eukaryotic cells prokaryotic cells in a non selective manner [71]. It is produced as a pro-protein (pro-Mellitin) that later gets formylated during its biosynthesis. The entire peptide consists of 26 amino acid residues that are cationic predominantly at the C- terminus where there is a stretch of positively charged amino acids See figure 2.2 while the N- terminus of the protein is mainly hydrophobic. The net charge of the protein is + 6 at physiological pH which will keep it in solution is able to keep it in solution but when exposed to naturally occurring membranes it will spontaneously insert [72, 73]. There is an asymmetric distribution of hydrophilic and hydrophobic amino acids that will make the peptide amphipatic upon folding into alpha-helix conformation. At low concentration Mellittin is monomeric and random coiled. At high concentration the alpha helical Mellitin will aggregate as a tetramers with very little structure difference [74], they are all helical with a kink around the prolin at position 14 giving them a bent rod shape. Melittin will partition into model membranes composed of PC with a partitioning coefficient of ~ 10^3-10^5 M^{-1} [75] while forming an α-helix structure. This association takes place in the matter of milliseconds. In spite of this the affinity of melittin towards negatively charged membranes have been shown to be a 100 times greater than towards those composed solely of zwitterionic vesicles[76]. Fluorescence studies looking at the local environment of the tryptophan at position 19 indicate that it is situated at the headgroup interface. The location of the tryptophan is modulated with increasing concentration of charged lipids in the membrane indicating functional difference in the lytic activity in the different bilayers[77]. Several studies have also shown that the lytic activity of melittin is reduced when there is cholesterol present in the model membrane possibly due a decrease in binding efficiency.[78, 79] Using peptide orientation sensitive techniques like oriented circular dichroism the mode of membrane lysis by melittin has been shown to be consistent with the torroidal pore model [80]. At higher concentrations melittin seems to disrupt

model membranes in a fashion similar to that of detergent with the formation of micelles and membrane fusion [81].

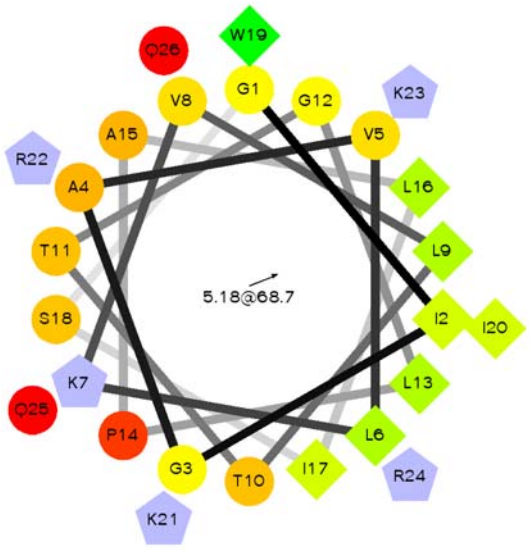

Figure 2.3: A schematic presentation of the helical wheel of Melittin with the helical moment displayed in the center. Hydrophilic residues as circles, hydrophobic residues as diamonds, potentially negatively charged as triangles, and potentially positively charged as pentagons. The most hydrophobic residue is green, and the amount of green is decreasing proportionally to the hydrophobicity, with zero hydrophobicity coded as yellow. Hydrophilic residues are coded red with pure red being the most hydrophilic (uncharged) residue, and the amount of red decreasing proportionally to the hydrophobicity.

2.3 Anionic and cationic peptides that contain cystein bridges

This group of peptides is mainly dominated by the AMP family known as Defensins. They were originally isolated from rabbit and human neutrophils but have but found in plants, insects, vertebrates and recently also fungi. All of the defensins are cationic and contain 6 to 8 much conserved cysteins that pair in three or four disulfide bonds. This high amount of disulfide bonds for a group of fairly small proteins 40 – 60 amino acids means that their secondary structure is much defined, often a mix between alpha helix and beta sheet. They are classified not only on the basis of their origin but also the pattern of disulfide bridging. For a classification of the defensins see table 1. Defensins are synthesized and as prepropeptides and are processed post translational into mature forms and in vertebrates they are then stored in granules. Several studies have shown that Defensins display a direct effect when used in concentrations above 2 µM killing bacteria, protozoa, fungi and also viruses. The modes by which they work seem to be that they cause disruption of the cell membrane by interacting with specific components both in the membrane and in the interior of the cell. Furthermore, it has been shown that defensins can activate a host immune response against the invading organism. This is done by phagocytoysis,

degranulation of mast cells, initiating gene transcription and also stimulation of the innate immune system.

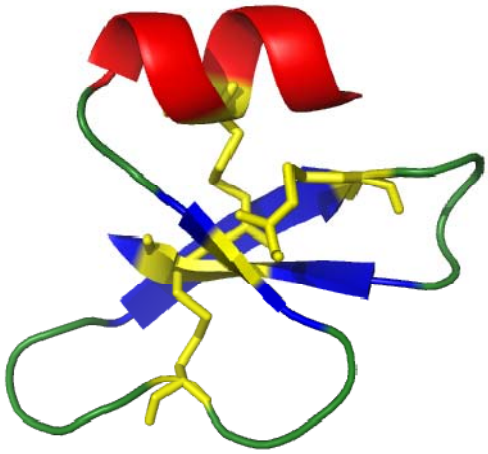

Figure 2.4: The structure of Human betadefensin – 2 with alpha helix indicated in red, beta sheet in blue and the cystein bridges are shown in yellow.

2.3.1 Example: Human betadefensin- 2

One example of this group is the Human beta-defensin-2; it is a cysteine rich, cationic 41 residues long Antimicrobial peptide. There tertiary structure is much locked with 3 cysteine bridges that connect cysteins 1-5, 2-4 and 3-6 (see figure 2.4) and it is this cysteine bridge pattern that define it as a beta defensin. At the C-terminus it has an alpha helix and it has a pair of hydrogen bonded beta sheets that that are connected by a short turn to form a beta hairpin. It was originally isolated from psoriatic skin in 1997 [82]. The production is as a unique feature from other defensins inducible by various pro inflammatory agents and gram positive and negative bacteria [82, 83]. Although the messenger rna coding for human betadefensin 2 can be found in most tissues it appears to be mainly localized to the tract epithelia and the skin. The main function of this peptide is the killing of bacteria or fungi and LD50 values as low as 100 ng/ml has been found. The mode of action is as yet not clear but Morgera and coworkers[84] have found that it might interact with membranes in a dimer form, as a cationic beta sheet platform presenting amphipatic helices for insertion into the bilayer. The interaction with of the peptides with the membrane then leads to the permeabilization which in turn could be part of the antimicrobial effect. The helix seems to modulate the antimicrobial activity with regards to membrane selectivity and killing kinetics.

2.4 Anionic Anti Microbial Peptides

The anionic peptides have not been described in much detail but include for example anionic peptides isolated from airway epithelial cells of humans, sheep and cattle. They are active against

2 The Role of Antimicrobial Peptides

both gram negative and gram positive bacteria are constituently produced and need zinc as a cofactor. Their mode of action has not been thoroughly investigated but it is suggested to be different from that of the linear cationic peptides where you have a charge interaction driving the association to bacterial membrane.

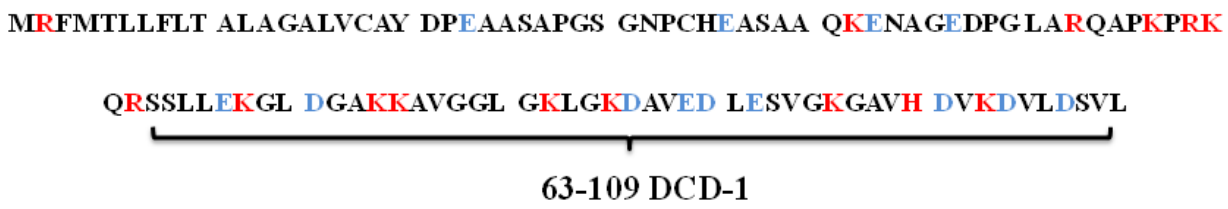

Figure 2.5: The protein sequence of Dermacidin with the proteolyticly cleaved Fragment DCD-1. Negatively charged amino acids are marked in blue while the positively charged are shown in red.

2.4.1 Example: Dermicidin

An example of the anionic anti microbial peptides is the 110 amino acid protein Dermicidin that was originally identified as the protein responsible for the 46 aa peptide proteolyticly processed product DCD-1 see figure 1 secreted from human sweat glands [85]. The full length protein has a pI of 6 and DCD-1 fragment has a pI of 5 based on calculation of the sequence seen in figure 2.5 making them both anionic at physiological pH. There is no homology to any AMPs known to date. Dermicidin is constitutively expressed in the human dermis and it is transported through the sweat, where it can be found in concentrations 1-10 µg/ml, to the surface of the skin. In contrast to the other known human AMPS such as beta defensin it is not induced in the keratonocytes of skin diseases such as psoriasis. The DCD-1 fragment consists of 41 amino acids but smaller fragments of Dermicidins have also been found. These fragments have shown in vitro antimicrobial effect against *Staphylococcus aureus*, *Escherichia coli*, *Enterococcus aecalis* and *Candida albicans*. The importance of this antimicrobial effect in vivo have been substantiated by the fact that low expressions levels in humans leads to a chronic infection of the skin.[86] The structure of Dermicidin has not been solved and no biophysical experiments have been conducted so it is unknown how it interacts with bacterial membrane especially since it would be expected that there would be charge repulsion between the negatively charge Dermicidin and negatively charged bacterial membranes. The complexity and diversity of how these peptides work is underlined by the fact that Dermicidin has been shown to both activate normal human keratonocytes [44] and increased the turnover of fat in adipose tissue in mouse models [87].

2.5 Anionic and cationic peptide fragments of larger proteins

This group of anti microbial peptides consists of a group of peptides that originate from larger proteins such as the peptide Casocidin derived from casein [13]. These fragments are created by either proteolytic auto cleaving or enzymes and then gain the antimicrobial activity although none was present in the paternal protein. The composition and structure of these AMP´s is

similar to those which we have already described and they do have any unique characteristics.

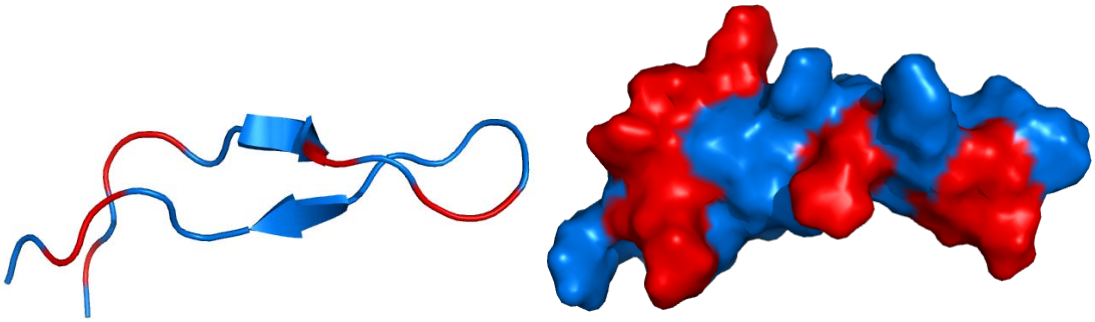

Figure 2.6 : the structure of Lactoferrin shown in a cartoon form and shown with the surface potential on the rigth where the red colour indicates positively charged residues.

2.5.1 Example: Lactoferricin

In 1992 Bellamy and coworkers isolated lactoferricin is a 25 amino acid residue antimicrobial peptide from Bovine Lactoferrin. Lactoferrin is a 80 KDA iron binding glycoprotein that is present in milk[88] and also in polymorphonuclear leukocytes where it is released during inflammatory responses[89]. Lactoferrin has been shown to provide a natural defense against a wide range of bacteria[90] and fungi.[91] Originally, it was thought that the antimicrobial activity of the intact protein was due solely to its iron-binding properties. Scavenging of iron by Lactoferrin would make it unavailable for bacteria, which need it for growth. Later however it was shown that a peptide fragment near the N-terminus was much more potent as an antibiotic than the full length protein. It is noteworthy that the proper cleavage of Lactoferrin to form lactoferricin is catalyzed by pepsin at low pH suggesting that this could be occurring naturally in the stomach after ingestion. This feature of deriving Lactoferricin from Lactoferrin has also been shown for the Human analogue as well but this does not have the same anti microbial potency. The structure of lactoferricin changes dramatically when it is cleaved off from the intact protein. It loses its alpha helical structure and adopts a twisted beta-sheet structure as can be seen in figure 2.6. This new structure also has the effect that the peptide becomes more or less amphipatic with all the hydrophobic residues on one side and the basic residues on the other side. This amphipacity is something which is well known from the AMP group linear cationic helical peptides and is believed to be essential in the interaction with negatively charged membranes. But the two Trp are also essential for the activity but they are also well known for working as membrane anchors in membrane proteins and the NMR in DPC reveals that they indeed buried in micelle[92]. The mode by which lactoferricin exhibits its antimicrobial effect is not exactly clear but there have been some experiments with model membranes that can give us some indications. Differential scanning calorimetry show that lactoferricin has a preferential interaction with negatively charged membranes which is also seen for many of the native antimicrobial peptides [93]. These experiments also showed that lactoferricin perturbs bilayers by inducing a positive membrane curvature. Fluorescence studies looking at quenching of the Trp fluorescence signal with binding to membranes have shown that lactoferricin bind more

tightly and seem to penetrate deeper when the PG is present in the model membranes [94]. Based on this they estimate that the Trp aromatic ring is laying close to the glycerol portion of the phospholipids. Vogel et al [93] have suggested that the membrane perturbation facilitates the internalization of the peptide where it might bind RNA and DNA and work as a transcription factor as this has been shown for the full length Lactoferrin [95].

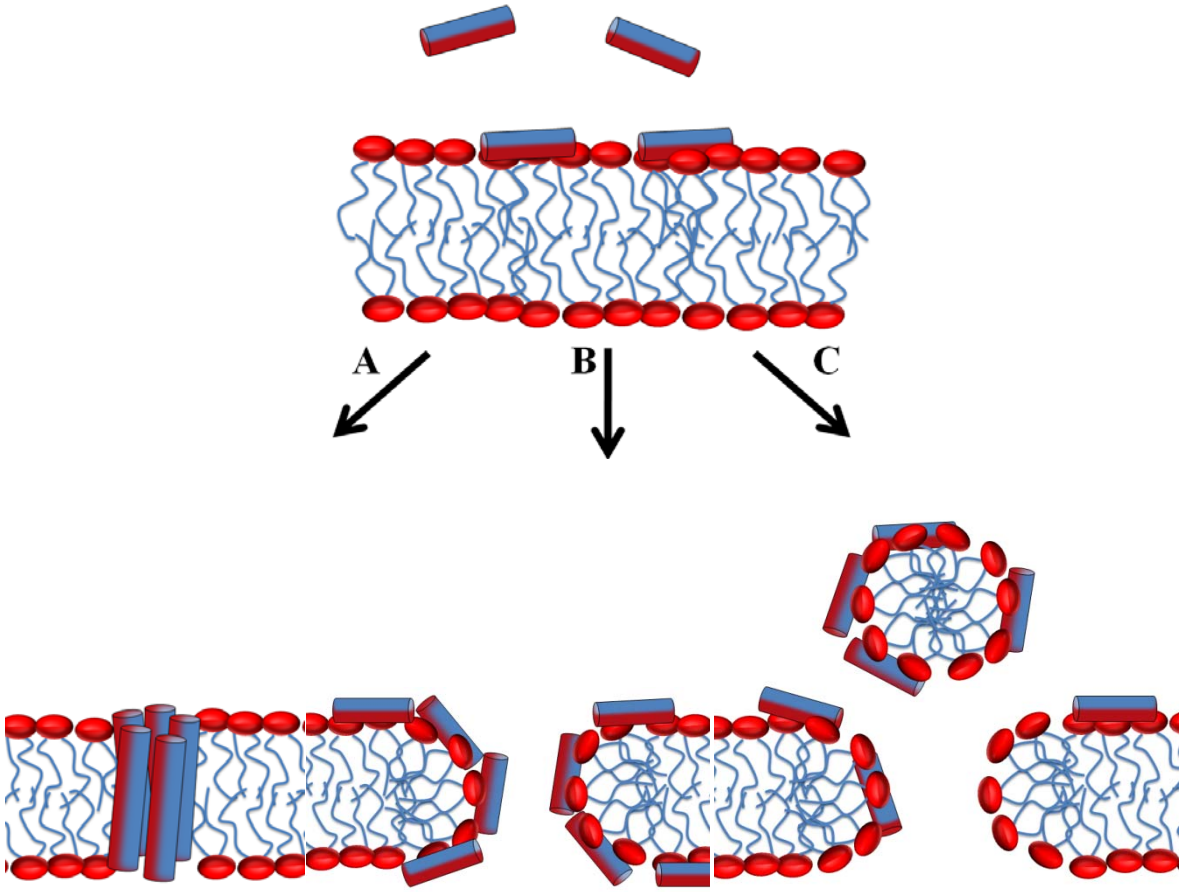

Figure 2.7: A schematic of the three most established ways of membrane disruption. They all go through an initial peptide binding step (top picture) and then either make a pore by the barrel stave mechanism the hydrophobic part of the amphipatic peptide is facing the interior of the membrane and the hydrophilic side is facing the water filled lumen inside the pore (A). The second mechanism torroidal pore mechanism (B) which forms pores by lying in the headgroup region of the lipids, thinning and increasing the curvature stress of the membrane until we see the formation semi stable pores the or finally by interacting with the lipids in a detergent like fashion which destroys the membrane integrity by pulling fragments of the membrane into solution also known as the carpet mechanism (C)

2.6 Mechanisms of bacterial resistance

The way by which bacteria gain resistance is basically selected evolution where the bacteria are reacting towards an environmental pressure; those bacteria that have the genetic makeup that allows them cope, will survive and pass on their genes. With conventional antibiotics this is usually accomplished by drug inactivation or modification by enzymes for example by

penicillin-resistant bacteria through the production of β-lactamases or Alteration of target site as in the case of PBP—the binding target site of penicillin's—in MRSA and other penicillin-resistant bacteria. With Anti microbial peptides the case is slightly different as they primarily interact with the bacterial membrane which is more difficult to obtain resistance against. The strategies applied by the bacteria to circumvent these events all have to do with the peptide mode of attachment, peptide insertion and membrane permeability. For Staphylococcus aureus it has been shown it can modify its anionic membrane by production of basic phospholipid Lysylphosphatidylglycerol. This is done by up regulating the lysyl phosphatidyl-glycerol-phosphate synthase that can transfer an L-Lysine from Lysyl-Trna to phosphatidylglycerol [96, 97]. The idea is then that these positively charged phospholipids will then repel the cationic charged AMP´s. The Gram negative bacteria have also found ways of reducing the affinity of the cationic AMP´s to their membranes by changing the net charge of the lipid A moiety of the LPS. This change in the net charge comes about by substituting the phosphate group of lipid A by a phosphorylethanolamine residue with a free amino group and also adding a amino aribidose group to the ester linked phosphate group of the glucosamine group[10]. Another way is to increase the number of acyl chains in LPS by addition of palmitate. This will increase the hydrophobic interactions and retard the insertion of the peptides into the membrane [98]. There have also been some reports from in vitro experiments that indicate AMP resistance could be obtained by secretion of proteases. An example of this is the linear cationic AMP LL37 have been shown to be degraded into non active fragments by the Metalloproteinase Aerolysin produced by *S Aureus* [99].

2.7 Experimental methods for characterizing AMP and lipid membrane interactions.

This chapter will go through some of the different biophysical measurements and structural techniques. This list does by no means cover all the techniques which can be used to look at peptide membrane interactions, but covers most of the aspects which can be investigated.

2.7.1 Nuclear Magnetic resonance (NMR)

NMR is a method that involves the observation of specific quantum mechanical magnetic properties of an atomic nucleus in the presence of an applied, external magnetic field. Without going into details with the technique it enough to say that it allows the building of an atomistic model of a given molecule be it a small drug compound or a medium sized protein. These three dimensional structures if obtained can give intimate details about the peptide - membrane interactions. Three-dimensional structures of antimicrobial peptides have been determined by solution NMR using short-chain phosphatidylglycerol micelles as a novel bacterial membrane-mimetic mode solution [100, 101]. In these cases the NMR signal of the peptide backbone and

2 The Role of Antimicrobial Peptides

sidechain residues has been measured to give the constraints that allows the three dimensional modeling. It is problematic to get information about small peptides in lipid bilayers due to their high mobility (see figure 2.8), but it has been done for example for the AMP Tachyplesin which revealed a β-sheet conformation in the bilayer [102, 103]. Another approach is to look at how the lipid membrane is affected by the presence of AMP´s, especially with regards to the order parameters of the lipids. This has been done with success for both Pardaxin and Aurein [104, 105] and showed how the binding of these affected the different parts of the lipids such the headgroup and the carbon atoms of the acyl chains.

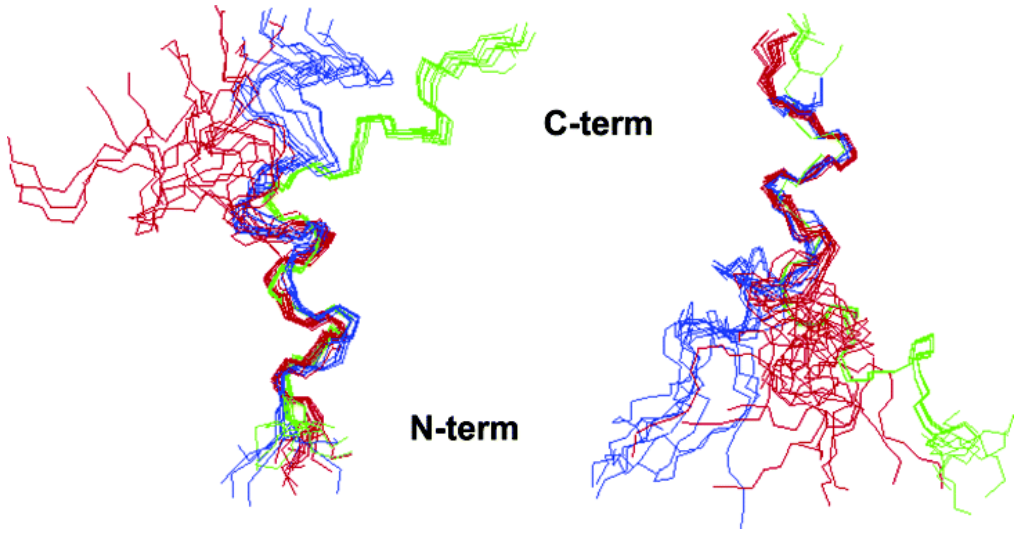

Figure 2.8 : Backbone alignment of the 10 best solution NMR structures of both the N- and C- termini of Novispirin in SDS (red), LTAB (blue), and TFE (green). It is obvious from these images that there is a high degree of mobility of the AMP Novispirin, seen by the lack of alignment, especially in detergents. Adapted from wimmer et al. [106]

2.7.2 X-ray diffraction

The use of x-ray for solving protein structures has been known since the structure of myoglobin was solved in 1958 by Phillips and coworkers [107]. The technique involves forming crystals of the desired protein. The crystal is then irradiated with an X-ray beam which will be scattered upon hitting the crystal. The method now depends on the analysis of these diffraction patterns from which an atomistic model of the protein can be rebuilt. When trying to apply the Crystallography method to AMP´s it is a problem that many of them are intrinsically very dynamic making them unsuitable for crystallization. One AMP which has been crystallized is Alamethisin which actually crystallized in a pore like structure in methanol and the with the absence of lipids [108]. This is the mayor drawback of crystallizing proteins, while the addition of various salts and organic solvents is needed, raising the question whether the observed structures represent natural phenomena. But instead of looking at the protein it is also possible to look at how AMP´s affect the lipid membrane by doing X-ray studies of the membrane. This has

revealed phenomena such as membrane thinning induced by the AMP LL37 and for Gramacidin S, cubic phase formation in the membrane [109-111]

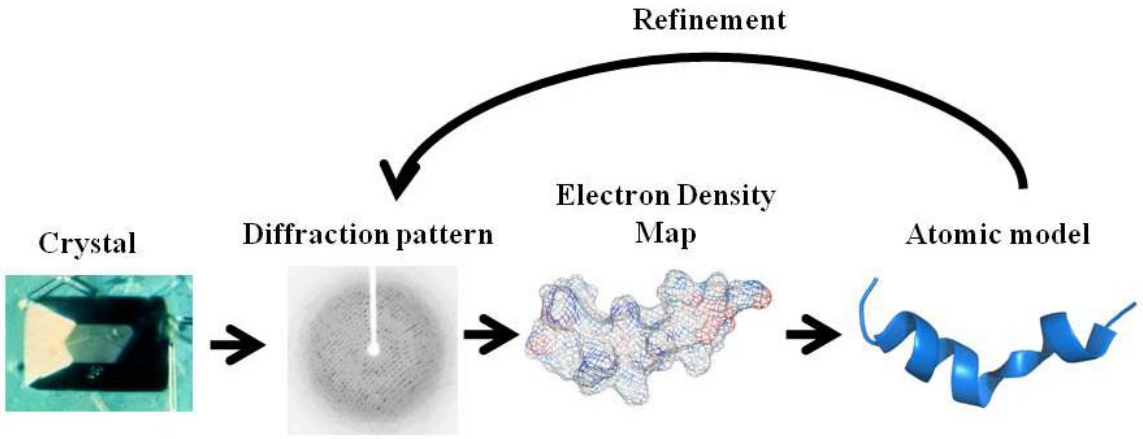

Figure 2.8: The general workflow for solving a protein structure by X-ray crystallography. Initially a protein crystal is obtained and radiated with X-rays giving a diffraction pattern. The phases for the diffraction pattern are solved allowing the building of a electron density map. The atomic model is build on the basis of the electron density map allowing for further refinement of the analysis of the diffraction pattern.

2.7.3 Fluorescence spectroscopy

Fluorescence is a phenomenon where the molecular absorption of a photon triggers the emission of a photon with a longer wavelength. The fluorescence of proteins is a mix of the fluorescence coming from the aromatic residues however mostly tryptophan residues, with some emissions due to tyrosine and phenylalanine. The normal maximum absorbance of Tryptophan is at 280 nm and the emission maximum from 300 to 350 nm. Tryptophan is a solvatochromic fluorophor which means that the maximum emission is sensitive to the solvent polarity of the local environment. This fact that can be used for the study of AMP and lipid membrane interactions for as the peptide inserts into the membrane the polarity of the environment surrounding the tryptophan to peptide. The shift in fluorescence can then be measured as a function of increasing lipid or AMP concentrations in order to describe the AMP binding to the membrane [112]. It also possible to look at how the AMPs affects vesicle integrity by including a fluorescent probe in the vesicles, that upon disruption of the vesicles will give rise to a change in the emission maxima or intensity [106]. It is also known that some AMP´s give rise to aggregation/fusion of vesicles and mixing of their contents. This can be shown with fluorescence by having a mix of two populations of vesicles containing separate fluorophors. If one of these fluorophors then quenches the other, this will give rise to a drop in fluorescence upon the aggregation/fusion of the vesicles which can be easily measured, as in the case of the AMP cryptdin4 [113]

2 The Role of Antimicrobial Peptides

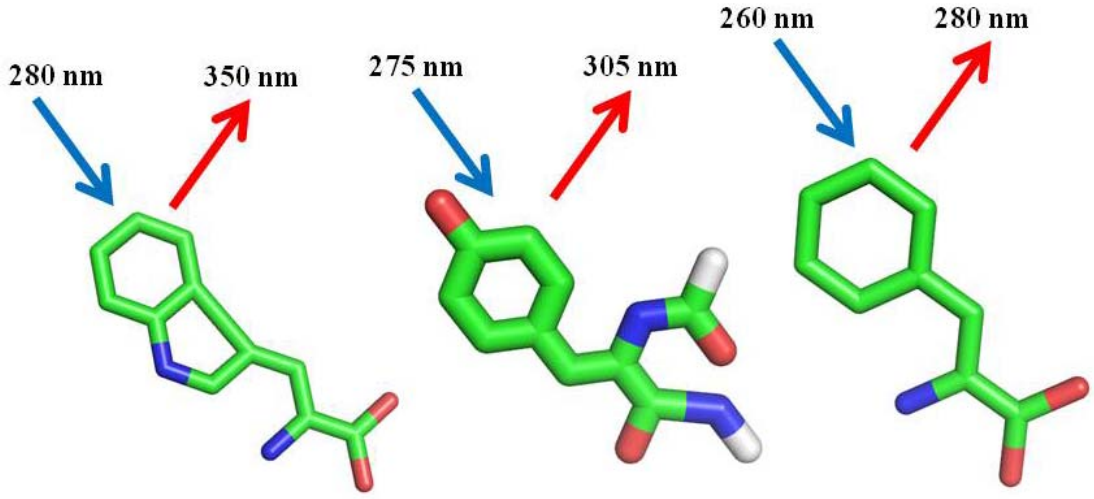

Figure 2.9: A stick figure representation of the aromatic residues Tryptophan (left) , tyrosine (middle) and phenylalanine (right) with the maximum absorption (blue arrow) and fluorescence emission (red arrow) at pH 7.

2.7.4 Circular Dichroism (CD)

CD is a technique that measures the differential absorption of left- and right-handed circularly polarized light as a function of either the wavelength or the temperature. When measuring on proteins in general the measurements are usually done in the Far UV which can reveal important characteristics of their secondary structure. CD spectra can be readily used to estimate the fraction of a molecule that is in the alpha-helix conformation, the beta-sheet conformation, the beta-turn conformation or random coil conformation (see figure 2.10). The CD cannot give details on which part of the protein the alpha helices etc are or even completely predict how many there are. Despite this, CD is a valuable tool, especially for showing changes in conformation as a function of for example additives or denaturants [114-116]. For some AMP´s the mode of action when absorbed to lipid membranes is linked to a change in the secondary structure. For this reason CD has been measured for AMP, initially just in solution [117] but also as a function of membrane mimicking detergents [118] and defined lipid vesicles [106]. The only prerequisite for CD samples is that there is a limitation with regards to the optical density of the sample and it has to be solubilized to give a signal.

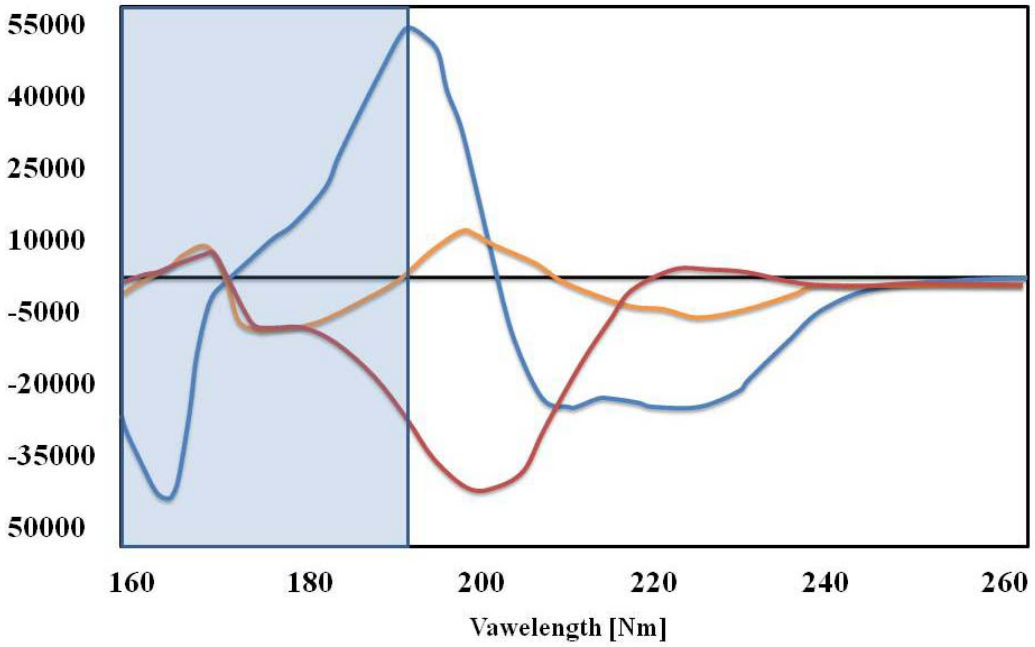

Figure 2.10: A representation of three different proteins composed solely of α-helical (blue), β-sheet (orange) and random coil (red) structural components. The area shaded in blue is usually not accessible by a commercial CD apparatus but only Synctron radiation CD´s due to limitations in the light intensity.

2.7.5 Molecular Dynamics (MD)

With the increase in processing power there have also been advances in the computer simulations of dynamic biological systems. This also includes the interaction of AMP´s and membranes on the single molecule level simulated with coarse grain modeling. The coarse grain modeling works by replacing an atomistic description of a biological molecule with a lower-resolution coarse-grained model that averages or smoothes away fine details. Coarse-grained models have been developed for investigating the longer time- and length-scale dynamics that are critical to many biological processes, such as lipid membranes and proteins (see figure 2.11). The main disputes regarding this technique are whether these simulations can reproduce the actual events that occur when peptides and membranes interact. Speaking in favor of this is the fact that it has been possible to see events which has been confirmed by biophysical measurements like the formation of pores by protegrin 1 [119] and a carpet like mechanism by maculatin [120]. The greatest limitations of this technique is the lack of processing power which is then reflected in the limited time lines which can be simulated and off course the reduction of atomistic details.

2 The Role of Antimicrobial Peptides

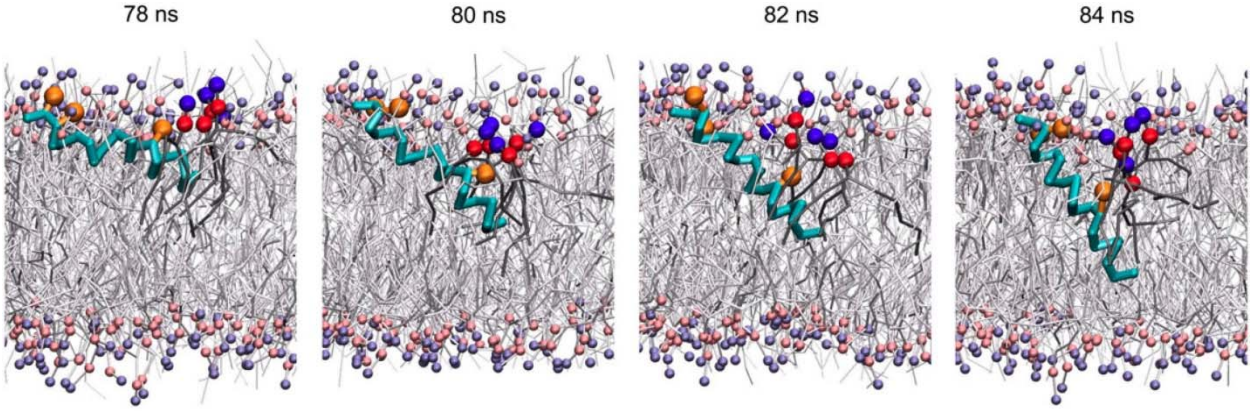

Figure 2.11: Timeline of the insertion of Pardaxin into the bilayer modeled by coarse grain dynamics. Adapted from Thøgersen *et al* [121]

2.7.6 Atomic Force spectroscopy (AFM)

The Atomic force microscopy is a technique that allows imaging and topography measurements of immobilized samples on the nanometer scale. The resolution is not yet at a stage where one can follow the organization of single AMP ´s into supra molecular structures like pores etc but rather gross morphological changes of the samples (see figure 2.12) . These experiments have included looking at events in the AMP - membrane interaction like membrane thinning [122] or phase separation [123] of model membranes. Furthermore there have also been studies looking at the formation of defects in live cells upon the addition of AMP´s [124, 125]. The limitations off this technique are the requirement for immobilization of the sample before measuring and differentiating between artifacts from immobilization and actual events.

3 Discussion of Papers I, II and III

3 Discussion of papers I, II and III

This chapter will try to elaborate on and compare the different systems we have looked in paper I (Divorcing folding from function: How acylation affects the membrane-perturbing properties of an anti-microbial peptide), paper II (The anti microbial peptide Pardaxin displays a charge dependent orientation in lipid bilayers) paper III (Kinetic partitioning between aggregation and vesicle permeabilization by modified ADan). The common feature of these papers is that they encompass what has been the main focus of this thesis namely the interaction between proteins and lipid membranes.

The three proteins we have been looking at have very individual features if we look at the net protein charge at a neutral pH we have the extreme of Novicidin that has a net charge of + 6 Pardaxin with a net charge of + 1 and SerAdan with a charge of -1. This difference in the charge is bound to influence how this peptide interacts with membranes as numerous studies have shown that there is a strong correlation between peptide charge and membrane binding activity [126-129]. Furthermore it has been shown that, charge interactions between the bilayer and the peptide, does not only influence the initial binding but also the latter orientation in the bilayer [130, 131]. Their structures are also somewhat different with SerAdan´s b-strand regions connected by loops [132] Pardaxin´s α-helix structure with a pronounced kink and the positive charges pointing in opposite directions[133] and Novicidin that forms an α-helix with a distinct amphipatic nature with charged residues located on one side of the helix (Personal communications Magnus Franzmann). There is however no specific rules with regards to what structural elements AMP´s should contain except some degree of amphipathicity. The amphipatic structure has been shown to be essential both for alpha helical and beta sheet peptides for the interaction with membranes [134].

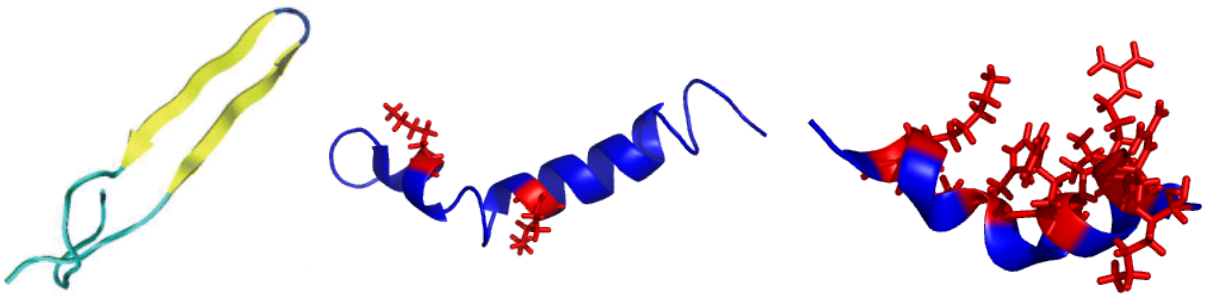

Figure 3.1: The structure of the three proteins on which the work in this thesis is based. On the left SerAdan, in the middle Pardaxin, and on the right Novicidin. For SerAdan the two β-strands are shown in yellow and the β-hairpin connecting them in dark blue. For Both Novicidin and Pardaxin the α-helices are shown in blue with positively charged residues shown in

3 Discussion of Papers I, II and III

3.1 Paper I: Kinetic partitioning between aggregation and vesicle permeabilization by modified ADan

We will start out by looking at the least characterized of the peptides with regards to anti microbial effect namely SerAdan. SerAdan is derived from the ADan peptide but is designed not to be oxidized by replacing the Cys5 and Cys22 with Ser [1]. SerAdan is produced in humans due to a decamer duplication of the Bri gene which produces a prepro protein that after Furin cleavage results in the 36 AA peptide SerAdan. There have been studies showing that SerAdan is cytotoxic to neurocytes [1] but is likely to assume that SerAdan and the parent peptide ADan is not in its evolution origin an antimicrobial peptide. This assumption is based on the fact that ADan is produced due to a very infrequent mutation but still we see a strong membrane perturbing effect with as low as 1/500 molar ratio. Despite its negative charge we clearly see a preference towards anionic vesicles. This preference is visible in the secondary structure where we see that in the presence of DOPG vesicles SerAdan retains a structure that is very similar to the freshly dissolved peptide which is the membrane active species. This is contrary to the usual mode of action for non disulfide bond AMP´s where a large structural change is either the prerequisite or consequence of membrane perturbation [135]. We also observe the anionic lipid preference in the maximum release which is 80 %, 25 % and 15 % for vesicles composed of DOPG, 1/1 of DOPC/ DOPG and DOPC vesicles respectively. This is contrary to Novicidin and Pardaxin where we need ~ 5 times more protein to disrupt anionic vesicles. Furthermore this is the only one of the three peptides were we are not able to induce complete vesicle disruption just by adding copious amounts of peptide to the lipids. The reason for this is most likely due to the other unique feature of this peptide, namely the time dependency of its membrane permeablising abilities. The kinetics and mode of adsorption is apparently driven by electrostatic interactions with vesicles but if this is slow, due to a lack of anionic lipids, the protein that is not adsorbed to the lipids are transformed in to the non membrane permeabilising species. There has been two suggested structures of ADan one is two strands connected by a beta turn [132] the other a triple beta sheet [136]. Both of the structures, separates the charged residues into the turn regions, but with a lack of obvious anionic patches to facilitate electrostatic interactions specifically with anionic lipid. If we try to classify SerAdan according to the different types of AMP´s, which was listed in the introduction there is no obvious category where SerAdan fits the given criteria. This lack of structure homology with known antimicrobial peptides is again maybe due to the fact that it is not the native role of this peptide. We were not able to investigate the mode of the membrane disruption by looking at how they disrupt GUV`s in the same fashion as we have with Pardaxin and Novicidin due to incompatibility with the experimental procedure. There would have been a large motivation for doing this as the membrane permeabilization by beta-sheet peptides is the least well understood and might have offered some new insights.

3 Discussion of Papers I, II and III

3.2 Paper II, The anti microbial peptide Pardaxin displays a charge dependent orientation in lipid bilayers

Pardaxin is peptide that been isolated from the fluid secreted from red sea mose´s sole *pardachirus marmoratusa* upon attack from predators like sharks. The pharyngeal cavity and the gills are the target organ for the repellent action of Pardaxin in shark [137] and the native role of the protein is not to work as an AMP but such activity has however been shown [138].

Pardaxin has a α-helical structure in solution and there are no observable changes upon binding to zwitterionic vesicles while we see a shift towards a more beta sheet like structure when it adsorbs to anionic vesicles. Contrary to SerAdan this structural difference is not due to a lack of binding of Pardaxin to zwitterionic lipids. We base this conclusion on the fact that Pardaxin was the peptide with the lowest concentrations needed for zwitter ionic vesicle disruption with an observable effect at Peptide to lipid molar rations of 1/6000. Hence we can assume that this indicates that the structural difference of lipid bound peptide reflects differences in the mode of interaction with the membrane. Our calcein release experiments further underline the differences in membrane interaction as a function of charge as we need ~5 times more peptide to disrupt Anionic vesicles. When we performed the GUV measurements we saw a very clear pattern in the mode of disruption, zwitterionic vesicles leaked out their contents but the membrane remained intact while anionic vesicles lost their membrane integrity coinciding with full contents release. It has been previously been shown that Pardaxin orientation in the membrane was dependent on the acyl chain but this was the first time that it was shown that the mode of action was dependent on the charge of the headgroup. There are two general accepted modes of pore-formation one is the torroidal pore the other is the barrel stave, where the main difference between the two is that in the torroidal pore the peptide only interacts with the headgroup region. We could distinguish which of the two Pardaxin forms pores with our Carbon abundance NMR which indicates where in the membrane that the peptides interact. We see that in the zwitterionic vesicles the order at the C-terminal is increased which we interpret this as a transmembrane barrel stave pore.

This is makes intuitively sense and is also in perfect agreement with others that have shown that a transmembrane protein will increase the acyl chain order [139, 140] while the formation of an α-helix at the membrane's surface is supposed to induce positive curvature strain, which decreases the headgroup hydration and acyl-chain order of lipids [141]. When we performed LSCM measurements of a mixed solution of Zwitterionic and anionic vesicles with Pardaxin we observed a repetition with regards to the mode of and they occurred simultaneous. This indicates that in vivo Pardaxin will interact with both mammalian and bacterial cell walls nondiscriminatory, which has previously been suggested by in vitro experiments [138].

3.3 Paper III, Divorcing folding from function: How acylation affects the membrane-perturbing properties of an anti-microbial peptide:

3 Discussion of Papers I, II and III

Novicidin was the only one the three peptides which in its origin was a confirmed AMP as it primary structure was mainly based N-terminal region of the cathelicidin peptide SMAP-29 from sheep. When Novicidin was in the presence of anionic vesicles the secondary structure changed quite significantly from random coiled to α-helical but as with Pardaxin this did not reflect a lack of binding to the zwitterionic vesicle. Surprisingly Novicidin showed a preference towards zwitterionic vesicles in the calcein release studies, this time with a factor of ~12 even though Novicidin is much more negatively charged than Pardaxin. The ratio shifts as we make the peptide more hydrophobic by acylation with a ratio of around ~ 3 suggesting that if the electrostatic interactions are the governing forces this in some way increases the concentrations needed for disruption of vesicles. The question was whether the differences in vesicle disruption also reflected differences in the mode of binding such as with Pardaxin. We investigated this by attaching an environmental sensitive probe to Novicidin and here the picture was clear. With anionic vesicles we saw a large increase in the probe fluorescence prior to disruption of the vesicles but not indicating that prior to the vesicle disruption Novicidin buried itself in the membrane. This did however not tell us whether Novicidin was forming a trans membrane pore or just lying in the interface region. There were some indications in the fact that we needed many factors more protein, than for what we had so convincingly shown was pore formation, by Pardaxin in zwitterionic vesicles. We then performed the GUV measurements similar to what we had done for Pardaxin and now we saw something completely different. There was not the same fine distinction between the vesicle types with regards to mode of action. For both Anionic and zwitterionic GUV´s we a mix of different modes of interaction vesicle collapse, pore formation and vesicle aggregation with different frequencies depending on the vesicle charge and degree of acylation. All of this suggesting, that Novicidin worked by a mix of the torroidal pore mechanism and the carpet mechanism but with different degrees of membrane insertion depending on the charge of the lipid headgroup. Dynamic simulations of Magainin have shown something similar where it existed in two different forms a random coiled loosely associated to the surface and another where it folds into an alpha-helix that is deeper immersed into the bilayer [142]. Another interesting feature which the LSCM measurements of a mixed solution of Zwitterionic and anionic vesicles showed was that the anionic vesicles bound most of or all of the free Novicidin leaving zwitterionic vesicles untouched. This was interesting for two reasons, one is that this is to our knowledge, the first case where we show a discrepancy between vesicle disruption in a homogeneous and heterogeneous vesicle suspension. The other is that even though we show that Novicidin disrupts zwitterionic vesicles, which could indicate hemolytic activity, in the co presence of anionic membranes like bacterial cell walls Novicidin will disrupt the later.

The methods in this thesis each have their own advantages and disadvantages and the study of peptide interactions with lipid membranes in this thesis clearly show that none of them on their own will give the full picture with regards to mode of interaction. We have shown by circular

3 Discussion of Papers I, II and III

dichroism that secondary structural changes of AMP´s are not a prerequisite for membrane perturbation but might rather decrease it. In our calcein release experiments we can observe clear differences in the amounts needed for vesicle disruption and kinetics suggesting distinctly different modes of interaction. An example is the differences in Pardaxin needed to permeate anionic and zwitter ionic which we show is due to total vesicle disruption and pore formation respectively. We suggest that molar ratios needed for vesicle disruption can also be compared to other proteins, to imply on their mode of action. An example hereof is the large difference in protein concentration needed for vesicle disruption by Pardaxin in zwitterionic and SerAdan in anionic vesicles clearly suggesting that SerAdan is not forming pores by the same mechanism as Pardaxin, if at all. But these results are however circumstantial and do unfortunately not give any definite answers with regards to the mode of interaction. The method of visualizing GUV´s after the addition of AMP´s by LSCM gives valuable information with regards to AMP mode of action. We can observe real-time the release of content and we determine pore sizes by encapsulating different size fluorophors. The work in this thesis also expands the use of the technique by looking at different types of vesicles simultaneously. We observed vesicles of two different types but given that the experimental set up will allow it one could easily imagine including more vesicle types. The drawback is that we lose the time resolution and it is not possible to stringently control the protein concentration which the vesicles are subjected to.

Table 3.1: A listing of SerAdan, Pardaxin and Novicidin interaction with lipids and possible modes of action.

Protein	SerAdan	Pardaxin	Novicidin
Concentration needed for membrane perturbation	Active at 1/500 protein to lipid ratio	Active at 1/6000 protein to lipid ratio	Active at 1/2000 protein to lipid ratio
Structural changes upon lipid association	Similar to monomer structure with anionic vesicles contrary to control	Shifting towards Beta sheet with anionic vesicles	From random coil to α-helical with anionic vesicles
Membrane orientation Zwitterionic lipids	Unknown	Perpendicular to the bilayer	In the plane of the bilayer
Membrane orientation Anionic lipids	Unknown	In the plane of the bilayer	In the plane of the bilayer
Mode of action Zwitterionic lipids	Unknown	Barrel stave	Carpet /torroidal pore
Mode of action Anionic lipids	Unknown	Carpet	Carpet /torroidal pore

3 Discussion of Papers I, II and III

3.4 PERSPECTIVES AND OUTLOOK

Since the first report of methicillin-resistant *Staphylococcus aureus* in the 1960s [143] there has been an increase in the frequency of bacterial strains that are resistant. Besides the methicillin-resistant *Staphylococcus aureus* there is now a prevalence of vancomycin-resistant *enterococci*, and extended spectrum β-lactamase-producing *Enterobacteriaceae* [144]. The strains that gain resistance are often highly virulent and quickly gain resistance against new antibiotics reducing the lifetime of a new antibiotic dramatically. This is also reflected in the fact that less ten new antibiotics have been licensed from 1999 to 2008 [145]. The few numbers are partially due to difficulties in coming up with new products but also because of the reduced profit turn over from antibiotics. The decreasing investment by major pharmaceutical companies in antimicrobial research has resulted in a rising concern from governmental health institutes around the world [146-148]. However one group of compounds that holds great potential is the AMP´s which so far seem to be more difficult to attain resistance against. The first AMP to undergo commercial development was the AMP Pexiganan a synthetic analogue of Magainin 2 derived the African clawed frog *Xenopus laevis.* Pexiganan demonstrated excellent *in vitro* broad-spectrum activity against 3109 bacterial clinical isolates. Resistant mutants could not be generated following repeated passage with sub inhibitory concentrations[149] . Unfortunately in 1999, FDA approval was denied because Pexiganan was deemed to be no more effective that other antibiotics used to treat foot ulcers and further development of Pexiganan was stopped [150]. After this there have been other AMP´s such as Neuprex, Iseganan, Omiganan and Histatin variants which have gone in to clinical trials. Some of these projects have been stopped due to a lack of successful results in phase II clinical trials and others despite positive results have yet to be approved for clinical use [151]. One antimicrobial peptide which has reached the market is the lipopeptide daptomycin which have been approved in many countries for the management of Gram-positive infections [152]. Despite the poor success rate of AMP´s for commercialization this is still a large commercial interest because of the lack of alternatives. In December of 2008 The International medicinal companies Novozymes and Sanofi-Aventis declared that they were launching a project with the AMP Plectasin NZ2114 that targets the treatment of severe infections, such as pneumonia and septicemia, caused by bacteria like *Staphylococcus* and *Streptococcus* [153]. The likelihood of getting from a promising AMP to a commercial product is a greater if we can understand the forces governing AMP membrane interactions. The way to obtain this is by systematic biophysical studies and atomic structures of membrane bound AMPs.

This thesis has mainly focused on the charge interactions between Membrane active peptides and lipids. To rule out other factors the lipid model membranes where primarily composed of only two different lipid types DOPC and DOPG. For future work it was be interesting to expand the scope of how SerAdan, Pardaxin and Novicidin interacts with membranes by looking at other factors as the presence of cholesterol. The effect of cholesterol in the membrane, is ordering of the acyl chains, increasing bilayer thickness and domain formation. This has been shown by *in*

3 Discussion of Papers I, II and III

vitro experiments to greatly influence peptide insertion. The cholesterol can both hinder the peptide insertion but also facilitate it followed by sequestering of the cholesterol into cholesterol rich domains [154-156]. These results have also been substantiated by experiments with mutant strains of live yeast cells producing different types of sterols, again showing a huge influence on peptide binding [157]. Another factor to investigate is the role of the lipid acyl chain lengths: as previously mentioned it can determine whether the peptide lays on the surface of the membrane or it transverses it. An NMR study has also shown that the interaction between lipids and peptides is very dynamic, the lipid can stretch the acyl chains or the peptide can tilt, depending what is most energetically favorable [158]. It would especially be interesting to compare Novicidin and Pardaxin as only the latter is long enough to transverse the 3-4 Å that usually comprises the membrane bilayer. Does the acyl chain length play an equally large role if the peptide only inserts in the headgroup region. Finally it would also be interesting to modulate the lateral membrane pressure by including lipids with the non bilayer forming headgroup PE or lipids with varying degrees of unsaturation, something that has not been studied systematically.

Another issue to address is the acquisition of NMR spectra that can be used for determining the atomistic modeling of AMPs in the presence of membrane mimicking detergents or lipids. In this study we looked at how the AMP´s affected the NMR signal of the lipid bilayer but it would be very interesting to combine these with atomic structures of the AMP´s. As mentioned previously there are some inherent problems with studying AMP´s by NMR as they comprise a very dynamic system. One possibility could be the addition of the paramagnetic relaxant Gadolinium while measuring. The Gadolinium will quench the NMR signal in a linear fashion away from the aqueous medium which for membrane AMP interactions can be used for determining how far away a give amino residue is from the aqueous solvent. It has already been shown that the technique can be used for determining the topology of alpha-helical membrane-proteins without the need for a complete NOE-based structure determination. [159, 160].

The fact that monomeric and prefibrillar aggregates of SerAdan displays membrane effects that are similar to those of actual AMP´s, is very interesting considering that this is not the obvious role of this protein *in vivo*. A study of prefibrillar HypF-N aggregates showed that the early toxicity of these where very much dependent on the cholesterol contents of the cell type which they were subjected to [161]. This is a feature which is also known from AMP´s where the lack of affinity towards cholesterol enriched membranes is used to ensure the selectivity towards bacterial cells. So the question is whether all proteins have some inherent membrane perturbing effect and if this is the evolutionary basis for AMP´s. Are the AMP´s deriving from proteins with other functions but then being selected for due to their evolutionary advantage. Supporting this more generic membrane perturbing effect of proteins, are studies that show that aggregates of disease-unrelated proteins display the same cytotoxicity as those formed by proteins and peptides associated with disease suggest that toxicity is a consequence of the common structure of

3 Discussion of Papers I, II and III

aggregates [162, 163]. It would be interesting to test the ability of an ensemble of proteins with known functions and testing their ability to permeate vesicles as a function of their path towards a correct structural fold. If this could be linked to atomic structures of the interactions between these otherwise non membrane active proteins, when they are situated in the membrane this would be a great leap in understanding not only the AMP membrane interactions. Furthermore it might also shed some light on the fundamentals of why, some otherwise good proteins suddenly turn bad.

4 References

4 References

1. Gibson, G., et al., *Oligomerization and neurotoxicity of the amyloid ADan peptide implicated in familial Danish dementia.* J Neurochem, 2004. **88**(2): p. 281-90.
2. Helms, J.B. and C. Zurzolo, *Lipids as targeting signals: lipid rafts and intracellular trafficking.* Traffic, 2004. **5**(4): p. 247-54.
3. Anderson, R.G. and K. Jacobson, *A role for lipid shells in targeting proteins to caveolae, rafts, and other lipid domains.* Science, 2002. **296**(5574): p. 1821-5.
4. Oresic, M., V.A. Hanninen, and A. Vidal-Puig, *Lipidomics: a new window to biomedical frontiers.* Trends Biotechnol, 2008. **26**(12): p. 647-52.
5. Sud, M., et al., *LMSD: LIPID MAPS structure database.* Nucleic Acids Res, 2007. **35**(Database issue): p. D527-32.
6. Vanden Boom, T.C., JE, *Genetics and regulation of bacterial lipid metabolism.* Annu Rev Microbiol., 1989: p. 317–343.
7. Yorek, M.A., *Phospholipids handbook.* Marcel Dekker, New York, 1993: p. 745-775.
8. Daleke, D.L., *Phospholipid flippases.* J Biol Chem, 2007. **282**(2): p. 821-5.
9. Devaux, P.F. and R. Morris, *Transmembrane asymmetry and lateral domains in biological membranes.* Traffic, 2004. **5**(4): p. 241-6.
10. Campos, M.A., et al., *Capsule polysaccharide mediates bacterial resistance to antimicrobial peptides.* Infect Immun, 2004. **72**(12): p. 7107-14.
11. Amiche, M., et al., *The dermaseptin precursors: a protein family with a common preproregion and a variable C-terminal antimicrobial domain.* FEBS Lett, 1999. **456**(3): p. 352-6.
12. Gazit, E., et al., *Interaction of the mammalian antibacterial peptide cecropin P1 with phospholipid vesicles.* Biochemistry, 1995. **34**(36): p. 11479-88.
13. Zucht, H.D., et al., *Casocidin-I: a casein-alpha s2 derived peptide exhibits antibacterial activity.* FEBS Lett, 1995. **372**(2-3): p. 185-8.
14. Zachowski, A., J.P. Henry, and P.F. Devaux, *Control of transmembrane lipid asymmetry in chromaffin granules by an ATP-dependent protein.* Nature, 1989. **340**(6228): p. 75-6.
15. Auland, M.E., et al., *Reconstitution of ATP-dependent aminophospholipid translocation in proteoliposomes.* Proc Natl Acad Sci U S A, 1994. **91**(23): p. 10938-42.
16. Greenberg, M.E., et al., *Oxidized phosphatidylserine-CD36 interactions play an essential role in macrophage-dependent phagocytosis of apoptotic cells.* J Exp Med, 2006. **203**(12): p. 2613-25.
17. Pereira, J., et al., *Platelet aging in vivo is associated with loss of membrane phospholipid asymmetry.* Thromb Haemost, 1999. **82**(4): p. 1318-21.
18. Kuypers, F.A. and K. de Jong, *The role of phosphatidylserine in recognition and removal of erythrocytes.* Cell Mol Biol (Noisy-le-grand), 2004. **50**(2): p. 147-58.
19. Ran, S., A. Downes, and P.E. Thorpe, *Increased exposure of anionic phospholipids on the surface of tumor blood vessels.* Cancer Res, 2002. **62**(21): p. 6132-40.

4 References

20. Morrison, D.C. and L.F. Kline, *Activation of the classical and properdin pathways of complement by bacterial lipopolysaccharides (LPS).* J Immunol, 1977. **118**(1): p. 362-8.
21. W., D., *Molecular basis for membrane phospholipid diversity: why are there so many lipids?* Annual Review of Biochemistry, 1997: p. 199-232.
22. Oppenheim, F.G., et al., *Histatins, a novel family of histidine-rich proteins in human parotid secretion. Isolation, characterization, primary structure, and fungistatic effects on Candida albicans.* J Biol Chem, 1988. **263**(16): p. 7472-7.
23. Schneider, M.F., et al., *Network formation of lipid membranes: triggering structural transitions by chain melting.* Proc Natl Acad Sci U S A, 1999. **96**(25): p. 14312-7.
24. Papahadjopoulos, D. and J.C. Watkins, *Phospholipid model membranes. II. Permeability properties of hydrated liquid crystals.* Biochim Biophys Acta, 1967. **135**(4): p. 639-52.
25. weissig, v.t.a.v., *liposomes, second edition.* practical approach, 2003.

.

26. Kaasgaard, T., O.G. Mouritsen, and K. Jorgensen, *Freeze/thaw effects on lipid-bilayer vesicles investigated by differential scanning calorimetry.* Biochim Biophys Acta, 2003. **1615**(1-2): p. 77-83.
27. Clerc, S.G. and T.E. Thompson, *A possible mechanism for vesicle formation by extrusion.* Biophys J, 1994. **67**(1): p. 475-6.
28. Schurtenberger, P., et al., *Preparation of monodisperse vesicles with variable size by dilution of mixed micellar solutions of bile salt and phosphatidylcholine.* Biochim Biophys Acta, 1984. **775**(1): p. 111-4.
29. Ueno, M., C. Tanford, and J.A. Reynolds, *Phospholipid vesicle formation using nonionic detergents with low monomer solubility. Kinetic factors determine vesicle size and permeability.* Biochemistry, 1984. **23**(13): p. 3070-6.
30. Menger, F.M. and J.S. Keiper, *Chemistry and physics of giant vesicles as biomembrane models.* Curr Opin Chem Biol, 1998. **2**(6): p. 726-32.
31. Needham, D. and E. Evans, *Structure and mechanical properties of giant lipid (DMPC) vesicle bilayers from 20 degrees C below to 10 degrees C above the liquid crystal-crystalline phase transition at 24 degrees C.* Biochemistry, 1988. **27**(21): p. 8261-9.
32. Yang, L. and M. Glaser, *Formation of membrane domains during the activation of protein kinase C.* Biochemistry, 1996. **35**(44): p. 13966-74.
33. Bagatolli, L.A., T. Parasassi, and E. Gratton, *Giant phospholipid vesicles: comparison among the whole lipid sample characteristics using different preparation methods: a two photon fluorescence microscopy study.* Chem Phys Lipids, 2000. **105**(2): p. 135-47.
34. Moscho, A., et al., *Rapid preparation of giant unilamellar vesicles.* Proc Natl Acad Sci U S A, 1996. **93**(21): p. 11443-7.
35. Angelova, M.I.a.D., D.S, *Liposome electroformation.* Faraday Discuss. Chem. Soc., 1986: p. 303–312.
36. Henriques, S.T., et al., *Energy-independent translocation of cell-penetrating peptides occurs without formation of pores. A biophysical study with pep-1.* Mol Membr Biol, 2007. **24**(4): p. 282-93.
37. Mechler, A., et al., *Specific and selective peptide-membrane interactions revealed using quartz crystal microbalance.* Biophys J, 2007. **93**(11): p. 3907-16.
38. Mecke, A., et al., *Membrane thinning due to antimicrobial peptide binding: an atomic force microscopy study of MSI-78 in lipid bilayers.* Biophys J, 2005. **89**(6): p. 4043-50.

4 References

39. Kamimori, H., et al., *Studies on the membrane interactions of the cyclotides kalata B1 and kalata B6 on model membrane systems by surface plasmon resonance.* Anal Biochem, 2005. **337**(1): p. 149-53.
40. Thompson, N.L., H.M. McConnell, and T.P. Burhardt, *Order in supported phospholipid monolayers detected by the dichroism of fluorescence excited with polarized evanescent illumination.* Biophys J, 1984. **46**(6): p. 739-47.
41. Richter, R.P. and A.R. Brisson, *Following the formation of supported lipid bilayers on mica: a study combining AFM, QCM-D, and ellipsometry.* Biophys J, 2005. **88**(5): p. 3422-33.
42. Botelho, A.V., et al., *Curvature and hydrophobic forces drive oligomerization and modulate activity of rhodopsin in membranes.* Biophys J, 2006. **91**(12): p. 4464-77.
43. Marsh, D., *Lateral pressure profile, spontaneous curvature frustration, and the incorporation and conformation of proteins in membranes.* Biophys J, 2007. **93**(11): p. 3884-99.
44. Niyonsaba, F., et al., *The human antimicrobial peptide dermcidin activates normal human keratinocytes.* Br J Dermatol, 2008.
45. Todar, K., *MECHANISMS OF BACTERIAL*

PATHOGENICITY: ENDOTOXINS. Todar's Online Textbook of Bacteriology, 2002.

46. Lerouge, I. and J. Vanderleyden, *O-antigen structural variation: mechanisms and possible roles in animal/plant-microbe interactions.* FEMS Microbiol Rev, 2002. **26**(1): p. 17-47.
47. Lukacova, M., I. Barak, and J. Kazar, *Role of structural variations of polysaccharide antigens in the pathogenicity of Gram-negative bacteria.* Clin Microbiol Infect, 2008. **14**(3): p. 200-6.
48. Gerrit van Meer, D.R.V.a.G.W.F., *Membrane lipids: where they are*

and how they behave. Nature reviews, 2008: p. 112-124.

49. Xu, T., et al., *Anticandidal activity of major human salivary histatins.* Infect Immun, 1991. **59**(8): p. 2549-54.
50. Sabatini, L.M. and E.A. Azen, *Histatins, a family of salivary histidine-rich proteins, are encoded by at least two loci (HIS1 and HIS2).* Biochem Biophys Res Commun, 1989. **160**(2): p. 495-502.
51. Schibli, D.J., P.M. Hwang, and H.J. Vogel, *Structure of the antimicrobial peptide tritrpticin bound to micelles: a distinct membrane-bound peptide fold.* Biochemistry, 1999. **38**(51): p. 16749-55.
52. Del Sal, G., et al., *cDNA cloning of the neutrophil bactericidal peptide indolicidin.* Biochem Biophys Res Commun, 1992. **187**(1): p. 467-72.
53. Selsted, M.E., et al., *Indolicidin, a novel bactericidal tridecapeptide amide from neutrophils.* J Biol Chem, 1992. **267**(7): p. 4292-5.
54. Rozek, A., C.L. Friedrich, and R.E. Hancock, *Structure of the bovine antimicrobial peptide indolicidin bound to dodecylphosphocholine and sodium dodecyl sulfate micelles.* Biochemistry, 2000. **39**(51): p. 15765-74.
55. Aley, S.B., et al., *Killing of Giardia lamblia by cryptdins and cationic neutrophil peptides.* Infect Immun, 1994. **62**(12): p. 5397-403.
56. Ahmad, I., et al., *Liposomal entrapment of the neutrophil-derived peptide indolicidin endows it with in vivo antifungal activity.* Biochim Biophys Acta, 1995. **1237**(2): p. 109-14.
57. Robinson, W.E., Jr., et al., *Anti-HIV-1 activity of indolicidin, an antimicrobial peptide from neutrophils.* J Leukoc Biol, 1998. **63**(1): p. 94-100.
58. Falla, T.J., D.N. Karunaratne, and R.E. Hancock, *Mode of action of the antimicrobial peptide indolicidin.* J Biol Chem, 1996. **271**(32): p. 19298-303.
59. Tossi, A., L. Sandri, and A. Giangaspero, *Amphipathic, alpha-helical antimicrobial peptides.* Biopolymers, 2000. **55**(1): p. 4-30.

4 References

60. Dathe, M. and T. Wieprecht, *Structural features of helical antimicrobial peptides: their potential to modulate activity on model membranes and biological cells.* Biochim Biophys Acta, 1999. **1462**(1-2): p. 71-87.
61. H, e.G.L., *electrically-gated ionic channels in lipid bilayers.* rev. biophys., 1977: p. 595-623.
62. Shai, Y. and Z. Oren, *From "carpet" mechanism to de-novo designed diastereomeric cell-selective antimicrobial peptides.* Peptides, 2001. **22**(10): p. 1629-41.
63. Yang, L., et al., *Crystallization of antimicrobial pores in membranes: magainin and protegrin.* Biophys J, 2000. **79**(4): p. 2002-9.
64. Zelezetsky, I., et al., *Tuning the biological properties of amphipathic alpha-helical antimicrobial peptides: rational use of minimal amino acid substitutions.* Peptides, 2005. **26**(12): p. 2368-76.
65. Zelezetsky, I. and A. Tossi, *Alpha-helical antimicrobial peptides--using a sequence template to guide structure-activity relationship studies.* Biochim Biophys Acta, 2006. **1758**(9): p. 1436-49.
66. Charpentier, S., et al., *Structure, synthesis, and molecular cloning of dermaseptins B, a family of skin peptide antibiotics.* J Biol Chem, 1998. **273**(24): p. 14690-7.
67. Yuan, Z. and V.H. Tam, *Polymyxin B: a new strategy for multidrug-resistant Gram-negative organisms.* Expert Opin Investig Drugs, 2008. **17**(5): p. 661-8.
68. Eisenberg, D., R.M. Weiss, and T.C. Terwilliger, *The hydrophobic moment detects periodicity in protein hydrophobicity.* Proc Natl Acad Sci U S A, 1984. **81**(1): p. 140-4.
69. Sitaram, N., C. Subbalakshmi, and R. Nagaraj, *Structural and charge requirements for antimicrobial and hemolytic activity in the peptide PKLLETFLSKWIG, corresponding to the hydrophobic region of the antimicrobial protein bovine seminalplasmin.* Int J Pept Protein Res, 1995. **46**(2): p. 166-73.
70. Habermann, E., *Bee and wasp venoms.* Science, 1972. **177**(46): p. 314-22.
71. Papo, N. and Y. Shai, *Exploring peptide membrane interaction using surface plasmon resonance: differentiation between pore formation versus membrane disruption by lytic peptides.* Biochemistry, 2003. **42**(2): p. 458-66.
72. Dasseux, J.L., et al., *A restatement of melittin-induced effects on the thermotropism of zwitterionic phospholipids.* Biochim Biophys Acta, 1984. **775**(1): p. 37-50.
73. Bernheimer, A.W. and B. Rudy, *Interactions between membranes and cytolytic peptides.* Biochim Biophys Acta, 1986. **864**(1): p. 123-41.
74. Anderson, D., et al., *Melittin forms crystals which are suitable for high resolution X-ray structural analysis and which reveal a molecular 2-fold axis of symmetry.* J Biol Chem, 1980. **255**(6): p. 2578-82.
75. Schwarz, G. and G. Beschiaschvili, *Thermodynamic and kinetic studies on the association of melittin with a phospholipid bilayer.* Biochim Biophys Acta, 1989. **979**(1): p. 82-90.
76. Beschiaschvili, G. and J. Seelig, *Melittin binding to mixed phosphatidylglycerol/phosphatidylcholine membranes.* Biochemistry, 1990. **29**(1): p. 52-8.
77. Ghosh, A.K., R. Rukmini, and A. Chattopadhyay, *Modulation of tryptophan environment in membrane-bound melittin by negatively charged phospholipids: implications in membrane organization and function.* Biochemistry, 1997. **36**(47): p. 14291-305.
78. Benachir, T. and M. Lafleur, *Study of vesicle leakage induced by melittin.* Biochim Biophys Acta, 1995. **1235**(2): p. 452-60.
79. Raghuraman, H. and A. Chattopadhyay, *Interaction of melittin with membrane cholesterol: a fluorescence approach.* Biophys J, 2004. **87**(4): p. 2419-32.
80. Yang, L., et al., *Barrel-stave model or toroidal model? A case study on melittin pores.* Biophys J, 2001. **81**(3): p. 1475-85.

4 References

81. Dufourcq, J., et al., *Morphological changes of phosphatidylcholine bilayers induced by melittin: vesicularization, fusion, discoidal particles.* Biochim Biophys Acta, 1986. **859**(1): p. 33-48.
82. Harder, J., et al., *A peptide antibiotic from human skin.* Nature, 1997. **387**(6636): p. 861.
83. Singh, P.K., et al., *Production of beta-defensins by human airway epithelia.* Proc Natl Acad Sci U S A, 1998. **95**(25): p. 14961-6.
84. Morgera, F., et al., *Structuring and interactions of human beta-defensins 2 and 3 with model membranes.* J Pept Sci, 2008. **14**(4): p. 518-23.
85. Schittek, B., et al., *Dermcidin: a novel human antibiotic peptide secreted by sweat glands.* Nat Immunol, 2001. **2**(12): p. 1133-7.
86. Rieg, S., et al., *Deficiency of dermcidin-derived antimicrobial peptides in sweat of patients with atopic dermatitis correlates with an impaired innate defense of human skin in vivo.* J Immunol, 2005. **174**(12): p. 8003-10.
87. Kim, K.A., et al., *Effect of dermcidin, an antimicrobial peptide, on body fat mobilization in normal mice.* J Endocrinol, 2008. **198**(1): p. 111-8.
88. P.L. Masson, a., J.F. Heremansa and C.H. Divea, *An iron-binding protein common to many external secretions.* Clinica Chimica Acta, 1966. **14**(16): p. 735-739
89. Castro-Malaspina, H., et al., *Human megakaryocyte stimulation of proliferation of bone marrow fibroblasts.* Blood, 1981. **57**(4): p. 781-7.
90. Arnold, R.R., M.F. Cole, and J.R. McGhee, *A bactericidal effect for human lactoferrin.* Science, 1977. **197**(4300): p. 263-5.
91. Soukka, T., J. Tenovuo, and M. Lenander-Lumikari, *Fungicidal effect of human lactoferrin against Candida albicans.* FEMS Microbiol Lett, 1992. **69**(3): p. 223-8.
92. Schibli, D.J., P.M. Hwang, and H.J. Vogel, *The structure of the antimicrobial active center of lactoferricin B bound to sodium dodecyl sulfate micelles.* FEBS Lett, 1999. **446**(2-3): p. 213-7.
93. Vogel, H.J., et al., *Towards a structure-function analysis of bovine lactoferricin and related tryptophan- and arginine-containing peptides.* Biochem Cell Biol, 2002. **80**(1): p. 49-63.
94. Schibli, D.J., et al., *Tryptophan-rich antimicrobial peptides: comparative properties and membrane interactions.* Biochem Cell Biol, 2002. **80**(5): p. 667-77.
95. He, J. and P. Furmanski, *Sequence specificity and transcriptional activation in the binding of lactoferrin to DNA.* Nature, 1995. **373**(6516): p. 721-4.
96. Kristian, S.A., et al., *MprF-mediated lysinylation of phospholipids in Staphylococcus aureus leads to protection against oxygen-independent neutrophil killing.* Infect Immun, 2003. **71**(1): p. 546-9.
97. Peschel, A., et al., *Staphylococcus aureus resistance to human defensins and evasion of neutrophil killing via the novel virulence factor MprF is based on modification of membrane lipids with l-lysine.* J Exp Med, 2001. **193**(9): p. 1067-76.
98. McPhee, J.B., S. Lewenza, and R.E. Hancock, *Cationic antimicrobial peptides activate a two-component regulatory system, PmrA-PmrB, that regulates resistance to polymyxin B and cationic antimicrobial peptides in Pseudomonas aeruginosa.* Mol Microbiol, 2003. **50**(1): p. 205-17.
99. Sieprawska-Lupa, M., et al., *Degradation of human antimicrobial peptide LL-37 by Staphylococcus aureus-derived proteinases.* Antimicrob Agents Chemother, 2004. **48**(12): p. 4673-9.
100. Anders, R., et al., *The NMR solution structure of the ion channel peptaibol chrysospermin C bound to dodecylphosphocholine micelles.* Eur J Biochem, 2000. **267**(6): p. 1784-94.
101. Esposito, G., et al., *High-resolution 1H NMR study of the solution structure of alamethicin.* Biochemistry, 1987. **26**(4): p. 1043-50.

4 References

102. Doherty, T., A.J. Waring, and M. Hong, *Membrane-bound conformation and topology of the antimicrobial peptide tachyplesin I by solid-state NMR.* Biochemistry, 2006. **45**(44): p. 13323-30.
103. Marcotte, I., et al., *Interaction of antimicrobial peptides from Australian amphibians with lipid membranes.* Chem Phys Lipids, 2003. **122**(1-2): p. 107-20.
104. Cheng, J.T., et al., *Effect of membrane composition on antimicrobial peptides aurein 2.2 and 2.3 from Australian southern bell frogs.* Biophys J, 2009. **96**(2): p. 552-65.
105. Hallock, K.J., et al., *Membrane composition determines pardaxin's mechanism of lipid bilayer disruption.* Biophys J, 2002. **83**(2): p. 1004-13.
106. Wimmer, R., et al., *Versatile interactions of the antimicrobial peptide novispirin with detergents and lipids.* Biochemistry, 2006. **45**(2): p. 481-97.
107. Kendrew, J.C., et al., *A three-dimensional model of the myoglobin molecule obtained by x-ray analysis.* Nature, 1958. **181**(4610): p. 662-6.
108. Fox, R.O., Jr. and F.M. Richards, *A voltage-gated ion channel model inferred from the crystal structure of alamethicin at 1.5-A resolution.* Nature, 1982. **300**(5890): p. 325-30.
109. Neville, F., et al., *Lipid headgroup discrimination by antimicrobial peptide LL-37: insight into mechanism of action.* Biophys J, 2006. **90**(4): p. 1275-87.
110. Staudegger, E., et al., *X-ray studies on the interaction of the antimicrobial peptide gramicidin S with microbial lipid extracts: evidence for cubic phase formation.* Biochim Biophys Acta, 2000. **1468**(1-2): p. 213-30.
111. Lohner, K. and E.J. Prenner, *Differential scanning calorimetry and X-ray diffraction studies of the specificity of the interaction of antimicrobial peptides with membrane-mimetic systems.* Biochim Biophys Acta, 1999. **1462**(1-2): p. 141-56.
112. Glukhov, E., et al., *Basis for selectivity of cationic antimicrobial peptides for bacterial versus mammalian membranes.* J Biol Chem, 2005. **280**(40): p. 33960-7.
113. Cummings, J.E. and T.K. Vanderlick, *Aggregation and hemi-fusion of anionic vesicles induced by the antimicrobial peptide cryptdin-4.* Biochim Biophys Acta, 2007. **1768**(7): p. 1796-804.
114. Otzen, D.E., *Folding of DsbB in mixed micelles: a kinetic analysis of the stability of a bacterial membrane protein.* J Mol Biol, 2003. **330**(4): p. 641-9.
115. Otzen, D.E., et al., *Aggregation of S6 in a quasi-native state by sub-micellar SDS.* Biochim Biophys Acta, 2008. **1784**(2): p. 400-14.
116. Otzen, D.E., P. Sehgal, and P. Westh, *Alpha-Lactalbumin is unfolded by all classes of surfactants but by different mechanisms.* J Colloid Interface Sci, 2009. **329**(2): p. 273-83.
117. Oh, J.E., S.Y. Hong, and K.H. Lee, *Structure-activity relationship study: short antimicrobial peptides.* J Pept Res, 1999. **53**(1): p. 41-6.
118. Ladokhin, A.S., M.E. Selsted, and S.H. White, *CD spectra of indolicidin antimicrobial peptides suggest turns, not polyproline helix.* Biochemistry, 1999. **38**(38): p. 12313-9.
119. Langham, A.A., A.S. Ahmad, and Y.N. Kaznessis, *On the nature of antimicrobial activity: a model for protegrin-1 pores.* J Am Chem Soc, 2008. **130**(13): p. 4338-46.
120. Bond, P.J., et al., *Coarse-grained simulations of the membrane-active antimicrobial Peptide maculatin 1.1.* Biophys J, 2008. **95**(8): p. 3802-15.
121. Thogersen, L., et al., *Peptide aggregation and pore formation in a lipid bilayer: a combined coarse-grained and all atom molecular dynamics study.* Biophys J, 2008. **95**(9): p. 4337-47.
122. Yu, L., et al., *Interaction of an artificial antimicrobial peptide with lipid membranes.* Biochim Biophys Acta, 2009. **1788**(2): p. 333-44.

4 References

123. Shaw, J.E., et al., *Mechanisms of antimicrobial peptide action: studies of indolicidin assembly at model membrane interfaces by in situ atomic force microscopy.* J Struct Biol, 2006. **154**(1): p. 42-58.
124. Li, A., et al., *Atomic force microscopy study of the antimicrobial action of Sushi peptides on Gram negative bacteria.* Biochim Biophys Acta, 2007. **1768**(3): p. 411-8.
125. Meincken, M., D.L. Holroyd, and M. Rautenbach, *Atomic force microscopy study of the effect of antimicrobial peptides on the cell envelope of Escherichia coli.* Antimicrob Agents Chemother, 2005. **49**(10): p. 4085-92.
126. Dathe, M., et al., *Optimization of the antimicrobial activity of magainin peptides by modification of charge.* FEBS Lett, 2001. **501**(2-3): p. 146-50.
127. Kim, Y.C., et al., *Biochemical enhancement of transdermal delivery with magainin peptide: Modification of electrostatic interactions by changing pH.* Int J Pharm, 2008. **362**(1-2): p. 20-8.
128. Bessalle, R., et al., *Augmentation of the antibacterial activity of magainin by positive-charge chain extension.* Antimicrob Agents Chemother, 1992. **36**(2): p. 313-7.
129. Vaz Gomes, A., et al., *Electric potentiation, cooperativity, and synergism of magainin peptides in protein-free liposomes.* Biochemistry, 1993. **32**(20): p. 5365-72.
130. Binder, H. and G. Lindblom, *Charge-dependent translocation of the Trojan peptide penetratin across lipid membranes.* Biophys J, 2003. **85**(2): p. 982-95.
131. Alves, I.D., et al., *Membrane interaction and perturbation mechanisms induced by two cationic cell penetrating peptides with distinct charge distribution.* Biochim Biophys Acta, 2008. **1780**(7-8): p. 948-59.
132. Surolia, I., G.B. Reddy, and S. Sinha, *Hierarchy and the mechanism of fibril formation in ADan peptides.* J Neurochem, 2006. **99**(2): p. 537-48.
133. Porcelli, F., et al., *Structure and orientation of pardaxin determined by NMR experiments in model membranes.* J Biol Chem, 2004. **279**(44): p. 45815-23.
134. Jin, Y., et al., *Antimicrobial activities and structures of two linear cationic peptide families with various amphipathic beta-sheet and alpha-helical potentials.* Antimicrob Agents Chemother, 2005. **49**(12): p. 4957-64.
135. Haney, E.F., et al., *Solution NMR Studies of Amphibian Antimicrobial Peptides: Linking Structure to Function?* Biochim Biophys Acta, 2009.
136. El-Agnaf, O.M., et al., *Effect of the disulfide bridge and the C-terminal extension on the oligomerization of the amyloid peptide ABri implicated in familial British dementia.* Biochemistry, 2001. **40**(12): p. 3449-57.
137. Primor, N., *Pharyngeal cavity and the gills are the target organ for the repellent action of pardaxin in shark.* Experientia, 1985. **41**(5): p. 693-5.
138. Oren, Z. and Y. Shai, *A class of highly potent antibacterial peptides derived from pardaxin, a pore-forming peptide isolated from Moses sole fish Pardachirus marmoratus.* Eur J Biochem, 1996. **237**(1): p. 303-10.
139. Tatulian, S.A. and L.K. Tamm, *Secondary structure, orientation, oligomerization, and lipid interactions of the transmembrane domain of influenza hemagglutinin.* Biochemistry, 2000. **39**(3): p. 496-507.
140. Epand, R.M., et al., *Mechanisms for the modulation of membrane bilayer properties by amphipathic helical peptides.* Biopolymers, 1995. **37**(5): p. 319-38.
141. Shintou, K., et al., *Interaction of an amphipathic peptide with phosphatidycholine/phosphatidylethanolamine mixed membranes.* Biophys J, 2007. **93**(11): p. 3900-6.

4 References

142. Shental-Bechor, D., T. Haliloglu, and N. Ben-Tal, *Interactions of cationic-hydrophobic peptides with lipid bilayers: a Monte Carlo simulation method.* Biophys J, 2007. **93**(6): p. 1858-71.
143. Eriksen, K.R. and I. Erichsen, *[Clinical Occurrence of Methicillin-Resistant Strains of Staphylococcus Aureus.].* Ugeskr Laeger, 1963. **125**: p. 1234-40.
144. Isturiz, R., *Global resistance trends and the potential impact on empirical therapy.* Int J Antimicrob Agents, 2008. **32 Suppl 4**: p. S201-6.
145. Lee, C., *Therapeutic challenges in the era of antibiotic resistance.* Int J Antimicrob Agents, 2008. **32 Suppl 4**: p. S197-9.
146. Boucher, H.W., et al., *Bad bugs, no drugs: no ESKAPE! An update from the Infectious Diseases Society of America.* Clin Infect Dis, 2009. **48**(1): p. 1-12.
147. Talbot, G.H., et al., *Bad bugs need drugs: an update on the development pipeline from the Antimicrobial Availability Task Force of the Infectious Diseases Society of America.* Clin Infect Dis, 2006. **42**(5): p. 657-68.
148. Finch, R. and P.A. Hunter, *Antibiotic resistance--action to promote new technologies: report of an EU Intergovernmental Conference held in Birmingham, UK, 12-13 December 2005.* J Antimicrob Chemother, 2006. **58 Suppl 1**: p. i3-i22.
149. Ge Y, M.D., Holroyd KJ, Thornsberry C, Wexler H, Zasloff M., *In vitro antibacterial properties of pexiganan, an analog of magainin.* Antimicrob Agents Chemother, 1999. **43**: p. 782–788.
150. A., M., *Biotech versus pharma: advantages and drawbacks*
in drug development. EMBO Rep, 2003. **4**: p. 114–117.
151. Gordon YJ, R.E., McDermott AM., *A review of antimicrobial peptides and their therapeutic potential as anti-infective drugs.* Curr Eye Res, 2005: p. 505-15.
152. Khardori, N., *Antibiotics--past, present, and future.* Med Clin North Am, 2006. **90**(6): p. 1049-76.
153. http://www.novozymes.com/en/MainStructure/PressAndPublications/PressRelease/2008/Novozymes+and+sanofi-aventis+announce+collaboration+for+an+innovative+antibiotic.htm, *Novozymes and sanofi-aventis announce collaboration for an innovative antibiotic* 2008.
154. Epand, R.F., A. Ramamoorthy, and R.M. Epand, *Membrane lipid composition and the interaction of pardaxin: the role of cholesterol.* Protein Pept Lett, 2006. **13**(1): p. 1-5.
155. Epand, R.M., et al., *An apolipoprotein AI mimetic peptide: membrane interactions and the role of cholesterol.* Biochemistry, 2004. **43**(17): p. 5073-83.
156. Epand, R.M., B.G. Sayer, and R.F. Epand, *Peptide-induced formation of cholesterol-rich domains.* Biochemistry, 2003. **42**(49): p. 14677-89.
157. Latoud, C., F. Peypoux, and G. Michel, *Interaction of iturin A, a lipopeptide antibiotic, with Saccharomyces cerevisiae cells: influence of the sterol membrane composition.* Can J Microbiol, 1990. **36**(6): p. 384-9.
158. Pabst, G., et al., *Membrane thickening by the antimicrobial peptide PGLa.* Biophys J, 2008. **95**(12): p. 5779-88.
159. Respondek, M., et al., *Mapping the orientation of helices in micelle-bound peptides by paramagnetic relaxation waves.* J Am Chem Soc, 2007. **129**(16): p. 5228-34.
160. Zangger, K., et al., *Positioning of Micelle-Bound Peptides by Paramagnetic Relaxation Enhancements.* J Phys Chem B, 2009.
161. Cecchi, C., et al., *Differing molecular mechanisms appear to underlie early toxicity of prefibrillar HypF-N aggregates to different cell types.* Febs J, 2006. **273**(10): p. 2206-22.
162. Stefani, M., *What the use of disease-unrelated model proteins can tell us about the molecular basis of amyloid aggregation and toxicity.* Ital J Biochem, 2003. **52**(4): p. 162-76.

4 References

163. Bucciantini, M., et al., *Prefibrillar amyloid protein aggregates share common features of cytotoxicity.* J Biol Chem, 2004. **279**(30): p. 31374-82.

Part II

Investigating the mechanical stability of an inner membrane protein by atomic force spectroscopy

5 Investigating the mechanical stability of an inner membrane protein by atomic force spectroscopy

Investigating the mechanical stability of an inner membrane protein by atomic force spectroscopy

Brian S. Vad[1], Alberto Imparato[2], Ole G. Mouritsen[3], Adam Cohen Simonsen[3], Daniel E. Otzen[1*]

[1] Interdisciplinary Nanoscience Center (iNANO), Department of Molecular Biology, University of Aarhus, Gustav Wieds Vej 10C, DENMARK

[2] Department of Physics and Astronomy, University of Aarhus, Ny Munkegade 120, DK – 8000 Aarhus C, DENMARK

[3] Center for Biomembrane Physics, Department of Physics and Chemistry, University of Southern Denmark, Campusvej 55, DK-5230 Odense M, Denmark

SUMMARY

This chapter involves the study of the mechanical stability of a membrane protein measured by dynamic Atomic force microscopy. This project was originally planned as the main goal of this thesis but due to problems with the data analysis of the force retraction curves; work was extended through the entire PhD. These studies will form the basis for additional studies to complete this work. All programming for the automatic determination of force peak size and length was done by Alberto Imparato.

5 Investigating the mechanical stability of an inner membrane protein by atomic force spectroscopy

5.1 INTRODUCTION

Dynamic force spectroscopy has been used to explore the energy landscape of specific interactions between biological relevant molecules and for studying the unfolding pathway of single proteins [1-15]. The basis for these experiments is very simple: a cantilever is brought into contact with the molecule to allow it to bind. The binding can for example be a nonspecific binding or a covalent binding like a gold-thiol bond [16]. The cantilever is then moved away from the sample at a constant speed and when the protein can extend no more, the bond is then broken. By measuring the displacement Δx of the cantilever, Hooke's law allows us to calculate the force F exerted on the cantilever:

$$|\Delta x| = \frac{F}{k} \qquad (1)$$

It has been shown by Daniel Müller and coworkers [10-12, 17] that for membrane proteins the unfolding of membrane proteins in their natural membranes gives rise not just to a single force peak but to a saw tooth pattern of force peaks. Each of these peaks is proposed to coincide with the unfolding of certain structural elements such as a α-helix. In the work by Daniel Muller et al on Bacteriorhodopsin they found that its transmembrane helices predominantly unfold in pairs, each of the helices may also unfold individually and in some cases even only partially [18]. If we assume that helices unfold individually the scenario is sketched out in figure 5.1 for a membrane protein with 4 alpha helices.

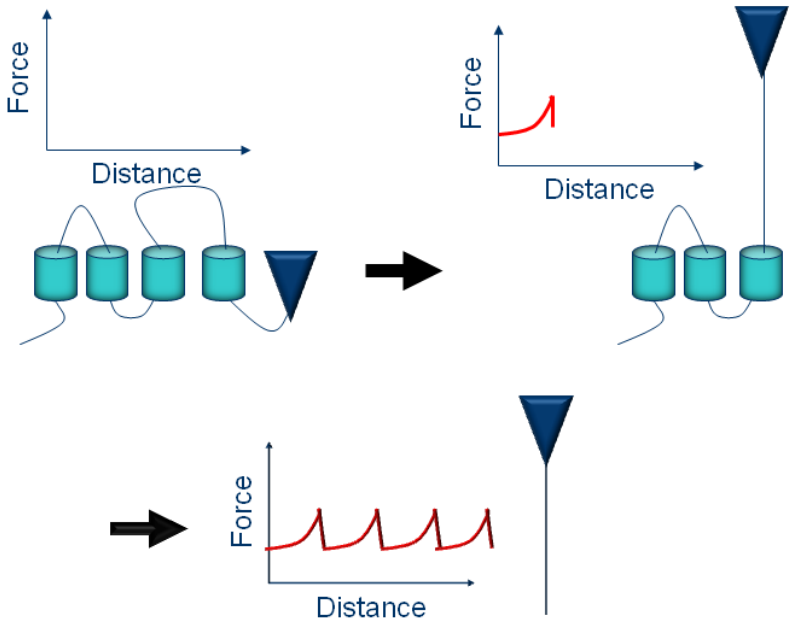

5 Investigating the mechanical stability of an inner membrane protein by atomic force spectroscopy

Figure 5.1: Schematic overview of the unfolding of a protein with four structural elements shown in light blue each of which gives rise to an unfolding peak shown in read.

The cantilever will bend until the structural elements unfold in a cooperative process reducing the force exerted on the cantilever to 0 again. The height of the peaks reflects the strength of interactions that are with the structural elements. To find the length of these structural elements the individual peaks can be fitted to the worm like chain model that gives a reasonable description of the behavior of the stretched protein [2, 19, 20]. The worm like chain model is model known from polymer physics and is used to describe the behavior of semi flexible polymers. The model assumes that the polymer is an isotropic rod that is continuously flexible. The model is especially suitable for describing stiffer polymers, with successive segments displaying a sort of cooperativity [21-23]. If this is done for all the peaks and compared to the primary structure of the protein this will give a map of the interactions that stabilize the protein [24] . The membrane proteins that have been unfolded so far all display multiple unfolding pathways each populated with different probabilities [5, 11, 13, 25-27]. These proteins have ranged from 6 to 12 transmembrane helices that have all been unfolded individually, pair wise or in triplets with unfolding forces ranging from 30-200 pN with some variations for the individual peaks. This will result in an ensemble of force curve patterns and to add on to the complexity the cantilever can in the case of a non specific binding attach at any given point of the protein. Therefore one of the obstacles for this technique is that quite a lot of data handling and sorting is involved. The Some methods have been developed for analyzing dynamic AFM data [28-30] but none of them have spawned a rise in the reported use of the dynamic AFM technique. To increase the likely hood of an attachment event people have used either 2 dimensional crystals of membrane proteins [31] or membranes that are naturally enriched in a specific protein like the purple membrane of bacteriorhodopsin [32] . However not all membrane proteins occur in high quantities in their natural membranes nor will they easily form 2D crystals. Therefore, for the technique to be of general use, it will have to be expanded to systems with a lower protein density. This is the task which we have undertaken in this work. We have chosen two different ways of immobilizing a membrane protein to a solid support. One is the use of a recombinantly produced membrane protein incorporated into phospholipid vesicles to form proteoliposomes. When transferred to a mica surface, the lipids will merge and form a bilayer containing the protein of interest. This has been applied with success to photosynthetic reaction centers which have been shown to retain both their structure and activity [33]. However there has also been reports of the opposite for example for the proton translocating nicotinamide nucleotide transhydrogenase protein were a loss of activity was observed subsequent to surface immobilization[34] possibly due to denaturation. If the protein denatures upon adsorption to the surface the dynamic force spectra will of course not contain peaks deriving from secondary structural elements. The other method is the tethering of a detergent solubilized membrane protein to a mica surface that has been functionalized with an amine reactive linker. This

5 Investigating the mechanical stability of an inner membrane protein by atomic force spectroscopy

technique was originally used for the soluble protein pea lectin [35] but has not previously been applied to a membrane protein. For the binding of the cantilever to the sample, both the unspecific binding and the use of a gold thiol bond were performed. The use of the gold thiol should increase the reproducibility of the experiments as the cantilever attachment point presumably would be the same every time.

The model protein we have chosen for this study is the Disulfide bond forming protein B (DsbB). DsbB is an inner membrane protein and is an integral part of the network of catalysts that are required for the oxidative protein folding in proteo bacteria [36]. The protein is roughly 20 KDa and consist of four transmembrane helices, a common feature of the whole DsbB family [36] and two large periplasmic loops [37] (see figure 5.2). Both periplasmic loops contain a conserved cysteine bridge at positions 41, 44 and 104,130 which have been shown to be crucial for the activity since removal results in loss of catalytic activity [38] DsbB has been co crystallized with Disulfide bond forming protein A and the crystal structure solved by Inaba and coworkers in 2005 [39-41] . The purpose was to see if we could get structural data from our dynamic AFM measurement that would coincide with the structural and stability data already obtained from the crystal structure[40] and other biophysical measurements [37, 42-50]. For the dynamic AFM experiments we used a mutant that lacked the cysteins at positions 41, 44, 49 104 and 130 but retained a single cysteine at the position 8 which allows the formation of a specific gold thiol bond with a gold coated cantilever in the N-terminal part of the protein. In the reaction with the functionalized mica there are 7 possible points of attachment to DsbB, 6 lysines at positions 39, 66, 118, 167, 169 and 170 and the N terminus. For an overview of the DsbB structure and the key residues see figure 5.2 A.

5 Investigating the mechanical stability of an inner membrane protein by atomic force spectroscopy

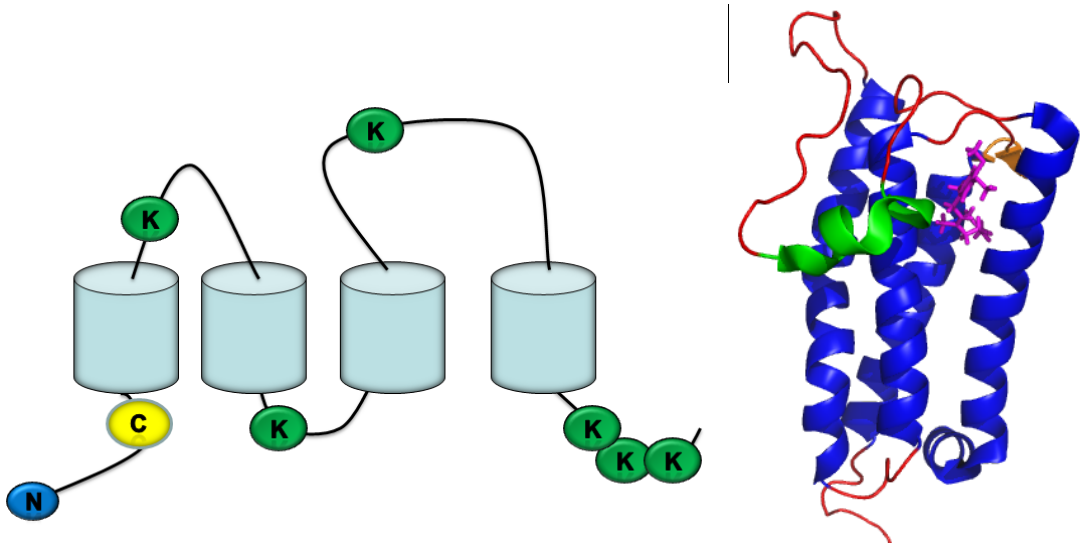

Figure 5.2: (A): Schematic drawing of a cystein deficient DsbB mutant showing the transmembrane helices in light blue the N-terminal in dark blue, the single cystein at position 8 is shown in yellow and lysines at positions 38, 65, 117, 166, 168 and 169 are shown in green. (B) The liquid state NMR structure of DsbB [51] in complex with Ubiquinone shown in purple. Transmembrane helices are shown in blue, helices area shown in green and beta sheet is shown in orange.

5 Investigating the mechanical stability of an inner membrane protein by atomic force spectroscopy

5.2 MATERIALS AND METHODS

Production and purification of DsbB: The purification protocol was adapted from Bardwell et al [52, 53]. C43(DE3) *E. coli* cells harboring the plasmid expressing the DsbB single cysteine mutant was transferred from a glycerol stock to two LB-agar agar plates containing 100µg/ml ampicillin grown overnight at 37°C. In the single cystein mutant cysteins at position 41,44,104 and 130 have been mutated into leusine Agar plates were washed with 20ml LB-medium and inoculated into 2 L shaking flask with 1 Liter of LB medium containing 100µg/ml ampicillin and grown for 2 hours. The medium was the centrifuged for 10 min at 3000 g. The cell pellet was resuspended in 50 ml LB medium and used to inoculate 10 l of medium in a fermentor at 37°C. At an OD_{600} of ~ 1 the culture was induced with 450 µl 0.1M IPTG stock pr L. The culture was grown for another 4 hours and harvested by centrifugation at 4000g for 10min. The pellets were resuspended in 60ml 50mM tris HCl buffer pH 8, containing 300mM NaCl and 1mM EDTA. Subsequently PMSF dissolved in isopropanol was added to a final concentration of 2mM. Cells were lysed by rod sonication 5 times 1min... Cell debris was centrifuged for 10min. at 10000G and supernatant was subsequently centrifuged at 100.000G for 90min. The pellet was resuspended with a glass homogenizer in 50mM NaP pH 8, containing 300mM NaCl and 1% w/v DDM and loaded onto a Ni NTA column. A Ni NTA column was equilibrated with 5mM sodium phosphate (NaP) buffer pH 8, containing 300mM NaCl and 0.02% w/v DDM 0.02% DDM corresponds to. 0.4 mM, which is ~twice the detergent's CMC value of 0.17 mM. The sample was loaded onto the column at a flow rate of 0.5ml/min, recycling the flow-through over the column overnight. The column was washed with 50mM NaP buffer pH 8 containing 300mM NaCl and 0.02% w/v DDM until baseline followed by an additional wash with 50ml containing 30mM imidazole. A gradient was run from 30-500mM imidazole at a flow rate of 1 ml per and collected in 4 ml samples and analyzed on a 12% SDS gel. The purest samples were collected, concentrated and used for experiments. The final yield was ~ 3 mg/L of cell culture.

Fluorescence labeling of DsbB: DsbB dissolved in 50 mM Phosphate buffer and 300 mM NaCl with 0.02 % DDM was bound on a Ni-NTA-agarose beads and incubated with a 3 molar excess of the thiol reactive Fluorescent probe 5 – iodacetamide fluorescein for 2 hours at 5°C with agitation. The beads were applied to an empty Pharmacia PD-10 column and washed with copious amounts of 50 mM PBS with 0.02 % DDM. The DsbB was then eluted by addition of 50 mM EDTA and subsequently dialyzed against 50 mM PBS with 0.02 % DDM.

Preparation of Small unilamellar vesicles: Lipid samples were prepared from chloroform stocks which were mixed and solvent was removed in a dessicator. Lipids were rehydrated to a concentration of 10 mg/ml in 50 mM PBS buffer pH 7.5 by vortexing. SUV´s were formed by inserting a rod sonicator in the liquid and pulse sonicating for 1 hour. The sample container was submerged in ice water to avoid lipid degradation due to elevated temperatures. Subsequently the

sample was centrifuged for 15 min in a table top centrifuge at 12000 rpm to remove titanium debris shed from the tip of the rod sonicator during operation.

Determination of hydrodynamic radius: The hydrodynamic radius of samples was measured on a PDDLS/coolbatch 90T Dynamic light scattering apparatus from postnova analytics. The sample time etc was set to and the spectra were normalized according to molecular weight. Samples were diluted to ~ 100 ng/ml DsbB in 50 mM PBS buffer that had been filtrated through a 0.2 μm disposable filter syringe.

Secondary structural changes measured by CD spectroscopy: Circular dichroism studies were performed on a Jasco J-810 spectropolarimeter (Jasco Spectroscopic Co., Hachioji City, Japan) with a Jasco PTC-348W1 temperature control unit. Scan speed was set to 100 nm min, slit width 2 nm. All experiments were carried out in 50 mM PBS buffer pH 7.5, at 25^{o}C using a 1 mm quartz cuvette. Samples were diluted to a protein concentration of 40μM.

Reconstitution of DsbB into lipid vesicles: DsbB was mixed with sonicated lipid vesicles at a 1:300 DsbB: lipid molar ratio with a DDM concentration of approximately 0.4 mM in 50 mM phosphate buffer with 300 mM NaCl. The samples were allowed to equilibrate with gentle agitation for an hour at 5^{o}C. DDM was removed by addition of a surplus of *Bio-Beads SM-2* Macro porous Beads (Bio-Rad) and left to incubate for 30 min with gentle agitation, this was repeated two times and samples were subsequently used for analysis. There was no observable protein aggregation when subjected to a visual inspection.

Functionalisation of mica: The functionalisation of mica with a primary amine reactive species was done according to the method described by Klein et al (ref): A water free solution of ethanolamine in dry DMSO (6.6 g in 12 mL) was heated up to 70^{o}C . To keep the solution anhydrous, molecular sieve beads (0.3 nm) were added. Freshly cleaved muscovite mica sheets were incubated overnight in this solution. The mica sheets were washed four times in DMSO and twice in ethanol. The mica sheets were then dried under a nitrogen flow. At this stage the mica should be derivatized to expose primary amine groups which can then be bound to a bis-NHS ester. This is done by incubating the mica for 3 h in a solution of chloroform with 1mg/ml ethylene glycol bis(succinimidyl succinate) and triethylamine (0.5% v/v). The mica sheets were washed in chloroform and dried in a nitrogen flow. The mica sheets were immediately used for protein coupling.

Activity measurements of DsbB

The activity measurements of DsbB exploit the fact that DsbA loses its fluorescence as it is oxidized by DsbB. The assay was performed at 30°C in a reaction mixture containing 50 mM sodium phosphate (pH 6.0), 300 mM NaCl, 0.5 mM EDTA, 0.1% DM, ubiquinone-1 (coenzyme

Q_1; Sigma), DsbB, and the reduced form of DsbA that was prepared as described [52, 53]. The rates were derived from the initial linear fluorescence decrease.

Fluorescence imaging

Fluorescence images of collapsed liposomes and immobilized fluorescently labeled DsbB were recorded on a Nikon TE2000 inverted microscope and using a 20× long working distance objective. Fluorescence excitation was done with a halogen lamb and using a G-2A filter cube (Nikon). Images were recorded with a high sensitivity CCD camera (Sensicam em, 1004×1002 pixels, PCO-imaging, Kelheim, Germany) and operated with Camware software (PCO)

AFM imaging and dynamic AFM of DsbB on solid supports: AFM images were done in a fluid chamber on a PicoSPM atomic force microscope (Molecular Imaging, Phoenix, AZ) in contact mode. For imaging of membranes the vesicles were deposited on a piece of freshly cleaved mica in 50 mM Phosphate buffer pH 7.5 with 300 mM NaCl and left for 1 hour to allow vesicle collapse and bilayer formation. Afterwards the sample was washed by exchanging the sample volume 10 times to remove excess layers of lipid. For binding of DsbB in DDM to amine reactive mica, the sample was placed on the mica for 1 hour to allow covalent binding, after which the sample fluid was replaced 10 times to remove any unbound protein. The dynamic AFM spectra were recorded on a JPK Nanowizard AFM system (JPK Instruments AG). The cantilevers had either triangular silicon nitride or silicon gold coated tip from budget sensors (Sofia, Bulgaria) with a nominal spring constant of 0.01 N/m and 0.06 N/m respectively. The pulling speed was set to 100 nm/sec and the cantilever was set to pause for 1 sec upon touching the sample surface. For every sample, ~1800 force curves were collected, and for every 25 spectra the tip was moved to a new spot on the sample surface. The data collection for each dataset took roughly 5 hours.

Dynamic AFM data analysis: The original was recalculated into force using Hooke's law:

$$|\Delta x| = \frac{F}{k} \qquad (1)$$

and the data was sorted manually into spectra contained force peaks and those that did not. The spectra were analyzed automatically by a program written in C++ by Alberto Imparato. The program determined the baseline by a linear fit to the final part of the force spectra and the point where this intersected with the initial pressure slope was set as the starting point of protein extension. Data were smoothed by averaging all values per nm extension which in average was ~ 15 points pr nm. The length and unfolding force of each force peak was then determined by fitting to the wormlike chain model [2, 19, 20] and was compiled in an output file together with the value of the offset.

5 Investigating the mechanical stability of an inner membrane protein by atomic force spectroscopy

5 Investigating the mechanical stability of an inner membrane protein by atomic force spectroscopy

5.3 RESULTS

5.3.1 Expression, purification, reconstitution and functional characterization of DsbB

The expression and purification of functional detergent solubilized DsbB has been established as a routine procedure both in our lab and by other group's [54-57]. However, it was necessary to establish a protocol for lipid reconstitution of DsbB and assay how this influenced the secondary structure and enzymatic stability. Both the wild type and cysteine deficient DsbB were successfully over expressed and Purified in DDM. The wt DsbB was then reconstituted into lipids containing both zwitterionic and anionic lipids. The samples turned slightly opaque upon removal of the detergents indicating a change in the vesicle morphology. This was tested by measuring the mean diameter of the vesicle suspension prior to and after DsbB reconstitution. Upon reconstitution an increase in the mean vesicle diameter of approximately 100 nm was observed (Table 5.1). There were no significant differences in the vesicle diameters as a function of the lipid composition.

Table 5.1: Mean hydrodynamic radius (R_h) of different DsbB-amphiphile complexes[a]

Protein	Amphiphile	R_h (nm)
DsbB	DM	6
-	DOPC	32
-	8DOPC:2DOPG	27
DsbB	DOPC	68
DsbB	8DOPC:2DOPG	72

Notes:

[a] All experiments at 25 degrees C in 50 mM Phosphate buffer with 300 mM NaCl.

The sample was centrifuged in order to sediment the lipid fraction. According to SDS-PAGE, more than 75 % of the proteliposomes could be centrifuged down by a normal table top centrifuge (Fig. 5.3), indicating that they have a size much larger than that which was given as the mean average in the DLS. The pellet had a clear purple hue indicating that the DsbB still bound a quinone. This is a strong indication that it has retained the native fold during the reconstitution into lipids.

5 Investigating the mechanical stability of an inner membrane protein by atomic force spectroscopy

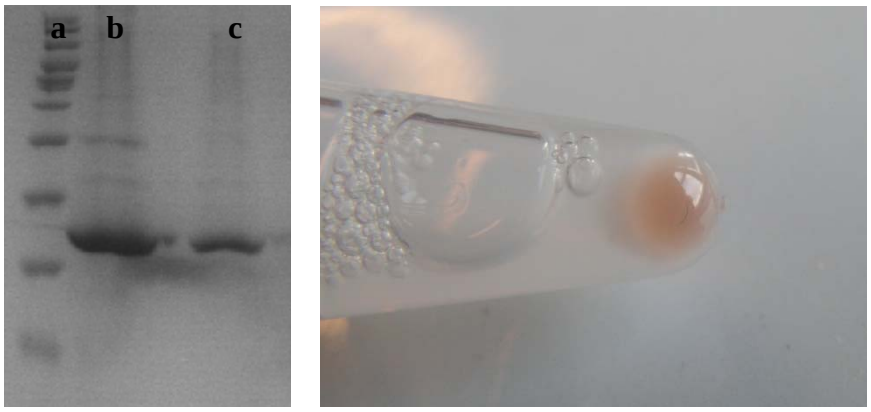

Figure 5.3: (A): 12% SDS gel with a molecular marker in lane (a), pellet (b) and supernatant (c) after centrifugation for 30 min at 12000 rpm in lane b. (B): pellet of DsbB solubilized in DOPC vesicles. After centrifugation a clear pink hue is seen.

The secondary structure was measured for DsbB both reconstituted in DDM, 100% DOPC and 20% DOPG: 80 % DOPC (Fig. 5.4 A). The structure of DsbB dissolved in DDM is clearly α-helical with two local minima at 208 and 222 nm. The lipid reconstituted DsbB displays two essentially identical CD spectra which retain the double-minimum shape characteristic of α-helices but with a slight shift in the wavelength of the initial minimum from 222 to 228 nm and the second minimum at 208 reduced to a shoulder compared to the detergent solubilized DsbB. Although the DDM- and lipid spectra are not completely identical, this is likely to reflect slight structural changes in the reconstitution process rather than actual protein unfolding. Furthermore, some artifacts may be introduced by light scattering from the liposomes.

Activity was measured by an assay which monitors the decrease in the fluorescence signal of the periplasmic protein DsbA at 355 nm upon interaction with DsbB (Fig. 5.4 B). This decrease in fluorescence is caused by the oxidation of DsbA by DsbB, which in turns changes the environment around DsbA´s tryptophan. Assuming random insertion of DsbB into lipid vesicles, activity will be halved compared to that of detergent solubilized DsbB. This is because only 50 percent of the DsbB molecules will present the long flexible loops that are responsible for the reoxidation of DsbA to the exterior of the vesicles. What we observe in the activity measurements is that there is activity but it is reduced by half for the DsbB reconstituted in 20% DOPG & 80 % DOPC and even more for the DsbB reconstituted in pure DOPC. Hence we conclude that DsbB is correctly inserted into vesicles, retaining its bound quinine, its secondary structure and to a large extent also the enzymatic activity.

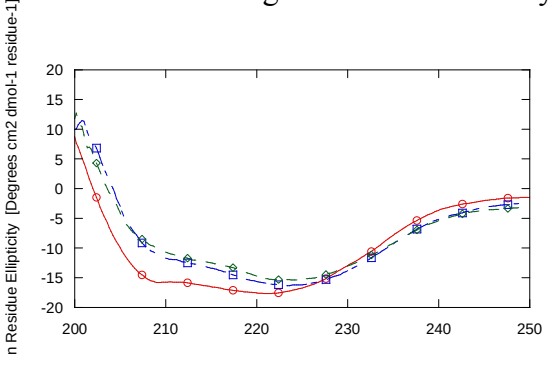

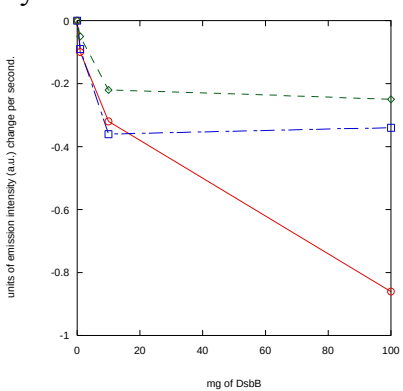

5 Investigating the mechanical stability of an inner membrane protein by atomic force spectroscopy

Figure 5.4: (A) Circular dichroism spectra of DsbB in 50 mM PBS buffer pH 7.5 DDM (○), DOPC (□) and 20% DOPG & 80 % DOPC (△). (B) Activity of DsbB in 50 mM PBS buffer pH 7.5 5 DDM (○), DOPC (□) and triangles 20% DOPG & 80 % DOPC (△).

5.3.2 The immobilization of DsbB on solid substrates

Our force spectroscopy measurements require us to immobilize DsbB to a solid support by (a) covalent binding of detergent solubilized DsbB or (b) collapse of proteoliposomes containing DsbB onto freshly cleaved mica. Once DsbB is immobilized, we are unable to check if it retains its secondary structure or activity. As an alternative, we examined the distribution and morphology of the deposits. To check whether we had a homogeneous distribution of DsbB in the supported bilayer, we fluorescently labeled DsbB with fluorescein and checked for localization of fluorescein fluorescence at the mica surface by fluorescence microscopy. Most of the mica surface showed a homogeneous fluorescence indicating an even distribution of DsbB (Fig. 5.5 A). There were however also areas where there was either a lack of DsbB in the lipid bilayer or defects in the bilayer itself indicated by dark patches indicated by arrow 1 (Fig. 5.5 A). There were also spots where increased fluorescence suggested aggregation of DsbB. Most often these two phenomena's could be observed in conjunction suggesting that the defects in the bilayer were caused by protein aggregation or vice versa. The same procedure was used to test whether the functionalized mica bound DsbB solubilized in DDM. Again the fluorescence could be localized just above the mica surface but the distribution was very different from what was observed in the lipid system. There are large contiguous regions of DsbB-fluorescence interrupted by spherical areas with low fluorescence, but there were no signs of protein aggregates on the surface of the type seen with lipids (Fig. 5.5 B). This would indicate that DsbB is bound to the surface but is very unevenly distributed. This might influence the data acquisition in dynamic AFM.

5 Investigating the mechanical stability of an inner membrane protein by atomic force spectroscopy

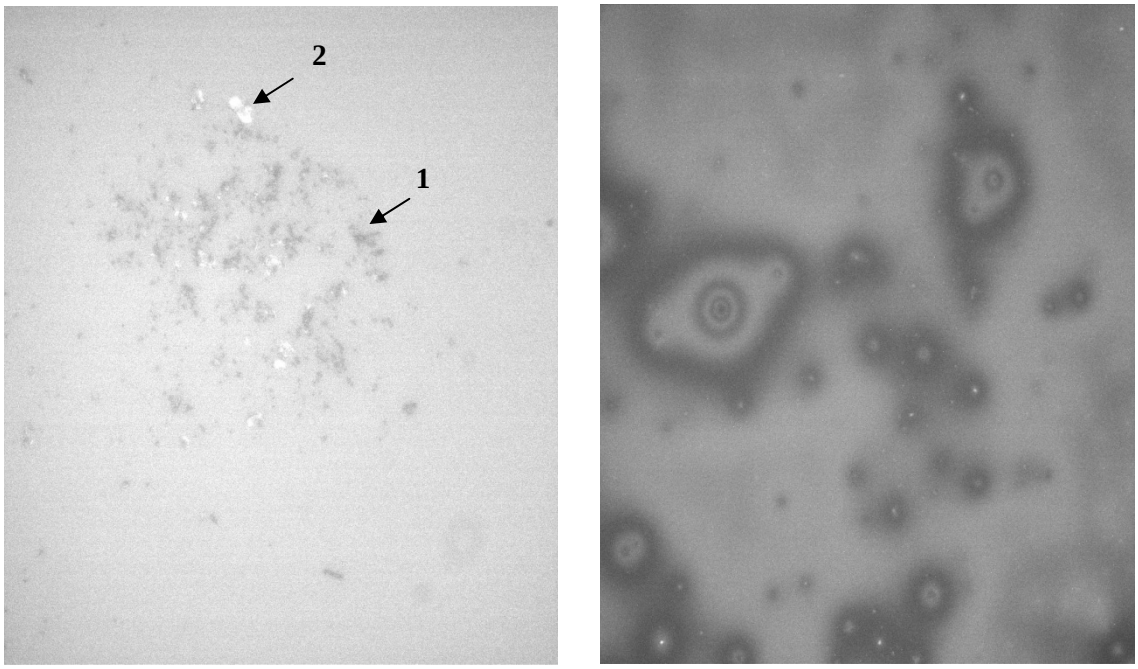

Figure 5.5: (A): Fluorescence image of fluorescein-labeled DsbB in DOPC vesicles collapsed on to a mica substrate. Arrow one indicating low fluorescence points possibly due to defects in the membrane. Arrow two indicating an area with increased fluorescence most likely due to the presence of protein aggregates. (B): Fluorescence image of amine reactive mica incubated with fluorescein-labeled DsbB in DDM. The fluorescence is shown in light color corresponding to the presence of fluorescein-labeled DsbB, which is very unevenly distributed.

To compare surface morphology of both DsbB in supported bilayers and on the functionalized mica surface, we imaged the surface by AFM. The lipid bilayer image (Fig. 5.6 A) shows a homogeneous flat bilayer with small perturbations with a height on the order of 1-2 nm and a width of 10-50 nm. These perturbations are too large to be individual DsbB molecules and most likely represent small protein aggregates. No defects could be observed in the bilayer but when applying excessive force on the membrane lipids, a layer could be peeled off that corresponds to the thickness of a bilayer. The surface of the functionalized mica with DsbB (Fig. 5.6 B) showed a much more rugged surface morphology with pronounced height variation but again in the 1-3 nm scale. Some defects in the surface coverage could be observed indicated in figure 5.6 B by arrow no 3. Thus, the AFM imaging confirmed our fluorescence microscopy observations; the sample surface is unevenly covered by DsbB, but without obvious indications of protein aggregation.

5 Investigating the mechanical stability of an inner membrane protein by atomic force spectroscopy

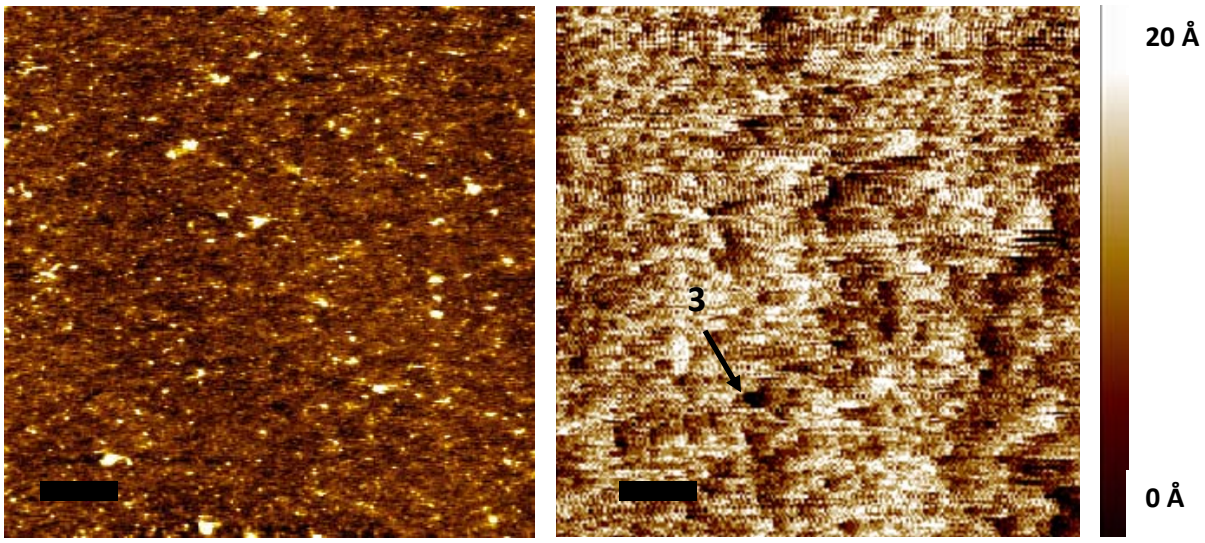

Figure 5.6: (A) Atomic Force Microscopy images of amine reactive mica incubated with fluorescein labeled DsbB in DDM in 50 mM Tris buffer pH 7.5 µm image arrow indicating small holes in the surface. The scale bare is 250nm. (B) Atomic force image of fluorescein labeled DsbB in 20% DOPG & 80% DOPC vesicles collapsed on to a mica substrate. A color height scale bar going from 0 to 20 Å is shown n the right.

5.3.3 Measuring Dynamic AFM on DsbB in DDM and Anionic lipid membranes

The dynamic AFM of measurements of DsbB in lipids and detergent was undertaken to establish a method of mapping the structural elements of DsbB. Approximately 1800 force spectra were recorded for each of the different conditions, leading to 2.5-12% data sets with force peaks (Table 5.4). The dataset set that contained the most unfolding events was the sample with detergent solubilized DsbB covalently bound to mica (unfolded with the gold cantilever) while the one with the fewest events was DsbB in lipids (also unfolded with the gold cantilever). When unfolded with the SiNi cantilever, both samples contained 6-7% unfolding events. None of the spectra contained more than 3 unfolding events, with the great majority (73-100%) containing only one unfolding event.

5 Investigating the mechanical stability of an inner membrane protein by atomic force spectroscopy

Table 5.4: The frequency of force peak events in the dynamic AFM data sets and also the number of force events.[a]

			Percentage of all curves	**Percentage of curves with force peaks**		
Amphiphile	Surface	Cantilever	Curves with force peaks	Single peak	Two peaks	Three peaks
8DOPC:2DOPG	Mica	SiNi	7.8	73	24	3
8DOPC:2DOPG	Mica	Gold	2.56	100	0	0
DDM	F.-mica[b]	SiNi	6.27	90	8	2
DDM	F.-mica[b]	Gold	12	84	13	3

Notes:

[a]All measurements in 50 mM PBS pH 7.5.

[b] Functionalized mica allowing DsbB to bind covalently to the surface via Lys residues.

When the rupture force and the rupture length of the unfolding peaks were plotted against their frequency, they displayed the signature of a normal distribution for all four experimental conditions except for the lipid reconstituted DsbB unfolded with SiNi cantilever where two overlapping sigmoidial distributions were observed. The sigmoidial curves were fitted to Gaussian functions and the peak values and widths are shown in Table 5.5.

Table 5.5: Rupture forces and lengths for unfolding of different preparations of DsbB[a]

Amphiphile	**Surface**	Cantilever	**Peak position Rupture force [pN]**	**Peak width rupture force[pN]**	**Peak position Rupture length [nm]**	**Peak width Rupture length [nm]**
8**DOPC:2DOPG**	Mica	SiNi	449	355	16.7&34.5	10.6 & 28.3
8**DOPC:2DOPG**	Mica	Gold	172	110	11.4	10.25
DDM	F.-mica[b]	SiNi	487	386	41.2	57.4
DDM	F.-mica[b]	Gold	78	52	11.8	21.1

Notes:

[a] All experiments performed in 50 mM PBS buffer at 15^{o}C. Data obtained from Gaussian distribution fits to the histograms of the distribution of rupture force and the rupture length shown in Fig. 6.

5 Investigating the mechanical stability of an inner membrane protein by atomic force spectroscopy

The peak rupture forces observed for the unfolding of lipid reconstituted and detergent solubilized unfolded with SiNi cantilevers displayed similar rupture forces ~ 500 pN. The rupture forces using a gold cantilever were significantly lower, with peak rupture forces of 172 and 78 pN for lipid reconstituted and detergent solubilized DsbB, respectively. The peak positions for the rupture length for the lipid reconstituted and detergent solubilized DsbB using a gold cantilever were very similar (~11 nm). This corresponds to roughly a sixth of the entire protein length indicating that the majority of the unfolding events represent the unfolding of a single helix. The rupture length of DsbB in DDM on functionalized mica with a SiNi cantilever was approximately 41 nm which could correspond to three out the four helices. Under the assumption that DsbB is bound to either of either the N terminal or the three leusines at the C terminal this would suggest that the cantilever preferably binds somewhere in which ever of the large periplasmic loops that is farthest away from the point of attachment. For the lipid reconstituted DsbB measured with a SiNi cantilever we see two rupture length populations one with a distribution around 17 nm and one around 34 nm. This would suggest that the cantilever attaches with an even frequency in either of the two periplasmic loops. The 5 most similar spectra of the force spectra, preferably with peaks around the most frequent rupture length where overlaid to elucidate on force peak characteristics, see figure 5.7.

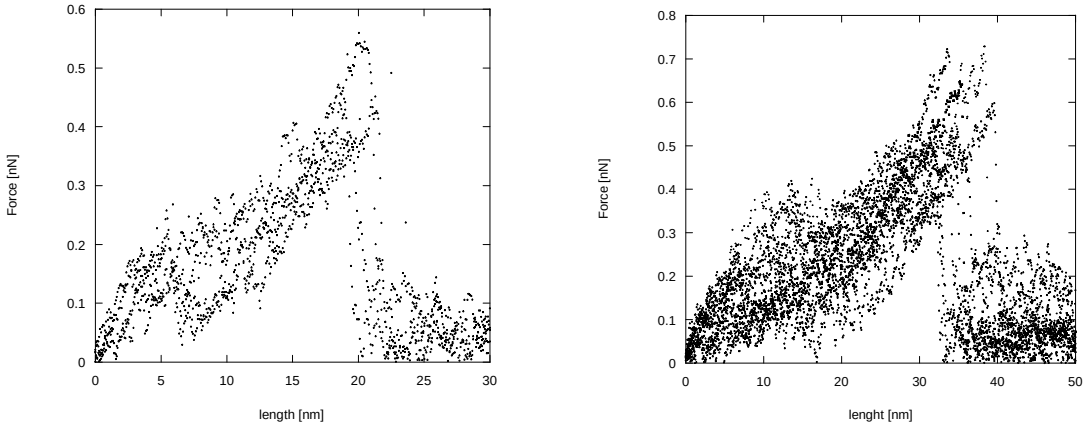

5 Investigating the mechanical stability of an inner membrane protein by atomic force spectroscopy

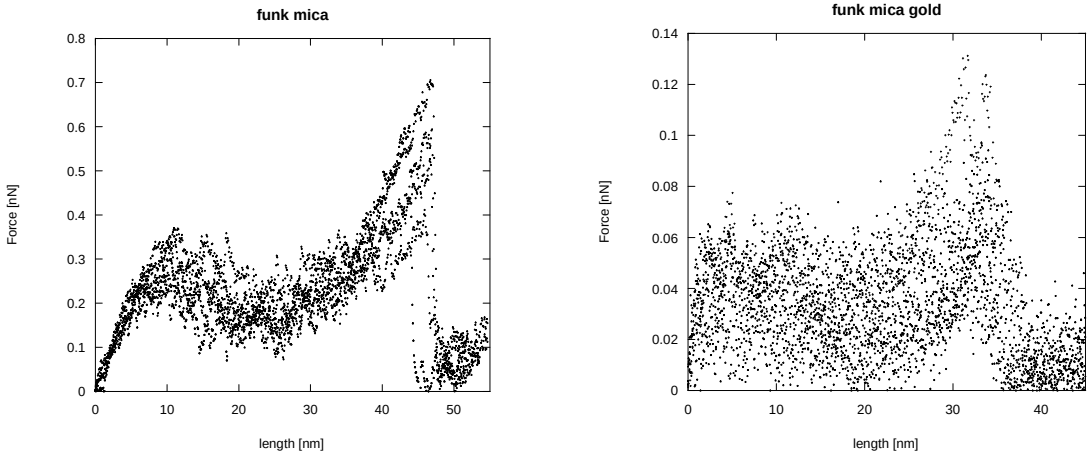

Figure 5.7: left: Overlay of 5 force curves with a rupture length at +/- 7 nm from the maximum values of the Gaussian fit to rupture length frequency for: DsbB in lipids and using a SiNi cantilever ~ 17 (top left) & 34 nm (top right), DsbB in DDM ~ 41 nm (bottom left) using a SiNi. The bottom right is DsbB in DDM using a Gold cantilever but here spectra could not be aligned at the maximum values of the Gaussian fit to rupture length frequency but where instead aligned for spectra with rupture lengths at ~34 nm.

None of the datasets that were collected contained sufficient spectra with unfolding curves that were similar to that of the full length protein ~ 63 nm for comparison and overlay. As seen in table 3 DsbB incorporated into lipids and unfolded with a SiNi cantilever predominantly two unfolding peaks with a contour length of 17 nm and another of 34 nm was observed. For both of these values 5 spectra could be overlaid displaying only a single unfolding peak but with some noise in the initial 5-10 nm. This indicates that the protein favors unfolding in a cooperative manner regardless of where the cantilever attaches to the protein. We observe the same for the unfolding of DsbB in DDM with a SiNi cantilever, 5 spectra could be overlaid with one prominent peak in this case at ~ 44 nm. These spectra overlaid better than the two previous but again some degree of noise can be observed within the initial 5-10 nm. For the unfolding of DsbB in DDM with a gold cantilever we could not overlay 5 spectra with peaks at the most frequent unfolding length ~11 nm. This was due to the very low signal to noise ratio but 5 spectra with peaks around 34 nm could be aligned with an acceptable result. For DsbB in lipids unfolded with a gold cantilever the lack of spectra meant that it was not possible to align 5 spectra with a satisfying result.

5 Investigating the mechanical stability of an inner membrane protein by atomic force spectroscopy

5.4 DISCUSSION

5.4.1 The reconstitution of DsbB in lipids

The meaning of measuring dynamic AFM on non Crystalline DsbB was to make the dynamic AFM method more generally applicable for measuring the mechanic unfolding of membrane proteins. The initial step was therefore to ensure that we started out with DsbB that was correctly folded which would be evaluated by CD measurements and activity measurements. From our centrifugation study we established that the main fraction of liposome-DsbB could be spun down with the lipid fraction of the sample. The liposome-DsbB retained the cofactor Q8 indicated by the purple color contrary to the Cys deficient mutant, which was yellow, and aggregated DsbB which is white (data not shown). The pink color is due to the charge-transfer interaction between Cys44 and ubiquinone Q8 [41, 58, 59] which strongly indicates that DsbB is properly folded upon insertion into lipids. The secondary structure of liposome - DsbB was more or less the same indicated by the CD measurements with a slight decrease of the signal intensity at 208 nm. However Otzen 2003 [60] showed that unfolding of DsbB by increasing fractions of SDS only changed the CD spectra intensity at 208 nm with a slight increase, the opposite of what we observe in lipids. All the experiments indicated that the lipid reconstitution of DsbB was successful. The activity was reduced by ~50% in lipids but this can be explained both by lack of substrate accessibility due to random insertion and scattering effects from the lipids at high protein concentrations. The protein insertion direction has been shown to be very dependent on the detergent addition and further work could be done to elucidate this [61].

5.4.2 Evaluating the morphology of DsbB on a solid substrate

We had no direct means of measuring how the structure of DsbB is affected by immobilization either in a supported bilayer or on functionalized mica. There are some reports that the structure of soluble proteins change upon immobilization on a solid substrate [62-64] but this does not seem to be transferable to membrane proteins [31, 32, 65]. Based on this we assume that DsbB retains its structure on the surface. We were able to evaluate the protein distribution and the gross morphology by Fluorescence microscopy and AFM respectively. We observed that DsbB seemed to be more evenly distributed in the lipid bilayers compared to the functionalized mica judging from the fluorescence images. When we zoomed in by the aid of AFM we observed what seemed to be more or less homogeneously covered surfaces. This would suggest that the inhomogeneous coverage of the functionalized mica does not pose a problem as long as a suitable surface area is chosen for dynamic AFM.

5.4.3 Dynamic AFM of DsbB reveal patterns in the unfolding events

The dynamic AFM measurements showed a force peak frequency in the order DsbB in DDM with gold cantilever > DsbB in lipids SiNi cantilever > DsbB in DDM with SiNi cantilever >

5 Investigating the mechanical stability of an inner membrane protein by atomic force spectroscopy

DsbB in lipids with gold cantilever. The low occurrence of force peaks in the DsbB in lipids with gold cantilever can easily be explained by lack of accessibility of the free Cysteine. If the free cysteine is facing the mica surface the cantilever has to penetrate the lipid bilayer in order to establish the covalent gold-thiol bond. The accessibility in combination with the formation of covalent bond could then explain why we observe the highest frequency of binding in the DsbB in DDM with gold cantilever. The main bulk of spectra obtained in DDM with gold cantilever was however not of lengths compatible with that of the full length protein or of a significantly better quality than those obtained with the SiNi cantilever. This work is the first to our knowledge that describes the unfolding of a detergent solubilized membrane protein by dynamic AFM. The force spectra obtained were of a quality similar to or better than those that were obtained for the lipid solubilized protein. The maximum number of force peaks observed in a single spectrum was three, indicating either that the single helices do not pose an unfolding barrier or that we have obtained an insufficient number of force trajectories. Dynamic AFM measurements have shown that not all transmembrane give rise to unfolding barriers for example Bacteriorhodopsin only shows 3 force peaks for 5 TM-helices [10] and AdiC only 7 force peaks for 12 TM-helices [65] The length of the force peaks suggest that this is due to pair wise unfolding of TM-helices. If the TM-helices of DsbB also unfold pair wise we should only observe 2 force peaks, which are supported by the lack of force spectra with 4 peaks. For three of the systems 5 spectra with a contour length comparable to that of the most frequent unfolding length were overlaid. They all displayed a single unfolding peak suggesting that primarily DsbB unfolds in a cooperative manner. These results does not exclude that more force peaks corresponding to helice pairs can be seen but the data available in this study does not support this. Less than 1 % of the total number of spectra contained spectra with a total length corresponding to that of DsbB. This meant that there were not enough contours to give a meaningful comparison by overlaying force spectra that had a contour of what would be expected for the full length protein. In a similar study on proteoliposomes by Fotiadis et al they recorded more than 400000 force spectra to get ~ 600 spectra they could overlay for pattern recognition. If we compare this to the total of ~8000 spectra that we recorded our work will have to be characterized as an initial study.

5.4.3 Perspectives and future work

This work described the immobilization of an inner Membrane protein to a solid support either solubilized in lipids or the detergent DDM. The sample preparation was standardized and could be routinely performed to a satisfactory degree confirmed by the techniques we had available such as fluorescence, CD and microscopy. The data analysis was also made partly automatic by the development of a program that determined both the protein rupture length and unfolding force. The bottleneck was the accumulation of sufficient amount of data which were suitable for

analysis and secondly the initial sorting of data into force spectra that contained force peaks and those that did not. The latter could be overcome by refining the data analysis program to be able do the initial data screening. The data acquisition could be optimized by creating a macro that would automate the procedure of moving and recalibrating the cantilever to a new point on the surface after a given number of measurements. This would make data acquisition a standalone process greatly increasing the number of force spectra that is feasible to obtain after protein immobilization. It would of great interest to pursue the path of mechanical unfolding of a membrane protein solubilized in detergent for several reasons. One is that one of the limitations of this technique has been the accessibility of pure protein sample material in high concentrations in a lipid suspension. The solubilization of membrane proteins in detergent is a standard procedure that is used in most membrane protein purifications [66-68]. Furthermore this would allow for example the inclusion of the detergent SDS which is known to destabilize proteins [69-72]. A series of experiments could be performed with an increasing concentration of SDS to methodically study the effect the destabilizing effect of SDS on the mechanical stability of DsbB. These results could then be compared to the results previously obtained by circular dichroism and stopped flow fluorescence [60, 73].

ACKNOWLEDGEMENTS

B.S.V. is supported by a pre-doctoral grant co-financed by the Villum Kann Rasmussen Foundation and Aalborg University. D.E.O., O.G.M. and A.C.S. are supported by the Villum Kann Rasmussen Foundation.

6 References

6 REFERENCES

1. Gao, M., M. Wilmanns, and K. Schulten, *Steered molecular dynamics studies of titin I1 domain unfolding.* Biophys J, 2002. **83**(6): p. 3435-45.
2. Rief, M., et al., *Reversible unfolding of individual titin immunoglobulin domains by AFM.* Science, 1997. **276**(5315): p. 1109-12.
3. Erickson, H.P., *Reversible unfolding of fibronectin type III and immunoglobulin domains provides the structural basis for stretch and elasticity of titin and fibronectin.* Proc Natl Acad Sci U S A, 1994. **91**(21): p. 10114-8.
4. Franz, C.M., et al., *Studying integrin-mediated cell adhesion at the single-molecule level using AFM force spectroscopy.* Sci STKE, 2007. **2007**(406): p. pl5.
5. Kedrov, A., et al., *Detecting molecular interactions that stabilize, activate and guide ligand-binding of the sodium/proton antiporter MjNhaP1 from Methanococcus jannaschii.* J Struct Biol, 2007. **159**(2): p. 290-301.
6. Janovjak, H., et al., *Imaging and detecting molecular interactions of single transmembrane proteins.* Neurobiol Aging, 2006. **27**(4): p. 546-61.
7. Bippes, C.A., et al., *Direct measurement of single-molecule visco-elasticity in atomic force microscope force-extension experiments.* Eur Biophys J, 2006. **35**(3): p. 287-92.
8. Puech, P.H., et al., *Measuring cell adhesion forces of primary gastrulating cells from zebrafish using atomic force microscopy.* J Cell Sci, 2005. **118**(Pt 18): p. 4199-206.
9. Janovjak, H., J. Struckmeier, and D.J. Muller, *Hydrodynamic effects in fast AFM single-molecule force measurements.* Eur Biophys J, 2005. **34**(1): p. 91-6.
10. Janovjak, H., et al., *Unfolding pathways of native bacteriorhodopsin depend on temperature.* Embo J, 2003. **22**(19): p. 5220-9.
11. Moller, C., et al., *Determining molecular forces that stabilize human aquaporin-1.* J Struct Biol, 2003. **142**(3): p. 369-78.
12. Scheuring, S., et al., *Sampling the conformational space of membrane protein surfaces with the AFM.* Eur Biophys J, 2002. **31**(3): p. 172-8.
13. Heymann, J.B., et al., *Conformations of the rhodopsin third cytoplasmic loop grafted onto bacteriorhodopsin.* Structure, 2000. **8**(6): p. 643-53.
14. Muller, D.J., W. Baumeister, and A. Engel, *Controlled unzipping of a bacterial surface layer with atomic force microscopy.* Proc Natl Acad Sci U S A, 1999. **96**(23): p. 13170-4.
15. Oesterhelt, F., et al., *Unfolding pathways of individual bacteriorhodopsins.* Science, 2000. **288**(5463): p. 143-6.
16. Muller, D.J., M. Amrein, and A. Engel, *Adsorption of biological molecules to a solid support for scanning probe microscopy.* J Struct Biol, 1997. **119**(2): p. 172-88.
17. Muller, D.J., et al., *Atomic force microscopy of native purple membrane.* Biochim Biophys Acta, 2000. **1460**(1): p. 27-38.

6 References

18. Muller, D.J., et al., *Stability of bacteriorhodopsin alpha-helices and loops analyzed by single-molecule force spectroscopy.* Biophys J, 2002. **83**(6): p. 3578-88.
19. Janshoff, A., et al., *Force Spectroscopy of Molecular Systems-Single Molecule Spectroscopy of Polymers and Biomolecules.* Angew Chem Int Ed Engl, 2000. **39**(18): p. 3212-3237.
20. Kellermayer, M.S., et al., *Folding-unfolding transitions in single titin molecules characterized with laser tweezers.* Science, 1997. **276**(5315): p. 1112-6.
21. **O. Kratky, G.P.**, *Röntgenuntersuchung gelöster Fadenmoleküle.* Rec. Trav. Chim. Pays-Bas, 1949: p. 1106-1123.
22. J. F. Marko, E.D.S., *Stretching DNA.* Macromolecules, 1995: p. 8759.
23. Bustamante, C., et al., *Entropic elasticity of lambda-phage DNA.* Science, 1994. **265**(5178): p. 1599-600.
24. Mueller, F., D.J. Muller, and D. Labudde, *Analysis assistant for single-molecule force spectroscopy data on membrane proteins--MPTV.* Bioinformatics, 2006. **22**(14): p. 1796-9.
25. Kedrov, A., et al., *Examining the dynamic energy landscape of an antiporter upon inhibitor binding.* J Mol Biol, 2008. **375**(5): p. 1258-66.
26. Cisneros, D.A., D. Oesterhelt, and D.J. Muller, *Probing origins of molecular interactions stabilizing the membrane proteins halorhodopsin and bacteriorhodopsin.* Structure, 2005. **13**(2): p. 235-42.
27. Janovjak, H., K.T. Sapra, and D.J. Muller, *Complex stability of single proteins explored by forced unfolding experiments.* Biophys J, 2005. **88**(5): p. L37-9.
28. Carl, P., et al., *Forced unfolding modulated by disulfide bonds in the Ig domains of a cell adhesion molecule.* Proc Natl Acad Sci U S A, 2001. **98**(4): p. 1565-70.
29. Kuhn, M., et al., *Automated alignment and pattern recognition of single-molecule force spectroscopy data.* J Microsc, 2005. **218**(Pt 2): p. 125-32.
30. Marsico, A., et al., *A novel pattern recognition algorithm to classify membrane protein unfolding pathways with high-throughput single-molecule force spectroscopy.* Bioinformatics, 2007. **23**(2): p. e231-6.
31. Kedrov, A., et al., *Controlled unfolding and refolding of a single sodium-proton antiporter using atomic force microscopy.* J Mol Biol, 2004. **340**(5): p. 1143-52.
32. Kessler, M. and H.E. Gaub, *Unfolding barriers in bacteriorhodopsin probed from the cytoplasmic and the extracellular side by AFM.* Structure, 2006. **14**(3): p. 521-7.
33. Salafsky, J., J.T. Groves, and S.G. Boxer, *Architecture and function of membrane proteins in planar supported bilayers: a study with photosynthetic reaction centers.* Biochemistry, 1996. **35**(47): p. 14773-81.
34. Annette Grane´li, †,‡ Jan Rydstro¨m,‡ Bengt Kasemo,† and Fredrik Ho¨o¨k, *Formation of Supported Lipid Bilayer Membranes on SiO2*
from Proteoliposomes Containing Transmembrane
Proteins. Langmuir, 2003: p. 842-850.
35. Klein, D.C., et al., *Covalent immobilization of single proteins on mica for molecular recognition force microscopy.* Chemphyschem, 2003. **4**(12): p. 1367-71.
36. Kimball, R.A., L. Martin, and M.H. Saier, Jr., *Reversing transmembrane electron flow: the DsbD and DsbB protein families.* J Mol Microbiol Biotechnol, 2003. **5**(3): p. 133-49.
37. Grauschopf, U., A. Fritz, and R. Glockshuber, *Mechanism of the electron transfer catalyst DsbB from Escherichia coli.* Embo J, 2003. **22**(14): p. 3503-13.
38. Bader, M., et al., *Reconstitution of a protein disulfide catalytic system.* J. Biol. Chem., 1998. **273**(2048): p. 10302-10307.

6 References

39. Inaba, K., *Protein disulfide bond generation in Escherichia coli DsbB-DsbA.* J Synchrotron Radiat, 2008. **15**(Pt 3): p. 199-201.
40. Inaba, K. and K. Ito, *Structure and mechanisms of the DsbB-DsbA disulfide bond generation machine.* Biochim Biophys Acta, 2008. **1783**(4): p. 520-9.
41. Inaba, K., et al., *Crystal structure of the DsbB-DsbA complex reveals a mechanism of disulfide bond generation.* Cell, 2006. **127**(4): p. 789-801.
42. Kadokura, H., et al., *Roles of a conserved arginine residue of DsbB in linking protein disulfide-bond-formation pathway to the respiratory chain of Escherichia coli.* Proc. Natl. Acad. Sci. U.S.A., 2000. **97**(2380): p. 10884-10889.
43. Kobayashi, T., et al., *Respiratory chain is required to maintain oxidized states of the DsbA-DsbB disulfide bond formation system in aerobically growing Escherichia coli cells.* Proc. Natl. Acad. Sci. U.S.A., 1997. **94**(2373): p. 11857-11862.
44. Otzen, D.E., *Folding of the α-helical membrane proteins DsbB and NhaA*, in *Biophysical Chemistry: Membranes and Proteins*, J. Seddon, Editor. 2002, Royal Society of Chemistry: London. p. 208-214.
45. Jander, G., N.L. Martin, and J. Beckwith, *Two cysteines in each periplasmic domain of the membrane protein DsbB are required for its function in protein disulfide bond formation.* EMBO J., 1994. **13**(3157): p. 5121-5127.
46. Otzen, D.E., *Folding of DsbB in mixed micelles: A kinetic analysis of the stability of a bacterial membrane protein.* J. Mol. Biol., 2003. **330**(3113): p. 641-649.
47. Regeimbal, J. and J.C.A. Bardwell, *DsbB catalyzes disulfide bond formation de novo.* J. Biol. Chem., 2002. **277**(3134): p. 32706-32713.
48. Inaba, K., Y.-H. Takahashi, and K. Ito, *DsbB elicits a red-shift of bound ubiquinone during the catalysis of DsbA oxidation.* J. Biol. Chem., 2004. **279**(3924): p. 6761-6768.
49. Inaba, K. and K. Ito, *Paradoxical redox properties of DsbB and DsbA in the protein disulfide-introducing reaction cascadee.* EMBO J., 2002. **21**(3925): p. 2646-2654.
50. Inaba, K., Y.-H. Takahashi, and K. Ito, *Reactivities of quinone-free DsbB from Escherichia coli.* J. Biol. Chem., 2005. **280**(3926): p. In press.
51. Zhou, Y., et al., *NMR solution structure of the integral membrane enzyme DsbB: functional insights into DsbB-catalyzed disulfide bond formation.* Mol Cell, 2008. **31**(6): p. 896-908.
52. Bader, M., et al., *Oxidative protein folding is driven by the electron transport system.* Cell, 1999. **98**(2): p. 217-27.
53. Bader, M., et al., *Reconstitution of a protein disulfide catalytic system.* J Biol Chem, 1998. **273**(17): p. 10302-7.
54. Pan, J.L., I. Sliskovic, and J.C. Bardwell, *Mutants in DsbB that appear to redirect oxidation through the disulfide isomerization pathway.* J Mol Biol, 2008. **377**(5): p. 1433-42.
55. Tapley, T.L., et al., *Kinetic characterization of the disulfide bond-forming enzyme DsbB.* J Biol Chem, 2007. **282**(14): p. 10263-71.
56. Tan, J., Y. Lu, and J.C. Bardwell, *Mutational analysis of the disulfide catalysts DsbA and DsbB.* J Bacteriol, 2005. **187**(4): p. 1504-10.
57. Bardwell, J.C., et al., *A pathway for disulfide bond formation in vivo.* Proc Natl Acad Sci U S A, 1993. **90**(3): p. 1038-42.
58. Kadokura, H. and J. Beckwith, *Four cysteines of the membrane protein DsbB act in concert to oxidize its substrate DsbA.* Embo J, 2002. **21**(10): p. 2354-63.
59. Malojcic, G., et al., *Preparation and structure of the charge-transfer intermediate of the transmembrane redox catalyst DsbB.* FEBS Lett, 2008. **582**(23-24): p. 3301-7.

6 References

60. Otzen, D.E., *Folding of DsbB in mixed micelles: a kinetic analysis of the stability of a bacterial membrane protein.* J Mol Biol, 2003. **330**(4): p. 641-9.
61. Knol, J., et al., *Unidirectional reconstitution into detergent-destabilized liposomes of the purified lactose transport system of Streptococcus thermophilus.* J Biol Chem, 1996. **271**(26): p. 15358-66.
62. Vallieres, K., et al., *AFM imaging of immobilized fibronectin: does the surface conjugation scheme affect the protein orientation/conformation?* Langmuir, 2007. **23**(19): p. 9745-51.
63. Bergkvist, M., J. Carlsson, and S. Oscarsson, *Surface-dependent conformations of human plasma fibronectin adsorbed to silica, mica, and hydrophobic surfaces, studied with use of Atomic Force Microscopy.* J Biomed Mater Res A, 2003. **64**(2): p. 349-56.
64. Koutsopoulos, S., et al., *Adsorption of trypsin on hydrophilic and hydrophobic surfaces.* Langmuir, 2007. **23**(4): p. 2000-6.
65. Bosshart, C., Frederix, Ratera, Bippes, Muller, Palacin, Engel and Fotiadis, *High-throughput single-molecule force spectroscopy for membrane proteins.* Nanotechnology, 2008.
66. Carpenter, E.P., et al., *Overcoming the challenges of membrane protein crystallography.* Curr Opin Struct Biol, 2008. **18**(5): p. 581-6.
67. Chiu, M.L., et al., *Over-expression, solubilization, and purification of G protein-coupled receptors for structural biology.* Comb Chem High Throughput Screen, 2008. **11**(6): p. 439-62.
68. Everberg, H., N. Gustavasson, and F. Tjerned, *Enrichment of membrane proteins by partitioning in detergent/polymer aqueous two-phase systems.* Methods Mol Biol, 2008. **424**: p. 403-12.
69. Andersen, K.K., P. Westh, and D.E. Otzen, *Global study of myoglobin-surfactant interactions.* Langmuir, 2008. **24**(2): p. 399-407.
70. Otzen, D.E., et al., *Aggregation of S6 in a quasi-native state by sub-micellar SDS.* Biochim Biophys Acta, 2008. **1784**(2): p. 400-14.
71. Hansen, J.H., et al., *Stable intermediates determine proteins' primary unfolding sites in the presence of surfactants.* Biopolymers, 2009. **91**(3): p. 221-31.
72. Otzen, D.E., P. Sehgal, and P. Westh, *Alpha-Lactalbumin is unfolded by all classes of surfactants but by different mechanisms.* J Colloid Interface Sci, 2009. **329**(2): p. 273-83.
73. Sehgal, P. and D.E. Otzen, *Thermodynamics of unfolding of an integral membrane protein in mixed micelles.* Protein Sci, 2006. **15**(4): p. 890-9.

Paper I: Kinetic partitioning between aggregation and vesicle permeabilization by modified Adan

Co-author statement for Paper 1

Brian Vad., Line Aagot Thomsen, Jan Mondrup Pedersen, Kresten Bertelsen, Thomas Vosegaard, Zuzana Valnickova, Magnus Franzmann, Reinhard Wimmer, Troels Skrydstrup, Jan J. Enghild, Niels Chr. Nielsen, Daniel Otzen .: **Divorcing Folding from Function: How Acylation Affects the Membrane-perturbing Properties of an Anti-microbial Peptide**

. *To be submitted*.

- Brian Vad performed all liposome calcein release work, Stopped flow fluorescence, Confocal Laser microscopy, Circular dichroism, fluorescence anisotropy measurements and wrote the bulk of the article
- Kresten Bertelsen performed, described and discussed the Solid state NMR experiments under supervision of Thomas Vosegaard and Niels Chr. Nielsen.
- Line Aagot Thomsen did preliminary purification and characterization of Novicidin.
- Magnus Franzmann did the solution state NMR under the supervision of Reinhard Wimmer.
- Jan Mondrup Pedersen performed the peptide synthesis under the supervision of Troels Skrydstrup.
- Zuzana Valnickova performed the β-galactosidase assay under the supervision of Jan Enghild.
- Niels Nielsen contributed to the interpretation of NMR data and writing of the article.
- Daniel Otzen supervised overall design and execution of the experiments, contributed extensively to the writing of the article and submitted the article..

Jan Mondrup Pedersen _____ 6th of april 2009

Line Aagot Thomsen _____ 6th of april 2009

Kresten Bertelsen _____ 6th of april 2009

Thomas Vosegaard _____ 6th of april 2009

Zuzana Valnickova _____ 6th of april 2009

Magnus Franzmann _____ 30th March 2009

Reinhard Wimmer  6th of april 2009

Jan J. Enghild 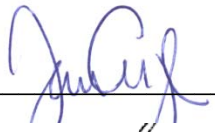 6th of april 2009

Niels Chr. Nielsen  6th of april 2009

Daniel Otzen 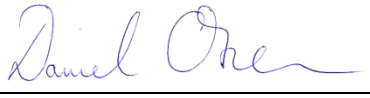 26th March 2009

Brian Stougaard Vad _____ 6th of april 2009

Signature Date

Biochimica et Biophysica Acta 1794 (2009) 84–93

Contents lists available at ScienceDirect

Biochimica et Biophysica Acta

journal homepage: www.elsevier.com/locate/bbapap

Kinetic partitioning between aggregation and vesicle permeabilization by modified ADan

Lise Nesgaard [a], Brian Vad [a,b], Gunna Christiansen [c], Daniel Otzen [a,b,*]

[a] Department of Life Sciences, Aalborg University, Sohngaardsholmsvej 49, DK-9000 Aalborg, Denmark
[b] Interdisciplinary Nanoscience Centre, Department of Molecular Biology, University of Aarhus, Gustav Wieds Vej 10C, DK-8000 Aarhus C, Denmark
[c] Institute of Medical Microbiology and Immunology, The Bartholin Building, University of Aarhus, DK-8000 Aarhus C, Denmark

ARTICLE INFO

Article history:
Received 18 June 2008
Received in revised form 19 September 2008
Accepted 28 September 2008
Available online 15 October 2008

Keywords:
Familial Danish Dementia
Non-amyloid aggregate
β-sheet structure
Oligomer
Vesicle permeabilization

ABSTRACT

The neurodegenerative illness Familial Danish Dementia (FDD) is linked to formation and aggregation of the 34-residue ADan peptide, whose cytotoxicity may be mediated by membrane interactions. Here we characterize the derived peptide SerADan, in which the two cysteines found in ADan have been changed to serines to emulate the reduced peptide. SerADan aggregates rapidly at pH 5.0 and 7.5 in a series of conformational transitions to form β-sheet rich fibril-like structures, which nevertheless do not bind amyloid-specific dyes, probably due to the absence of organized β-sheet contacts. Aggregation is prevented at neutral/acidic pH and low ionic strength by anionic lipid vesicles. These vesicles are permeabilized by monomeric SerADan assembling on the membrane to form stable β-sheet structures which are different from the solution aggregates. In contrast, solution ageing of SerADan first reduces and then abolishes permeabilization properties. The competition between lipid binding and aggregation may reflect bifurcating pathways for the ADan peptide *in vivo* between accumulation of inert aggregates and formation of cytotoxic permeabilizing species. Our work demonstrates that non-fibrillar aggregates can assemble in a series of steps to form a hierarchy of higher-order assemblies, where rapid formation of stable local β-sheet structure may prevent rearrangement to amyloid proper.

1. Introduction

Familial Danish Dementia, first described in 1970 [1] as *heredopathia ophthalmo-oto-encephalica*, is an example of a degenerating neurofibrillar disease of the same type as the more common and better characterized Alzheimer's disease (AD) [2]. The illness involves progressive dementia and is fatal with death occurring at the age of 50–60. The earliest clinical manifestation is cataract formation before the age of thirty followed by progressive hearing loss and cerebellar ataxia. A 34-amino acid peptide, ADan, has been identified in circulation and in plaques in post-mortem tissue samples [2]. In contrast to the Aβ aggregates formed in AD, these plaques appear to be predominantly pre-amyloid in nature with amorphous morphology containing sparse and disperse fibrils, and are negative for staining with the amyloid-specific dyes Congo red and thioflavin S [3]. The ADan peptide is formed due to a decamer duplication in the 3′-end of the *Bri* gene causing a frameshift and generating a larger-than-normal precursor protein [2]. C-terminal degradation of the precursor by furin yields the 34-amino acid ADan peptide rather than the native 23-amino acid Bri peptide [4] (Fig. 1). Both wild-type Bri and mutant ADan peptide circulate in plasma, but only ADan has been found to accumulate in tissue [5]. The oxidation state of the two cysteines in serum-circulating and plaque-deposited ADan is controversial, with some groups claiming it to be reduced [6] and others oxidized between Cys5 and Cys22 [7]. The deposited form of the peptide is highly heterogeneous [7], with the N-terminal glutamate modified to pyroglutamate in a large percentage of the peptide chains, which are also N- and C-terminally processed at position 3, 28 and 33.

Previous studies of the aggregational tendencies of ADan in both the reduced and oxidized forms [8,9] did not observe classical fibril-formation of the type routinely observed for Aβ and similar fibrillation protein peptides under physiological conditions. Formation of amyloid-like material was only possible for the oxidized form of ADan under mildly acidic conditions (pH 4.8) and after extensive ageing (10–15 days). At other experimental condition, including a wide range of pH values and peptide concentrations, oxidized and reduced ADan were found to readily aggregate into various amorphous structures. However, studies using SH-SY5Y or neuro2a cell lines showed that the reduced form of ADan had higher cytotoxicity than the oxidized form and led to marked caspase activation [8]. The distinct prevalence of pre-amyloid over amyloid deposits makes ADan an interesting case

Abbreviations: AD, Alzheimer's Disease; DLS, Dynamic light scattering; DOPC, 1,2-Dioleoyl-*sn*-glycero-3-phosphocoline; DOPG, 1,2-Dioleoyl-*sn*-glycero-3-[phospho-*rac*-(1-glycerol)]; FDD, Familial Danish Dementia; IAPP, Islet Amyloid Polypeptide

* Corresponding author. Interdisciplinary Nanoscience Centre, Department of Molecular Biology, University of Aarhus, Gustav Wieds Vej 10C, DK-8000 Aarhus C, Denmark. Tel.: +45 89 42 50 46; fax: +45 98 12 31 78.
E-mail address: dao@inano.dk (D. Otzen).

1570-9639/$ – see front matter © 2008 Elsevier B.V. All rights reserved.
doi:10.1016/j.bbapap.2008.09.021

```
wtBri     EASNCFAIRHFENKFAVETLICS
ADan    pEASNCFAIRHFENKFAVETLICFNLFLNSQEKHY
SerADan   EASNSFAIRHFENKWAVETLISFNLFLNSQEKHY
          #   *          ¤       *------------
```

Fig. 1. Primary structure of wildtype Bri (wtBri), ADan and SerADan peptides. #: Location of pyroglutamate found in physiological aggregates of ADan peptide. *: Mutation of cysteine to serine. ¤: Mutation of phenylalanine to tryptophane. -: Elongation found in physiological aggregates of ADan peptide.

study, that may provide further insight into the nature of aggregate cytotoxicity. Here we examine the aggregational properties of a modified ADan-like peptide, termed SerADan, designed to prevent any oxidation by replacing Cys5 and Cys22 with Ser. Besides mimicking the reduced state which has been shown to be more neurotoxic than the oxidized state in cell cultures [8], it also avoids the formation of covalent crosslinks that complicate *in vitro* studies of ADan. Additionally, the phenylalanine in position 14 was replaced with the fluorescent probe tryptophan, which may also be considered a conservative mutation. To address charge effects, the peptide was investigated at both the approximately neutral pH-value 7.5 and the slightly acidic pH 5.0, which is similar to the pH-value at which the oxidized variant form amyloid-like structures. These two pH values are on either side of the estimated isoelectric point of pH 6.05.

In order to elucidate the possible mechanism of cytotoxicity, we investigated the direct interaction of SerADan with lipid membranes. Several fibrillation-prone peptides are known to interact with anionic lipid membranes but with different outcomes. Anionic membranes stimulate fibrillation of Islet Amyloid Polypeptide (IAPP) [10,11], while $A\beta_{40}$ is protected from fibrillation when fully inserted in anionic membranes but experiences accelerated fibrillation when surface bound [12]. Interestingly, zwitterionic lipids may also reverse fibrillation of amyloid and lead to cytotoxic species [13]. The anionic lipid phosphatidylserine has been shown to trigger fibril formation for a number of peptides and proteins including lysozyme, insulin and transthyretin [14]. In contrast, annular structures that exhibit heterogeneous single-channel conductance have been observed for ADan bound to zwitterionic phosphatidylcholine membranes in a manner highly similar to those of other fibrillation-prone peptides *e.g.* α-synuclein and Aβ [15]. We consequently examined peptide-membrane interactions using fluorescence spectroscopy and calcein release assays for vesicles of anionic and zwitterionic phospholipids.

2. Materials and methods

2.1. Materials

SerBri (EASNSFAIRH FENKWAVETL ISS) and SerADan (EASNSFAIRH FENKWAVETL ISFNLFLNSQ EKHY, in which Cys5 and Cys22 found in ADan are replaced by Ser) peptides were obtained >90% pure (EZBiolab Inc., Westfield, IN, USA). 1,2-Dioleoyl-*sn*-glycero-3-phosphocoline (DOPC) and 1,2-Dioleoyl-*sn*-glycero-3-[phospho-*rac*-(1-glycerol)] (DOPG) were from Avanti Polar Lipids (Alabaster, AL). Thioflavin T and other chemicals were from Sigma (Sigma-Aldrich, St. Louis, MO).

2.2. Preparation of SerADan samples

Freeze-dried SerADan peptide was dissolved in 10 M urea and allowed to disaggregate overnight at room temperature to obtain a monodisperse monomeric population in the random coil conformation according to circular dichroism. Concentration was monitored by absorbance at 280 nm (extinction coefficient estimate obtained using the ProtParam tool at http://www.expasy.org) and found to be within 5% of the weighed amount. Stock concentration was adjusted to 2.5 mM. Stock aliquots were flash frozen and stored at −80 °C. They were thawed and centrifuged immediately before use. Samples for aggregation were prepared by freshly thawed peptide stock to the appropriate concentration (10–75 μM) in either 50 mM sodium acetate (pH 5.0) or 50 mM Tris (pH 7.5) with or without 100 mM NaCl.

2.3. Preparation of liposomes and calcein release assay

Vesicles were prepared from stock solutions of lipids dissolved in chloroform and dried overnight in vacuum. Lipids were then resuspended by vortexing in milliQ water to a final concentration of 10 g/L (~14 mM), exposed to at least seven cycles of freezing in liquid nitrogen, followed by thawing in a 50 °C water bath, before extrusion through a 100 nm pore filter 12 times using a 10 mL thermo barrel extruder (Northern Lipids, Vancouver, Canada). Vesicle size was verified by DLS and vesicles were used the same day they were made.

Calcein-containing vesicles, which were made immediately before each experiment, were prepared similarly, except that lipid was dispersed in 1.5 mL calcein-containing buffer (70 mM calcein, 50 mM Tris, pH 7.5) prior to freeze–thawing and extrusion. Vesicles were isolated from the calcein buffer by filtration through a pre-equilibrated Pharmacia PD-10 column and small aliquots of the collected fractions were monitored by fluorescence (excitation 490 nm, emission 500–600 nm) using Triton X-100 to obtain release of calcein and thereby increased fluorescence of vesicle-containing fraction(s). Those with the highest signal-to-background ratio were selected for further use. The fluorescence measurements were conducted on a Cary Eclipse Fluorescence Spectrophotometer (Varian, Palo Alto, CA) using a 10 mm quartz cuvette with magnetic stirring. The vesicles were diluted in 50 mM Tris buffer pH 7.5 to a concentration of ~0.017 mg/mL (21 μM), yielding a maximum signal of around 90 U under these settings. For ageing experiments, SerADan was diluted from a 2.5 mM stock in 10 M urea to 10 μM peptide and 0.04 M urea in 50 mM Tris buffer pH 7.5. At different time points, 10 μL of this solution was diluted 10-fold to 1 μM SerADan in the presence of 21 μM calcein-filled vesicles and calcein release was monitored by measuring fluorescence emission intensity at 515 nm (excitation at 490 nm, 5 nm slits for both monochromators) every 11 s until it reached a plateau. Spectra were normalized with regards to maximum fluorescence, *i.e.* the fluorescence level achieved when 1% of Triton X-100 is added. For permeabilization experiments with different concentrations of SerADan, the peptide was first diluted from 2.5 mM stock in urea to 50 μM peptide and immediately diluted to the appropriate concentration in the presence of 21 μM calcein vesicles.

2.4. Circular dichroism

Circular dichroism (CD) spectra were recorded on a Jasco J-810 spectropolarimeter (Jasco, Hachioji, Tokyo, Japan; 110QS cuvette, Hellma, Müllheim, Germany) using averaging over 10 scans, resolution 0.1 nm and 10–50 μM peptide.

2.5. Fourier transform infrared spectroscopy

Spectra were recorded on a Bruker Tensor 27 infrared spectrometer (Bruker Optik GmbH, Ettlingen, Germany) with a Specac Golden Gate single-reflection ATR unit (Specac Ltd., Orpington, UK). Aged aggregates were washed twice in milliQ water and isolated by centrifugation. Three independent samples were investigated (64 scans, 2 cm^{-1} resolution). The secondary structure was estimated using OPUS 5.5. If needed, the presence of water vapor was corrected for by subtraction of a fresh vapor spectrum or the inbuilt atmospheric compensation function. Peaks were assigned from the 2nd derivative and deconvolution of spectra [16]. The non-deconvoluted spectra were fitted using the Levenberg–Maquardt method, the areas of individual peaks calculated and the secondary structure content estimated.

2.6. Fluorescence spectroscopy

Time-resolved fluorescence spectroscopy was performed on a Cary Eclipse fluorometer (Varian, Palo Alto, CA), excitation at 290 nm and emission measured at 350 nm. Freshly thawed peptide stock was diluted to 10–50 μM in buffer with or without lipid (LP 0.1–10). Aggregation was monitored for 30 min in 10 s increments and for the following 600–1200 min in 1 min increments. Initial reaction rates were calculated by linear regression as the slope of the timecurve over the initial 10 min. Emission spectra were obtained at start and at end points before and after vigorous agitation of the sample to resuspend sediments. Time resolved emission spectra were recorded similarly on a LS55 fluorometer (Perkin-Elmer, Wellesley, MA), excitation at 290 nm, emission 310 nm–390 nm.

2.7. Dynamic light scattering

Time-resolved estimates of the hydrodynamic radius were obtained by dynamic light scattering on a PDDLS/CoolBatch+90T system (Precision Detectors, Bellingham, MA). Buffers were filtrated to remove dust particles. Samples were prepared by dilution of freshly thawed and centrifuged peptide stock into buffer (50 μM peptide, 50 mM Tris, pH 7.5) with or without freshly prepared and centrifuged lipid vesicles (LP 0.1–10). Temperature was held at 22.5 °C and R_{hyd} estimates were obtained every 2–3 min.

2.8. Electron microscopy

Electron microscopy was performed as described [17] by placing 5 μL aliquots on 400-mesh carbon-coated, glow-discharged grids for 30 s followed by washing with distilled water and staining with phosphotungstic acid (pH 6.8). Samples were visualized using a Jeol 1010 transmission electron microscope. For time-based electron microscopy on the hour timescale, aliquots were removed directly from the aging sample. For longer experimental periods, the aliquots were flash-frozen in liquid nitrogen and stored at −80 °C.

3. Results

3.1. SerADan is sparsely soluble and quickly forms β-rich but non-amyloid aggregates

The serine-variant of the short non-toxic wildtype Bri peptide (SerBri) readily dissolves in dilute buffer to adopt a predominantly random coil-like structure when examined with circular dichroism (data not shown). In contrast, the longer SerADan peptide forms large, insoluble aggregates when diluted from 10 M urea to 0.2 M urea at pH 5.0 (Fig. 2) and 7.5 (Fig. 3) as shown by time-resolved electron microscopy. The aggregates can be observed within minutes of dilution (Figs. 2A–B, 3A) and have μm-scale dimensions, consisting of thin filaments that persist over the entire visualized time-span of 5 days (Figs. 2D, 3C, E). At pH 5.0, a more electron-dense and less organized morphology can be observed for samples obtained 19 min after dilution, but not for later time points. Smaller, transient amorphous structures were also present during the first hour of aggregation (Fig. 3B, shown for pH 7.5 only) but slowly disappeared. When studied by attenuated total reflection infrared spectroscopy (ATR-FTIR, Fig. 4A) the secondary structure of aged (12 h) and washed samples, which are structurally stable over a period of several days, appear rich in β-sheet with similar sheet content for pH 5.0 and 7.5 (34–36%). Circular dichroism spectra (Fig. 4B) show that β-structure with a characteristic minimum around 215 nm appears within a few minutes of dilution from the stock solution (within the dead-time of the measurement), suggesting that the peptide rapidly collapses into a β-rich structure in solution. Over time, the spectra diminish in intensity, particularly within the first 100 min of incubation (insert to Fig. 4B), but retain the overall β-sheet appearance. At pH 7.5 there is a lag phase of around 30 min before the ellipticity starts to decline, while the lag phase is absent at pH 5.0.

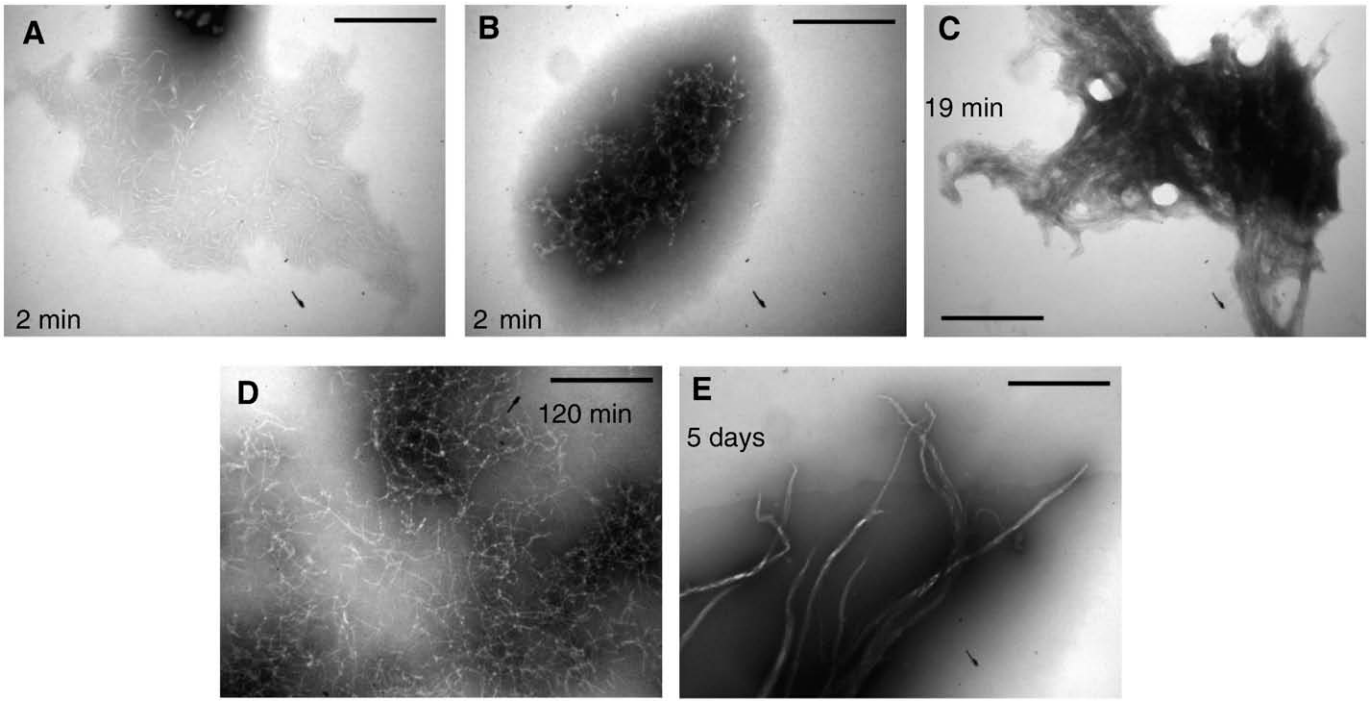

Fig. 2. Time-resolved electron micrographs of 50 μM SerADan at pH 5.0. Black bar corresponds to 400 μm. (A) Thin filaments observed within the method deadtime (2–3 min). (B) Same sample as A. but showing a more electron-dense morphology. (C) Sample obtained after 19 min showing dense, less organized morphology, which coexisted with the type of structures shown in B. (D) Sample obtained after 2 h and frozen for later imaging. Morphology consists of long, thin filaments. (E) Sample obtained and frozen after 5 days aging. The shown morphology coexists with thin filaments.

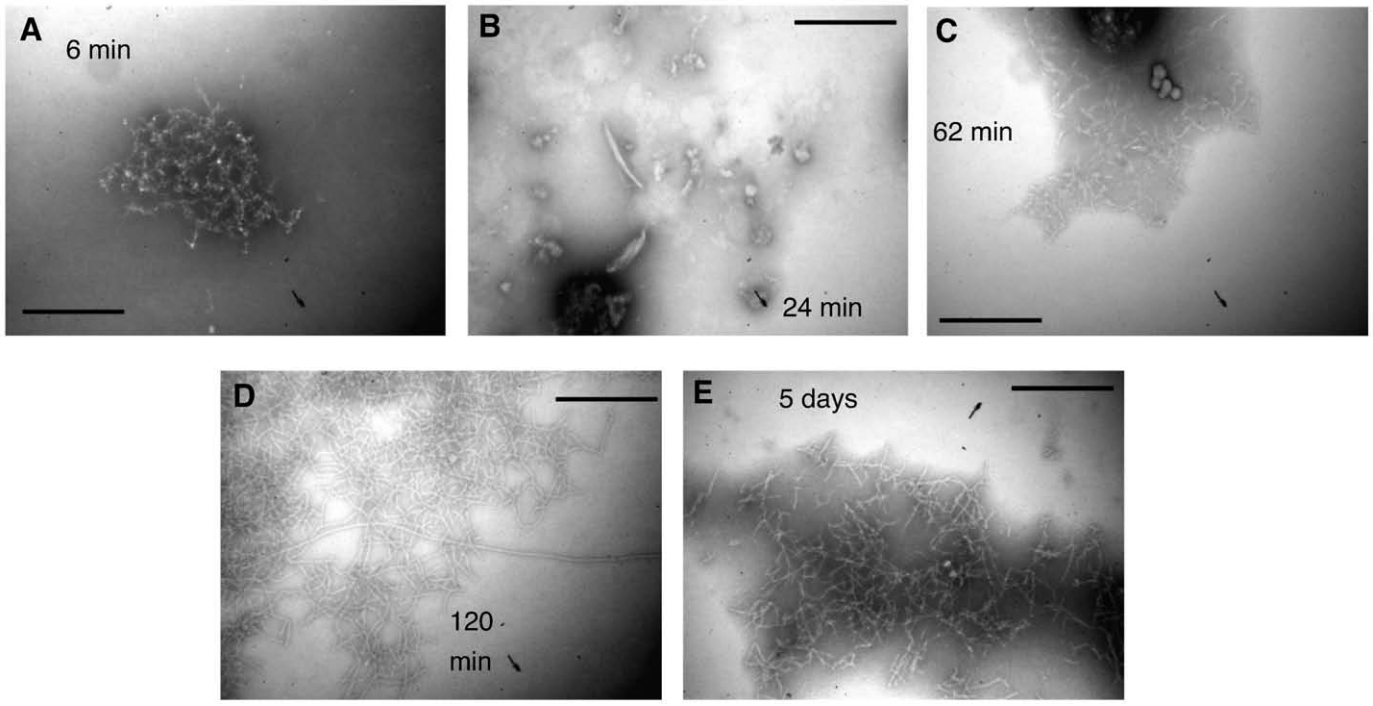

Fig. 3. Time-resolved electron micrographs of 50 μM SerADan at pH 7.5. Black bar corresponds to 400 μm. (A) Morphology after 6 min. (B) Amorphous structures observed after 24 min. Structures coexistent with structure of the type shown in A. (C) Sample obtained after 62 min contains filaments and amorphous elements. (D) Long, thin filaments of clear morphology obtained after 2 h and frozen for later imaging. (E) Sample obtained and frozen after 5 days aging. Thin filaments persist as dominating structure.

The fibril-like structure and β-sheet signature are amyloid hallmarks. However, no binding of Congo Red or Thioflavin T can be observed (data not shown), just as reported for wildtype ADan deposits [2,3]. This indicates a different arrangement of the β-structure within the observed filaments. Our previous X-ray fiber diffraction data show a strong signal at 4.76 Å arising from the distance between adjacent β-strands [18]. However, signals at 10–11 Å (which are strong in regular amyloid fibrils and reflect inter-sheet distances) are essentially absent for pH 7.5 aggregates and very diffuse for the pH 5.0 aggregates [18], indicating a lack of organized higher-order structure.

3.2. Time-resolved fluorescence data shows two distinct phases

The images obtained by EM show that the aggregates form within a very short time span of a few minutes. The Phe11Trp substitution provides a fluorescent probe to follow the time course of the aggregate formation (Fig. 5A).

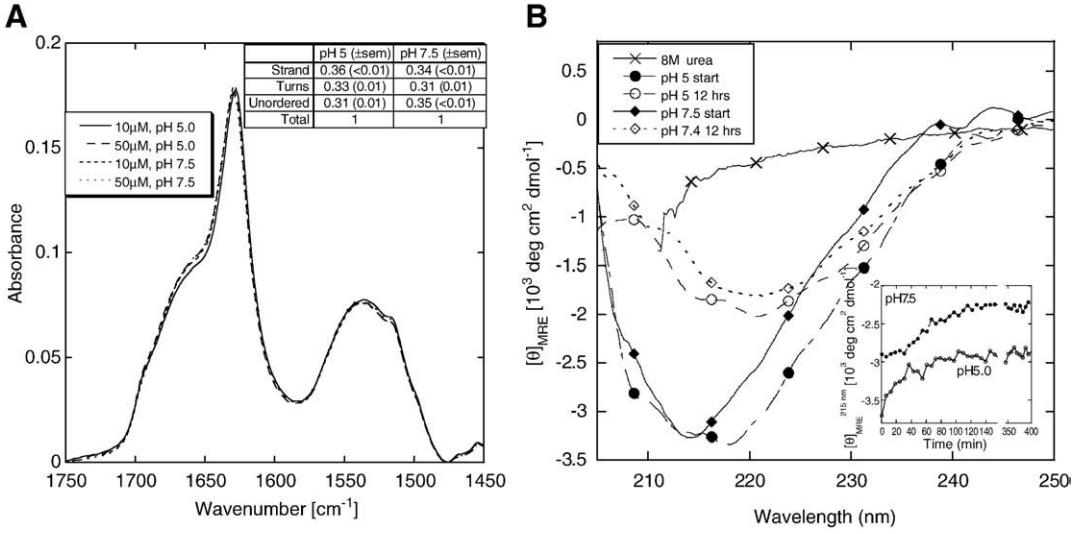

Fig. 4. Secondary structure of aggregated SerADan. (A) Fourier transform infrared spectroscopy of 10 and 50 μM SerADan at pH 5.0 and 7.5, aged for 12 h at 10 and 50 μM peptide. The aggregates were washed in water and found to be stable over several days. The secondary structure appears independent of pH and concentration. Table: Estimate of secondary structure content by curve fitting. (B) CD spectra of 50 μM SerADan in 10 M urea (no buffer) and at pH 5.0 and 7.5 after 50-fold dilution into 0.2 M urea. Immediately after dilution, there is a clear minimum around 215–220 nm, indicative of β-sheet structure. The spectra reduce in intensity over the next 12 h but retain minimum around 215–220 nm. Insert: change in molar ellipticity at 215 nm over time when 50 μM SerADan is diluted into 0.2 M urea from 10 M urea, indicating that most of the ellipticity change occurs over the first 100 min. Ellipticity levels for the two runs have been offset for clarity. Note the lag phase at pH 7.5 which is absent at pH 5.0.

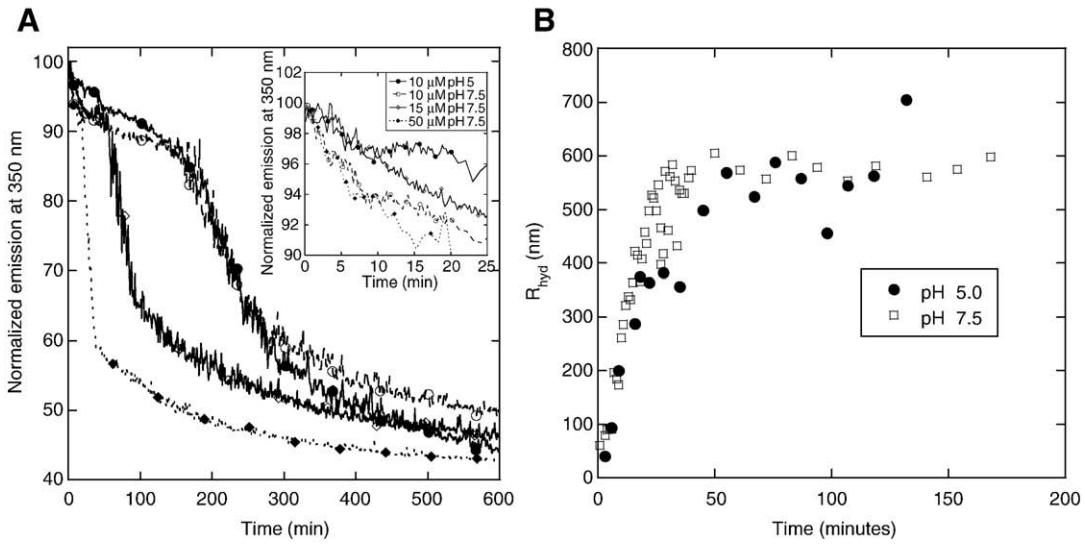

Fig. 5. Aggregation behavior of SerADan at pH 7.5 and 22.5 °C. (A) Time-resolved intrinsic fluorescence (excitation 290 nm, emission 350 nm) at 10 μM, 15 μM and 50 μM, respectively. An exponential decline of ~5–7% is followed by a linear decline of ~5%, a steep drop of ~30% and a slower decline of ~20%. Insert shows a blow-up of the first 25 min of the reaction. (B) Dynamic light scattering data for 50 μM SerADan at pH 5.0 and 7.5 followed over time. Note the immediate increase in particle size in contrast to the lag observed by CD and fluorescence.

When 10–50 μM SerADan is incubated at pH 7.5 and 22.5 °C and the fluorescence emission was monitored over time, we observe a rapid and only slightly concentration-dependent ~5–7% decline in the signal over the first 5–10 min, followed by a ~5% linear decline (~5%). After an additional 10–100 min (depending on concentration), there is a very steep decline over 10–100 min in emission down to ~60% of the initial fluorescence intensity, which slowly declines further by ~20% over the next 6–9 h. Incubation at pH 5.0 also leads to a similar 20% decline in signal although the change is somewhat slower (Fig. 5A, insert). In conjunction with the differences in the time-profile for the CD signal between pH 5.0 and 7.5 (Fig. 4B), this suggests subtle differences in the initial conformational changes at these two pH values. The rapid fluorescence phase completed within 5–10 min at pH 7.5 coincides with the formation of β-sheet structure within the dead-time of the recording of the first CD spectrum (Fig. 4B). The subsequent 5% signal change occurs over the next ~100 min at 10 μM peptide, and the rate of the linear decline (raw fluorescence emission intensity per time unit) scales with protein concentration with a slope of 1 in a log–log plot, indicating that this step does not involve a change in the molecularity of the SerADan aggregate formed at this stage (data not shown). However, the length of this phase (ending at the onset of the steep fluorescence decline) is shortened dramatically at 50 μM to around 15 min, indicating that the next step involves aggregation. In fact we have two observations that indicate that the large decline in emission to around 60% is simply caused by bulk sedimentation of aggregated material. Firstly, there is no decline if the experiment is performed with agitation, which prevents sedimentation (data not shown). Secondly, resuspension of the aggregates returns fluorescence to the plateau value reached after the first 20% decline in signal (data not shown).

Emission spectra recorded at different times at both pH-values reveals that change in fluorescence signal within the initial exponential phase and slow linear decline (prior to the sedimentation step) is due to changes in fluorescence intensity rather than a major shift in maximum emission wavelength, since we only observe a slight blue-shift from ~353 nm to ~350 nm (data not shown).

The rapid fluorescence decline to a 60% level (completed after 20 min at a concentration of 50 μM SerADan) is complemented by DLS data for 50 μM SerADan at both pH 5.0 and 7.5 which show an increase in particle size to a plateau level within 20–30 min (Fig. 5B). During this period there is no change in the CD signal at 50 μm SerADan (Fig. 4B insert). Rather, the slow decline in CD signal seen for 50 μM SerADan (Fig. 4B insert) coincides with the slower decay over several hundreds of seconds from ~60 to ~40% intensity after the rapid fluorescence decline. Thus there appears to be several phases in the sedimentation process, of which only the last one is detected by CD. As a reporter of tertiary and quaternary structure, Trp fluorescence is a more sensitive reporter of protein changes than CD signal and it is therefore not unexpected that more phases are revealed by the former method.

Early onset of formation of large aggregates and thereby sedimentation can also be triggered by addition of seeds of preformed aggregates, which is a well-known characteristic of batch fibrillation *in vitro*. Thus, addition of 1.5% seeds reduces the sedimentation half-time from around 200 to around 120 min, while 15% seeds have little further effect (data not shown).

3.3. SerADan interacts with the anionic lipid DOPG

Wildtype ADan is cytotoxic to the commonly used SH-SY5Y neuronal cell line [8,9] in both oligomeric and more extensively aggregated forms. The known interaction between cytotoxic peptides and cell membranes prompted us to study the membrane interactions of the SerADan peptide. Fibrillation of numerous proteins has previously been shown to be stimulated by the presence of anionic lipids [10–12,14] so we investigated the effect on aggregation by both the zwitterionic DOPC and anionic DOPG. While little interaction was observed with DOPC at both pH values (data not shown), DOPG interacted strongly with freshly diluted peptide. The presence of anionic lipid prevented the sedimentation of large aggregates (Fig. 6A). This effect was pronounced at even 1:10 lipid:protein ratios at pH 7.5 while 10:1 lipid:protein ratios were required at pH 5.0 (data not shown). For pH 7.5, the anti-sedimentation effect was abolished for all but the highest lipid concentration (LP 10) by the presence of 100 mM NaCl, indicating electrostatic forces as an important factor in the interaction. However, the lone tryptophan also appears involved in the interaction as the peptide fluorescence spectrum shows a clear blueshift from ~353 nm to ~340 nm when incubated with lipid (Fig. 6B insert). In contrast, the far-UV CD spectrum has a minimum around 210 nm (Fig. 6B) which is different from and more intense than that in the absence of lipid (Fig. 4B). Furthermore, it does not undergo any significant band shifts or intensity changes over time. Interestingly, the small pre-sedimentation exponential decay in emission (within the first 20 min, Fig. 5A) is not affected by lipids, suggesting

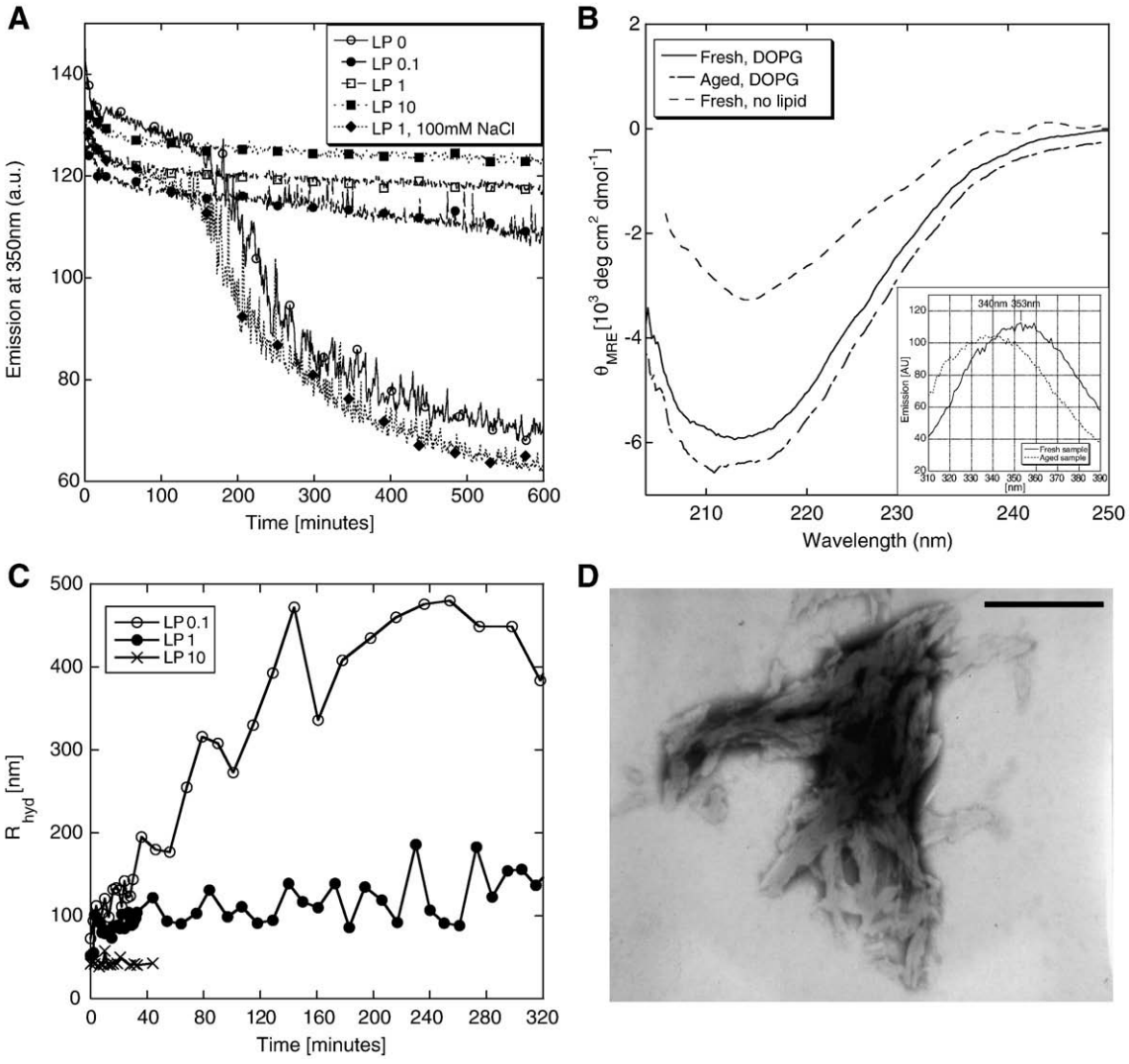

Fig. 6. Spectroscopic and microscopic investigations of SerADan lipid interactions at pH 7.5 and 22.5 °C. (A) The effect of anionic lipid (DOPG) at high and low ionic strength on the change in fluorescence signal (excitation 290 nm, emission 350 nm) of 10 μM SerADan over time. The presence of lipids prevents sedimentation but the effect is abolished by the presence of 100 mM NaCl at lipid-to-protein ratios (LP) of 1 and below. (B) CD spectra for fresh (immediately after dilution from stock in 10 M urea) and aged (12 h after dilution) SerADan (10 μM) in the presence of DOPG, LP 10 at pH 7.5 (no NaCl). Fresh spectrum in absence of DOPG (from Fig. 4B) included for comparison. Insert: Emission spectra showing significant blue-shifting. (C) Time-resolved DLS of 10 μM SerADan showing inhibition of aggregation at LP 1 and 10. (D) Electron micrograph of 50 μM SerADan with DOPG (LP 10) at pH 7.5 after 5 days aging. Black bar corresponds to 400 μm. The previously observed thin filaments are absent in favour of amorphous material.

that this conformational change is a prerequisite for lipid binding or can occur on the lipid surface.

When examined at pH 7.5 by DLS, the formation of large species is highly dependent on the presence of lipids (Fig. 6C). As described previously the formation of large species is fast in the absence of lipids, while the presence of small amounts (LP 0.1) slows the formation of large species considerably. At higher lipid concentrations, the formation of large species is negligible within the observed time window. Electron microscopy of samples aged for 16 h or 6 days did not show straight fibril-like structures but rather small amounts of wool-like morphologies (Fig. 6D), suggesting mixed, amorphous lipid/peptide material. This suggests that the presence of anionic lipid prevents the formation of fibril-like aggregates instead of just preventing their sedimentation.

3.4. SerADan affects release of calcein from vesicles in competition with ageing

To investigate more closely the interactions of SerADan with lipids, we studied the ability of the peptide to release calcein from different vesicles. In this assay, calcein is initially trapped in vesicles at self-quenching concentrations and subsequent release of calcein leads to a large rise in fluorescence which for SerADan follows an approximately exponential time course (Fig. 7A). This permeabilization ability towards DOPG vesicles is maintained at peptide:lipid molar concentrations down to 1:500 (Fig. 7B). SerADan's ability to release calcein is highly dependent on its age. While SerADan freshly diluted from a stock in 10 M urea is able to affect release of almost 60% of all trapped calcein from 21 μM DOPG vesicles, this figure drops precipitously to around 30% within 15 min of ageing (Fig. 7C), and subsequently remains at a plateau until it drops further after around 3 h of ageing (corresponding to the onset of precipitation seen in Fig. 5A). Over the same 15 min ageing time range, the rate constant at which calcein release occurs (approximated by a first order fitting to the release data) drops by around a factor of 10, after which it remains at a very low value. The ability to release calcein is also sensitive to vesicle type. SerADan diluted from a stock in 10 M urea and aged for about 10 min is able to effect only release of around 31% of the trapped calcein from pure DOPG vesicles (Fig. 7A) over a period of about an hour, and the figure

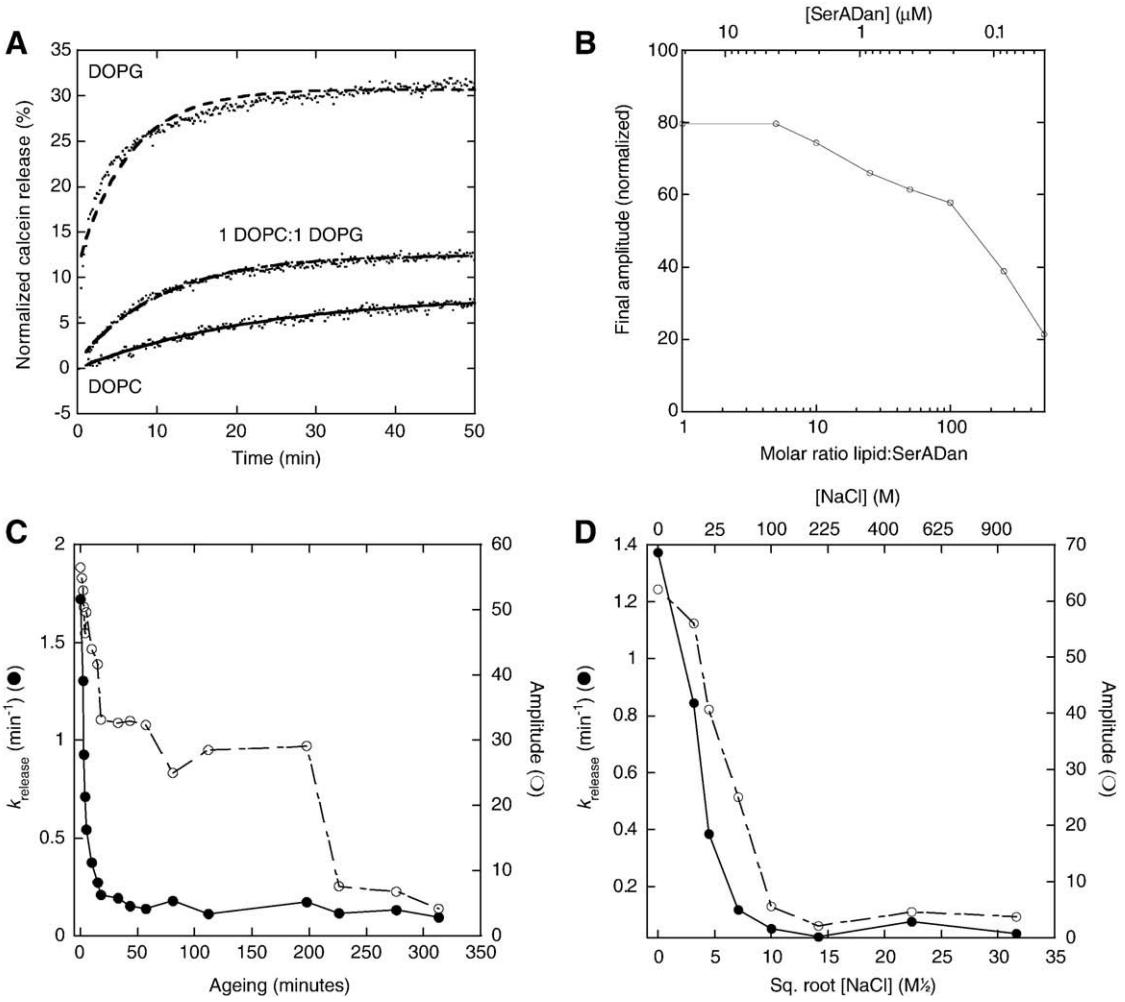

Fig. 7. Ability of SerADan to permeabilize vesicles at pH 7.5 and 22.5 °C. (A) Time profile of the release of calcein from 21 μM of vesicles of different compositions by 1 μM SerADan (50-fold diluted from a 50 μM solution in 0.2 M urea that had been aged for an hour after 50-fold dilution from a 2.5 mM stock in 10 M urea). Lines indicate best fits to single exponential decays. The fit is not particularly good for DOPG, but the associated rate constant and amplitude provide useful (if approximate) measures of the efficacy of permeabilization. (B) Ability of different concentrations of freshly diluted SerADan to permeabilize 21 μM calcein-filled DOPG vesicles. SerADan was first diluted from 2.5 mM peptide in 10 M urea to 50 μM peptide in 0.2 M urea, and then immediately diluted to the indicated concentrations in the presence of vesicles. SerADan permeabilizes a significant proportion of the vesicles at molar protein:lipid ratios down to 1:500. (C) Effect of ageing on ability of SerADan to permeabilize DOPG vesicles, measured in terms of the rate constant and amplitude of calcein release (derived from exponential decays as in panel A). SerADan was aged at a concentration of 10 μM in 0.04 M urea (diluted 250-fold from a 2.5 mM stock in 10 M urea) and subsequently diluted to 1 μM in the presence of 21 μM DOPG. The time profile thus reports on the ageing at 10 μM concentration. (D) Effect of ionic strength on ability of 1.0 μM SerADan to permeabilize 21 μM DOPG vesicles, measured as in panel A.

declines to around 13 and 8% for 1:1 DOPG:DOPC vesicles and pure DOPC vesicles, respectively. Just as high NaCl concentrations abolish the interaction between lipids and SerADan (Fig. 6A), they also prevent SerADan from permeabilizing vesicles (Fig. 7D).

4. Discussion

4.1. The multifaceted nature of SerADan aggregation

SerADan is an interesting model aggregation system for several reasons. Firstly, the close similarity to the original ADan peptide provides a direct link to aggregation processes occurring *in vivo*. Secondly, despite the preponderance of β-sheet structure and the overall amyloid-like appearance of the aggregates at longer time points, it presents no *bona fide* amyloid structure (according to both tinctorial assays and X-ray fiber diffraction studies). Diffraction data [18] indicate that the peptide is able to form organized β-stranded structure at the local level, but cannot assemble the ensuing β-sheets into supramolecular structures that are sufficiently organized to provide binding sites for amyloid-specific dyes such as Thioflavin T and Congo Red. In this sense SerADan occupies an intermediate position between classical amyloid and more diffuse protein aggregates, which may occur naturally as reversible associations in secretory granules [19]. These less well organized structures can be stabilized by local interactions in competition with proper amyloid structures [20] or may be held together by *e.g.* complementary charges mediated by detergent molecules [21].

The conformational and functional transitions identified for SerADan based on the use of 6 different techniques (circular dichroism, FTIR, Trp fluorescence, dynamic light scattering, electron microscopy and the release of calcein entrapped in vesicles) indicate that non-fibrillar aggregates can also assemble in numerous steps. We can thus build up a rather detailed picture of the different steps involved in SerADan aggregation after it has been diluted out from 10 M urea into buffer (summarized in Fig. 8). The following data pertain to behavior at pH 7.5 but are essentially the same at pH 5.0 unless indicated otherwise. SerADan is calculated to have a negative charge of −1 to −2 at pH 7.5 and ~+1 at pH 5, but the minor difference in behavior at these two pH values reveals that the overall charge does not play a significant role.

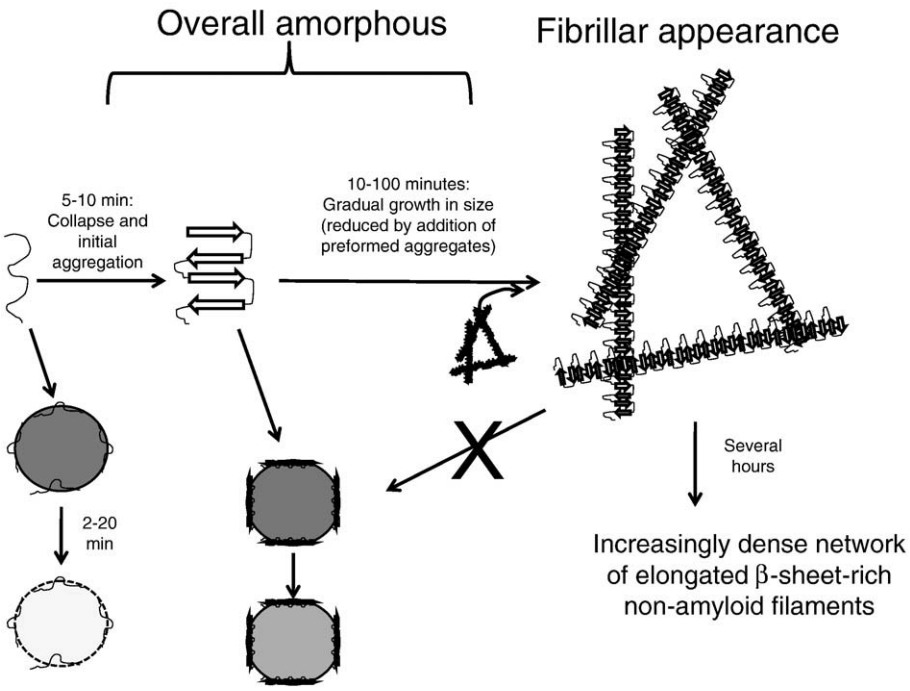

Fig. 8. Model of the different aggregation steps for SerADan and its interaction with lipids. Times indicate the approximate lengths required to complete the step in question (at concentration ranges spanning 10–50 μM SerADan). The first phase (first 10 min) involves formation of β-sheet structure, a ~5% loss in Trp fluorescence, initial aggregation and ~50% loss of permeabilization ability. Over the next 10–100 min aggregation levels increase, leading eventually to a multi-step sedimentation of large aggregates with loss of permeabilization ability, CD and Trp signals. Calcein-containing vesicles are denoted by circles. The different shades of grey indicate different levels of ability of SerADan aggregates to permeabilize the vesicles.

Within the first 5–10 min, there is a small (~15%) concentration-independent decline in Trp fluorescence; concomitantly a large amount of β-sheet structure forms rapidly according to circular dichroism, after which it stabilizes temporarily. In this period, SerADan's ability to permeabilize calcein-loaded membranes declines 50% in terms of the amount of calcein that can be released and around 10-fold in terms of the rate constant of permeabilization. This initial Trp decline is not so evident at pH 5.0, and at this pH the CD signal starts to decline straight away, suggesting that the rearrangement step occurs more rapidly at pH 5.0 or is bypassed to some extent. Over the next 5–100 min (depending on peptide concentration), there is a minor (~5%) linear and concentration-independent decline in fluorescence which may indicate a modest conformational rearrangement, but no change in permeabilization efficiency or CD signal at pH 7.5. Compared to the initial non-aggregated species which can permeabilize up to 60% of the vesicles, the aggregates present at this stage have a two-fold reduced membrane permeabilization activity, perhaps based on a limited ability to dissociate and re-aggregate productively in the membrane environment. Alternatively, these aggregates do not rearrange in the membrane, but simply possess a more modest permeabilization activity than the aggregated species formed by assembly of monomers in the membrane environment; the assembly process in the membrane is likely to be different from that in solution and also leads to β-sheet assemblies with stronger CD signals and more blue-shifted Trp fluorescence than in solution. In this time range, we also observe a marked growth in aggregate size by dynamic light scattering and the transient appearance and disappearance of amorphous aggregates according to electron microscopy. Although we do not include this as a separate step, it is likely that there is a gradual build-up of soluble species of increasing size in this period. From 2 h onwards, fibril-like aggregates (which already appear after a few minutes but not as the major species) dominate the EM images and there is a marked increase in aggregate size (probably due to the formation of intermeshed structures), leading to precipitation from solution and the complete loss of membrane permeabilization activity. This aggregation process is complex and proceeds in several stages; the steep drop in fluorescence to around 60% of the initial value (which is not paralleled by CD changes) is followed by a more measured fluorescence decline towards 40% over the next 2–10 h as well as a decline in CD signal. Although EM provides no categorical distinction between the different levels of aggregation on these time scales, the final decline is nevertheless accompanied by the consolidation of large filament-like structures by EM (Fig. 3). No major rearrangements occur over longer time intervals at the level of secondary structure (FTIR) or ultrastructure (EM). The modest decline in fluorescence prior to precipitation can be viewed as an apparent lag phase, as it represents the time required for accumulation of aggregates of a certain size. Similar to other nucleation-limited process, precipitation can be accelerated by the addition of preformed aggregates around which the smaller aggregates can coalesce as well as by an increase in the protein concentration.

In the presence of sufficient amounts of lipids, and provided there is not significant amount of electrostatic screening, there is only a small decline in Trp fluorescence (*i.e.* no precipitation) but a marked increase in β-sheet structure compared to the absence of lipids. Nevertheless EM does not indicate formation of straight fibril-like structure in lipids but rather wool-like threads. The decline in Trp fluorescence is accompanied by a ~13 nm blueshift, suggesting direct hydrophobic interaction between the aromatic residue and lipid. In contrast, the lipid-free process associated with the 15% Trp fluorescence decline gives rise to a negligible shift. Thus there is a kinetic partitioning between lipid binding and aggregation. In fact the inability of fresh SerADan to permeabilize vesicles 100% could be due to dead-time formation of aggregated species. Aggregation will dominate under physiological conditions (cfr. the screening effect of 100 mM NaCl), but permeabilization is not completely abolished and will be facilitated by higher lipid: peptide ratios, so that its effects may accumulate over longer time spans.

4.2. Similarities between SerADan and ADan

The previous studies of the reduced form of ADan showed no formation of amyloid-like structures but did demonstrate the presence of a dimer in fresh samples, which aggregated over several days [8,9] into an electron-dense matrix. That matrix shares some morphological similarities with the electron micrographs we present here although a stronger similarity can be seen with so-called immature fibers formed by oxidized ADan [9]. However, the kinetics of SerADan aggregation at pH 5.0 and 7.5 alike are an order of magnitude more rapid than those previously measured for the cysteine-containing ADan variants. This acceleration of aggregation is unexpected given the nature of the substitutions (Cys→Ser and Phe→Trp). These do not significantly alter the β-sheet propensity [22,23] or, in the case of F15W, the propensity for β-aggregation [24]. For C5S and C22S, the substitution theoretically lowers the β-aggregation propensity rather than increasing it. However, due to the proximity to the theoretical pKa for cysteine (~8.0), ~17% of the Cys residues in reduced ADan will be charged at pH 7.5. In principle, the elimination of charge by the mutations in SerADan could play a role at pH 7.5, but not at pH 5.0 where only 0.1% of the Cys residues will be charged. However, since the kinetics are rapid at both pH 5.0 and 7.5, we conclude that charge elimination by the Cys-Ser mutations will not contribute significantly. An alternative explanation for the effect of the mutations is that the elimination of cysteine prevents shuffling and formation of intermolecular disulphide bonds that could trap the peptide in 'aggregation-protected' conformations. Thus the mutations in SerADan allow us to filter out the covalent interactions and focus entirely on how non-covalent interactions affect the aggregation process.

4.3. SerADan interacts strongly with anionic phospholipids

SerADan shows the preference for anionic lipids that is seen for most other lipid-interacting aggregating proteins. These interactions are mediated by electrostatics, as they are reduced at medium ionic strength. At pH 7.5, the charge is predicted to be −1 to −2, leading to overall repulsion from anionic lipid membranes. Inspection of the primary structure does not reveal an obvious basic region that could account for the interaction with the negatively charged lipid. However, several authors have attempted molecular modeling of the ADan peptide based on (a) the 101–123 segment of transthyretin [9] or (b) a previous model for the related ABri peptide [8,25]. The former (a) resulted in a double-stranded β-sheet stabilized by disulphide and hydrogen bonding and terminating in a long loop with the C-terminal tyrosine residue hydrogen bonded to the β-sheet. The latter (b) showed a triple β-sheet in which strands one and two are similar to the double-stranded model while the third strand consist of the C-terminal region. Both of these models are interesting in that they largely isolate the charged residues at one or both ends of the β-sheet albeit not in a manner that creates a clear cationic region. In addition, the peptide contains two histidine residues and local environmental effects could very well shift the effective pK_a of this group. The residue corresponding to the single tryptophan in SerADan is also located at one end of both models. Together with the observed strong blueshifting of the emission spectrum in SerADan, it is tempting to speculate that Trp is buried within the core or border region of the membrane while a local basic region of the peptide interacts with the lipid head group; this whole interacting region is located at one end of a double- or triple-stranded β-sheet.

4.4. SerADan share characteristics with antimicrobial peptides

The rapid release of calcein from vesicles demonstrates that SerADan (and by implication ADan) has a potent perturbing effect on lipid membranes at molar peptide:lipid ratios down to 1:500, which is comparable to *bona fide* antimicrobial peptides [26]. Unlike small antimicrobial peptides such as Novispirin [27], lipid-bound SerADan does not contain notable amounts of α-helical structure. However, amphiphilic antimicrobial peptides forming β-hairpins in the active form have been identified such as the cationic β-defensins and bactenecin [28,29], and self-assembling β-sheet peptides are able to form transient pores in membranes [30]. Furthermore, formation of α-helix structure is not a prerequisite for the ability of Novicidin to permeabilize *e.g.* zwitterionic lipids (B.S. Vad and D.E. Otzen, unpublished observations).

SerADan's predilection for β-sheet structure in lipids is in marked contrast to IAPP, which in the presence of anionic lipids is able to form α-helical assemblies that lead to membrane leakage and subsequent fibril assembly through α-to-β conversion within the α-helical assembly [31]. Similarly, the fibrillating polypeptides α-synuclein [32] and Aβ [33] both form α-helical structures in lipid bilayers which may be intermediates in fibril formation [34]. Although programmes such as TANGO [35] predict Aβ to have a significantly higher β-sheet propensity in buffer than SerADan (whose propensity in turn is much higher than that of IAPP), this may be overruled by the pronounced tendency of SerADan to associate rapidly by a more general collapse. SerADan's inability to form highly organized fibrillar structures may thus reflect that it is quickly trapped in locally well-organized aggregates that are unable to reorganize at the molecular level to make regular β-sheet contacts. It is tempting to speculate that the swiftness with which these oligomeric structures are formed in solution and in lipid bilayers is a key factor that will facilitate an aggressive behavior towards cellular membranes at the monomeric and early oligomeric level.

Acknowledgements

L.W.N. and B.S.V. are supported by pre-doctoral grants from Aalborg University, the Danish Research Training Council and the BioNET research network, funded by the Villum Kann Rasmussen Foundation. D.E.O. is supported by the Villum Kann Rasmussen Foundation and the Danish Research Foundation.

References

[1] E. Strömgren, A. Dalby, M.A. Dalby, B. Ranheim, Cataract, deafness, cerebellar ataxia, psychosis and dementia—a new syndrome. Acta Neurol. Scand. 46 (Suppl. 43) (1970) 97–98.
[2] R. Vidal, T. Revesz, A. Rostagno, E. Kim, J.L. Holton, T. Bek, M. Bojsen-Moller, H. Braendgaard, G. Plant, J. Ghiso, B. Frangione, A decamer duplication in the 3′ region of the BRI gene originates an amyloid peptide that is associated with dementia in a Danish kindred, Proc. Natl. Acad. Sci. U. S. A. 97 (2000) 4920–4925.
[3] J.L. Holton, T. Lashley, J. Ghiso, H. Braendgaard, R. Vidal, C.J. Guerin, G. Gibb, D.P. Hanger, A. Rostagno, B.H. Anderton, C. Strand, H. Ayling, G. Plant, B. Frangione, M. Bojsen-Moller, T. Revesz, Familial Danish dementia: a novel form of cerebral amyloidosis associated with deposition of both amyloid-Dan and amyloid-beta, J. Neuropathol. Exp. Neurol. 61 (2002) 254–267.
[4] S.H. Kim, J.W. Creemers, S. Chu, G. Thinakaran, S.S. Sisodia, Proteolytic processing of familial British dementia-associated BRI variants: evidence for enhanced intracellular accumulation of amyloidogenic peptides, J. Biol. Chem. 277 (2002) 1872–1877.
[5] A. Rostagno, Y. Tomidokoro, T. Lashley, D. Ng, G. Plant, J. Holton, B. Frangione, T. Revesz, J. Ghiso, Chromosome 13 dementias, Cell. Mol. Life Sci. 62 (2005) 1814–1825.
[6] B. Austen, O.M.A. El-Agnaf, S. Nagala, B. Patel, N. Gunasekera, M. Lee, V. Lelyveld, Properties of neurotoxic peptides related to the BRI gene, Biochem. Soc. Trans. 30 (2002) 557–559.
[7] Y. Tomidokoro, T. Lashley, A. Rostagno, T.A. Neubert, M. Bojsen-Møller, H. Brændgaard, G. Plant, J.M. Holton, B. Frangione, T. Revesz, J. Ghiso, Familial Danish dementia: co-existence of Danish and Alzheimer amyloid subunits (ADan AND Aβ) in the absence of compact plaques, J. Biol. Chem. 280 (2005) 36883–36894.
[8] G. Gibson, N. Gunasekera, M.T. Lee, V. Lelyveld, O.M.A. El-Agnaf, A. Wright, B. Austen, Oligomerization and neurotoxicity of the amyloid ADan peptide implicated in familial Danish dementia, J. Neurochem. 88 (2004) 281–290.
[9] I. Surolia, G.B. Reddy, S. Sinha, Hierarchy and the mechanism of fibril formation in ADan peptides, J. Neurochem. 99 (2006) 537–548.

[10] J.D. Knight, A.D. Miranker, Phospholipid catalysis of diabetic amyloid assembly, J. Mol. Biol. 341 (2004) 1175–1187.
[11] Y.A. Domanov, P.K. Kinnunen, Islet amyloid polypeptide forms rigid lipid–protein amyloid fibrils on supported phospholipid bilayers, J. Mol. Biol. 376 (2008) 42–54.
[12] M. Bokvist, F. Lindstrom, A. Watts, G. Grobner, Two types of Alzheimer's beta-amyloid (1–40) peptide membrane interactions: aggregation preventing transmembrane anchoring versus accelerated surface fibril formation, J. Mol. Biol. 335 (2004) 1039–1049.
[13] I.C. Martins, I. Kuperstein, H. Wilkinson, E. Maes, M. Vanbrabant, W. Jonckheere, P. Van Gelder, D. Hartmann, R. D'Hooge, B. de Strooper, J. Schymkowitz, F. Rousseau, Lipids revert inert Aβ amyloid fibrils to neurotoxic protofibrils that affect learning in mice, EMBO J. 27 (2008) 224–233.
[14] H. Zhao, E.K. Tuominen, P.K. Kinnunen, Formation of amyloid fibers triggered by phosphatidylserine-containing membranes, Biochemistry 43 (2004) 10302–10307.
[15] A. Quist, I. Doudevski, H. Lin, R. Azimova, D. Ng, B. Frangione, B. Kagan, J. Ghiso, R. Lal, Amyloid ion channels: a common structural link for protein-misfolding disease, Proc. Natl. Acad. Sci. U. S. A. 102 (2005) 10427–10432.
[16] D.M. Byler, H. Susi, Examination of the secondary structure of proteins by deconvolved FTIR spectra, Biopolymers 25 (1986) 469–487.
[17] J.S. Pedersen, G. Christiansen, D.E. Otzen, Modulation of S6 fibrillation by unfolding rates and gatekeeper residues, J. Mol. Biol. 341 (2004) 575–588.
[18] L. Nesgaard, A. Malmendal, S.V. Hoffmann, D.E. Otzen, Characterization of dry globular proteins and proteins fibrils by synchrotron radiation circular dichroism, Biopolymers 89 (2008) 779–795.
[19] C. Keeler, M.E. Hodsdon, P.S. Dannies, Is there structural specificity in the reversible protein aggregates that are stored in secretory granules? J. Mol. Neurosci. 22 (2004) 43–49.
[20] O.P. Bliznyukov, L.D. Kozmin, L.L. VYsotskaya, A.K. Golenkov, V.M. TIshchenko, M.P. Samyolovich, V.B. Klimovich, Human immunoglobulin light chains lambda form amyloid fibrils and granular aggregates in solution, Biochemistry (Mosc.) 70 (2005) 458–466.
[21] D.E. Otzen, L. Nesgaard, K.K. Andersen, J.H. Hansen, G. Christiansen, H. Doe, P. Sehgal, Aggregation of S6 in a quasi-native state by monomeric SDS, Biochim. Biophys. Acta 1784 (2008) 400–414.
[22] P.Y. Chou, G.D. Fasman, Conformational parameters for amino acids in helical, beta-sheet, and random coil regions calculated from proteins, Biochemistry 13 (1974) 211–222.
[23] P. Koehl, M. Levitt, Structure-based conformational preferences of amino acids, Proc. Natl. Acad. Sci. U. S. A. 96 (1999) 12524–12529.
[24] A.P. Pawar, K.F. DuBay, J. Zurdo, F. Chiti, M. Vendruscolo, C.M. Dobson, Prediction of "Aggregation-prone" and "Aggregationsusceptible" regions in proteins associated with neurodegenerative diseases, J. Mol. Biol. 2005 (2005) 379–392.
[25] O.M. El-Agnaf, J.M. Sheridan, C. Sidera, G. Siligardi, R. Hussain, P.I. Haris, B.M. Austen, Effect of the disulfide bridge and the C-terminal extension on the oligomerization of the amyloid peptide ABri implicated in familial British dementia, Biochemistry 40 (2001) 3449–3457.
[26] R.E.W. Hancock, H.G. Sahl, Antimicrobial and host-defense peptides as new anti-infective therapeutic strategies, Nat. Biotechnol. 24 (2006) 1551–1557.
[27] R. Wimmer, K. Andersen, B. Vad, M. Davidsen, S. Mølgaard, L.W. Nesgaard, H.H. Kristensen, D.E. Otzen, Versatile interactions of the antimicrobial peptide Novispirin with detergents and lipids, Biochemistry 45 (2006) 481–497.
[28] M. Pazgier, X. Li, W. Lu, J. Lubkowski, Human defensins: synthesis and structural properties, Curr. Pharm. Des. 13 (2007) 3096–3118.
[29] D. Romeo, B. Skerlavaj, M. Bolognesi, R. Gennaro, Structure and bactericidal activity of an antibiotic dodecapeptide purified from bovine neutrophils, J. Biol. Chem. 263 (1988) 9573–9575.
[30] J.M. Rausch, J.R. Marks, R. Rathinakumar, W.C. Wimley, Beta-sheet pore-forming peptides selected from a rational combinatorial library: mechanism of pore formation in lipid vesicles and activity in biological membranes, Biochemistry 46 (2007) 12124–12139.
[31] J.D. Knight, J.A. Hebda, A.D. Miranker, Conserved and cooperative assembly of membrane-bound alpha-helical states of islet amyloid polypeptide, Biochemistry 45 (2006) 9496–9508.
[32] E. Jo, J. McLaurin, C.M. Yip, P. St. George-Hyslop, P.E. Faser, alpha-Synuclein membrane interactions and lipid specificity, J. Biol. Chem. 275 (2000) 34328–34334.
[33] E. Terzi, G. Holzemann, J. Seelig, Interaction of Alzheimer beta-amyloid peptide (1–40) with lipid membranes, Biochemistry 36 (1997) 14845–14852.
[34] M.D. Kirkitadze, M.M. Condron, D.B. Teplow, Identification and characterization of key kinetic intermediates in amyloid beta-protein fibrillogenesis, J. Mol. Biol. 312 (2001) 1103–1119.
[35] A.M. Fernandez-Escamilla, F. Rousseau, J. Schymkowitz, L. Serrano, Prediction of sequence-dependent and mutational effects on the aggregation of peptides and protein, Nat. Biotechnol. 22 (2004) 1302–1306.

Paper II: The anti microbial peptide Pardaxin displays a charge dependent orientation in lipid bilayers

Co-author statement for Paper 2

Brian Vad, Kresten Berthelsen, Charlotte Hau Johansen, Jan Mondrup Pedersen and Daniel E. Otzen: The anti microbial peptide Pardaxin displays a charge dependent orientation in lipid bilayers**:** *To be submitted.*

- Brian Vad purified Pardaxin, performed the LSCM measurements in collaboration with Charlotte Hau Johansen, did all the calcein release experiments and wrote the article in collaboration with Kresten Bertelsen, Niels Chr. Nielsen and Daniel Otzen.
- Charlotte Hau Johansen did the circular dichroism measurements on Pardaxin.
- Kresten Bertelsen did the Solid state NMR experiments.
- Jan Mondrup Pedersen performed the peptide synthesis.
- Daniel E. Otzen supervised the experiments and the writing of the article.

Kresten Berthelsen 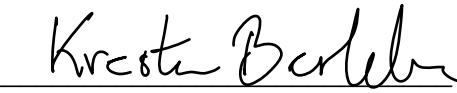 6th of april 2009

Jan Mondrup Pedersen _____ 6th of april 2009

Charlotte Hau Johansen  6th of april 2009

Daniel E. Otzen  26th March 2009

Brian Vad _____ 6th of april 2009

Signature Date

Paper III: Divorcing folding from function: How acylation affects the membrane-perturbing properties of an anti-microbial peptide

The anti microbial peptide Pardaxin displays a charge dependent orientation in lipid bilayers

Brian Vad[1,2], Kresten Berthelsen[3], Charlotte Hau Johansen[2], Jan Mondrup Pedersen[3], Troels Skrydstrup[3], Niels Chr. Nielsen[3] and Daniel E. Otzen[1,2]*

[1]Interdisciplinary Nanoscience Center (iNANO), Centre for Insoluble Protein Structures, Department of Molecular Biology, Gustav Wieds Vej 10C, University of Aarhus, DK-8000 Aarhus C, Denmark

[2] Department of Life Sciences, Aalborg University, Sohngaardsholmsvej 49, DK – 9000 Aalborg.

[3] Centre for Insoluble Protein Structures, Department of Chemistry, Langelandsgade 140, University of Aarhus, DK – 8000 Aarhus C, Denmark.

* To whom correspondence should be addressed at Department of Molecular Biology, Gustav Wieds Vej 10C, University of Aarhus, DK-8000 Aarhus C, Denmark. E-mail dao@inano.dk, tel. + 45 89 42 46 50, fax + 45 86 12 31 78.

ABSTRACT

Pardaxin is a 33 amino acid neurotoxin from the Red Sea Moses sole *Pardachirus marmoratus* that has been studied intensively as a model peptide membrane interaction. There are different proposals for its mode of action in terms of peptide aggregation and the effect of pH and lipid composition. Many of the techniques that have been used to characterize the interaction between amps and lipids all have limitations with regards to describing the specific interactions and mode of action for the amp. For example looking at the general release of dye entrapped in lipid vesicles will give you an indication of how the interaction is but it will be ensemble measurements. Here we combine optical spectroscopy and standard dye release experiments with natural abundance ^{13}C NMR and Laser Scanning Confocal Microscopy to provide a more complete picture of how Pardaxin interacts with lipids. We demonstrate that there is a pH/charge dependent release of entrapped fluorophor from both LUV´s and GUV´s with respect to the time release profile and the mode of action. In DOPC GUV´s there is either formation of stable or transient pores that allow release of contents without loss of vesicle integrity while the presence of DOPG facilitates a total vesicle collapse. NMR results show that in the presence of 14-O-PC: 6-O-PC bicelles Pardaxin is transmembrane where as Pardaxin interacts only with the headgroup of the lipids when 14-O-PG is mixed in.

Introduction

There is an increasing occurrence of bacterial strains that are resistant to conventional antibiotics which demands a steady output of new antimicrobial agents. The mode by which the bacteria gain resistance against a single antibiotic has a tendency to improve their tolerance to that entire group of antibiotics like the quinolones, sulfonamides, penicillins and cephalosporins. This means that even though the cost for developing antibiotic compounds becomes even more difficult and costly, their longevity for treating bacterial strains decreases. For exactly these reasons the Antimicrobial peptides have become an attractive alternative as new antibiotic compounds. The rate with which bacteria can become resistant towards anti microbial peptides is much lower if at all and the resistance against one type does not seem to induce a general increase in anti microbial peptide resistance.

The mechanism by which cationic linear anti microbial peptides interacts and permeates membranes has been thoroughly studied and a consensus has been reached with regards to three different models, the barrel-stave - [1], carpet -[2], and toroidal pore model [3]. The barrel stave model is the only one that requires that the protein interacts with the hydrophobic core of the protein while in the two other systems they are lying on the surface or in the headgroup region of the lipid bilayer.

Pardaxin is a 33 amino acid neurotoxin that was originally isolated from the Red Sea Moses sole *Pardachirus marmoratus* in 1986 [4]. Over the years, many studies have been done on Pardaxin looking into the mode of action [5, 6] its connection to peptide aggregation [7, 8] and how it is influenced by factors such as pH and lipid composition [8-12]. Several techniques have been used to elucidate how Pardaxin interacts with phospholipid membranes. Hallock et al showed by differential scanning calorimetry that very low concentrations of Pardaxin reduced the fluid lamellar-to-inverted hexagonal phase transition temperature of POPC vesicles. The presence of anionic lipids or cholesterol was found to reduce the peptide's ability to disrupt bilayers [13] They speculated that this indicated that Pardaxin worked by the barrels stave mechanism in POPC vesicles but could not make definite conclusions about the effect of POPG. Solid state ^{2}H NMR was employed by Ramamoorthy and co-workers to demonstrate that Pardaxin induces considerable disorder in both the head-groups and the hydrophobic core of the POPG bilayers [14]. Remarkably, solid state ^{15}N NMR spectroscopy on mechanically aligned bilayers showed that Pardaxin aligned in the plane of POPC bilayers but perpendicular to DMPC bilayers [13]. Thus, Pardaxin mode of action is sensitive to the acyl chain of the bilayer, using a barrel stave mechanism in DMPC and the carpet mechanism in POPC. A combination of a vesicle permeation assay and fluorescently labeled Pardaxin has been used to conclude that Pardaxin forms pores with ~ 6 molecules per pore [7]. Interpretation is complicated by the fact that the lipids used were a mix of naturally derived lipids which consist of a mix of carbon lengths from 16 to 20 with varying degree of saturation. Given that pore formation appears to be very lipid specific, a combination of different peptide-membrane interactions might be taking place under

these conditions. In this study we use lipids with a defined acyl chainlegths in order to keep the focus on the relevance of charge interactions. In addition to this the NMR studies of Pardaxin where done at a relative low pH somewhat from the pH in vivo in cells and in seawater which lies between 7.5 and 8.4 meaning charge dependent differences in the binding . Given that Pardaxin interactions are sensitive to lipid composition such as lipid headgroup charge, we decided to make a thorough investigation of the role of electrostatics in Pardaxin-membrane interactions. This was done in three ways. Firstly, the effect of headgroup charge (lipid composition) and Pardaxin protenation (at different pH values) on the kinetics of vesicle disruption. Secondly, Real-time analysis of Pardaxin's disruption of individual vesicles using Confocal Laser Scanning Microscopy. Thirdly, structural analysis of the interaction between Pardaxin and lipids using solid state natural abundance ^{13}C NMR on anionic and zwitterionic bicelles. We find that the kinetics of vesicle permeation by Pardaxin is affected by the pH and vesicle charge but in a discrete way that cannot be linked to favorable electrostatic interactions. Confocal Laser Scanning Microscopy measurements clearly show that Pardaxin forms pores in GUV´s composed of zwitterionic vesicles while it causes complete loss of membrane integrity when the GUV´s contain anionic lipids. The solid state natural abundance ^{13}C NMR show that Pardaxin interacts with the zwitterionic lipids all along the lipid molecule indicating a Trans membrane conformation. A different mode of interaction is measured when anionic lipid are mixed in. In this case Pardaxin interacts only with the upper layer of the lipid membrane.

MATERIALS AND METHODS

Chemicals: All lipids were from Avanti Polar Lipids (Alabaster, AL). Protected amino acids, 1,2-ethane dithiole (EDT), triisopropylsylane (TIPS), Di-chloromethane (DCM), Dimethylformamide (DMF), N,N-Diisopropylethylamine (DIPEA), 1H-Benzotriazolyl)-1,1,3,3-tetramethyl-uronium hexafluorophosphate (HBTU), acetonitrile chromasolv gradient grade, trifluoroacetic acid (TFA), Sucrose 99.5 % purity and D(+) Glucose 99.5 % purity were from Sigma (St. Louise, MO). DiIC18(3) and Alexa^{488} and Alexa^{633} hydrazide were from Invitrogen (Carlsbad, California). Calcein disodium salt was from Fluka (Buchs, Switzerland).

Peptide synthesis: Pardaxin (sequence GFFALIPKIISSPLFKTLLSAVGSALSSSGGQE) was synthesized on an automatic CEM liberty microwave assisted peptide synthesizer by solid phase synthesis using standard Fmoc chemistry on Wang resin. Wang resin was used with the C-terminal Glu residue coupled to the linker group at a concentration of 0.66 mmol Glu/g_{resin}. The resin was initially swelled with DCM for 30 min, followed by 5 repeating washes with DMF. The Fmoc protective group was removed with 20% piperidine solvated in DMF. Fmoc-amino acids were coupled to the resin bound peptide in 4 times molar excess together with 4 times molar excess of HBTU and 8 times molar excess of DIPEA solvated in DMF. The resin was washed with DMF and the procedure was repeated for each residue. The Lysine side chains had BOC as a protective group. The crude peptide mix was run on a on a Dionex Ultimate 3000 HPLC system with a Reverse Phase semi-preparative C16 column and an AJO-7371 guard column in an AJO-7220 guard column system. Prior to each purification, the column was equilibrated with 15% acetonitrile. After loading the peptide to the column, an initial step with 15% acetonitrile was run for 2 min followed by a gradient from 15% acetonitrile from 15% to 99.9% acetonitrile over a period of 30 min. The column was allowed to run another 30 min at 99.9 % acetonitrile followed by a gradient from 99,9% acetonitrile to 15% acetonitrile over a period of 30 min. The eluent solutions all contained 0.1 % TFA. The fractions containing peptides were freeze dried and the peptide dissolved in the appropriate buffer.

Calcein release assay measured by fluorescence: LUV´s (Large unilamellar vesicles) containing calcein were prepared from stock solutions of lipids dissolved in chloroform and dried overnight in a Heto VR-1 centrifuge vacuum drier. Lipids were then resuspended by vortexing in the respective buffers plus an additional 40 mM calcein sodium salt, to a final concentration of 10 g/L (~14 mM). The vesicles were exposed to at least seven cycles of freezing in liquid nitrogen, followed by thawing in a 50^{o}C water bath, before extrusion through a 200 nm pore filter 12 times using a 10 ml thermo barrel extruder (Northern Lipids, Vancouver, Canada). The lipid solutions were run on a PD10 column pre-equilibrated with 50 mM NaCl solution. Eluent fractions were gathered and tested by fluorescence measurements with and without the addition of Triton X-100

to test for calcein release. Those with the highest signal-to-background ratio were selected for further use. All extruded vesicles were used within two days from when they were made.

All fluorescence measurements were conducted on a Cary Eclipse Fluorescence spectrophotometer (Varian, Palo Alto, CA). Release of free calcein from the vesicles and the subsequent increase in fluorescence, was monitored by excitation at 490 nm, recording emission at 515 nm every second using a slit width of 2.5 nm for both monochromators. The time delay between each measurement was set to 0.2 seconds. The vesicles were diluted in buffers with the desired pH values to a concentration of ~ 0.017 g/L, leading to a maximum emission signal of around 200 units under these settings. A 10 mm quartz cuvette with magnetic stirring was used and the vesicle solution was allowed to equilibrate thermally for a minute before starting to record fluorescence. For each recording, Pardaxin was injected and emission was followed until it reached a plateau (typically after several minutes). Since calcein fluorescence is pH sensitive and varies by approximately a factor of 5 within the concentration range used here, we normalized the spectra at each pH with regards to maximum fluorescence. This is operationally defined as the fluorescence level obtained when 1% of Triton X-100 is added. Data are normalized using the equation:

$$Dye\ leakage(\%) = 100 * \frac{(F_t - F_o)}{(F_{\max} - F_o)}$$

where F_t is the time-dependent fluorescence intensity induced by Pardaxin and F_o and F_{max} are fluorescence intensities prior to Pardaxin addition and with Triton X-100, respectively.

Laser confocal microscopy measurements: GUVs (giant unilamellar vesicles) were prepared by the electroformation method originally described by Angelova and Dimitrov [15]. The GUVs were electroporated using a home-built electroformation chamber partly built on the specifications published by Baggatoli and Gratton [16]. GUVs were prepared from chloroform stocks containing 10 g/L lipid as well as 0,01 g/L DiI. ~10 µl of chloroform lipid stocks were spread on each platinum electrode. The chamber was incubated at 50^{o}C for 2 hours to evaporate any remaining solvents and then filled with a solution of 200 mM sucrose containing Alexa^{488} or Alexa^{633} hydrazide. The platinum wires were connected to a function generator (Digimess FG 100, Grundig Instruments, Nurnberg, Germany), and a low-frequency alternating field sinusoidal wave function with a frequency of 10 Hz and amplitude of 1,5 V was applied for 90 min followed by 30 min at 1 Hz and amplitude of 3 V. The GUV´s were removed from the platinum electrodes by gently pipetting up and down. The excess free fluorophor was removed by running the GUV´s over a PD10 column pre-equilibrated with 200 mM glucose. The eluent from the column was collected in 0.5 ml fractions; samples were selected on the basis of absorption of free fluorophor and transferred to an eight-well microscopy chamber (Lab-Tek Brand Products, Naperville, IL). Tris pH 8 was added to a final concentration of 10 mM and the GUVs were left

overnight at 4^{o}C to allow them to sediment at the bottom of the viewing chamber prior to viewing.

Vesicles were equilibrated to room temperature on the microscope slide for 15-20 minutes before measuring. GUVs were observed with a LSM 510 scanning confocal microscope (Zeiss GmbH, Jena, Germany). Excitation of Alexa^{488}, Alexa^{633} and DiI was done at 488, 633 and 543 nm, respectively. Fluorescence emission was measured at 505-548, 650-700 and 558-612 nm for Alexa^{488}, Alexa^{633} and DiI respectively. 10µl of Pardaxin of 30 µM dissolved in Mq was injected into the microcopy chamber outside the field of vision, and the measurements started immediately afterwards with images recorded every 15 s. Typically no changes were observed for the first 10-15 min after injection, probably due to slow diffusion of peptides into the field of vision in the viscous sucrose medium. Vesicle lysis was usually preceded by fluctuating vesicle movement associated with bulk solution changes, indicating the arrival of peptides diffusing in a lower-viscosity solution. Controls with addition of equivalent amounts of deionized water and buffer were performed but none of them showed signs of vesicle disruption.

Secondary structural changes measured by CD spectroscopy: Circular dichroism studies were performed on a Jasco J-810 spectropolarimeter (Jasco Spectroscopic Co., Hachioji City, Japan) with a Jasco PTC-348W1 temperature control unit. Scan speed was set to 100 nm min, slit with 2 nm. All experiments were carried out at 25^{o}C using a 1 mm quartz cuvette. Each spectrum in titration experiments represents a unique sample which was mixed 2-5 min before measuring. Each spectrum was based on an average of three scans. Background spectra for the different buffer and additive solutions without peptide were measured and subtracted to yield the final spectra. Pardaxin concentrations kept at 20 µM and diluted into 20 mM Tris pH 8.

Changes in lipid chain mobility measured by NMR: Bicelles were made from 14-O-PC(1,2-Di-O-Tetradecyl-*sn*-Glycero-3-Phosphocholine), 6-O-PC(1,2-Di-O-Hexyl-*sn*-Glycero-3-Phosphocholine) and 14-O-PG(1,2-Di-O-Tetradecyl-*sn*-Glycero-3-[Phospho-*rac*-(1-glycerol)]). All lipids except 14-O-PG were solubilized in chloroform except for 14-O-PG which was purchased as a dry powder. Two different bicelle samples were prepared, one containing only 14-O-PC and 6-O-PC at a molar ratio of 3.2:1 and the other containing 14-O-PC, 14-O-PG and 6-O-PC at a molar ratio of 2.6:0.6:1. Each sample contained a total of 56mg of lipids. The lipids were dried separately over a stream of nitrogen and left on vacuum over night. 200µL of a 10mM phosphate buffer (pH=6.8) was added to the dry 6-O-PC and briefly vortexed until solubilized. The clear solution of 6-O-PC was added to the dry 14-O-PC/14-O-PG and vortexed in an ice bath for 20 minutes. After a few heat and freeze cycles the sample was transferred to a 3cm long 5mm tube and sealed. It was left at room temperature for 10 days. The final sample is clear and viscous at ambient temperatures and becomes fluid below 10 °C. The Pardaxin was added to the bicelles suspension as a lyophilized powder followed by agitation to allow solubilization.

All experiments were performed on a Bruker Avance 400 spectrometer with a 9.4 T magnet employing a custom 5 mm Bruker triple-resonance probe for static experiments in double-resonance configuration. The ^{1}H RF field strength was 35 kHz for the 90 pulse while it was reduced to 20 kHz during the 3 ms CP period as well as the t_1 period of the PISEMA experiment. The ^{15}N RF field strength was 20 kHz during CP and t_1 of the PISEMA experiment. SPINAL-64 was employed for decoupling of the 1H during detection. The PISEMA experiment employed 45 t_1 increments, each acquired using 64 scans. Upon processing, the scaling factor of sqrt (2/3) in the indirect dimension was accounted for by increasing the spectral width accordingly. The temperature was 32^{o}C for samples containing only PC lipids while it was 30^{o}C for samples containing PG lipids. The temperatures chosen gave the best possible spectra.

RESULTS

Conformational changes in Pardaxin as function of solutes

The motivation for these measurements was to determine whether the secondary structure of Pardaxin was sensitive to the presence of amphipatic molecules like phospholipids and in turn how this was affected by the pH. It was also tested how the strengthening of intramolecular bonds affected Pardaxin's secondary structure by adding TFE and again as measuring it as a function of the pH. We measured the CD Spectra for Pardaxin in the presence of 50 % TFE, DPC, 100% DOPC and mixed vesicles containing 20% DOPG: and 80 % DOPC as a function of pH from 2 till 10 in increments of 1 pH unit but no differences in the spectra characteristics could be observed when we normalized for protein concentration (Fig. 1). At pH 6-8, ~ 20 % of the Pardaxin solution precipitated (according to Bradford assays on the supernatant left after centrifugation). In both 50% TFE and DPC, we observe spectra that resemble that of classical alpha helical spectra with two local minima at 222 and 208 nm. It should be noted here that we have chosen the lipid/TFE/DPC concentrations were we observe the most intense CD spectra. For DOPC the local minimum at 208 nm is much less pronounced than in DOPC and TFE. This suggests a lower degree of helix formation and it becomes much clearer when we include 20 % of the anionic DOPG. The local minimum at 208 almost completely disappears indicating that we have a shift towards a random coiled structure. This is underlined by the clear decrease in signal intensity.

The degree and kinetics of vesicles disruption depends on pH and lipid charge

Having established that the ensemble structure of Pardaxin is not affected by changes in pH and thus peptide protenation, we next investigated how the protenation of Pardaxin affected its ability to permeate vesicles of both zwitterionic and anionic composition. We measured the release of the fluorescent probe calcein from vesicles consisting of DOPC and 20% DOPG & 80 DOPC at pH 5.5, 8 and 10 where Pardaxin has a net charge of + 2, 0 and -1 respectively according to simple side chain titration calculations. In the same pH range, DOPC has a net charge of 0 and DOPG a net charge of -1.

The release of calcein from DOPC vesicles at all the pH values could be fitted to an equation involving two exponential decays, suggesting that the release of vesicle contents occurs in a two step (either consecutive or parallel) process (Fig. 2). The same is observed for vesicles consisting of 20% DOPG and 80% DOPC, except at pH 8 where we consistently observe two specific processes that do not overlap in their time course (Fig. 2). Such a step-type function can be rationalized as a three-phase process, in which the second (intermediate) phase has an amplitude that is opposite in sign to the first (fast) and last (slow) phase, leading to an apparent lag phase. Accordingly, the kinetics of the calcein release pattern of 20% DOPG and 80 DOPC vesicles at pH 8 could be fitted to an equation involving three exponential decays. However, the inherent

singularity problems associated with the fitting of multiple exponential decays reduced reproducibility significantly compared to the two-exponential fits used for the other kinetic profiles.

In contrast to the pH invariance displayed by the CD spectra, the kinetics of calcein release are highly sensitive to both pH and lipid type. Comparison of the two lipid types (Figs. 3A and 3B) reveals that five-tenfold less Pardaxin is required for maximum disruption of DOPC vesicles (~20 nM) compared to DOPC:DOPG vesicles (~100 nM at pH 5.5, ~240 nM at pH 8 and ~180 nM at pH 10). This indicates a remarkable difference in the mode of interaction. Furthermore, the maximum amount of calcein release from DOPC vesicles is independent of the pH; whereas the mixed vesicles are permeabilized 2-3 fold more efficiently at pH 5.5 compared to pH 8 and 10. The reason for this is most likely preferential electrostatic interactions between Pardaxin (which has a net charge of +2 at pH 5.5) and the anionic lipids.

Several interesting features are revealed when we plot the half lives of the different exponential phases versus Pardaxin concentration (Fig. 4). Although there is very little difference between the 3 pH-values in terms of the amount of Pardaxin needed for complete disruption of the vesicles, it is clear that release occurs much more rapidly at pH 10 than at pH 5.5 and 8 (Fig. 4A and 4C). Furthermore, the half life of release reaches a plateau at pH 10 at 2-3 fold lower Pardaxin concentrations than at pH 5.5 and 8. The kinetic plateau at pH 5.5 and 8 (~20 nM) coincides nicely with the amplitude plateau (Fig. 3A), whereas the kinetic plateau at pH 10 is ~7 nM in contrast to ~30 nM for the amplitude plateau. This indicates a difference in the mechanism of interaction at the three pH values and highlights a remarkable attraction between negatively charged Pardaxin and zwitterionic lipids. The plateau presumably reflects a situation in which the rate limiting step changes from diffusion-controlled protein association on the vesicle to unimolecular rearrangements on the vesicle.

In contrast, for the DOPC: DOPG vesicles the situation is completely reversed. For the fast phase, kinetics are fastest at pH 5.5 for all Pardaxin concentrations, followed by pH 10 and then pH 8 (Fig. 4B); furthermore, the plateau level is reached first at pH 5.5 followed by pH 10 and then pH 8, but in all cases the plateau level is reached at a ~2 fold higher concentration than the amplitude plateau (Fig. 3B). The same trend is seen for the slow phase although it is less distinct (data at pH 8 are complicated by the triple exponential decay).

Thus pH and lipid composition combine to make the kinetics of Pardaxinlipid interactions very variable and subtle.

Pardaxin displays a charge dependent disruption of Giant unilamellar vesicles

The use of LSCM and giant unilamellar vesicles allows us to visualize how Pardaxin disrupts individual lipid vesicles. This is achieved by loading the GUVs with a water soluble fluorophor

and incorporating a lipid specific dye in the vesicles. This setup allows monitoring how the release of entrapped fluorophor corresponds with disruption of the GUVS and distinguishing between for example disruption by pore formation or a more global vesicle disruption. For DOPC vesicles we observe the release of vesicle contents over a time course of roughly 15 min but insubstantial loss of vesicle integrity (Fig. 5). So there is an efflux of vesicle contents in a semi controlled manner indicating that we may have pore formation.

When the GUV´s contain 20 % DOPG the effects are quite different. We observe the same lag time as with DOPC vesicles but upon binding there is release of fluorophor with simultaneous loss of membrane integrity. The time scale on which this occurs is also much faster than with DOPC vesicles, from initial interaction to disruption of more than 95 % of the vesicles it takes a maximum of 50 minutes. These two distinct modes of vesicle disruption are also apparent when we have a mixture of the two types of vesicles. This means that we can exclude the possibility that what we observe is an effect of small differences in experimental conditions. Furthermore we observe that the two processes happen at equal time rates meaning in heterogeneous solution there no preference towards neither zwitterionic nor anionic vesicles. (Data not shown).

Carbon NMR shows that Pardaxin interacts with the lipid acyl chain is charge dependent

To complement our spectroscopic and microscopic studies, we finally turn to solid-state NMR spectroscopy to analyze the conformation/orientation of Pardaxin when incorporated into or binding to the two lipid types. As mimics of vesicles and phospholipid bilayers, we use bicelles [17] composed of a mixture of long-chain (14-O-PC with and without 14-O-PG) and short-chain (6-O-PC) phospholipids. In these phospholipids, the ester bonds linking the two acyl chains to the glycerol backbone are replaced with a non-hydrolysable ether bond. This increases the chemical stability of the lipids but does not affect the secondary structure of Pardaxin according to circular dichroism spectra (data not shown). Bicelles mixed using appropriate stoichiometry will align when placed in a strong magnetic field, making them especially useful for oriented-sample solid-state NMR spectroscopy. Such studies aim at determining the orientation of anisotropic nuclear spin interactions (e.g., ^{13}C-^{1}H dipole-dipole couplings, being collinear with the internuclear axis) and through these establish information about the orientation of the molecules relative to the external magnetic field. With the bicelles oriented as disks with the normal of the disk perpendicular to the magnetic field, it is possible to obtain information about the orientation of peptides relative to the bicelles they are binding to or incorporated into. Furthermore, we can observe changes in the conformation of the lipid molecules upon interacting with the peptides. The latter approach has the advantage that it may be conducted with both lipids and peptides in natural abundance (i.e., without incorporating ^{15}N or ^{13}C isotope labels).

We recorded ^{13}C natural abundance PISEMA [18] NMR spectra of the two types of bicelles, and observe differences when Pardaxin is added. In the present context, the PISEMA spectrum correlates ^{13}C chemical shifts with the ^{1}H-^{13}C heteronuclear dipole–dipole coupling reflecting the

binding of the carbon to directly attached protons. The dipole-dipole coupling (and to a smaller extent the chemical shift) is very sensitive to reorientation of the lipids and thereby changes in lipid order. Therefore changes between PISEMA spectra with and without Pardaxin provide information on how Pardaxin interacts with the lipid bilayer at individual atomic sites as described previously by Ramamoorthy and coworkers [19, 20]. The change in the lipid conformation may conveniently be expressed in terms of an order parameter (28). Fig. 6 shows a 2D PISEMA spectrum (A) and 1D slices obtained for a bicelle composed of 14-O-PC:DHPC (molar ratio 3.2:1.0) lipids [21] and 14-O-PC:14-O-PG:6-O-PC(molar ratio 2.6:0.6:1,0) lipids (E-G). In the slices (extracted from the 2D spectra), we focus on ^{1}H-^{13}C dipole-dipole couplings observed for three representative carbon sites along the 14-O-PC molecule, namely C_{α} (d,e), C_3 (c,f), and C_{14} (d,g) with the slice in red representing pure lipids while the slice in black represents the case where Pardaxin is incorporated. It is evident that Pardaxin interacts differently with lipid bilayers depending on their surface charge. Fig. 6B-6D show that the order parameter changes at carbon sites all along the lipid molecule, indicating that Pardaxin is incorporated in a transmembrane configuration when the lipid head groups have a net charge of zero. This agrees very well with the formation of pores according to GUV analyses (Fig. 5). A different pattern is observed for bicelles containing a mixture of 14-O-PC:14-O-PC:6-O-PC as illustrated in Figs. 6E-6G. In these bicelles, only the order parameters for the head group region (C3 (E) and Cα (D)) change upon addition of Pardaxin, while that of C14 remains invariant (F). Accordingly, in this case the NMR data suggest that Pardaxin is positioned flat on the surface of the PC/PG bicelle and only interacts with the head group. This also correlates very well with our GUV data (Fig. 5).

Figs. 6H and 6I provide a color code representation of the relative changes in order parameters when Pardaxin is added to PC bicelles (6H) and PC:PG mixed bicelles (6I). Red indicates an increase in the order parameter, while blue represents a decrease. The diameters of the spheres in Figs. 6H and 6I are proportional to the measured order parameter in bicelles without Pardaxin. It is not surprising that the headgroup order generally decreases as peptide is added to the bicelles. We interpret this as the peptide interacts with the lipids and the conformational average ordering of the bilayers is disturbed (i.e., decreased) upon accommodation of the peptide. Similarly it appears intuitively correct that the order of the very disordered C_{14} site increases when Pardaxin is suggested to be transmembrane. An explanation could be that the free rotation of the acyl methyl group is restricted when Pardaxin is transmembrane. This would make the methyl group less dynamic and more ordered. Similar arguments apply to g_1 (The first carbon in the glycerol linker region of the lipid molecule) which also becomes slightly more ordered when Pardaxin is added to PC bicelles (Fig. 6I).

For the PG-containing bicelles we observe no change in the conformation order of the acyl chains in the deeper parts of the bicelles. This is indicated by the generally white color of the C4-C14 in Fig. 6I reflecting the data in Fig. 6E- 6G where only small changes in the dipolar splitting (and thereby the order parameter) are observed.

DISCUSSION

Calcein release patterns are dependent on lipid headgroup charge

There has been numerous studies looking at the interaction of Pardaxin with lipid membranes [7-14, 22-28] but none of them have methodically investigated how the rate of vesicle permeation was affected by the pH of the solution and the charge of the lipid headgroup. In this study the vesicle permeation was studied by measuring the fluorescence increase upon the contents release from Calcein loaded vesicles. The Calcein release patterns show that Pardaxin mediated lipid permeations are dependent on lipid headgroup charge and show subtle kinetic effects. From the maximum calcein release data in figure 3 A & B it was clear that we only observe a dependence of Pardaxin protenation with vesicles containing the anionic DOPG lipid. We needed less protein to permeate anionic vesicles when Pardaxin had a net charge of + 1. Despite of this 5 times less Pardaxin was needed to permeate purely zwitterionic vesicles. It is known that there is large difference in the concentrations needed to permeate vesicles by either pore formation or the carpet mechanism with the later being the most protein demanding [29]. These findings suggest that the differences in Pardaxin concentration needed for permeation reflects differences in the mode of action with zwitterionic and anionic vesicles. This is further supported by a similar lipid dependence shown for the anti microbial peptide Mellitin which was found to form pores in zwitterionic vesicles and aggregation/fusion [30]. This study reported on a 10 fold increase in the Mellitin concentrations needed for permeating anionic vesicles compared to zwitterionic vesicles.

The kinetics of the membrane disruption by Pardaxin reveals two distinct processes, an initial fast process and a subsequent slow process. The measured release time profiles represent the final result(s) of permeabilization, i.e. they are not just intermediate rearrangements of Pardaxin (as one might interpret e.g. a Trp fluorescence time profile in a refolding experiment). Thus it seems as if there are several more or less distinct ways of perturbing the membrane. The kinetics of membrane disruption by the AMP Cecropin also displays two distinct kinetic processes. The two processes consist of an initial fast step that relates to initial peptide binding and a second slower process that is linked to the more specific mode of action like the formation of pores or shedding of membrane fragments. Sawyer et al are able to show that the kinetics of vesicle disruption is markedly slower for a Cecropin mutant that works by the carpet mechanism contrary to the pore formation by wt Cecropin [31]. A similar scenario is observed with Pardaxin with regards to the kinetics of membrane disruption of zwitterionic and anionic vesicles. We observe that the T(1/2) for both the fast and the slow process vesicle disruption process has reached a minimum plateau with zwitterionic vesicles before there is any measureable disruption of anionic vesicles. This should be viewed in the light that the Gouy-Chapman theory describes how negative charge on the acidic membrane creates a membrane potential which causes cationic peptides to redistribute to the membrane [32, 33]. This passive accumulation of peptides near an anionic membrane surface will results in a high apparent

binding constant. If the initial fast process relates to peptide binding it should be expected that these would either be of the same order of magnitude or even more pronounced for anionic vesicles. Hence the initial fast process must relate to an initial step in the mode of action for Pardaxin be it pore formation or carpet mechanism.

Another important point that this study reveals is the step process by which Pardaxin seems to permeate vesicle at low peptide concentrations at pH 8. Simulations conducted using the kinetics software program KinTek [34] revealed that the characteristic step-pattern observed for pardaxin at pH 8 could be satisfactorily reproduced by a three-step mechanism (A ↔ B ↔ C ↔ D) in which each step represents the formation of a species with a specific level of permeabilization activity (D.E. Otzen, data not shown). The reason why this feature has not been shown before is due to the fact that previous studies have looked at endpoint permeation and not the release as a function of time [8-10, 23, 25]. The LSCM experiments did not reveal any phenomena that could explain this behavior which means it might not be related to changes in the mode of action.

GUV experiments reveal two distinct vesicle disruption patterns

There have previously been suggested that the mode of action of Pardaxin is sensitive to the charge of the lipid groups with clear indications of pore formation in pure POPC vesicles which appeared to change upon the inclusion of anionic lipids [13]. With these GUV experiments we can without a doubt say that Pardaxin forms pores in pure DOPC vesicles and disrupts anionic vesicles in a none or all fashion indicative of the carpet mechanism. There have previously been studies that combine the use of GUV´s and LSCM to elucidate on the mode of action of AMP´s. These studies included Maculatin, Citropin, Aurein and Magainin 2 and proved capable of resolving whether the peptides worked by either pore formation or the carpet mechanism in vesicles composed of a mixture of zwitterionic and anionic lipids[35, 36]. This study of Pardaxin is however the first that is able to show that the mode of action can be dependent on the lipid composition of the vesicles. These findings are cooperated both by the calcein vesicle disruption assay and the NMR data. Furthermore we were able to reproduce the specific modes of action in a heterogeneous mixture composed of anionic vesicles and zwitterionic vesicles. These two different modes of action were observed on the same timescale showing there was no preference for either lipid composition. This demonstrates the robustness of the method as Pardaxin has been shown *in vitro* to be active against the anionic membranes of bacteria and the zwitterionic membranes of mammals [6].

The interaction of Pardaxin with membranes changes the lipid

The use of 2D NMR experiments, of natural abundance ^{13}C observed from bicelles containing DMPC and DHPC lipid molecules were developed by Ramamoorthy and coworkers. The technique allows probing the interactions of molecules with lipid membranes without the addition of exotic probes to the sample which might in turn effect the molecule-lipid interactions.

It has been used in for studying the membrane interactions of the antidepressant Desipramine [37] but also the AMP Pexiganan[19, 38]. Pexiganan has been shown by various techniques as has been established via fluorescence assays, calorimetric techniques, microscopy, and solid-state NMR spectroscopy and neutron diffraction to work by a toroidal pore mechanism. In the natural abundance ^{13}C NMR experiments this resulted in an increase in the disorder of DMPC mainly at the headgroup group region and the upper part of the acyl chain. Given that Pexiganan works by the toroidal pore mechanism, the NMR signal is a mixture of the signal from the bilayer forming lipids and the lipids that line the toroidal pore making specific interpretations of peptide induced changes in the lipid conformation. The calcein release measurements and the LSCM results for Pardaxin revealed two distinct vesicle disruption patterns compatible with pore formation and the carpet mechanism for zwitterionic and anionic vesicles respectively. This is then reflected in the natural abundance ^{13}C 2D NMR measurements. For bicelles composed only of zwitterionic vesicles there was a slight disordering of the lipid headgroup and an increase in the order of the acyl chain. This is the opposite of what was observed for Pexiganan indicating that Pardaxin does not form toroidal pores. The increase in acyl chain order is rather what would be expected if the Pardaxin was transmembrane and thereby restricting the movement of the acyl chains. This ordering effect on lipid acyl chains by transmembrane peptides has been reported previously [39, 40] corresponding to the formation of pores by the barrel stave mechanism [41]. For the bicelles containing anionic lipids a disordering of the headgroup region is observed when Pardaxin is added. From the LSCM measurements we have shown that Pardaxin works by a none or all mechanism as would be expected from a peptide that worked by the carpet mechanism. All though it has been shown that the toroidal pore formation is followed by membrane disruption at higher concentration [42] no pore formation was observed by lowering the Pardaxin concentration. These results indicate that there is a significant difference in the impact on acyl chain order induced by the toroidal pore formation and the carpet mechanism. This is interesting from the standpoint that in both processes the peptide is lying in the lipid headgroup and acyl chain interface [43-46]. If this is a general characteristic of natural abundance ^{13}C NMR for these two mechanism this would allow for an easy way of distinguishing between but this would require testing on more systems to exclude that these results are not peptide specific.

This paper describes how the combination of a vesicle disruption assay, LSCM and natural abundance ^{13}C NMR allowed the determination of mode of action of Pardaxin and the underlying kinetics of these. There is a clear difference in the peptide concentrations needed for the permeation of zwitterionic and anionic vesicles with more peptides needed for the latter regardless of the protenation state of Pardaxin. These findings alone are a strong indicator in differences in the mode of action but it is further confirmed by the LSCM measurement. Real-time images taken Zwitterionic and anionic GUV´s after the addition Pardaxin revealed that the Pardaxin formed pores in zwitterionic GUV´s and disrupted anionic vesicles by an all or none mechanism. Natural abundance ^{13}C NMR finally showed that Pardaxin forms pores by the barrel stave mechanism in zwitterionic lipids and disrupts anionic lipid membranes by the carpet mechanism.

REFERENCES

1. H, e.G.L., *electrically-gated ionic channels in lipid bilayers.* rev. biophys., 1977: p. 595-623.
2. Shai, Y. and Z. Oren, *From "carpet" mechanism to de-novo designed diastereomeric cell-selective antimicrobial peptides.* Peptides, 2001. **22**(10): p. 1629-41.
3. Yang, L., et al., *Crystallization of antimicrobial pores in membranes: magainin and protegrin.* Biophys J, 2000. **79**(4): p. 2002-9.
4. Lazarovici, P., N. Primor, and L.M. Loew, *Purification and pore-forming activity of two hydrophobic polypeptides from the secretion of the Red Sea Moses sole (Pardachirus marmoratus).* J Biol Chem, 1986. **261**(35): p. 16704-13.
5. Shai, Y., D. Bach, and A. Yanovsky, *Channel formation properties of synthetic pardaxin and analogues.* J Biol Chem, 1990. **265**(33): p. 20202-9.
6. Oren, Z. and Y. Shai, *A class of highly potent antibacterial peptides derived from pardaxin, a pore-forming peptide isolated from Moses sole fish Pardachirus marmoratus.* Eur J Biochem, 1996. **237**(1): p. 303-10.
7. Rapaport, D., et al., *Reversible surface aggregation in pore formation by pardaxin.* Biophys J, 1996. **70**(6): p. 2502-12.
8. Rapaport, D. and Y. Shai, *Interaction of fluorescently labeled pardaxin and its analogues with lipid bilayers.* J Biol Chem, 1991. **266**(35): p. 23769-75.
9. Shai, Y., Y.R. Hadari, and A. Finkels, *pH-dependent pore formation properties of pardaxin analogues.* J Biol Chem, 1991. **266**(33): p. 22346-54.
10. Epand, R.F., A. Ramamoorthy, and R.M. Epand, *Membrane lipid composition and the interaction of pardaxin: the role of cholesterol.* Protein Pept Lett, 2006. **13**(1): p. 1-5.
11. Kolusheva, S., et al., *Pardaxin, a fish toxin peptide interaction with a biomimetic phospholipid/polydiacetylene membrane assay.* Peptides, 2008. **29**(9): p. 1620-5.
12. Pouny, Y. and Y. Shai, *Interaction of D-amino acid incorporated analogues of pardaxin with membranes.* Biochemistry, 1992. **31**(39): p. 9482-90.
13. Hallock, K.J., et al., *Membrane composition determines pardaxin's mechanism of lipid bilayer disruption.* Biophys J, 2002. **83**(2): p. 1004-13.
14. Porcelli, F., et al., *Structure and orientation of pardaxin determined by NMR experiments in model membranes.* J Biol Chem, 2004. **279**(44): p. 45815-23.
15. Angelova, M.L., and D. S. Dimitrov, *Liposome electroformation.* Faraday Discuss. Chem. Soc, 1986: p. 303-311.
16. Bagatolli, L.A. and E. Gratton, *Two-photon fluorescence microscopy observation of shape changes at the phase transition in phospholipid giant unilamellar vesicles.* Biophys J, 1999. **77**(4): p. 2090-101.
17. Prosser, R.S., J.S. Hwang, and R.R. Vold, *Magnetically aligned phospholipid bilayers with positive ordering: a new model membrane system.* Biophys J, 1998. **74**(5): p. 2405-18.
18. C. H. Wu, A.R., and S. J. Opella, *High-resolution heteronuclear dipolar solid-statenmr-spectroscopy.* Journal of Magnetic Resonance Series A, , 1994(109): p. 270–272.
19. Dvinskikh, S., et al., *A high-resolution solid-state NMR approach for the structural studies of bicelles.* J Am Chem Soc, 2006. **128**(19): p. 6326-7.
20. John D. Gross, D.E.W., and Robert G. Griffin, *Dipolar Recoupling in MAS NMR: A Probe for Segmental Order in Lipid Bilayers* J. Am. Chem. Soc, 1997. **119**: p. 796 -802.
21. Coutte, L., et al., *Subtilisin-like autotransporter serves as maturation protease in a bacterial secretion pathway.* EMBO J., 2001. **20**(2726): p. 5040-5048.

22. Rapaport, D., S. Nir, and Y. Shai, *Capacities of pardaxin analogues to induce fusion and leakage of negatively charged phospholipid vesicles are not necessarily correlated.* Biochemistry, 1994. **33**(42): p. 12615-24.
23. Rapaport, D., et al., *pH- and ionic strength-dependent fusion of phospholipid vesicles induced by pardaxin analogues or by mixtures of charge-reversed peptides.* Biochemistry, 1993. **32**(13): p. 3291-7.
24. Rapaport, D. and Y. Shai, *Aggregation and organization of pardaxin in phospholipid membranes. A fluorescence energy transfer study.* J Biol Chem, 1992. **267**(10): p. 6502-9.
25. Lelkes, P.I. and P. Lazarovici, *Pardaxin induces aggregation but not fusion of phosphatidylserine vesicles.* FEBS Lett, 1988. **230**(1-2): p. 131-6.
26. Thennarasu, S. and R. Nagaraj, *Solution conformations of peptides representing the sequence of the toxin pardaxin and analogues in trifluoroethanol-water mixtures: analysis of CD spectra.* Biopolymers, 1997. **41**(6): p. 635-45.
27. Shi, Y.L., C. Edwards, and P. Lazarovici, *Ion selectivity of the channels formed by pardaxin, an ionophore, in bilayer membranes.* Nat Toxins, 1995. **3**(3): p. 151-5.
28. Primor, N., *Pharyngeal cavity and the gills are the target organ for the repellent action of pardaxin in shark.* Experientia, 1985. **41**(5): p. 693-5.
29. Steiner, H., D. Andreu, and R.B. Merrifield, *Binding and action of cecropin and cecropin analogues: antibacterial peptides from insects.* Biochim Biophys Acta, 1988. **939**(2): p. 260-6.
30. van den Bogaart, G., et al., *The lipid dependence of melittin action investigated by dual-color fluorescence burst analysis.* Biophys J, 2007. **93**(1): p. 154-63.
31. Chen, H.M., et al., *Kinetics of membrane lysis by custom lytic peptides and peptide orientations in membrane.* Eur J Biochem, 2001. **268**(6): p. 1659-69.
32. Matsuzaki, K., et al., *Physicochemical determinants for the interactions of magainins 1 and 2 with acidic lipid bilayers.* Biochim Biophys Acta, 1991. **1063**(1): p. 162-70.
33. Kuchinka, E. and J. Seelig, *Interaction of melittin with phosphatidylcholine membranes. Binding isotherm and lipid head-group conformation.* Biochemistry, 1989. **28**(10): p. 4216-21.
34. Johnson, K.A., Z.B. Simpson, and T. Blom, *Global Kinetic Explorer: A new computer program for dynamic simulation and fitting of kinetic data.* Anal Biochem, 2009. **387**(1): p. 20-9.
35. Ambroggio, E.E., et al., *Direct visualization of membrane leakage induced by the antibiotic peptides: maculatin, citropin, and aurein.* Biophys J, 2005. **89**(3): p. 1874-81.
36. Tamba, Y. and M. Yamazaki, *Single giant unilamellar vesicle method reveals effect of antimicrobial peptide magainin 2 on membrane permeability.* Biochemistry, 2005. **44**(48): p. 15823-33.
37. Dvinskikh, S.V., et al., *High-resolution 2D NMR spectroscopy of bicelles to measure the membrane interaction of ligands.* J Am Chem Soc, 2007. **129**(4): p. 794-802.
38. Gottler, L.M. and A. Ramamoorthy, *Structure, membrane orientation, mechanism, and function of pexiganan - A highly potent antimicrobial peptide designed from magainin.* Biochim Biophys Acta, 2008.
39. Marcotte, I., et al., *Interaction of antimicrobial peptides from Australian amphibians with lipid membranes.* Chem Phys Lipids, 2003. **122**(1-2): p. 107-20.
40. Koenig, B.W., J.A. Ferretti, and K. Gawrisch, *Site-specific deuterium order parameters and membrane-bound behavior of a peptide fragment from the intracellular domain of HIV-1 gp41.* Biochemistry, 1999. **38**(19): p. 6327-34.
41. Yang, L., et al., *Barrel-stave model or toroidal model? A case study on melittin pores.* Biophys J, 2001. **81**(3): p. 1475-85.
42. Sengupta, D., et al., *Toroidal pores formed by antimicrobial peptides show significant disorder.* Biochim Biophys Acta, 2008. **1778**(10): p. 2308-17.

43. Murzyn, K. and M. Pasenkiewicz-Gierula, *Construction of a toroidal model for the magainin pore.* J Mol Model, 2003. **9**(4): p. 217-24.
44. Wi, S. and C. Kim, *Pore structure, thinning effect, and lateral diffusive dynamics of oriented lipid membranes interacting with antimicrobial peptide protegrin-1: 31P and 2H solid-state NMR study.* J Phys Chem B, 2008. **112**(36): p. 11402-14.
45. Wieprecht, T., et al., *Influence of the angle subtended by the positively charged helix face on the membrane activity of amphipathic, antibacterial peptides.* Biochemistry, 1997. **36**(42): p. 12869-80.
46. Oren, Z. and Y. Shai, *Selective lysis of bacteria but not mammalian cells by diastereomers of melittin: structure-function study.* Biochemistry, 1997. **36**(7): p. 1826-35.

FIGURE LEGENDS

Figure 1. CD spectra of 20 μM Pardaxin in 20 mM PBS buffer pH 7.5 in the prescence of TFE (○), DPC(□), 100 % DOPC vesicles(◊), 20%DOPG - 80% DOPC vesicles(+).

Figure 2: Two representative time profiles from the calcein release experiments. The addition of Pardaxin to DOPC: PG vesicles at pH 8 shows a step-type time profile that can be fitted to a triple exponential decay, while Pardaxin at all other conditions (pH 5.5-10 and both vesicle types) follows a double-exponential decay.

Figure 3 Maximum release of calcein by Pardaxin from (A) DOPC vesicles and (B) 20 % DOPG and 80 % DOPC vesicles at pH 5.5, 8 and 10. In all the experiments the lipid concentration was held constant at 20 μM

Figure 4 the $t_{(1/2)}$ for both the initial (A & C) and the second phase (B & D) of the calcein release plotted for DOPC (top) and 20% DOPG & 80 %DOPC vesicles as a function of the protein concentration.

Figure 5: Time course of the fluorescence from a water soluble fluorophor (green) and a membrane specific (blue) after the addition of 5 μM Pardaxin to GUV composed of DOPC (top) and 20% DOPG & 80 % DOPC (bottom).

Figure 6:Static solid state natural abundance NMR data of oriented PC or PC/PG bicelles with and with out pardaxin. (a) 2D PISEMA spectrum of a PC bicelle with Pardaxin.[21] 1D slices from 2D PISEMA spectra of PC bicelles with(black) and without(red) Pardaxin. From b to d the slices represent Ca, C3 and C14. (e-g) 1D slices from 2D PISEMA spectra of PC:PG bicelles with(black) and without(red) Pardaxin.(h) 14-O-PC molecule size of spheres represent are proportional to measured order parameter in pure PC:PG bicelles, larger means less ordered. The colors represent the relative change in order parameter as Pardaxin is added. More disordered sites are blue while more ordered sites are red white is no measured change. (i) 14-O-PC with order parameters and relative change in order parameters for Pardaxin added to PC:PG bicelles.

Vad et al. Figure 1

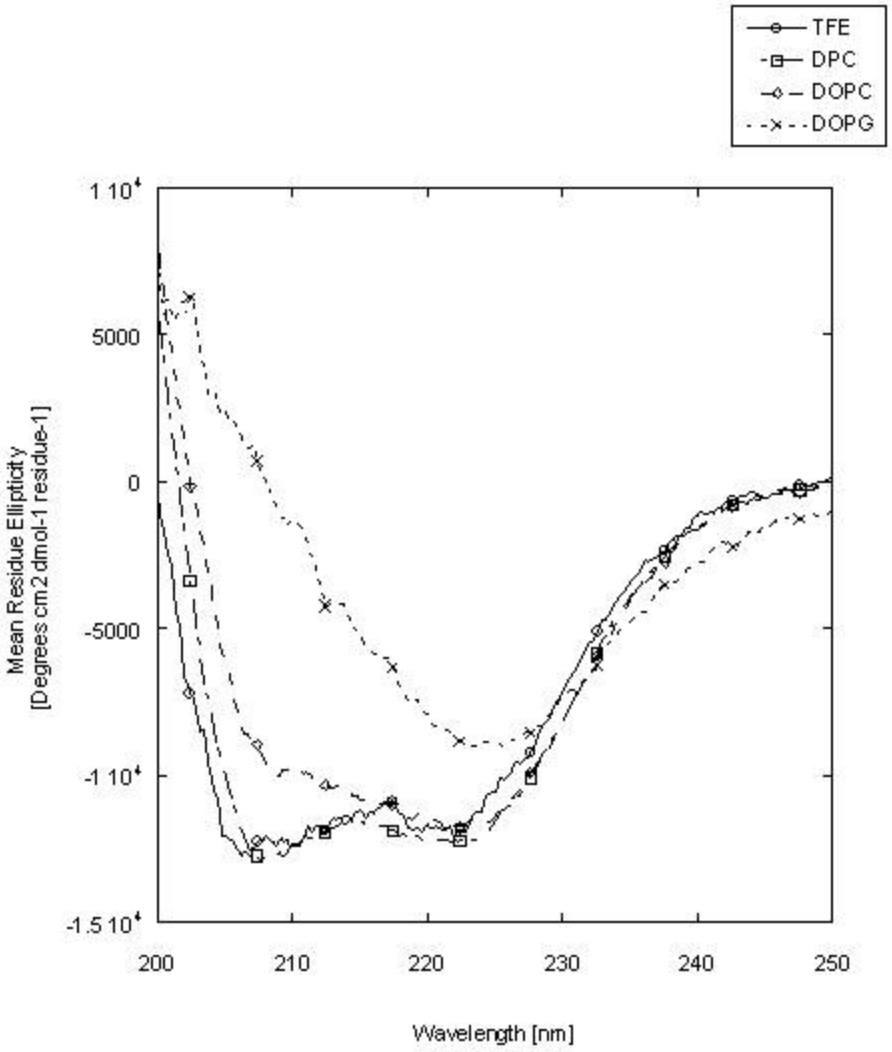

Vad et al. Figure 2

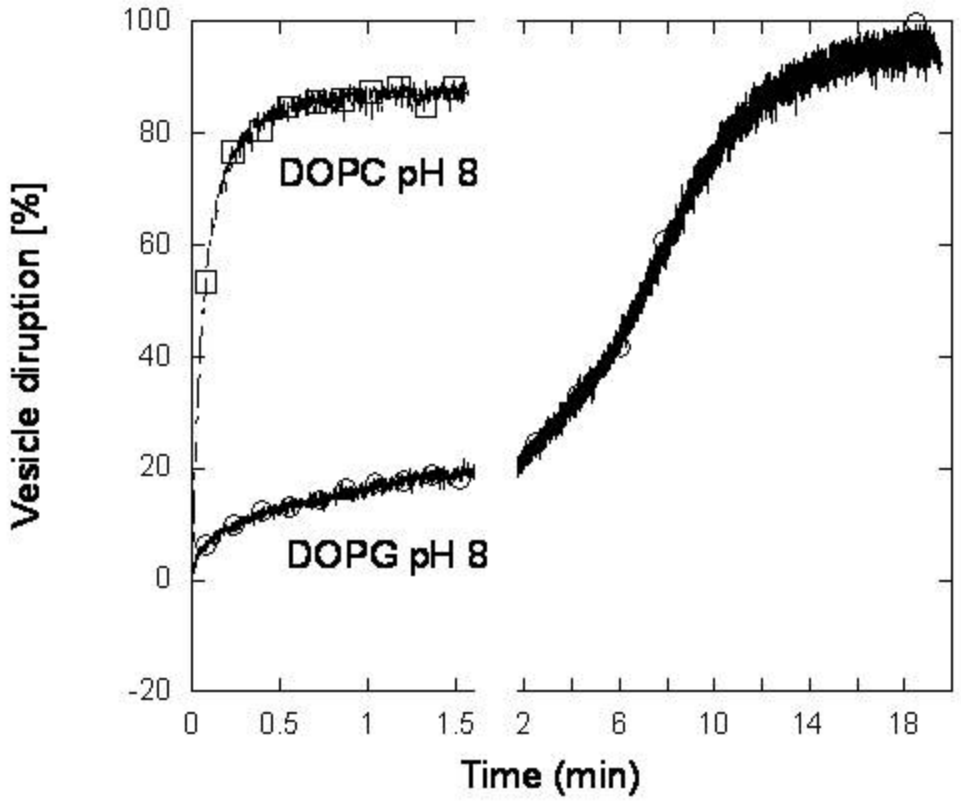

Vad et al. Figure 3

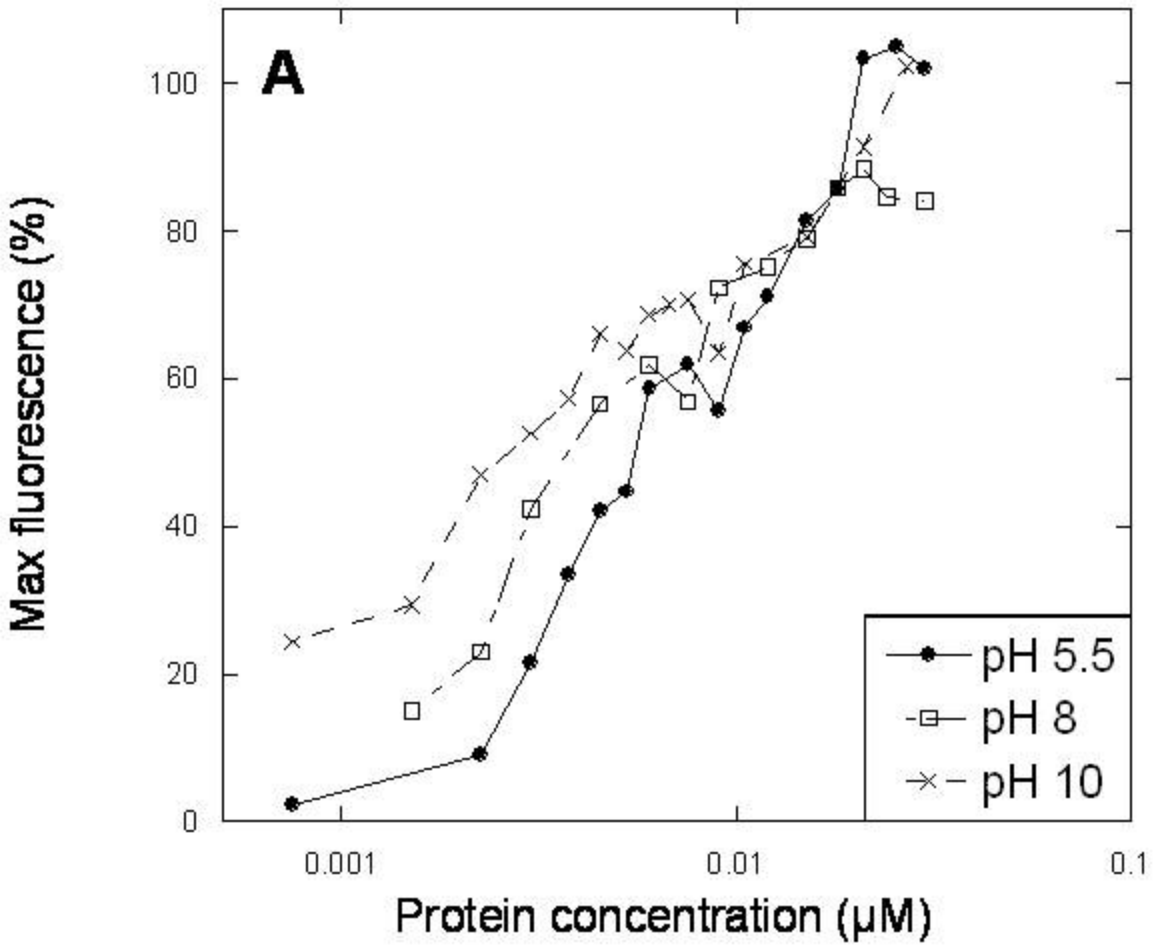

Vad et al. Figure 3

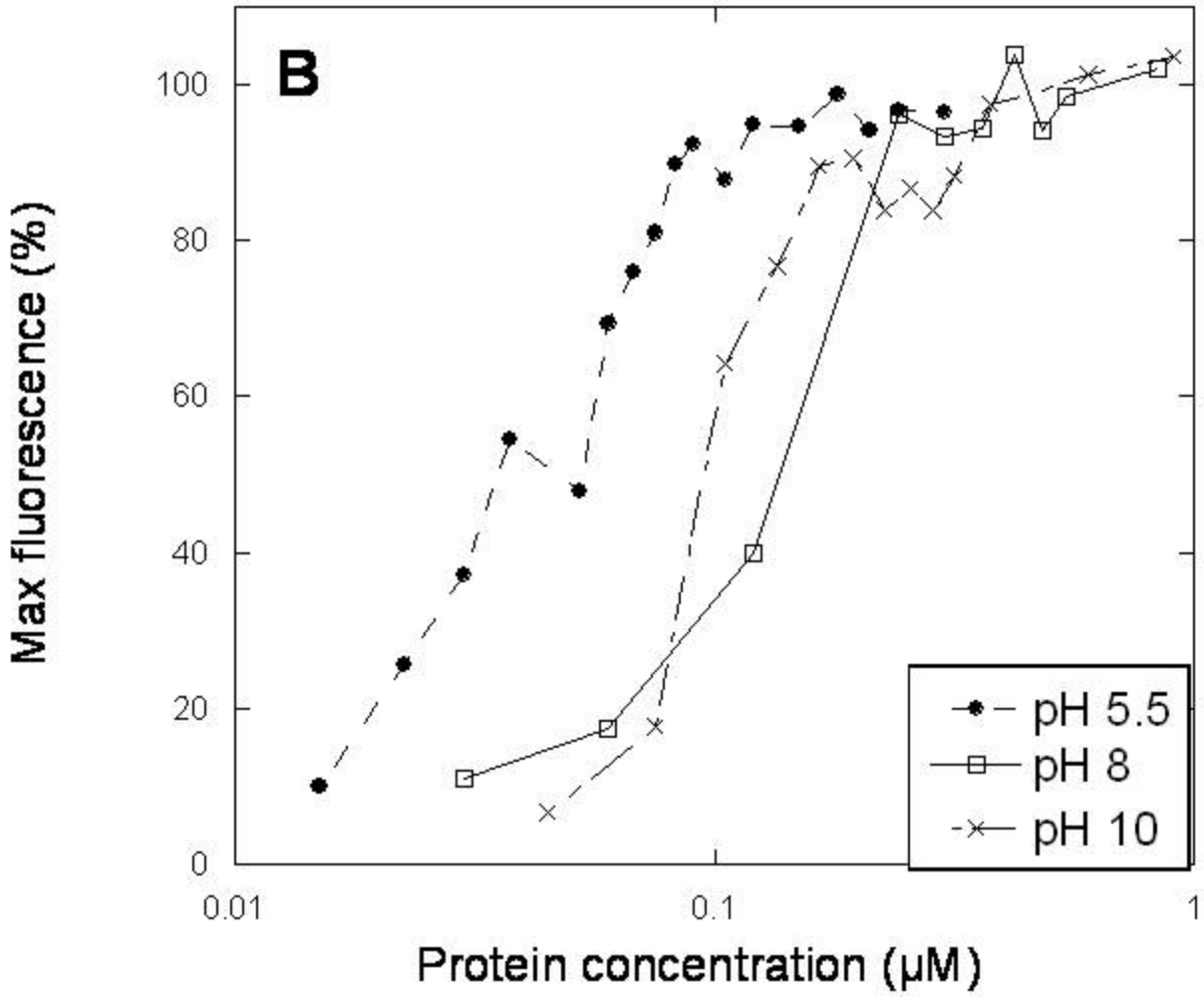

Vad et al. Figure 4

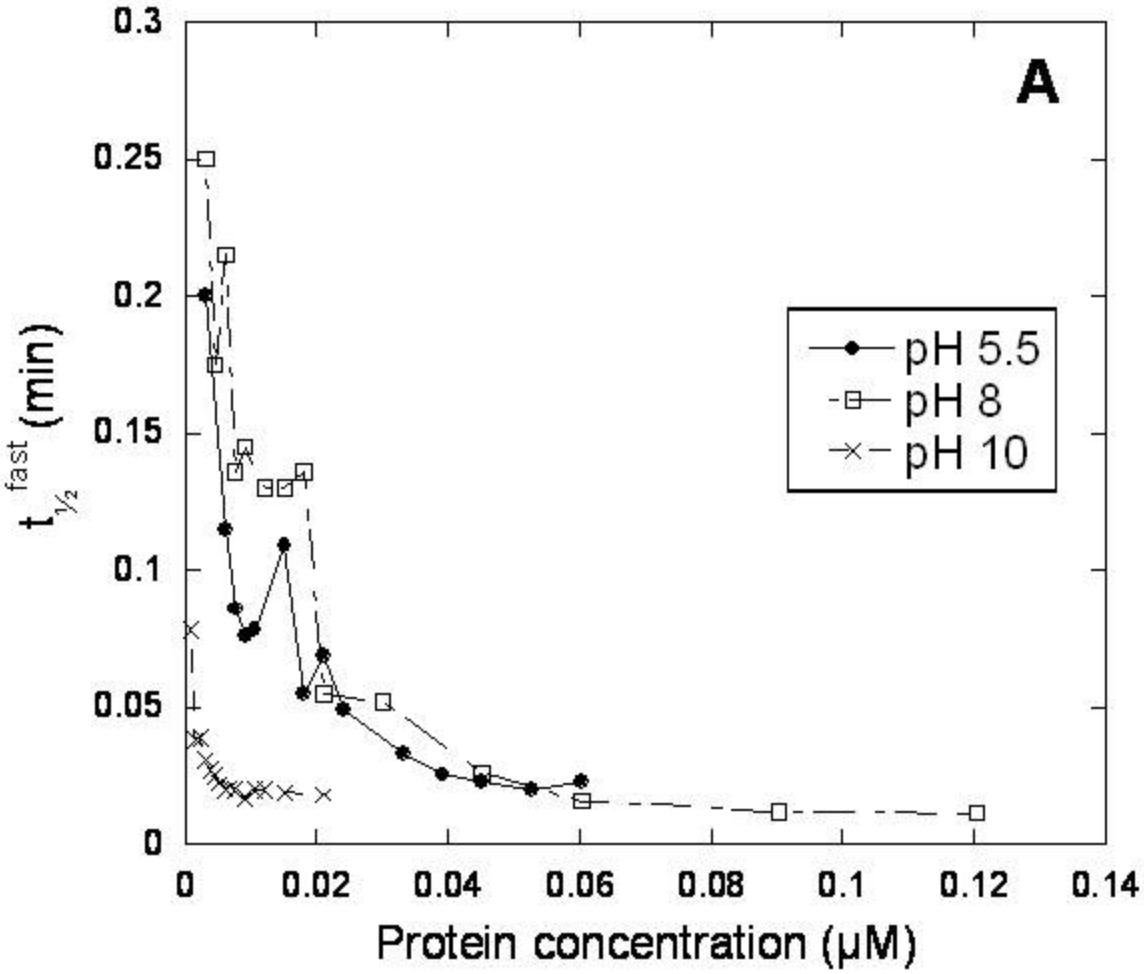

Vad et al. Figure 4

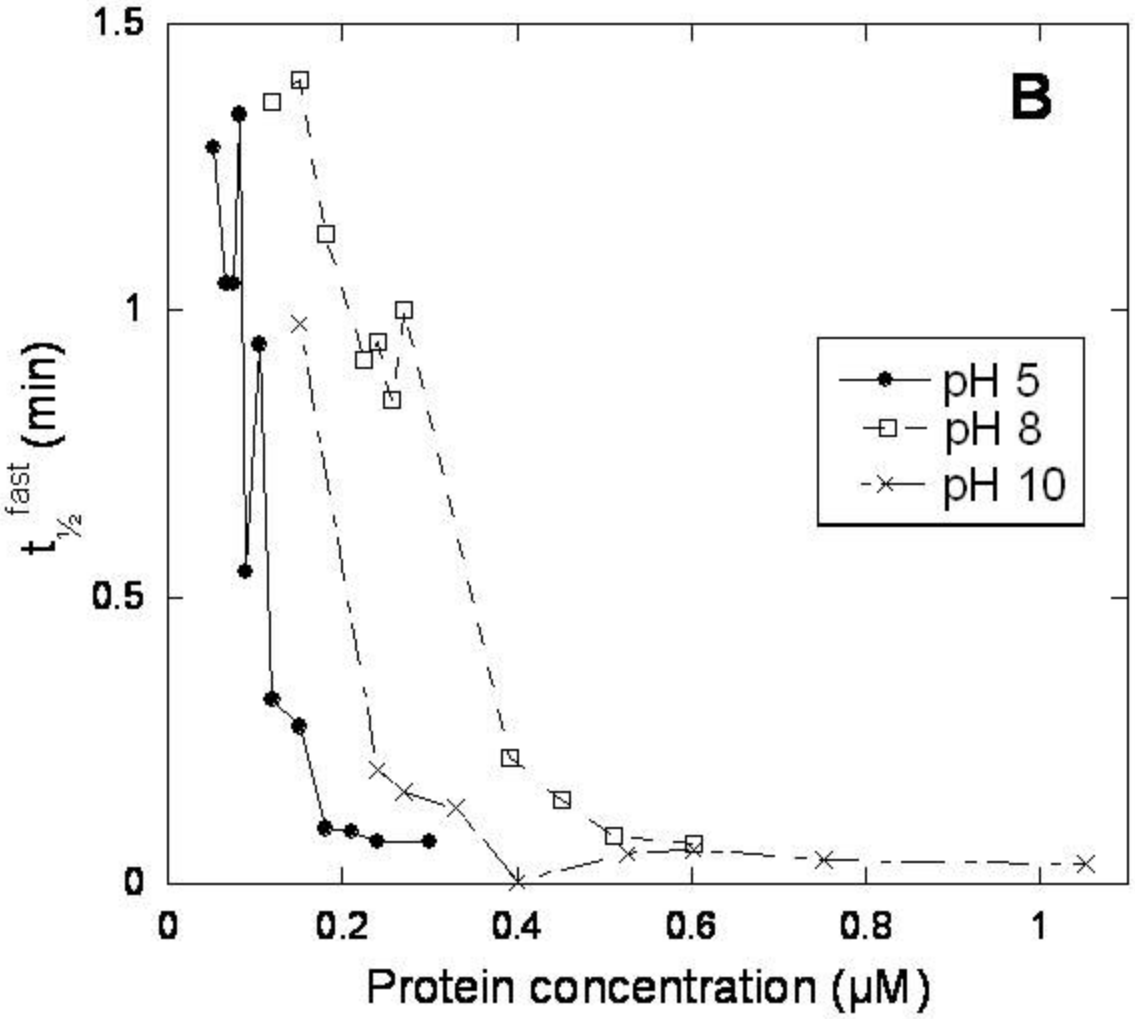

Vad et al. Figure 4

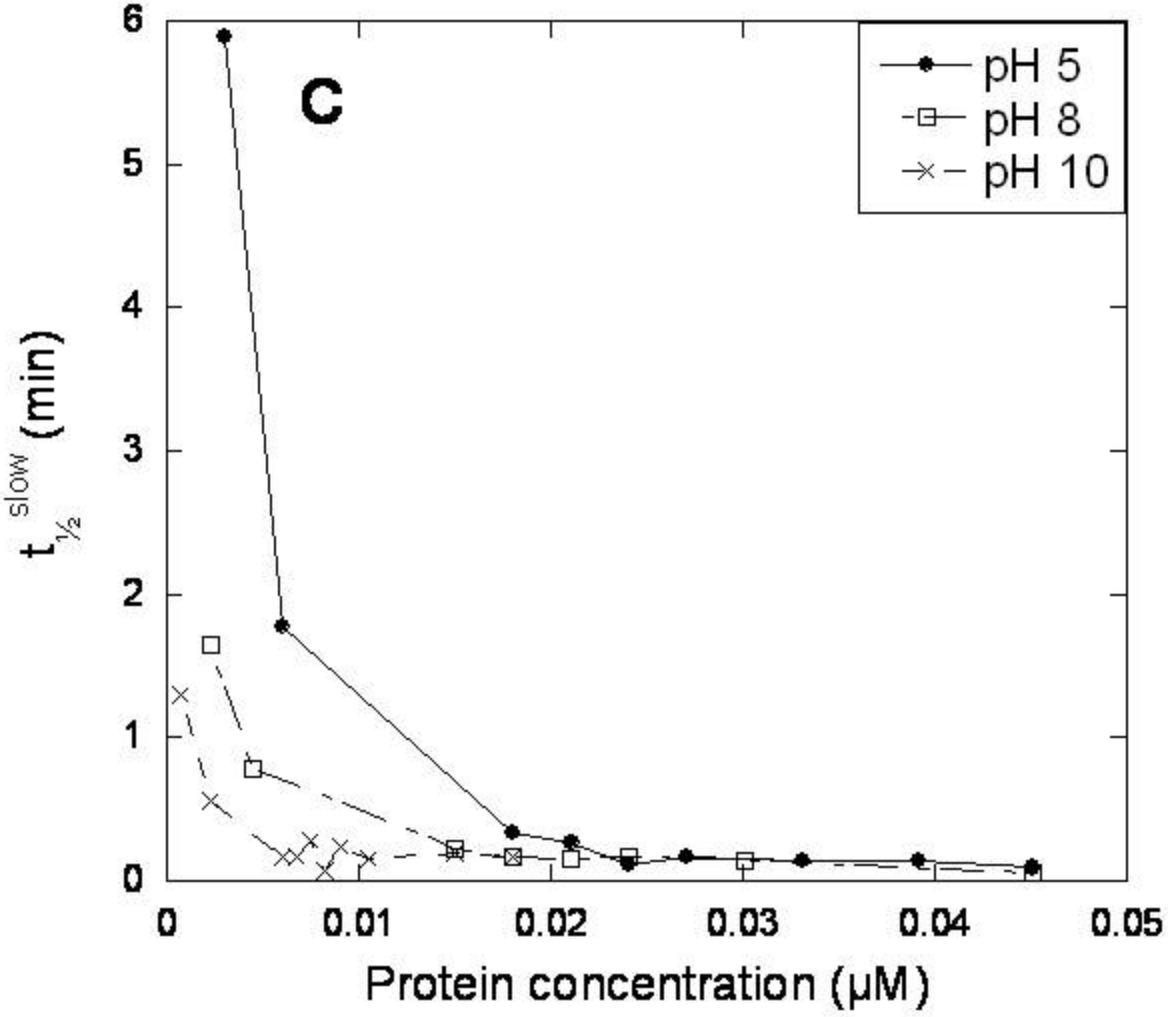

Vad et al. Figure 4

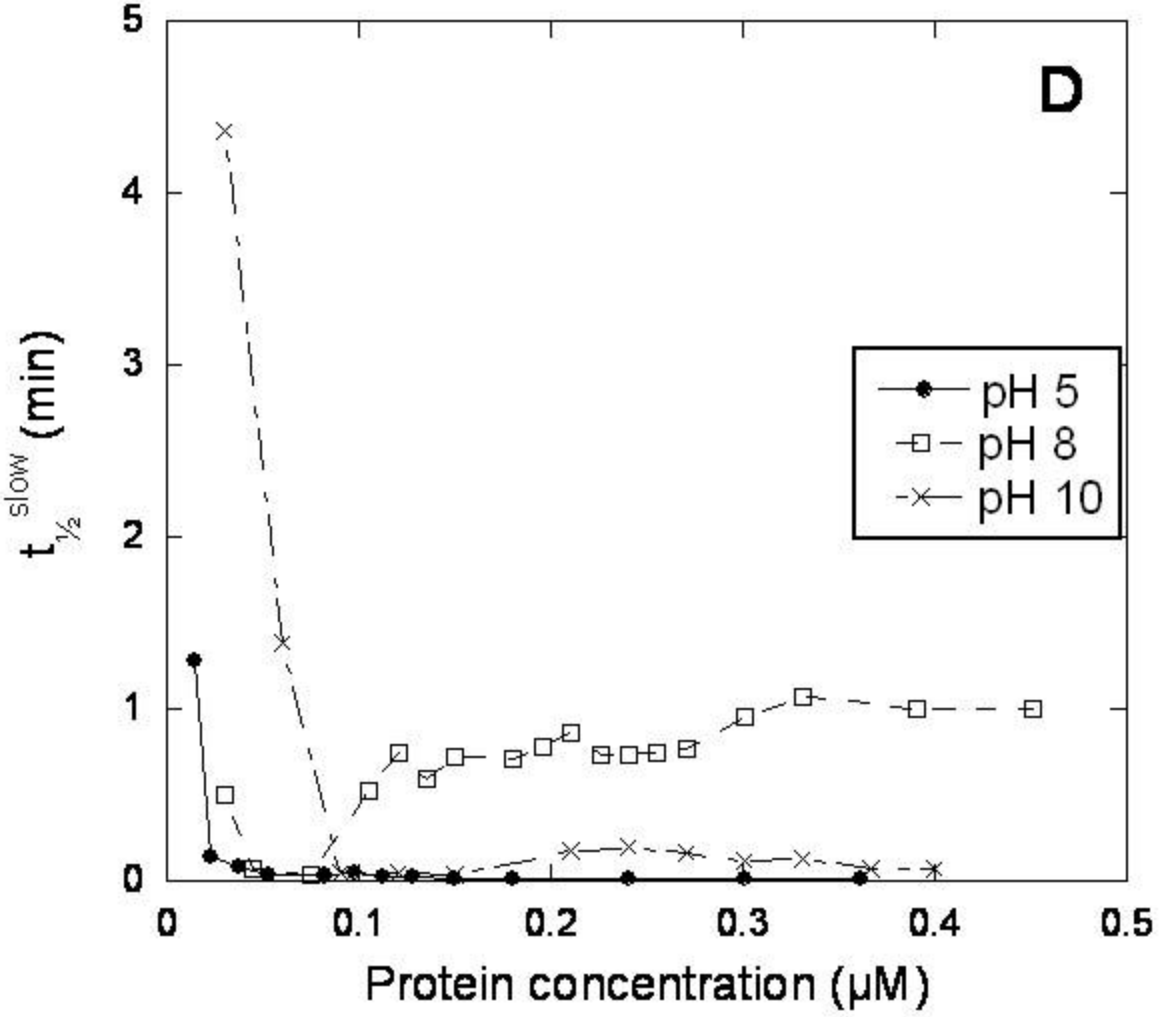

Vad et al. Figure 5

DOPC

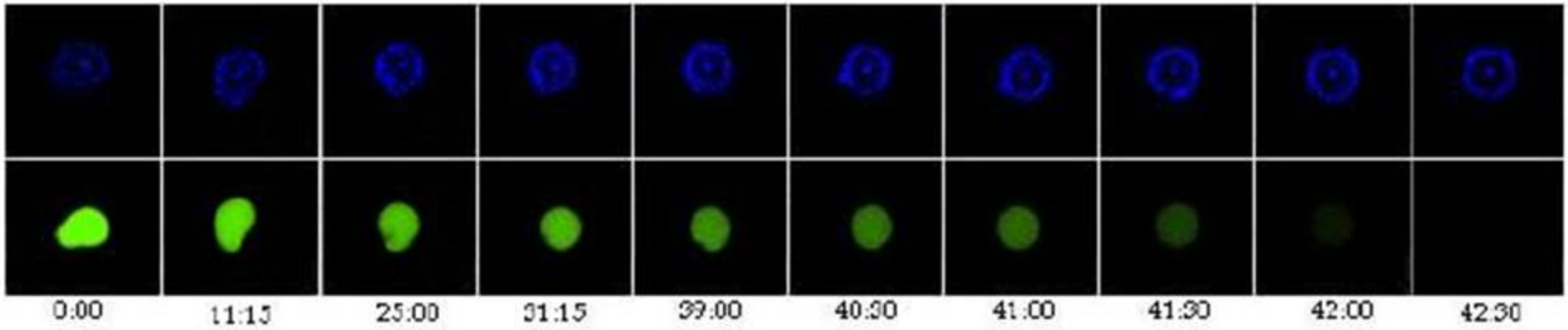

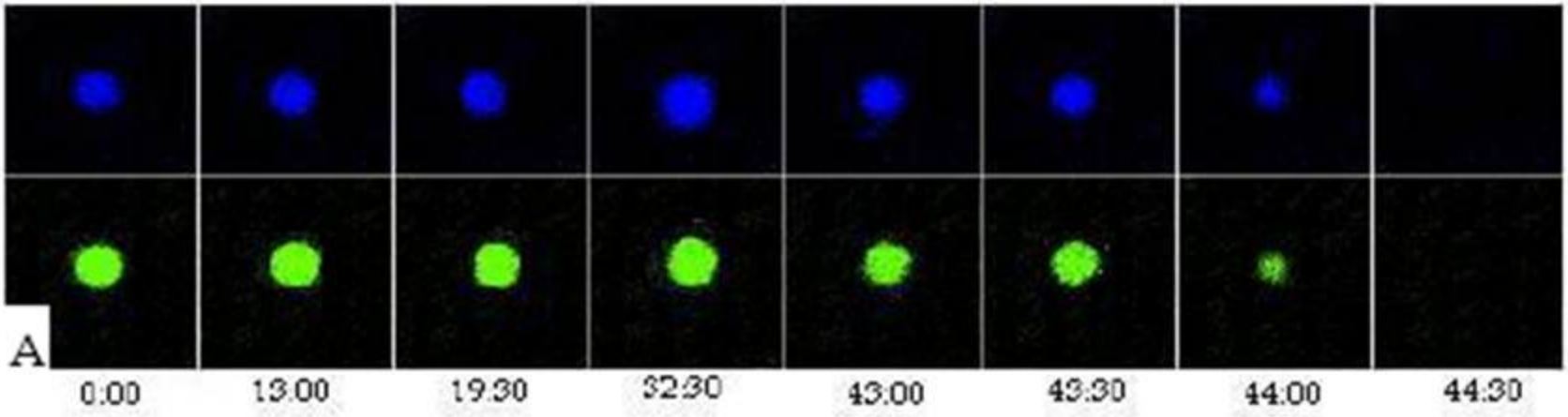

20%DOPG:80% DOPC

Vad et al. Figure 6

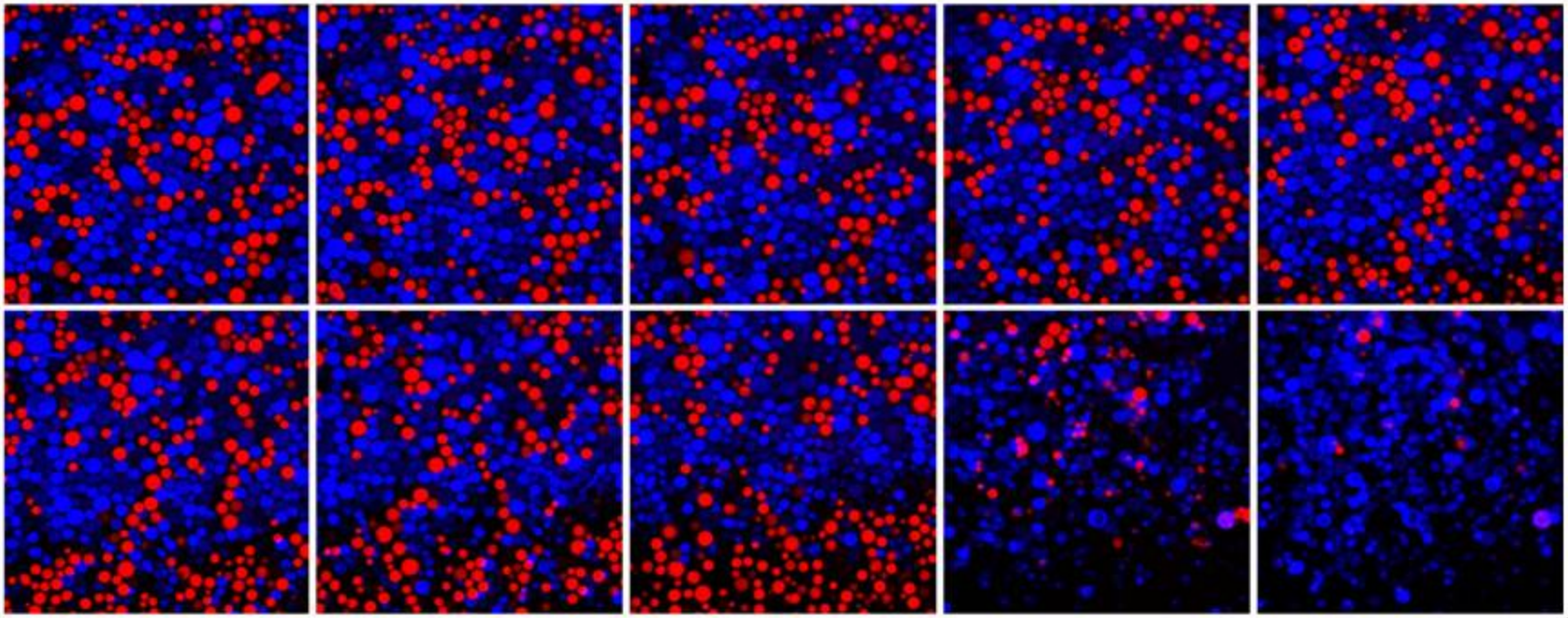

Vad et al. Figure 7

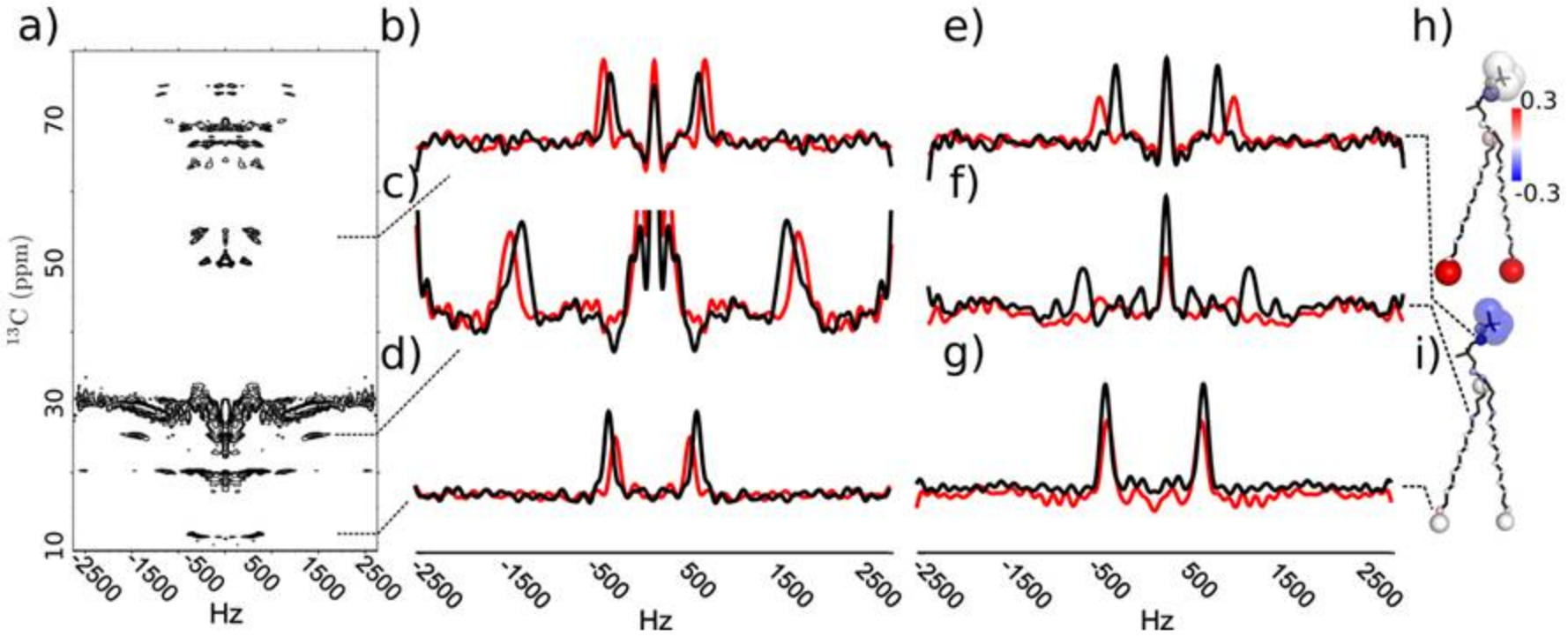

Co-author statement for Paper 3

Nesgaard, L., Vad, B., Christiansen, G. and Otzen, D.: Kinetic partitioning between aggregation and vesicle permeabilization by modified ADan. *Biochim Biophys Acta* (2009) 1794 p. 84-93.

- Lise W. Nesgaard performed all experimental work except electron microscopy and liposome calcein release and wrote the article with Daniel Otzen
- Brian Vad performed and communicated all liposome calcein release work.
- Gunna Christiansen performed all electron microscopy.
- Daniel Otzen supervised design and execution of the experiments, contributed extensively to the writing of the article and took care of submission, revision and galley proofs.

Lise W. Nesgaard	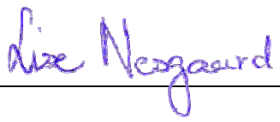	6th of april 2009
Gunna Christiansen	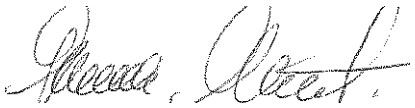	6th of april 2009
Daniel Otzen	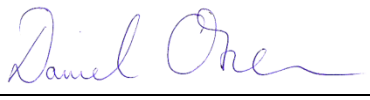	26th March 2009
Brian Vad		6th of april 2009
	Signature	Date

Elsevier Editorial System(tm) for Journal of Molecular Biology
Manuscript Draft

Manuscript Number:

Title: Divorcing Folding from Function: How Acylation Affects the Membrane-perturbing Properties of an Anti-microbial Peptide

Article Type: Full Length Article

Section/Category: Protein and nucleic acid structure, function, and interactions

Keywords: Novicidin; membrane permeabilization; confocal laser scanning microscopy; circular dichrosim; liquid- and solid-state NMR

Corresponding Author: Professor Daniel Otzen, Ph.D.

Corresponding Author's Institution: Aarhus University

First Author: Brian S Vad

Order of Authors: Brian S Vad; Line A Thomsen; Kresten Bertelsen; Magnus Franzmann; Jan M Pedersen; Thomas Vosegaard; Zuzana Valnickova; Troels Skrydstrup; Jan J Enghild; Reinhard Wimmer; Niels Christian Nielsen; Daniel Otzen, Ph.D.

Abstract: Many small cationic peptides, which are unstructured in aqueous solution, have antimicrobial properties. These properties are assumed to be linked to their ability to permeabilize bacterial membranes, accompanied by the transition to an alpha-helical folding state. Here we focus on the link between folding of the antimicrobial peptide Novicidin (Nc) and its membrane permeabilization. N-terminal acylation with C8-C16 alkyl chains, as well as the inclusion of anionic lipids, both increase Nc's ability to form alpha-helical structure in the presence of vesicles. Nevertheless, both acylation and anionic lipids reduce the extent of permeabilization of these vesicles as well as intact E. coli cells, and lead to slower permeabilization kinetics. This suggests that significant induction of alpha-helical structure in this class of antimicrobial peptides is not a

prerequisite for membrane perturbation. Our data suggests that induction of alpha-helical structure rather than facilitating membrane disruption may inhibit it, and that a more peripheral interaction may be a more efficient permeabilization mechanism. Furthermore, acylation leads to a deeper embedding in the membrane, which could lead to an anti-permeabilizing "plugging" effect. We observe multiple modes of interaction between antimicrobial peptides and simple model membranes, suggesting that antimicrobial peptide interactions with bacterial membranes may be even more varied in the complex environment of live bacterial membranes.

Dear Editor,

we hereby submit the article ”Divorcing Folding from Function: How Acylation Affects the Membrane-perturbing Properties of an Anti-microbial Peptide” which we hope you will consider for publication in *Journal of Molecular Biology*. We believe this work is of interest for readers of JMB because it highlights some surprising features about the action of the antimicrobial peptide Novicidin (derived from a slightly longer sheep antimicrobial peptide), namely the lack of coupling between folding and function. Novicidin is unstructured in water and remains predominantly unstructured in the presence of lipid vesicles composed of zwitterionic phospholipids; however, the presence of even a small amount of anionic phospholipids in the vesicles (or the acylation of Novicidin) induces alpha-helical structure. Nevertheless, calcein release assays reveal that Novicidin is in fact more efficient at permeabilizing vesicles under conditions where it is essentially unstructured. We confirm by stopped-flow kinetics that Novicidin appears more peripherally associated with zwitterionic vesicles and back up this analysis with both liquid state NMR (structure of acylated Novicidin and its effect on the immersion of Novicidin into amphiphilic environments) and solid state NMR studies. Finally, we propose a “plugging” effect to explain the reduced permeabilization efficacy of acylated Novicidin. We believe that this work may shed new light on the way in which antimicrobial peptides can work on bacterial membranes.

Yours sincerely

Daniel Otzen

Suggested referees:

1. Burkhard Bechinger, Department of Chemistry, University of Strasbourg, burkhard.bechinger@chimie.u-strasbg.fr.
2. Anne Ulrich, Institute of Organic Chemistry, University of Karlsruhe, 76131 Karlsruhe, Germany. E-mail: anne.ulrich@ibg.fzk.de
3. Y. Shai, Department of Biological Chemistry, The Weizmann Institute of Science, Rehovot 76100, Israel**.** E-mail: Yechiel.Shai@weizmann.ac.il.
4. Luis Bagatolli, Department of Biochemistry and Molecular Biology, University of Southern Denmark, Campusvej 55, DK-5230 Odense M, DENMARK. E-mail: bagatolli@memphys.sdu.dk
5. T. Heimburg, Niels Bohr Institute, University of Copenhagen. theimbu@nbi.dk

6. José-Luis Neira, Department of Molecular and Cellular Biology, University of Miguel Hernandez, jlneira@umh.es.

Divorcing Folding from Function: How Acylation Affects the Membrane-perturbing Properties of an Anti-microbial Peptide

Brian Vad[1,2], Line Aagot Thomsen[2], Kresten Bertelsen[3], Magnus Franzmann[2], Jan Mondrup Pedersen[3], Thomas Vosegaard[3], Zuzana Valnickova[1], Troels Skrydstrup[3], Jan J. Enghild[1], Reinhard Wimmer[2], Niels Chr. Nielsen[3*] and Daniel E. Otzen[1,2*]

[1] *Center for Insoluble Protein Structures (inSPIN), Interdisciplinary Nanoscience Center (iNANO) and Department of Molecular Biology, Gustav Wieds Vej 10C, University of Aarhus, DK-8000 Aarhus C, Denmark*

[2] *Department of Biotechnology, Chemistry and Environmental Engineering, Aalborg University, Sohngaardsholmsvej 49, DK – 9000 Aalborg*.

[3] *Center for Insoluble Protein Structures (inSPIN), Interdisciplinary Nanoscience Center (iNANO) and Department of Chemistry, Langelandsgade 140, University of Aarhus, DK – 8000 Aarhus C, Denmark.*

* To whom correspondence should be addressed at dao@inano.dk, tel. + 45 89 42 46 50, fax + 45 86 12 31 78 (D.E.O.) or ncn@inano.dk, tel. +45 89 42 38 41, fax + 45 86 19 61 99 (N.C.N.).

Running title: Activity, folding and acylation of Novicidin

ABSTRACT

Many small cationic peptides, which are unstructured in aqueous solution, have antimicrobial properties. These properties are assumed to be linked to their ability to permeabilize bacterial membranes, accompanied by the transition to an α-helical folding state. Here we focus on the link between folding of the antimicrobial peptide Novicidin (Nc) and its membrane permeabilization. N-terminal acylation with C8-C16 alkyl chains, as well as the inclusion of anionic lipids, both increase Nc's ability to form α-helical structure in the presence of vesicles. Nevertheless, both acylation and anionic lipids reduce the extent of permeabilization of these vesicles as well as intact *E. coli* cells, and lead to slower permeabilization kinetics. This suggests that significant induction of α-helical structure in this class of antimicrobial peptides is not a prerequisite for membrane perturbation. Our data suggests that induction of α-helical structure rather than facilitating membrane disruption may inhibit it, and that a more peripheral interaction may be a more efficient permeabilization mechanism. Furthermore, acylation leads to a deeper embedding in the membrane, which could lead to an anti-permeabilizing "plugging" effect. We observe multiple modes of interaction between antimicrobial peptides and simple model membranes, suggesting that antimicrobial peptide interactions with bacterial membranes may be even more varied in the complex environment of live bacterial membranes.

Abbreviations used: CD, circular dichroism; D-Nc, Novicidin consisting of D-amino acids; Nc, Novicidin; Nc-CX, N-terminally acylated Nc where X refers to the number of carbon atoms in the acyl chain; PRE, paramagnetic relaxation enhancement.

Keywords: Novicidin; membrane permeabilization; confocal laser scanning microscopy; circular dichrosim; liquid- and solid-state NMR; peptide acylation.

INTRODUCTION

Over the past two decades, more than 800 antimicrobial peptides (AMPs) have been reported from sources as diverse as animals, plants, insects, and fungi [1; 2; 3; 4]. As parts of the innate immune system in vertebrates, AMPs are often the first line of defence against an invading organism, and thus show activity against a broad range of targets. Microorganisms do not easily evolve resistance to them, making them of great interest as alternatives to small-molecule antibiotics. Over the recent few years significant resources have been directed towards their commercialization. So far, only a few products have succeeded, while several promising candidates have been halted because of adverse effects or effects similar to existing antibiotics [5]. The lack of success most likely reflects limited understanding of their mechanism of action and microbial specificity. At present the common procedure is to search for naturally occurring AMP´s and then subsequently mutate them to change their specificity [6; 7; 8; 9; 10]. More detailed insight into AMP activity may ultimately allow design *in silico* [11].

AMPs are generally understood to target the bacterial plasma membrane and can do so in a variety of ways, including a barrel-stave model, a carpet model, and a toroidal pore model [12]. In the barrel-stave model, the peptides completely traverse the membrane by pore formation, quickly ruining the electrochemical gradient and killing the cell. This mode of action is mostly driven by hydrophobic interactions between an amphipatic peptide and the lipid's acyl chains and is therefore less specific towards membranes of different lipid compositions. A minimum of 22 and 8 amino acids is necessary to straddle the bacterial membrane for an α-helical- and a β-sheet peptide, respectively. In the carpet model, the positively charged peptides cover the membrane surface in a carpet-like fashion until they reach a concentration where they permeabilize the cell by disrupting the membrane curvature. As opposed to the barrel-stave model, the peptide does not need to assume a specific oligomeric structure and the peptides are always in contact with the lipid headgroups at the interface with the acyl chains. This mode of action is more sensitive to the lipid headgroup charge, explaining why it is more specific towards the negatively charged surface of bacteria [13; 14; 15]. Finally, the toroidal-pore model is a mixture between the carpet model and the barrel-stave model. Defined pores are formed as in the barrel-stave model but the peptides lie in the lipid headgroup-acyl chain interface. This is possible because the peptides induce a sharp bending of the lipids so that lipid headgroups can line the interior of the pore.

It may be possible to modulate the mode of antimicrobial action, and thus the spectrum of applications, by modifying the AMPs with acyl chains, since this modification will increase AMP hydrophobicity and potentially also its membrane affinity. This has been studied in two different approaches: Makovitzki *et al.* [16] synthesized tetrapeptides with acyl chains of length 8-16 (number carbons in the acyl chain) and found that the tetrapeptides conferred bacterial species specificity while their aggressiveness correlated with acyl chain length. The same group also showed that conjugation of the AMP magainin with acyl chains of length 7, 11, and 16 had important effects on magainin activity, with the membrane permeabilizing ability increasing uniformly with chain length. Furthermore, the attachment of the acyl chains also resulted in a change of the secondary structure of C11 magainin and C16 magainin in solution from that of the wildtype Magainin. While the C7-Magainin, like the wild type, was disordered and monomeric in solution, both C11 Magainin and C16 Magainin adopted α-helical structure. The C11 Magainin was only α-helical above a threshold concentration indicating detergent-like properties in which the protein assumed an α-helical structure in the micellar state. In contrast, C16 Magainin remained α-helical at all investigated concentrations, suggesting that the longer acyl chain was able to sequester the hydrophobic residues in the folded Magainin at the monomer level.

To explore in greater detail how acylation can modulate membrane binding properties, we report here a detailed study on the effect of acylation on the AMP Novicidin (Nc) [7; 17; 18; 19; 20]. This AMP is a variant of the 18-residue Ovispirin, which in turn is derived from the N-terminal region of the cathelicidin peptide SMAP-29 from sheep. Ovispirin (sequence KNLRR IIRKI IHIIK KYG) showed unacceptably high haemolytic activity, but the mutation Ile10→Gly (Novispirin) reduced this to more appropriate levels. Subsequently, the C-terminal mutation Gly18→Phe (Novicidin, abbreviated Nc) led to improved efficacy towards microorganisms (personal communication, Hans-Henrik Kristensen). Novispirin and Nc are unstructured in solution but readily adopt α-helical structures in the presence of anionic lipids and detergents, as well as to a smaller extent in the presence of cationic and zwitterionic detergents [21], in agreement with its amphipathic character (Fig. 1A). We focus on the structural and vesicle-disruptive properties of Nc, its D-amino acid diastereomer D-Nc, and its N-terminally acylated derivatives. Surprisingly, we find that the induction of measurable amounts of α-helical structure is not a prerequisite for membrane permeabilizing properties and that acylation actually reduces

permeabilization efficiency. We suggest that a more peripheral membrane contact may be the most productive mode of action for at least some AMPs.

RESULTS

Interaction of Nc and acyl derivatives with lipids

We start by analyzing the degree to which zwitterionic (100% DOPC) and mixed, partially anionic (80% DOPC:20% DOPG) lipid vesicles induce structure in the different Nc variants. These vesicles were used as simple mimics of the mammalian plasma membrane (predominantly zwitterionic) and the outer leaflet of the bacterial cell membrane (at least 25% anionic lipid in *E. coli*). The secondary structure of Nc, D-Nc, and the acylated derivatives (termed Nc-CX, where X refers to the number of carbon atoms in the acyl chain) was monitored by far-UV CD. Figure 1B shows the CD spectra of Nc, D-Nc, Nc-C8, Nc-C12, and Nc-C16. Note that the CD spectrum of D-Nc is the mirror image of Nc because of its D-amino acids. Nc, D-Nc, Nc-C8, and low concentrations (40 μM) of Nc-C12 display CD spectra characteristic of a random coil. At high concentrations (200 μM), the CD spectrum of Nc-C12 changes to a distinct α-helical profile with minima at 209 and 222 nm. Nc, D-Nc, and Nc-C8 remain unstructured at 200 μM (data not shown). The CD spectrum of C16 is primarily α-helical over the entire accessible concentration range (20-200 μM). In the presence of 0-2 mg/ml DOPC, Nc and D-Nc shows only a slight change in their CD spectra, retaining the features of a random coil structure (data not shown) though there is a small increase in ellipticity between 0 and 2 mg/ml lipid (Fig. 2A). This agrees with the observation that high (several hundred mM) concentrations of non-ionic and zwitterionic surfactant are required to induce helical structure in the closely related peptide Novispirin [21]. In contrast, Nc-C8 and Nc-C12 both change from random coil to α-helical structure with increasing concentrations of lipid over the range probed (data for Nc-C8 shown in Fig. 1B). In the presence of DOPC:PG vesicles, the spectra of Nc, Nc-C8, and Nc-C12 changed dramatically from random coil to α-helix (representative spectra shown in Fig. 1B, summarized in Fig. 2B). The ellipticity at 208 nm, which is indicative of α-helical structure, shows a reasonably linear increase with lipid concentration, apart from a more hyperbolic behavior for Nc-C12 in DOPC (Fig. 2A). As we have previously reported for Novispirin [21], this slope most likely represents the initial linear stage of a hyperbolic binding curve, whose slope (summarized in Table 1) is directly proportional to the lipid binding affinity. To avoid artifacts from light scattering, we did not record data at higher lipid concentrations. For both lipid compositions, wt

Nc shows the lowest lipid affinity of all the peptides (measured in terms of α-helix induction), although it has a clear preference for DOPC:PG vesicles where the slope is ~7 times higher. Nc-C12 has slightly greater affinity for DOPC than Nc-C8, but the switch to DOPC:PG vesicles only increases Nc-C12 affinity by around 30% while that of Nc-C8 increases 5-fold. D-Nc displays an affinity towards mixed lipids similar to those of Nc-C8. The CD spectra of Nc-C16 remained essentially unchanged by the addition of both lipid types.

Acylation leads to a marked decrease in the efficiency of lipid permeabilization

We now turn to a functional analysis of the Nc peptides, *i.e.* their ability to permeabilize vesicles, using a manual calcein release assay. We prepared LUV´s containing calcein at a concentration (50 mM) in which calcein fluorescence is self-quenched, and measured the release of calcein as function of peptide concentration, using the addition of Triton X-100 to obtain the fluorescence level associated with 100% release. The presence of calcein did not affect the ability of lipids to induce structural changes in the peptides (data not shown), nor did Triton X-100 influence the fluorescence of calcein (data not shown).

Three distinct calcein release patterns were observed (Fig. 3A): (*i*) instantaneous (<10 s) calcein release, followed by a steady baseline, (*ii*) relatively rapid release of calcein which could be described by first order kinetics with a plateau being reached after a few minutes, or (*iii*) rapid overshoot of fluorescence to a value well above that of free calcein, followed by a decrease to a signal corresponding to roughly 100 % calcein release. The fraction of calcein released as a function of peptide concentration in the two different lipid compositions is illustrated in Fig. 3B-C. The efficacy of release is quantified by the amount of peptide needed to effectuate 50% calcein release (R_{50}). In all cases, very high concentrations of peptide lead to a drop in calcein release (data not shown), possibly due to vesicle aggregation (*vide infra*).

The ranking order of the lipolytic effect of the peptides is as follows (summarized in Fig. 3D): Nc > D-Nc > Nc-C8 > Nc-C16 > Nc-C12. For all of the peptides, it was apparent that R_{50} increased in DOPC:PG vesicles. The ratio $R_{50}^{DOPC:PG}/R_{50}^{DOPC}$ (the higher this ratio, the greater the preference for DOPC) decreased in the order Nc>Nc-C8>D-Nc-Nc-C12-Nc-C16, reaching a plateau of around 3 for D-Nc, Nc-C12 and Nc-C16. This indicates that the more hydrophobic the peptide, the lower the preference for DOPC vesicles. Interestingly, it also highlights a change in the lipid affinity between D- and L-Nc. For Nc-C8 and Nc-C12 these permeabilization data

contrast with the structural data provided by CD, which reveal that acylation decreases the preference for DOPC:PG vesicles in terms of inducing α-helicity.

Exposure of *E. Coli* to Nc variants show that acylation reduces the efficacy of Nc as an antimicrobial peptide

To compare the data on synthetic vesicles with Nc's biological targets, *i.e.* bacteria, we measured the lysis of *E. Coli* at different concentrations of the Nc variants. Lysis was measured by the release of cytosolic β-galactosidase, monitored by the hydrolysis of the chromogenic substrate *o*-nitrophenyl galactose. All peptides lead to the same level of release at concentrations around 20-40 μM (Fig. 4), but differ at lower concentrations. When we quantify this as $[NcX]^{50\%}$, the concentration of Nc at which release is 50% of the maximal value, we obtain a value of ~1 μM for Nc wildtype and values of 5-7 μM for all 3 acylated peptides. Thus, both in calcein assays and biological assays, unacylated Nc permeabilizes more efficiently than acylated Nc.

Fluorescence anisotropy measurements show that Nc mobility is decreased upon mixing with DOPC and DOPC:PG vesicles

The calcein release measurements indicate that Nc binds to and permeabilizes both neutral and partially anionic vesicles, although CD titration data show that α-helical structure is only induced in the partially anionic vesicles. This suggests that induction of α-helix structure in peptides that are unstructured in solution is not a prerequisite for AMP action. To monitor binding independent of folding, we used a Dansyl-labelled variant of unacylated Nc to measure how the fluorescence anisotropy of the dansyl group changes as lipid is added. Immobilization of the peptide on the vesicle surface is expected to lead to a significant increase in anisotropy. Upon increasing the concentrations of lipid, we observe a hyperbolic binding curve which for both DOPC and DOPC:PG vesicles reaches a plateau at a lipid:protein molar ratio of ~250 (Fig. 5). Lipids were added stepwise to a single Nc solution. We were able to probe higher lipid:peptide ratios than in the CD experiments because of the low concentrations of Nc required for these experiments. To obtain reproducible results, we had to let the system equilibrate for a few minutes, particularly at the lower concentrations. This is most likely due to reorganization of the lipids into micellar-like structures as we can see from our calcein-release measurements that the

binding happens on a much faster timescale. We observe a slightly larger increase in fluorescence anisotropy for the DOPC vesicles. This could tentatively be interpreted as increased propensity to aggregate and thus permeabilize these vesicles compared to DOPC:PG vesicles (cf. Fig. 3D).

Dansyl-labelled Nc highlights differences in peptide insertion into different lipids

We combined the time-resolution of stopped-flow kinetics with the environmental sensitivity of a Dansyl fluorophor, attached to the N-terminus of unacylated Nc, to investigate the coupling between peptide binding and calcein release. When Dansyl-Nc is mixed with DOPC vesicles, we observe a slight increase in Dansyl fluorescence prior to vesicle disruption (indicated by the increase in calcein fluorescence), indicating a modest degree of peptide interaction with the membrane before disruption (Fig. 6A). However, when Dansyl-Nc is added to DOPC:PG vesicles, we observe a 10-fold higher increase in Dansyl fluorescence (compared to DOPC), which also precedes vesicle disruption (Fig. 6B). This increased Dansyl-fluorescence in DOPC:PG vesicles compared to DOPC vesicles indicates that Novicidin undergoes a greater change in environmental polarity when it inserts into DOPC:PG vesicles. This suggests that Nc inserts more deeply into the DOPC:PG membrane than into the pure DOPC membrane. We also observe an additional increase in Dansyl fluorescence during the process of calcein release from DOPC:PG vesicles, suggesting a further rearrangement of Dansyl-Nc in the DOPC:PG membrane upon vesicle disruption.

Visualization of vesicle leakage, aggregation and lysis

Confocal laser scanning microscopy (CLSM) with giant unilamellar vesicles (GUVs) provides an alternative way of elucidating the mechanism of action of the different peptides, since we can focus on individual vesicles rather than measuring ensemble changes. The GUVs contained a lipid fluorophor (DiIC18) and were loaded with membrane impermeable water-soluble fluorophors (Alexa 488 for DOPC:PG vesicles and Alexa 633 for DOPC vesicles), allowing us to monitor changes in both membrane integrity and permeability. The increased imaging facilities come at the expense of kinetic resolution, because diffusion limitation led to typical lag times between 10~15 min until the added peptide reached the field of vision, which makes it unrealistic to compare with the time-profile provided by stopped-flow experiments. As

illustrated in Fig. 7 and summarized in Table 2, the interactions between peptide and vesicle could be classified into three groups: (i) slow leakage that led to complete release of the vesicle content over 5-10 min, leaving an empty but intact vesicle behind; (ii) vesicle aggregation where the vesicles clump together, without necessarily facilitating the release of trapped fluorophor and (iii) vesicle lysis, causing immediate release of the vesicle content and complete loss of vesicle structure. Within the framework of current models for AMP action, (i) is most simply interpreted as pore formation and (iii) as the carpet model for membrane lysis, whereas (ii) represents an alternative class of interactions which do not occur in the absence of Nc and which to our knowledge has not been described before using CLSM. Images recorded at different stages of the process are provided in the supplementary material.

Nc added to DOPC vesicles caused both vesicle lysis and aggregation (Table 2). The fused vesicles seemed partially stabilized, as they were the last to rupture and little to no leakage was observed. For Nc, it was clear that there was a higher degree of vesicle aggregation when the vesicles contained 20% DOPG. The aggregation caused partial entrapment of the water-soluble probe and leads to larger particles with greater light-scattering properties, could very well explain the overshoot in steady-state measurements at high concentrations that was more prominent with DOPG vesicles. Both lysis of the vesicles and slow leakage was observed during and after the aggregation of the vesicles. The increase in vesicle aggregation observed with DOPC:PG vesicles might be explained by favorable electrostatic interactions between adsorbed (cationic) Nc and neighboring (anionic) vesicles. We have also observed aggregation of the related peptide Novispirin in the presence of different concentrations of SDS [21].

The addition of Nc-C8 to either DOPC vesicles or DOPC:PG vesicles did not cause vesicle aggregation to any observable degree, but we did observe vesicle lysis. Vesicle leakage was only evident for DOPC:PG vesicles. The leaky vesicles retained their structural integrity despite the fact that they did not aggregate, in contrast to observations with Nc. Nc-C12 did not cause slow leakage from neither DOPC nor DOPC:PG vesicles but resulted in vesicle lysis, and, in contrast to Nc-C8, vesicle aggregation. Thus, vesicle aggregation seems to be independent of whether the peptide causes lysis or leakage. For Nc-C16 the vesicle leakage behavior was comparable to that of Nc for both DOPC and DOPC:DOPG vesicles but Nc-C16 caused an equally high degree of aggregation of vesicles irrespective of their lipid composition.

We also investigated the behavior of Nc when presented with a mixed population of different vesicles. In the presence of both DOPC and DOPC:PG vesicles, we see a clear preference for the vesicles containing DOPG. We distinguish between the two vesicle types by filling them separately with different water-soluble fluorophores (Alexa 488 for DOPC versus Alexa 633 for DOPC:PG). While the DOPC:PG vesicles behave more or less in the vesicle mixture as we have observed for neat DOPC:PG vesicles (both aggregation, lysis and leakage are observed), we only observe rupturing of a few of the DOPC vesicles in the mixture. This indicates that the DOPC:PG vesicles compete effectively with pure DOPC vesicles in attracting free Nc (Fig. 8).

Nc-C16 is more deeply embedded in micelles than Nc wt

In order to analyze the effect of acylation on Nc's anchoring in amphiphilic environments, we have used solution state NMR to determine the structure and extent of insertion of Nc-C16 in zwitterionic (DPC) micelles. The structure was determined with traditional homonuclear 2D-spectra for the proton shift assignment and ^{1}H-^{13}C-HSQC natural abundance spectra for the C^{α} and C^{β} shifts assignment. Key values of the structure calculation are listed in Table 4. The structure of Nc-C16 consists of a single slightly bent amphiphatic α-helix with the acyl-chain attached to the N-terminal part of the peptide (Fig. 9A). Similar structures have been reported for the homolog peptides Ovispirin and Novispirin in SDS micelles[36; 37; 38]. The only NOE cross peaks between the peptide and the attached acyl group that could be assigned were the correlation between the H^{N} of residue 1-3 and the protons located on the fatty acid α-carbon atom. In the calculated structures the acyl-chain therefore appears highly flexible without this necessarily being correct.

To determine the relative insertion depths of Nc and Nc-C16 in DPC micelles, samples with the micelle bound peptides were titrated with the paramagnetic agent Gd(DTPA-BMA) that is known not to interact with peptides and micelles[32; 33]. T_1 relaxation values for the H^{α} protons in the peptides were calculated from peak volumes of cross peaks with the H^{α} atom appearing in the indirect dimension of inversion-recovery weighted NOESY spectra. The R_1 relaxation rates of the H^{α} atoms measured at different concentration of Gd(DTPA-BMA) were subsequently plotted against the concentration of the paramagnetic agents giving the PRE values of the atoms.

In Fig. 9B the H^{α} PRE values of Nc and Nc-C16 can be seen as a function of the residue numbers. The PRE curves of both peptides give a wavelike pattern with a wavelength of either 3

or 4 residues between the maxima of the PRE curves which for both peptides are located at the residues Asn-2, Arg-5, Lys-9, His-12 and Lys-16 corresponding to the hydrophilic side of the amphipathic helix.

As the PRE values depend on the inverse of the sixth power of the distance between the hydrogen and the paramagnetic atom[33] the results shows that the hydrophilic side of the helix is facing the outside of the micelle as expected. The PRE values of the Nc atoms are significantly larger than the corresponding atoms in Nc-C16 which clearly indicates that the acylated variant of Novicidin is buried deeper into the micelles. This difference is most pronounced for Asn2 in the N-terminal part of the peptides where the acyl-chain of Nc-C16 is attached, which suggests that the hydrophobic acyl-chain of Nc-C16 is pulling the N-terminus of the peptide towards the hydrophobic core of the micelle.

Solid-state NMR experiments reveal stronger interactions of acylated Nc with lipids

We now turn from Nc-detergent to Nc-lipid interactions using solid-state NMR spectroscopy. Atomic-resolution details on the insertion of novicidin and acylated variants of novicidin into different phospholipids may be obtained by recording ^{1}H-^{13}C PISEMA spectra [34] of natural abundance samples with the peptides reconstituted into bicelles. Such experiments may be used correlate ^{13}C chemical shifts with ^{1}H-^{13}C dipole-dipole couplings for the abundant lipid molecules as demonstrated previously for other systems by Ramamoorthy and coworkers [39; 40]. By monitoring the positions and lineshapes of the resonances for various lipid carbons in 2D PISEMA spectra, it is possible to probe small differences in local dynamics and orientation of the lipid functional groups and thereby get information about the influence of the peptides on the various parts of the lipids. This is illustrated in Fig. 10 by excerpts from 2D PISEMA spectra recorded for pure lipid (red line), lipid and wt Nc (green line), lipid and Nc-C8 (blue line), and lipid and Nc-C16 (magenta line) with the lipids being either pure zwitterionic bicelles (DMPC together with DHPC, left column) or a mixtures of zwitterionic and anionic bicelles (DMPC:DMPG in ratio 4:1 together with DHPC; center column). The spectra report the perturbation of headgroup (C_α), a central carbon (C_3), and a terminal acyl carbon (C_{14}) according to the structural model given in Fig. 10g. In addition to contour plots from relevant parts of the 2D PISEMA spectra for the four different samples, the individual panels also contain sum projections (left and top) onto the ^{13}C chemical shift axis (vertical) and the ^{1}H-^{13}C dipolar axis

(horizontal). The individual panels also contain (right and bottom) the corresponding traces taken through the maximum point of the 2D spectra for the pure bicelles. While changes in the local environment (structure/orientation and time averaged dynamics) may be monitored from the 2D contours as well as the projections, it is evident that most sensitivity towards minor changes in peak positions will be probed through the traces. We note that all samples were prepared with approximately the same peptide concentration, and that we based on information from calcein release data (Fig. 3) might expect Nc to display stronger interactions with zwitterionic vesicles than with the mixed zwitterionic and anionic vesicles; on the other hand, the CD data (Fig. 2) suggest that DOPC:PG vesicles bind Nc more strongly.

From the upper panels in Fig. 10, it becomes evident that Nc as well as the acylated Nc variants interact with the headgroup of both types of lipids. This is seen from the position and shape of the contours, and very clearly from the traces taken at the position of the resonance in the pure lipid spectra. A closer inspection of the spectra provides a more diverse set of observations for a deeper penetration of the peptides into the various lipids. From the left-hand column of Fig. 10, it is seen that Nc-C16 interacts with all carbon sites of the zwitterionic lipids and thereby may adapt a transmembrane (or transiently transmembrane) configuration with significant effect on the carbons on the central region of the lipids. In contrast, it appears that largely only the headgroup region (Cα and C3 carbons) are affected by the peptides with shorter or no acylation. Turning to the PC:PG lipid bicelles (center column), it appears that the perturbing effect from the various peptides on the local environment of the lipids are somewhat less pronounced (weaker interactions) and to a large extend only influence the headgroup region. For the wt Nc sample only a slight shift in the resonance position is observed for the α and β (not shown) carbons, indicating a relatively weak perturbation as compared to the interaction with the pure bicelles.

The observed changes (summarized in Table 3) overall indicate that novicidin and its acylated variants mainly interact with the surface of bicelles composed of zwitterionic and anionic lipids, while more pronounced interactions are observed for the pure zwitterionic lipids. In the latter case is seems that addition of acyl chains accelerates the interaction with perturbation of the inner parts of the membrane for the Nc-C16 acylation. We note that the ^{1}H-^{13}C PISEMA experiments do not provide information on whether this transmembrane perturbation is caused by the formation of ion channels (barrel stave) or static/transient incorporation of

monomer/oligomers of acylated peptides. We note that, in full consistency with the NMR observations, the biophysical measurements report the strongest membrane perturbation for the DOPC vesicles, with the requirement of less peptide to penetrate/perturb the vesicles relative to the DOPC:PG vesicles – although this appears to occur with very little induction of secondary structure.

DISCUSSION

In this study, we have increased the hydrophobicity of the antimicrobial peptide Nc by adding acyl chains of various lengths to the N-terminus. These modifications do not directly alter the intrinsic secondary structure of the peptide but modify the extent to which it interacts with amphiphilic environments by virtue of their own hydrophobicity. Closer association with the membrane will also induce folding of Novicidin, since the membrane environment requires the formation of organized secondary structure such as α-helices to satisfy the peptide's hydrogen bonding requirements. In this way we can test how increased association with the lipid membrane and increased structure changes its functional profile. We have studied how vesicle disruption changes with peptide concentration and how the peptides' preferences for two different lipid compositions change with increased hydrophobicity.

Acylation promotes higher order assemblies and α-helical structure

The CD spectra of Nc and the acylated derivatives in buffered solution clearly shows that the C12 and C16 chain changed the peptide structure through their change of the local environment of the peptide chains towards a more lipid-like environment. Nc-C12 is random coil at 40 μM but α-helical at 200 μM, whereas Nc-C16 was α-helical at all measured concentrations (10-100 μM). For Nc-C12, this can be explained by the peptides arranging in a surfactant like fashion with a critical micelle concentration (CMC) between 40 and 200 μM. Micelle formation results in an α-helical structure, as described by Makovitzki *et al.* [41]. For Nc-C16, the CMC is either below the peptide concentration tested in this study (i.e. < 10 μM) or the structure is stabilized in a different fashion, possibly existing only as a monomer. Solution-state NMR experiments on pure samples of Nc-C12 and Nc-C16 in the absence of lipids showed that both derivatives at ~1 mM in aqueous buffer formed aggregates that did not yield any useful NMR signals (M. F. and R. W., unpublished data). However, when dispersed in DPC, Nc-C16 yielded well-defined NMR spectra. In addition, Dufour *et al.* [42] have studied linearized versions of the lipopeptide surfactin and found that C10, C14, and C18 surfactin had CMC values of 1113, 301, and 8 μM respectively. These values are consistent with our own observations and also support the Nc-C16

micellization. In principle, the acyl chain could also pack against the peptide at the monomer level provided a suitably hydrophobic binding surface was available as suggested by Makovitzki *et al.* [41]. A helix projection of Nc (Fig. 1A) highlights a perfectly amphipathic helix with a sharp distinction between a hydrophobic face (only interrupted by Gly10) and a cationic face, where the acyl chain is attached to first residue placed in the middle of the cationic face. Nevertheless, Nc-C16's apparent micellization suggests that the C16 chain engages in inter- rather than intra-molecular packing. It is likely that the precise site of attachment of the acyl chain will dictate whether it is more favorable for the chain to dock against the peptide, engage with other acyl chains in an intermolecular micellar arrangement, or even combine the two types to form small micelles that also incorporate the peptide, as suggested for the lipopeptides elegantly developed by Privé and coworkers [43]. For D-Nc, we do not observe any marked differences with regards to the CD spectra compared to wt Nc. This agrees with reports by Scolnik *et al.* [44] who only observe very subtle differences between for synthetic *D*- and *L*-polyglutamic acid by CD apart from the expected inversion of the signal.

It is worth considering how these aggregative tendencies may influence subsequent vesicle interactions: We have a system with two defined states, one monomeric where the peptide has a random conformation, the other most likely multimeric where the peptide has a α-helical structure. Let us assume that the peptide initially inserts as a monomer into the lipid bilayer (even if it binds as a multimer it is likely to rearrange its higher-order arrangement in the bilayer, and possibly monomerize, due to the change in environment). In that case binding will need to be preceded by micelle dissociation above the CMC of the lipopeptide micelle (which is < 10 μM for Nc-C16 and between 40 and 200 μM for Nc-C12). Detergent micellar dynamics typically involve two relaxation processes, namely the dissociation of monomer from micelles (on the μs scale) and micelle break-up (on the minute scale depending on the biophysical properties of the detergent) [45]. Thus, we do not consider it likely that monomer dissociation from micelles is rate-limiting for the kinetics of binding of acylated Nc to membranes. Any changes in disruption kinetics are most likely to reflect changes in the binding to the membrane and/or structural rearrangements in this environment. Let us therefore address these issues.

Changes in secondary structure caused by addition of lipids

Nc and D-Nc folding in vesicles is strongly dependent on the lipid headgroup. Nc remains largely random coil in 100% zwitterionic lipids, but mixed lipids containing 20% DOPG induce α-helical structure. However, the increase in secondary structure does not in itself favour permeabilization but makes it less efficient.

Since we know from our calcein release and fluorescence anisotropy studies that Nc binds at least as well to DOPC vesicles as to DOPC:PG vesicles, the differences in structure may reflect different arrangements on the vesicle surface and/or membrane traversion. One scenario could be that Nc is loosely attached to DOPC vesicles, allowing it to remain relatively unstructured and thus cover a larger surface on the vesicle, while in DOPC:PG vesicles Nc is buried at the headgroup-acyl chain interface, favoring an amphipatic α-helix structure. This is consistent with our stopped-flow experiments with Dansyl-Nc where we observe a higher degree of interaction with DOPC:PG vesicles both prior to and after vesicle disruption. Our solid-state NMR observations also show that Nc mainly interacts with the lipid headgroups. Previously we observed that the closely related peptide Novispirin was able to bind to the positively charged surfactant LTAC to a more superficial extent than to the complementary SDS micelles, highlighting different levels of interaction [21]. Other studies also indicate that binding and permeabilization can be separate processes, and that binding alone is not sufficient for membrane permeabilization. For example, the amyloid-β peptide can bind to both crystalline and liquid disordered phases but only permeabilize the liquid disordered state [46].

Acylated peptides are α-helical in the presence of zwitterionic vesicles, suggesting that the acyl chain causes the peptides to adsorb to the vesicles in a manner that facilitates the formation of α-helix. One could imagine that the acyl chains work as “anchors” that pull the peptides into the headgroup-acyl chain interface where it then folds into an α-helix, supported by our PRE-data which indicate deeper penetration into micelles by Nc-C16 than Nc wt (Fig. 9B). This anchoring effect may also explain our solid-state NMR observation where we not only observe perturbation of the lipid head groups but also effects in the central and tail parts of the lipids – where α-helical secondary structure would support membrane penetration (static or transient). Graham and Phillips [47] reported that adsorption of rigid molecules to lipid membranes caused a slower increase in surface pressure compared to flexible molecules. This, in combination with “plugging” effects mentioned below, could help to explain why we do not see an increased vesicle disruption because of the increased peptide rigidity induced by α-helix formation. In

addition, the increased submersion into the lipid bilayer will make the acylated peptides less sensitive to the nature of the headgroup and will thus decrease the preference for zwitterionic lipids shown by Nc.

Changes in lipid specificity caused by acylation

In the steady-state fluorescence measurements of vesicle disruption, we observe that Nc causes calcein release from DOPC vesicles at 12-fold lower concentration than those needed for disruption of DOPC:PG vesicles. Solid-state NMR data also reveal a stronger interaction between the peptide and the DMPC membranes than the DMPC:PG membranes. Peptide acylation increases the concentrations needed for vesicle disruption, and leads to a decreased preference for zwitterionic vesicles compared to partially anionic vesicles (Fig. 3D). However, this decreased functional efficiency does not reflect a lower degree of overall binding to vesicles, as we need less lipid to induce changes in secondary structure for both Nc-C8 and Nc-C12 compared to Nc. To explain this apparent discrepancy, we speculate that the peptide's N-terminal acyl chain to some degree is able to counteract membrane disruption. The observed faster release rates could then be explained by the higher surface concentration of peptide that has been able to accumulate up to this level without disrupting the membrane because of the "plugging" effects of the acyl chain which help retain membrane integrity (see model in Fig. 11). The "plugging" effect could very well be what we observe in the solid-state NMR spectra. It is clear that the C16 acylated Nc interacts with central parts of the lipid bilayer as seen in Figs. 10 c,f. We note that from the present NMR data, we cannot distinguish whether it is the peptide itself or it is its acyl chains that interact with the central parts of the lipids. Data which could be interpreted in the same light have been observed for the lipopeptide surfactin where an increase in acyl chain length lowers the surface pressure of vesicles [48]. *In vivo* these effects would presumably lead to a decrease in the haemolytic activity of the peptide as the outer leaflet of red blood cell is primarily composed of the zwitterionic phosphatidylcholine and phosphatidylethanolamine [49].

It should be mentioned that the decreased preference of acylated Nc for zwitterionic lipids differs significantly from the work of Dathe *et al* [50] and Wieprecht *et al* [51], who report an increased affinity towards zwitterionic vesicles as a result of increased hydrophobicity. However, in their studies they have made point mutations in order to increase the hydrophobicity, rather

than acylating the peptide. Although it has been reported that antimicrobial peptides composed solely of the D- enantiomer amino acids have the same antimicrobial effect [52; 53], we also observe a slight decrease in the permeabilizing ability of D-Nc towards neutral lipids, although it binds to lipids just as well as Nc does. As with the acylated variants, this emphasizes the separation of folding and function.

Vesicle aggregation

The overshoot observed in our calcein release assay is presumably a scattering effect caused by vesicle aggregation. Apparently the aggregated vesicle aggregates are subsequently dissolved as we observe the overshoot to decrease over time. This is confirmed in our CLSM experiments where we in some cases clearly observe vesicle aggregation followed by vesicle disruption. Peptide induced aggregation of vesicles has been reported previously for antimicrobial peptides such as Cryptidin-4 and polylysine, measured by FRET and dynamic light scattering [54; 55; 56]. The aggregation is believed to be driven primarily by preferential electrostatic interactions, bilayer deformation, and lipid head group dehydration [55; 57]. We do observe a link between the aggregation and the acylation, since increasing chain lengths increase the aggregation (though Nc-C8 has reduced aggregation capability compared to non-acylated Nc). One explanation could be that the previously suggested plugging effect gives the peptide-lipid complexes time to interact and subsequently aggregate.

In a mixed population of vesicles charge interactions are the governing forces of peptide-lipid interactions

For the mixed populations of purely zwitterionic and zwitterionic-anionic vesicles, the peptides show a marked preference towards the (partially) negatively charged DOPC;PG vesicles over the zwitterionic DOPC vesicles. This preference differs from our calcein release measurements but does not contradict them. Rather, they simply reveal that long-range interactions in solution, mediated by electrostatics, can be sufficient to trap peptides on or close to a membrane surface for subsequent folding and membrane interactions. Although the visualization of vesicle contents release by peptides and small molecules has been reported previously [58; 59; 60; 61], to our knowledge this is the first example of the microscope-based analysis of mixed vesicle populations. This allows us to compare the affinity of wildtype and modified

peptides for a specific lipid composition in the presence of competing lipids, and thus ultimately model complex *in vivo* systems, such as the human digestive track, where the antimicrobial peptides are exposed to a diverse range of possible targets [62; 63].

In summary, we present the following working model on how Nc and acylated versions interact with DOPC and DOPC:PG vesicles (Fig. 11): Nc attaches peripherally to DOPC vesicles since there is no significant change in the secondary structure upon binding although we still observe vesicle disruption. In the presence of DOPG, Nc is submerged more extensively in the bilayer most likely at the acyl chain headgroup interface, leading to increased α- helix structure and an increase in the fluorescence of the dansyl-labeled Nc prior to to vesicle disruption. The acylation of Nc pulls the peptide deeper into the DOPC vesicles as we have formation of α-helix. Nevertheless the insertion is different from that in DOPC:PG vesicles, since there are still clear differences in the vesicle disruption kinetics and concentrations needed for the two types of vesicles. The acyl chain helps to counter act the vesicle destabilizing effect of the peptide, leading to the need for higher concentrations of peptides to disrupt the vesicles, irrespective of the lipids used.

MATERIALS AND METHODS

Chemicals

DMPC (1,2-Di-myristoyl-sn-Glycero-3-Phosphocholine), DHPC (1,2-Di-hexanoyl-sn-Glycero-3-Phosphocholine), DMPG (1,2-Di-myristoyl-sn-Glycero-3-[Phospho-rac-(1-glycerol)]), DOPC (1,2-Di-oleoyl-sn-Glycero-3-Phosphocholine) and DOPG (1,2-Di-oleoyl-sn-Glycero-3-[Phospho-rac-(1-glycerol)]) were from Avanti Polar Lipids (Alabaster, AL). Protected amino acids, 1,2-ethane dithiole (EDT), triisopropylsylane (TIPS), Di-chloromethane (DCM), Dimethylformamide (DMF), N,N-Diisopropylethylamine (DIPEA), 1H-Benzotriazolyl)-1,1,3,3-tetramethyl-uronium hexafluorophosphate (HBTU), octanoic, dodecanoic- and hexadecanoic acid, and *O*-(7-azabenzotriazol-1-yl)-*N*,*N*,*N*',*N*'-tetramethyluronium hexafluorophosphate (HATU) were from Iris Biotech (Marktredwitz, Germany). Acetonitrile chromasolv gradient grade, trifluoroacetic acid (TFA), Sucrose 99.5 % purity and D(+)Glucose 99.5 % purity were from Sigma (St. Louise, MO). DiIC18(3) and Alexa^{488} hydrazide were from Invitrogen (Carlsbad, California). Calcein disodium salt was purchased from Fluka (Buchs, Switzerland). DPC was purchased as DPC-d_{38} from Cambridge Isotope Laboratories Inc. (Andover, MA) and Gd-(DTPA-BMA) was generously provided by Klaus Zangger.

Peptide synthesis, acylation and purification

Synthesis of the acylated Nc peptides was carried out in two steps. Firstly, the Nc peptide (sequence KNLRR IIRKG IHIIK KYF) was synthesized on an automatic CEM liberty microwave assisted peptide synthesizer (Matthews, North Carolina) by solid-phase synthesis using standard Fmoc chemistry on Wang resin. Secondly, the fatty acid was attached to the N-terminus of the resin-bound peptide also using Fmoc chemistry. Wang resin was used with the C-terminal Phe residue coupled to the linker group at a concentration of 0.66 mmol Phe/g_{resin}. The resin was initially swelled with DCM for 30 min, followed by 5 repeating washes with DMF. The Fmoc protective group was removed with 20% piperidine solvated in DMF. Fmoc-amino acids (Sigma) were coupled to the resin bound peptide in 4 times molar excess together with 4 times molar excess of HBTU and 8 times molar excess of DIPEA solvated in DMF. The resin was washed with DMF and the procedure was repeated for each residue. The following side

chain protective groups were used for reactive amino acids: Lys: BOC, Asn: Trityl, Arg: PBF, Tyr: Tert butyl and His: Trityl.

In the second step, Nc was manually acylated with either octanoic-, dodecanoic-, or hexadecanoic acid. The appropriate fatty acid, HATU and DIPEA were added to the resin bound peptide in 5, 5, and 10 times molar excess, respectively, and agitated for 1 h. The acylated peptidyl resin was washed, dried and cleaved from the resin with TFA, water, TIPS, and EDT in a 88:5:15:2 molar ratio. The reaction was allowed to proceed for 3 h before allowing the solvents to evaporate. Subsequently, the peptide was washed in tert-butyl-methyl ether five times, each time with a centrifugation step where the peptide was sedimented and the supernatant removed. The last remains of tert-butyl-methylether were evaporated before purification. The purification was done on a Dionex Ultimate 3000 HPLC system (Sunnyvale, California) with a Reverse Phase semi-preparative C5 column and an AJO-7371 guard column in an AJO-7220 guard column system. Prior to each purification, the column was equilibrated with 15% acetonitrile. After loading the peptide to the column, an initial step with 15% acetonitrile was run for 2 min followed by a gradient from 15% acetonitrile from 15% to 99.9% acetonitrile over a period of 30 min. The column was allowed to run another 30 min at 99.9 % acetonitrile followed by a gradient from 99,9% acetonitrile to 15% acetonitrile over a period of 30 min. The eluent solutions all contained 0.1 % TFA. The fractions containing peptides were freeze-dried and the peptide dissolved in the appropriate buffer.

Synthesis of dansyl-Nc

Nc was synthesized as for the fatty acid derivatives using SPPS. In the second step, Nc was manually acylated with the dansyl moeity. Dansyl-chloride (Aldrich) and DIPEA were added to resin bound peptide in 5 and 10 times molar excess, respectively, and agitated for 1 h. The dansyl acylated peptidyl resin was washed, dried and cleaved from the resin as for the fatty acid derivatives to provide the N-terminal dansylated Nc.

Preparation of LUV liposomes

LUV´s (large unilamellar vesicles) containing calcein were prepared from stock solutions of lipids dissolved in methanol and dried overnight in a Heto VR-1 centrifuge vacuum drier. Lipids were then resuspended by vortexing in 20 mM Tris HCl, pH 7.5 containing 40 mM calcein

sodium salt, to a final concentration of 10 g/L (~14 mM), exposed to at least seven cycles of freezing in liquid nitrogen, followed by thawing in a 50^{o}C water bath, before extrusion through a 200 nm pore filter 12 times using a 10 ml thermo barrel extruder (Northern Lipids, Vancouver, Canada). The lipid solutions were run on a PD10 column pre-equilibrated with 20 mM Tris HCl, pH 7.5. Eluent fractions were gathered and tested by fluorescence measurements with and without the addition of Triton X-100 to test for calcein release. Those with the highest signal-to-background ratio were selected for further use. All extruded vesicles were used on the same day that they were made.

Preparation of GUV liposomes

GUVs (giant unilamellar vesicles) were prepared by the electroformation method originally described by Angelova and Dimitrov [22]. The GUVs were made using a home-built electroformation chamber partly built on the specifications published by Bagatolli and Gratton [23]. GUVs were prepared from chloroform stocks containing 10 g/L lipid as well as 0,01 g/L DiIC18. The chloroform lipid stocks were spread on platinum electrodes with approximately 10µl on each. The chamber was placed at 50°C for 2 h to evaporate any remaining solvents. The chamber was filled with a solution of 200 mM sucrose containing Alexa-488 or Alexa-633 hydrazide. The platinum wires were connected to a function generator (Digimess FG 100, Grundig Instruments, Nürnberg, Germany) and a low-frequency alternating field sinusoidal function with a frequency of 10 Hz and amplitude of 1.5 V was applied for 90 min followed by 30 min at 1 Hz and amplitude of 3 V. The platinum electrodes were gently washed by pipetting up and down to release loosely bound GUVs. To remove free fluorophor, the GUVs were run over a PD10 column pre-equilibrated with 200 mM glucose. The eluent from the column was collected in 0.5 ml fractions, samples were selected on the basis of absorption of free fluorophor and transferred to an eight-well microscopy chamber (Lab-Tek Brand Products, Naperville, IL). For mixed vesicle experiments the GUV´s were mixed in a 1:1 ratio in the microscopy chamber. GUVs were left overnight at 4°C to allow them to sediment at the bottom of the viewing chamber prior to viewing.

Laser confocal microscopy measurements

Vesicles were equilibrated to room temperature on the microscope slide for 15-20 min before measuring. GUVs were observed with a LSM 510 scanning confocal microscope (Zeiss GmbH, Jena, Germany). Excitation of Alexa^{488}, Alexa^{633} and DIIC18 was done at 488, 633, and 543 nm, respectively. Fluorescence emission was measured at 505-548, 650-700, and 558-612 for Alexa^{488}, Alexa^{633}, and DiIC18, respectively. 10µl of peptide solution was injected into the microcopy chamber outside the field of vision, and the measurements started immediately afterwards with images recorded every 15 s. Typically no changes were observed for the first 10-15 min after injection, probably due to slow diffusion of peptides into the field of vision in the viscous sucrose medium. Vesicle lysis was usually preceded by fluctuating vesicle movement associated with bulk solution changes, indicating the arrival of peptides diffusing into a lower-viscosity solution. The fluorescence intensity inside GUVs and the average GUV size were quantified using the public domain program Image J (Image Processing and Analysis in Java).

Manual calcein release assay

All measurements were conducted on an LS55 fluorimeter (PerkinElmer, Waltham, USA). To monitor the release of free calcein from the vesicles and the concomitant rise in fluorescence, the solution was excited at 490 nm, measuring emission at 515 nm every second using a slit width of 2.5 nm for both monochromators. The vesicles were diluted in Tris buffer pH 7.5 to a concentration of ~ 0.05 g/L, yielding a maximum emission maximum signal of around 350 units under these settings. A 10 mm quartz cuvette with magnetic stirring was used and the vesicle solution was allowed to equilibrate for ~1 min before starting to record fluorescence. During the recording, peptide was injected and the fluorescence was followed until it reached a plateau (this typically took ~1 min). Spectra were normalized with regards to maximum fluorescence (the fluorescence level achieved when 1% of Triton X-100 is added) using the equation:

$$Dye\ leakage\ (\%)\ =\ 100 * \frac{(F - F_o)}{(F_t - F_o)}$$

where F is the fluorescence intensity achieved by the peptides and F_0 and F_t are fluorescence intensities without the peptides and with Triton X-100, respectively.

Stopped Flow measurements

Kinetic experiments were carried out on an Applied Photophysics SX-18MV reaction analyzer (Applied Photophysics, Leatherhead, Surrey) in fluorescence detection mode. For the calcein release measurements, the solution was excited at 490 nm and a 510-nm glass filter was used to measure emission intensity. The calcein vesicles and peptides were mixed in 10:1 volume ratio and at least three measurements were averaged for each concentration. Final concentrations of lipid were around 50 μM while final peptide concentrations varied from 0.2 μM to 72 μM. In measurements using Dansyl-Nc, the samples were excited at 335 nm and a 530 nm glass filter was used. The lipid concentration was held constant at 20 μM while the peptide concentration was varied from 1 to 10 μM.

Secondary structural changes measured by CD spectroscopy

Circular dichroism studies were performed on a Jasco J-810 spectropolarimeter (Jasco Spectroscopic Co., Hachioji City, Japan) with a Jasco PTC-348W1 temperature control unit. Scan speed was set to 100 nm/min, slit width 2 nm. All experiments were carried out in 20 mM Tris-HCl pH 7.5, at 25°C using a 1 mm quartz cuvette. The measurements were conducted as one-pot titrations with an initial peptide concentration of 200 μM and stepwise addition of lipids. After addition of each new lipid aliquot, the sample was allowed to equilibrate for at least 1 min before a spectrum was recorded. Samples at each concentration were measured in three scans and averaged to yield the final spectrum. Background spectra without peptide were subtracted and the CD signal was corrected for dilution.

Peptide lipid binding measured by fluorescence anisotropy

All measurements were done on an LS55 fluorimeter (PerkinElmer, Waltham, USA) in a 200 μL Hellma quartz cuvette. The excitation was set to 335 nm and emission was measured at 515 nm. Slit width was set to 7.5 nm for both the vertical and horizontal filter. For each sample the G-Factor was measured before measuring the anisotropy. Dansyl-Nc concentration was held

constant at 25 μM and increasing amounts of lipid was added. The samples were mixed by pipetting and allowed to equilibrate for 2 min before measuring anisotropy.

Interaction of Nc variants with *E. coli* cells

E. coli BL21(DE3) was grown to exponential phase (OD_{600} 0.7) in 250 ml LB media. The cells were harvested by centrifugation at 3000 *g* and washed 3 times in 10 mM sodium phosphate pH 7.5 and 130 mM NaCl. The cell pellet was resuspended in 10 ml of this buffer and further diluted five-fold in the same buffer. 10 μL containing 0-10 μg of acylated or non-acylated Nc was added to 100μl of this cell suspension and the samples were incubated for 2 h at 37°C, with occasional mixing. Following the incubation, the supernatant was separated from the cells by centrifugation at 3000 *g* and checked for cell lysis by β-galactosidase assay, which was performed essentially as described previously, with some modifications [24]. In short, 50 μl of cell supernatant was transferred to microtiter plates in duplicates and 30 μl of 0.1M NaH_2PO_4, pH 7.5 containing 33 mM $MgCl_2$ was added. To some wells, 50 μL of buffer was added instead of cell lysate as blanks. Reaction was initiated by addition of 20 μL of substrate (o-nitrophenyl galactose, ONPG). The plate was placed in a plate reader (FLUOstar Omega, BMG Labtech) set at 37°C and the OD_{410} was read at various time intervals, ranging from 15 min to 17 h. Blanks were subtracted from each value. The obtained numbers from each time interval reading were plotted as a function of the amount of Nc peptide(s) added in μg.

Solution-state NMR experiments

NMR samples containing 1 mM Nc-C16 or 2 mM Nc were dissolved in 90 mM DPC-d_{38}, 10 mM phosphate buffer, 0.05% sodium azide, 5% D_2O, pH 6 to a final volume of 500 μL. All NMR measurements were conducted at 37 ^{o}C on a Bruker DRX600 spectrometer operating at a field strength of 14.1 T, equipped with a TXI(H/C/N) probe with triple-axis gradients. [^{1}H, ^{1}H]-TOCSY spectra with 50 and 80 ms mixing time were recorded using a clean-TOCSY pulse sequence with a 15 kHz spin-lock and a WATERGATE water suppression[25]. 2QF-COSY, [^{1}H-^{13}C]-HSQC in the aromatic and aliphatic regions and a 2D NOESY spectra with a mixing time of 80 ms and WATERGATE water suppression[25] were recorded. All NMR spectra were processed using Topspin version 1.3, and assignment was performed using the program CARA version 1.5.5[26] while the NEASY subroutine of CARA[27] was used for integration of the NOE cross

peaks. The program TALOS[28] provided 13 φ/ψ backbone torsion angle restraints based on the H^{α} / C^{α} / C^{β} chemical shifts and the CALIBA[29] subroutine in CYANA was used to convert integrated cross-peak intensities from the NOESY spectra into distance constraints. The NOE upper distance constraints were combined with the angle constraints in the input for the structure calculation using the torsion angle dynamics program CYANA[30]. Structure calculations were subsequently started from 80 conformers with random torsion angle values and the 20 calculated structures with the lowest CYANA target function were selected for the final ensemble representing the tertiary structure of the peptide. The software program PYMOL version 0.99[31] was used for structural analysis and visualization.

The PRE measurements of Nc-C16 were performed as previously described in detail[32]. The Nc-C16 NMR sample were titrated with Gd(DTPA-BMA)[33] to final concentrations of 2, 5 and 10 mM. Eight inversion recovery NOESY spectra with recovery delay times of 1, 50, 150, 400, 700, 1200, 2600, 4000 ms were recorded for each titration point in order to obtain the T_1 relaxation time.

Preparation of lipid bicelles for solid-state NMR spectroscopy

The NMR bicelle samples were made from DMPC, DHPC, and DMPG. All lipids except DMPG were solubilized in chloroform. Two different bicelle samples were made with DMPC:DMPG:DHPC molar ratios of 3.2:0.0:1.0 and 2.6:0.6:1.0, respectively. The lipids were dried separately over a stream of nitrogen and left under vacuum over night. 200 µL of a 10mM sodium phosphate buffer pH 6.8 was added to the dry DHPC and briefly vortexed until the lipid was solubilized. The clear solution of DHPC was added to the dry powders of DMPC/DMPG and Nc, and subsequently vortexed in an ice bath for 20 min. After 3-5 freeze-thaw cycles, the sample was transferred to a 3 cm long 5mm (o.d.) NMR tube and sealed. All samples contained 3 ± 0.2 mg peptide and 56 mg lipid.

Solid-state NMR experiments

All experiments were performed on a Bruker Avance 400 spectrometer (Bruker BioSpin, Rheinstetten, Germany) operating at 9.4 T corresponding to 400 MHz for protons. The spectrometer was equipped with a standard Bruker 5 mm triple-resonance MAS flatcoil probe, which for the present experiments were used for static-sample experiments in a ^{1}H-^{13}C double-

resonance configuration. The ^{1}H RF field strength was 35 kHz for the initial 90° pulse, while it was reduced to 20 kHz during cross polarization (CP; 3 ms contact period) as well as the t_1 period of the PISEMA experiment [34]. The ^{15}N RF field strength was 20 kHz during CP and the t_1–period of the PISEMA experiment. SPINAL-64 [35] was employed for ^{1}H-decoupling during detection (20 ms). The PISEMA experiment employed 45 t_1 increments, each using 64 or 100 scans. The sample was allowed to equilibriate for 5 s between each scan. Upon processing, a scaling factor of $\sqrt{2/3}$ from Lee-Goldburg homonuclear decoupling in the indirect dimension was accounted for by increasing the spectral width accordingly and the intensity was adjusted according to the number of transients. The incubation temperature was 305°K for samples containing only PC lipids and 303°K for samples containing PG lipids.

ACKNOWLEDGEMENTS

This work was supported by the Danish National Research Foundation through the Center for Insoluble Protein Structures (inSPIN). B.S.V. and M.F. are supported by pre-doctoral grants co-financed by Aalborg University and the Villum Kann Rasmussen Foundation through BioNET. We are very grateful to Drs. Hans Henrik Kristensen and Per Holse Mygind, Novozymes A/S, for generous donations of Nc and D-Nc as well as for useful discussions. The NMR laboratory at Aalborg University is supported by the Obel Foundation.

REFERENCES

1. Hale, J. D. & Hancock, R. E. (2007). Alternative mechanisms of action of cationic antimicrobial peptides on bacteria. *Expert Rev Anti Infect Ther* **5**, 951-9.
2. Lohner, K. & Blondelle, S. E. (2005). Molecular mechanisms of membrane perturbation by antimicrobial peptides and the use of biophysical studies in the design of novel peptide antibiotics. *Comb Chem High Throughput Screen* **8**, 241-56.
3. Zasloff, M. (2002). Antimicrobial peptides of multicellular organisms. *Nature* **415**, 389-395.
4. Brogden, K. A. (2005). Antimicrobial peptides: pore formers or metabolic inhibitors in bacteria? *Nat Rev Microbiol* **3**, 238-50.
5. Gordon, Y. J., Romanowski, E. G. & McDermott, A. M. (2005). A review of antimicrobial peptides and their therapeutic potential as anti-infective drugs. *Curr Eye Res* **30**, 505-15.
6. Andra, J., Howe, J., Garidel, P., Rossle, M., Richter, W., Leiva-Leon, J., Moriyon, I., Bartels, R., Gutsmann, T. & Brandenburg, K. (2007). Mechanism of interaction of optimized Limulus-derived cyclic peptides with endotoxins: thermodynamic, biophysical and microbiological analysis. *Biochem J* **406**, 297-307.
7. Taboureau, O., Olsen, O. H., Nielsen, J. D., Raventos, D., Mygind, P. H. & Kristensen, H. H. (2006). Design of novispirin antimicrobial peptides by quantitative structure-activity relationship. *Chem Biol Drug Des* **68**, 48-57.
8. Pistolesi, S., Pogni, R. & Feix, J. B. (2007). Membrane insertion and bilayer perturbation by antimicrobial peptide CM15. *Biophys J* **93**, 1651-60.
9. Fazio, M. A., Jouvensal, L., Vovelle, F., Bulet, P., Miranda, M. T., Daffre, S. & Miranda, A. (2007). Biological and structural characterization of new linear gomesin analogues with improved therapeutic indices. *Biopolymers* **88**, 386-400.
10. Landon, C., Barbault, F., Legrain, M., Menin, L., Guenneugues, M., Schott, V., Vovelle, F. & Dimarcq, J. L. (2004). Lead optimization of antifungal peptides with 3D NMR structures analysis. *Protein Sci* **13**, 703-13.
11. Taboureau, O., Olsen, O. H., Nielsen, J. D., Raventós, D., Mygind, P. H. & Kristensen, H.-H. (2006). Design of Novispirin Antimicrobial Peptides by Quantitative Structure–Activity Relationship. *Chem. Biol. Drug Des.* **68**, 48-57.
12. Shai, Y. & Oren, Z. (2001). From "carpet" mechanism to de-novo designed diastereomeric cell-selective antimicrobial peptides. *Peptides* **22**, 1629-1641.
13. Gazit, E., Boman, A., Boman, H. G. & Shai, Y. (1995). Interaction of the mammalian antibacterial peptide cecropin P1 with phospholipid vesicles. *Biochemistry* **34**, 11479-88.
14. Pouny, Y. & Shai, Y. (1992). Interaction of D-amino acid incorporated analogues of pardaxin with membranes. *Biochemistry* **31**, 9482-90.
15. Shai, Y. (1995). Molecular recognition between membrane-spanning polypeptides. *Trends Biochem Sci* **20**, 460-4.
16. Matsuzaki, K., Mitani, Y., Akada, K. Y., Murase, O., Yoneyama, S., Zasloff, M. & Miyajima, K. (1998). Mechanism of synergism between antimicrobial peptides magainin 2 and PGLa. *Biochemistry* **37**, 15144-53.

17. Khandelia, H. & Kaznessis, Y. N. (2005). Molecular dynamics simulations of helical antimicrobial peptides in SDS micelles: What do point mutations achieve? *Peptides* **26**, 2037-49.
18. Sawai, M. V., Waring, A. J., Kearney, W. R., McCray, P. B. J., Forsyth, W. R., Lehrer, R. I. & Tack, B. F. (2002). Impact of single-residue mutations on the structure and function of ovispirin/novispirin antimicrobial peptides. *Prot. Eng.* **15**, 225-232.
19. Jacobsen, F., Mohammadi-Tabrisi, A., Hirsch, T., Mittler, D., Mygind, P. H., Sonksen, C. P., Raventos, D., Kristensen, H. H., Gatermann, S., Lehnhardt, M., Daigeler, A., Steinau, H. U. & Steinstraesser, L. (2007). Antimicrobial activity of the recombinant designer host defence peptide P-novispirin G10 in infected full-thickness wounds of porcine skin. *J Antimicrob Chemother* **59**, 493-8.
20. Khandelia, H. & Kaznessis, Y. N. (2006). Molecular dynamics investigation of the influence of anionic and zwitterionic interfaces on antimicrobial peptides' structure: implications for peptide toxicity and activity. *Peptides* **27**, 1192-200.
21. Wimmer, R., Andersen, K., Vad, B., Davidsen, M., Mølgaard, S., Nesgaard, L. W., Kristensen, H.-H. & Otzen, D. E. (2006). Versatile interactions of the antimicrobial peptide Novispirin with detergents and lipids. *Biochemistry* **45**, 481-497.
22. Angelova, M. I., and D. S. Dimitrov. (1986). Liposome electroformation. *Faraday Discuss. Chem. Soc* **81**, 301-311.
23. Bagatolli, L. A. & Gratton, E. (1999). Two-photon fluorescence microscopy observation of shape changes at the phase transition in phospholipid giant unilamellar vesicles. *Biophys J* **77**, 2090-101.
24. Nicholas, S. B. & Philipson, K. D. (1999). Cardiac expression of the Na(+)/Ca(2+) exchanger NCX1 is GATA factor dependent. *Am J Physiol* **277**, H324-30.
25. Griesinger, C., Otting, G., Wuethrich, K. & Ernst, R. (1988). Clean TOCSY for proton spin system identification in macromolecules. *J Am Chem Soc* **110**, 7870 - 7872.
26. Keller, R., 'OPTIMIZING THE PROCESS OF NUCLEAR MAGNETIC RESONANCE SPECTRUM ANALYSIS AND COMPUTER AIDED RESONANCE ASSIGNMENT' obtained from the website www.nmr.ch.
27. Bartels, C., Xia, T., Billeter, M., Güntert, P. & Wüthrich, K. (1995). The program XEASY for computer-supported NMR spectral analysis of biological macromolecules. *J. Biomol NMR* **6**, 1-10.
28. Cornilescu, G., Delaglio, F. & Bax, A. (1999). Protein backbone angle restraints from searching a database for chemical shift and sequence homology. *J Biomol NMR* **13**, 289-302.
29. Guntert, P., Braun, W. & Wuthrich, K. (1991). Efficient computation of three-dimensional protein structures in solution from nuclear magnetic resonance data using the program DIANA and the supporting programs CALIBA, HABAS and GLOMSA. *J Mol Biol* **217**, 517-30.
30. Guntert, P., Mumenthaler, C. & Wuthrich, K. (1997). Torsion angle dynamics for NMR structure calculation with the new program DYANA. *J Mol Biol* **273**, 283-98.
31. DeLano, W. L. (2002). *The PyMOL Molecular Graphics System, www.pymol.org*.
32. Respondek, M., Madl, T., Gobl, C., Golser, R. & Zangger, K. (2007). Mapping the orientation of helices in micelle-bound peptides by paramagnetic relaxation waves. *J Am Chem Soc* **129**, 5228-34.

33. Pintacuda, G., Keniry, M. A., Huber, T., Park, A. Y., Dixon, N. E. & Otting, G. (2004). Fast structure-based assignment of 15N HSQC spectra of selectively 15N-labeled paramagnetic proteins. *J Am Chem Soc* **126**, 2963-70.
34. Wu, C. H., Ramamoorthy, A. & Opella, S. J. (1994). High-resolution heteronuclear dipolar solid-state NMR Spectroscopy. *J. Magn. Reson.* **109**, 270-272.
35. Fung, B. M., Khitrin, A. K. & Ermolaev, K. (2000). An improved broadband decoupling sequence for liquid crystals and solids. *J. Magn. Reson.* **142**, 97-101.
36. Sawai, M. V., Waring, A. J., Kearney, W. R., McCray, P. B., Jr., Forsyth, W. R., Lehrer, R. I. & Tack, B. F. (2002). Impact of single-residue mutations on the structure and function of ovispirin/novispirin antimicrobial peptides. *Protein Eng* **15**, 225-32.
37. Wimmer, R., Andersen, K. K., Vad, B., Davidsen, M., Molgaard, S., Nesgaard, L. W., Kristensen, H. H. & Otzen, D. E. (2006). Versatile interactions of the antimicrobial peptide novispirin with detergents and lipids. *Biochemistry* **45**, 481-97.
38. Kalfa, V. C., Jia, H. P., Kunkle, R. A., McCray, P. B., Jr., Tack, B. F. & Brogden, K. A. (2001). Congeners of SMAP29 kill ovine pathogens and induce ultrastructural damage in bacterial cells. *Antimicrob Agents Chemother* **45**, 3256-61.
39. Dvinskikh, S., Dürr, U., Yamamoto, K. & Ramamoorthy, A. (2006). A high-resolution solid-state NMR approach for the structural studies of bicelles. *J. Am. Chem. Soc.* **128**, 6326-6327.
40. Dvinskikh, S., Dürr, U., Yamamoto, K. & Ramamoorthy, A. (2007). High-Resolution 2D NMR Spectroscopy of Bicelles To Measure the Membrane Interaction of Ligands. *J. Am. Chem. Soc.* **129**, 794-802.
41. Makovitzki, A., Avrahami, D. & Shai, Y. (2006). Ultrashort antibacterial and antifungal lipopeptides. *Proc. Natl. Acad. Sci. USA* **103**, 15997-16002.
42. Dufour, S., Deleu, M., Nott, K., Wathelet, B., Thonart, P. & Paquot, M. (2005). Hemolytic activity of new linear surfactin analogs in relation to their physico-chemical properties. *Biochim Biophys Acta* **1726**, 87-95.
43. McGregor, C.-L., Chen, L., Pomroy, N. C., Hwang, P., Go, S., Chakrabartty, A. & Privé, G. G. (2003). Lipopeptide detergents designed for the structural study of membrane proteins. *Nature Biotechnol.* **21**, 171-176.
44. Scolnik, Y., Portnaya, I., Cogan, U., Tal, S., Haimovitz, R., Fridkin, M., Elitzur, A. C., Deamer, D. W. & Shinitzky, M. (2006). Subtle differences in structural transitions between poly-L- and poly-D-amino acids of equal length in water. *Phys Chem Chem Phys* **8**, 333-9.
45. Patist, A., Kanicky, J. R., Shukla, P. K. & Shah, D. O. (2002). Importance of micellar kinetics in relation to technological processes. *J Colloid Interface Sci* **245**, 1-15.
46. Wong, P. T., Schauerte, J. A., Wisser, K. C., Ding, H., Lee, E. L., Steel, D. G. & Gafni, A. (2009). Amyloid-β membrane binding and permeabilization are distinct processes influenced separately by memrane charge and fluidity. *J. Mol. Biol.* **386**, 81-96.
47. Phillips, D. E. G. a. M. C. (1979). Proteins at liquid interfaces : I. Kinetics of adsorption and surface denaturation. *Journal of Colloid and Interface Science* **7**, 403-414.
48. Eeman, M., Berquand, A., Dufrene, Y. F., Paquot, M., Dufour, S. & Deleu, M. (2006). Penetration of surfactin into phospholipid monolayers: nanoscale interfacial organization. *Langmuir* **22**, 11337-11345.
49. Verkleij, A. J., Zwaal, R. F., Roelofsen, B., Comfurius, P., Kastelijn, D. & van Deenen, L. L. (1973). The asymmetric distribution of phospholipids in the human red cell

membrane. A combined study using phospholipases and freeze-etch electron microscopy. *Biochim Biophys Acta* **323**, 178-93.
50. Dathe, M., Wieprecht, T., Nikolenko, H., Handel, L., Maloy, W. L., MacDonald, D. L., Beyermann, M. & Bienert, M. (1997). Hydrophobicity, hydrophobic moment and angle subtended by charged residues modulate antibacterial and haemolytic activity of amphipathic helical peptides. *FEBS Lett* **403**, 208-12.
51. Wieprecht, T., Dathe, M., Beyermann, M., Krause, E., Maloy, W. L., MacDonald, D. L. & Bienert, M. (1997). Peptide hydrophobicity controls the activity and selectivity of magainin 2 amide in interaction with membranes. *Biochemistry* **36**, 6124-32.
52. Vunnam, S., Juvvadi, P., Rotondi, K. S. & Merrifield, R. B. (1998). Synthesis and study of normal, enantio, retro, and retroenantio isomers of cecropin A-melittin hybrids, their end group effects and selective enzyme inactivation. *J Pept Res* **51**, 38-44.
53. Hetru, C., Letellier, L., Oren, Z., Hoffmann, J. A. & Shai, Y. (2000). Androctonin, a hydrophilic disulphide-bridged non-haemolytic anti-microbial peptide: a plausible mode of action. *Biochem J* **345 Pt 3**, 653-64.
54. Matsuzaki, K., Fukui, M., Fujii, N. & Miyajima, K. (1993). Permeabilization and morphological changes in phosphatidylglycerol bilayers induced by an antimicrohial peptide, tachyplesin I. *Colloid & Polymer Science* **271**, 901-908.
55. Cummingsa, J. E. & Vanderlick, T. K. (2007). Aggregation and hemi-fusion of anionic vesicles induced by the antimicrobial peptide cryptdin-4. *Biochimica et Biophysica Acta (BBA)* **1768**, 1796-1804.
56. Fujii, G., Horvath, S., Woodward, S., Eiserling, F. & Eisenberg, D. (1992). A molecular model for membrane fusion based on solution studies of an amphiphilic peptide from HIV gp41. *Protein Sci* **1**, 1454-64.
57. Stegmann, T., Doms, R. W. & Helenius, A. (1989). Protein-mediated membrane fusion. *Annu Rev Biophys Biophys Chem* **18**, 187-211.
58. Henriques, S. T., Quintas, A., Bagatolli, L. A., Homble, F. & Castanho, M. A. (2007). Energy-independent translocation of cell-penetrating peptides occurs without formation of pores. A biophysical study with pep-1. *Mol Membr Biol* **24**, 282-93.
59. Ambroggio, E. E., Separovic, F., Bowie, J. H., Fidelio, G. D. & Bagatolli, L. A. (2005). Direct visualization of membrane leakage induced by the antibiotic peptides: maculatin, citropin, and aurein. *Biophys J* **89**, 1874-81.
60. Tamba, Y. & Yamazaki, M. (2005). Single giant unilamellar vesicle method reveals effect of antimicrobial peptide magainin 2 on membrane permeability. *Biochemistry* **44**, 15823-33.
61. Tamba, Y., Ohba, S., Kubota, M., Yoshioka, H., Yoshioka, H. & Yamazaki, M. (2007). Single GUV method reveals interaction of tea catechin (-)-epigallocatechin gallate with lipid membranes. *Biophys J* **92**, 3178-94.
62. Montes, L. R., Alonso, A., Goni, F. M. & Bagatolli, L. A. (2007). Giant unilamellar vesicles electroformed from native membranes and organic lipid mixtures under physiological conditions. *Biophys J* **93**, 3548-54.
63. Dethlefsen, L., McFall-Ngai, M. & Relman, D. A. (2007). An ecological and evolutionary perspective on human-microbe mutualism and disease. *Nature* **449**, 811-8.

FIGURE LEGENDS

Figure 1

(A) Sequence of Novicidin and a helical projection highlighting its amphipathic character. (B) CD spectra of Nc and acylated derivatives in 50 mM PBS buffer pH 7.5: 40 μM wt Nc (filled circles), 40 μM D-Nc (empty circles), 40 μM Nc-C8 (empty diamonds), 40 μM Nc-C12 (empty squares), 200 μM Nc-C12 (filled squares), 40 μM Nc-C16 (+), 40 μM Novicidin in vesicles containing 20% DOPG and 80% DOPC (x), and 40 μM Nc-C8 in vesicles containing 100% DOPC.

Figure 2

Development of CD spectra at 208 nm with the addition of increasing concentrations of (A) 100% DOPC and (B) 20%DOPG and 80% DOPC to Nc wt (filled circles), D-Nc (empty circles), Nc-C8 (diamonds) Nc-C12 (filled squares) and Nc-C16 (+)

Figure 3.

(A) Time profile of calcein release by Nc and derivatives. Signal normalized relative to signal upon addition of Triton X-100 (see Materials and Methods). With the addition of Nc and acylated derivatives to calcein loaded vesicles three distinct calcein release release patterns are observed in stedy-state fluorescence measurements. A slow release leading with the curve displaying second order characteristics (■), a fast release with a fluorescence increase between 0- and a 100 %(□), and finally a fast release with an overshoot which would after ~1 min reach decrease to a 100% (△). Injection occurs in all cases at 50s. (B and C) Nc, NcD and the acylated derivatives were added to calcein-loaded vescicles composed of (B) 100% DOPC and (C) 20 % DOPG and 80 % DOPC (data for Nc in 100% DOPC included for comparison). The normalised maximum fluorescence was plotted as a function of protein concentration. (D) The bars indicate the peptide concentrations needed for 50% calcein release (R_{50}) from 100% DOPC vesicles (gray bars) and 20 % DOPG and 80% DOPC vesicles (black bars) and also the ratio between these two (striped bars).

Figure 4: Degree of release of β-galactosidase from *E. coli* by different concentrations of Nc and acylated variants hereof.

Figure 5: Anisotropy measurements of Dansyl-Nc in increasing concentrations of pure DOPC and 80:DOPC:20%DOPG. The vesicles were allowed to equillibrate for 1 min before each measurement.

Figure 6: Stopped-flow analysis of Nc interactions with lipids. Upon addition of Dansyl Nc we observe an increase for the dansyl flourescence for both vesicles composed of DOPC (A) and 20% DOPG 80 % DOPC (B) before an increase in the calcein fluorescence. The arrow A(I) indicates an initial small increase in dansyl fluorescence due to binding while arrow A(II) shows the simultaneous release of vesicle contents for DOPC vesicles. For the 20% DOPG 80 % DOPC vesicles the arrow B(I) indicates a large fluorescence increase from the dansyl probe indiating Novicidin membrane insertion prior to vesicle disruption shown by arrow B(III) followed by another increase in dansyl fluorescence B(II) which might be due lipid rearrangement.

Figure 7: Representative multicolour fluorescence images of Alexa 488 (green colour) loaded lipid vesicles with DiIC18 (red colour) incorporated in the membrane obtained by confocal laser scanning microscopy. In the presence of Nc and acylated derivatives, we observe three distinct modes of action, namely (A) vesicle leakage, (B) vesicle aggregation and (C) vesicle lysis. The relative preferences for the three modes of action are summarized in Table 2,

Figure 8: CLSM images of vesicle contents release from DOPC (red, filled with Alexa 488) and 20% DOPG and 80% DOPC (green, filled with Alexa 633) GUV´s after addition of Nc. Each image represent ~ a 2 min interval. Peptide was injected at $t = 0$.

Figure 9. (A) Structure of Nc-C16 in the presents of DPC. Superposition of the 20 backbone conformers with the lowest cyana target function representing the 3D NMR structure. The bundle is obtained by superimposing the backbone C^{α}, C ,N atoms of residues 2-17. The carbon atoms of the acyl chain is clearly seen extending from the N-terminal part of the peptide. (B)

PRE values of H^{α} nuclei of Nc (▲) and Nc-C16 (■) as a function of residue numbers. Error bars indicate variations in PRE values obtained from fitting several peaks.

Figure 10. Solid-state NMR spectra of novicidin and acetylated variants in pure and mixed lipids. (a-f) Each panel describe four different bicelle samples containing either; pure lipid bicelle (red), lipid and wt Nc (green), lipid and C8-Nc (blue) and lipid with Nc-C16 (magenta). Each panel consists of an excerpt from 2D ^{1}H-^{13}C PISEMA spectra of DMPC:DHPC or DMPC:DMPG:DHPC bicelles as well as sum projections and traces along the position of the pure bnicelle for both the ^{1}H dimension and the 13C dimension.(a-c) describe the spectral changes observed for zwitterionic bicelles.
(d-f) describe the spectral changes observed for a mixture of zwitterionic and anionic bicelles. The focus is on three representative regions describing the lipid head group (a,d), the central part of the lipid molecule (b,e) and the lipid tail region (c,f).
The location of the carbon atoms in the lipid molecule is indicated in (g).

Figure 11: A schematic model to illustrate why much less wt Nc is required compared to the acylated versions to cause the same degree of vesicle permeabilization. Wt Nc binds either the membrane-water interface (zwitterionic vesicles) or the headgroup - acyl chain interface (anionic vesicles), leading to membrane disruption. Acylated Nc binds at the headgroup - acyl chain interface, but the inserted acyl chain helps to counter the peptide induced membrane disruption.

TABLES

Table 1

Increase in ellipticity at 208 nm of Nc peptides as a function of lipid concentration (units of molar ellipticity per mg/ml lipid x 10^{-3}).[a,b]

Peptide	**100% DOPC**	**20% DOPG 80 %DOPC**
Wt Nc	-1.21	-8.98
D-Nc	1.21	27.57
Nc-C8	-6.56	-29.56
Nc-C12	-8.84[c]	-11.87
Nc-C16	-0.58	-1.15

Notes:

[a] All data carried out in 20 mM Tris-HCl pH 7.5 at 25°C. Fits based on data shown in Fig. 2.

[b] These values are not actual affinity constants (since the ellipticity generally increases linearly and does not level off to a plateau level over the concentration range tested) but serve to illustrate the degree to which different lipids can increase the secondary structure of the Nc peptides over the experimentally accessible concentration range.

[c] Data have been fitted to a parabolic equation to derive the slope at zero molar lipid.

Table 2: Summary of confocal laser scanning microscopy experiments with Nc and acylated derivatives, indicating the propensities of the peptides for three different kinds of vesicle interactions (illustrated in Fig. 7)[a].

Vesicle leakage		
Peptide	DOPC vesicles	20%DOPG vesicles
Wt Nc	+	+++
Nc-C8	-	+
Nc-C12	-	-
Nc-C16	+	+++

Vesicle Fusion		
Peptide	DOPC vesicles	20%DOPG vesicles
Wt Nc	+	+++
Nc-C8	-	-
Nc-C12	++	+
Nc-C16	+++	+++

Vesicle lysis		
Peptide	DOPC vesicles	20%DOPG vesicles
Wt Nc	++	+
Nc-C8	+++	++
Nc-C12	+++	+++
Nc-C16	++	+

Notes:

[a] For practical reasons, all experiments were performed at pH 6 and at 15 ^{o}C. The degree of leakage, fusion and lysis was based on a relative comparison between the different samples.

Table 3. Summary of peptide induced-perturbation of CH_n groups in the headgroup (C_α), central (C_3), and tail (C_{14}) region of zwitterionic (DMPC) and mixed zwitterionic and anionic (DMPC:DMPG) bicelles[a]

	Peptide	**DMPC**	**DMPC:DMPG (4:1)**
Headgroup (C_α)	Nc	++	+
	Nc-C8	+++	++
	Nc-C16	+++	++
Central (C_3)	Nc	++	-
	Nc-C8	++	+
	Nc-C16	++	++
Tail (C_{14})	Nc	-	-
	Nc-C8	-	-
	Nc-C16	+++	+

Notes:

[a] See labelling of lipid functional groups in Fig. 10g

Table 4
Quality Criteria for the Calculated Nc-C16 Structures

number of distance constraints	271
- of which intraresidual	136
- of which sequential	69
- of which medium-range ($2 \leq \Delta_{res} \leq 4$)	66
number of angle constraints[a]	26
- of which φ	13
- of which ψ	13
CYANA residual target function	0.89 ± 0.04 Å^2
distance restraints violated by more than 0.2Å	0
angle restraints violated more than 5°[b]	0
rmsd residues 2-17[c]	0.13 ± 0.08 Å
% of residues in Ramachandran plot	
- in most favored regions	91.5
- less favored regions	7.6
- generously allowed regions	0.9
- disallowed allowed regions	0

Notes:

[a] Only those derived from TALOS.

[b] Per molecule.

[c] For backbone atoms C', C^{α} and N, as calculated by CYANA from the pairwise rmsd values of each of the 20 structures against a mean structure.

[d] as calculated by PROCHECK_NMR.

Vad et al. Fig. 1A

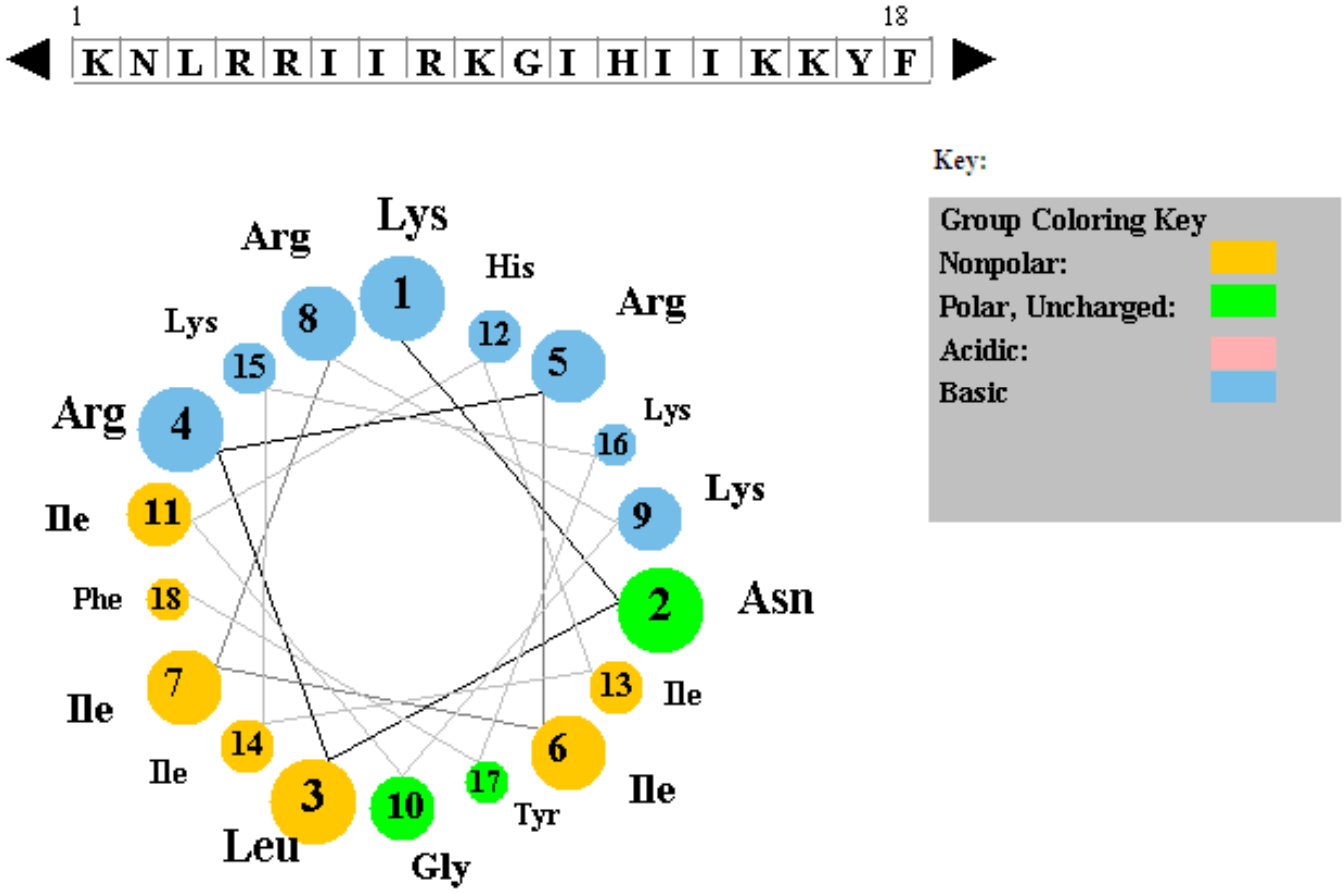

Vad et al. Fig. 1B

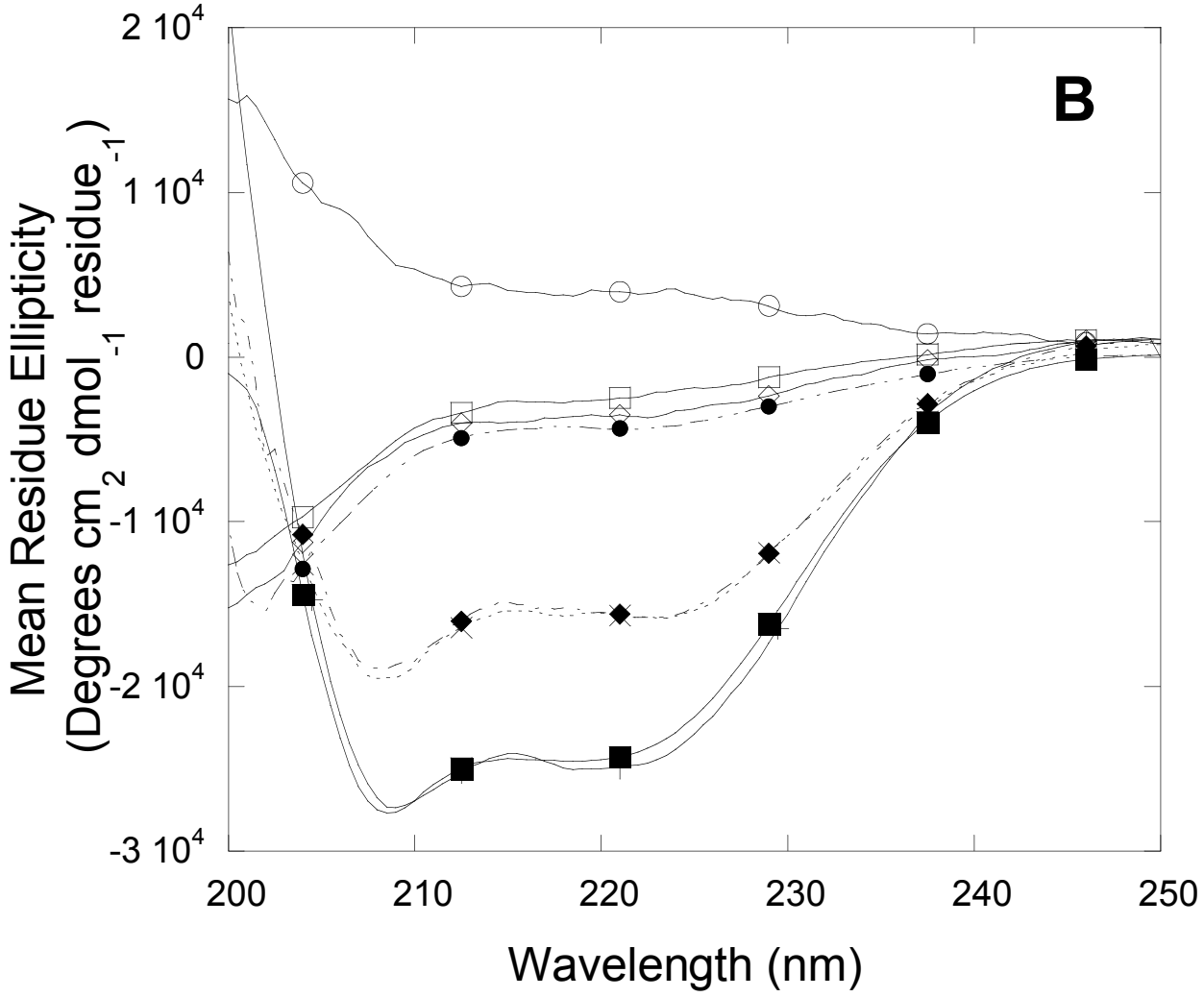

Vad et al. Fig. 2A

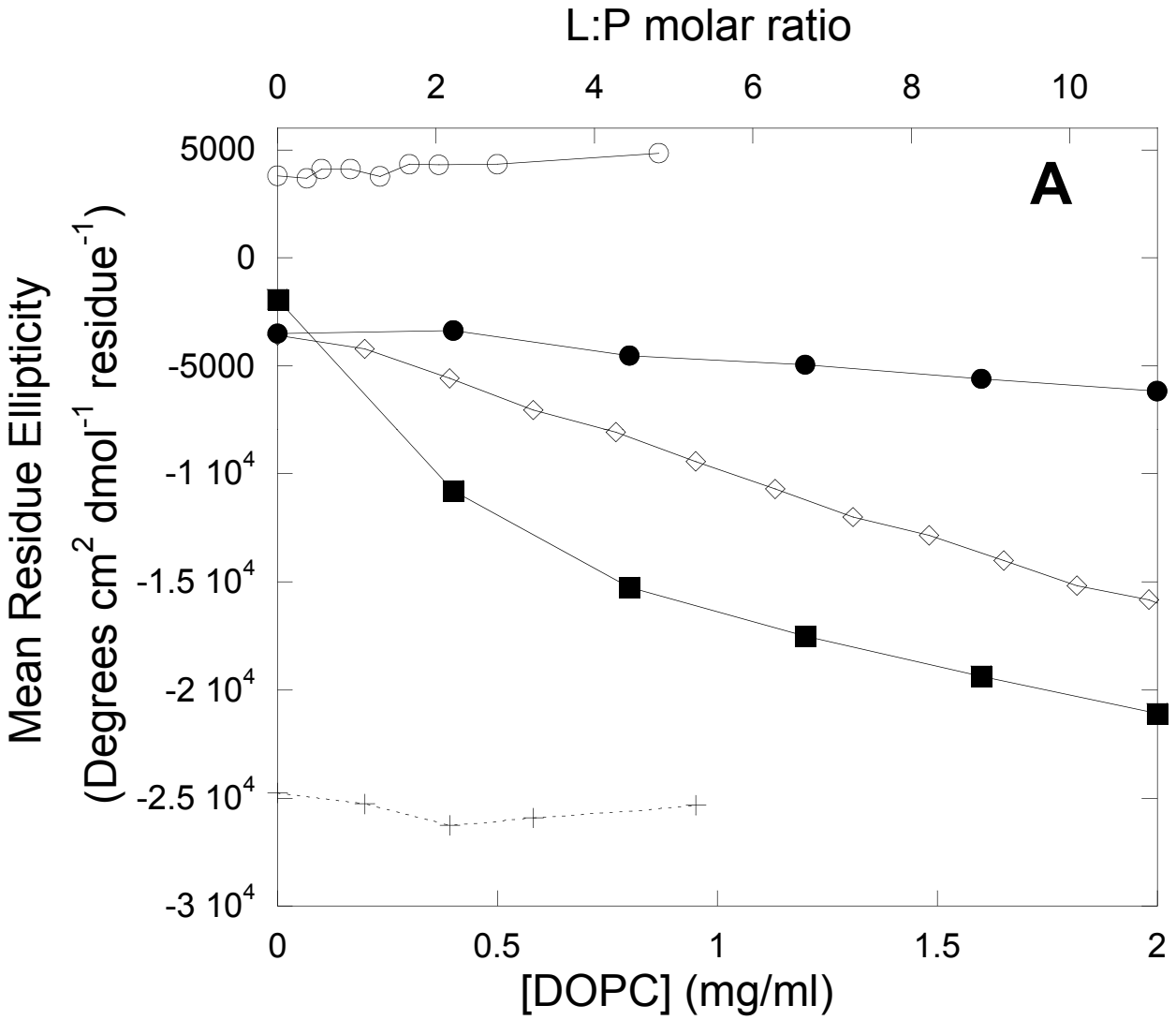

Vad et al. Fig. 2B

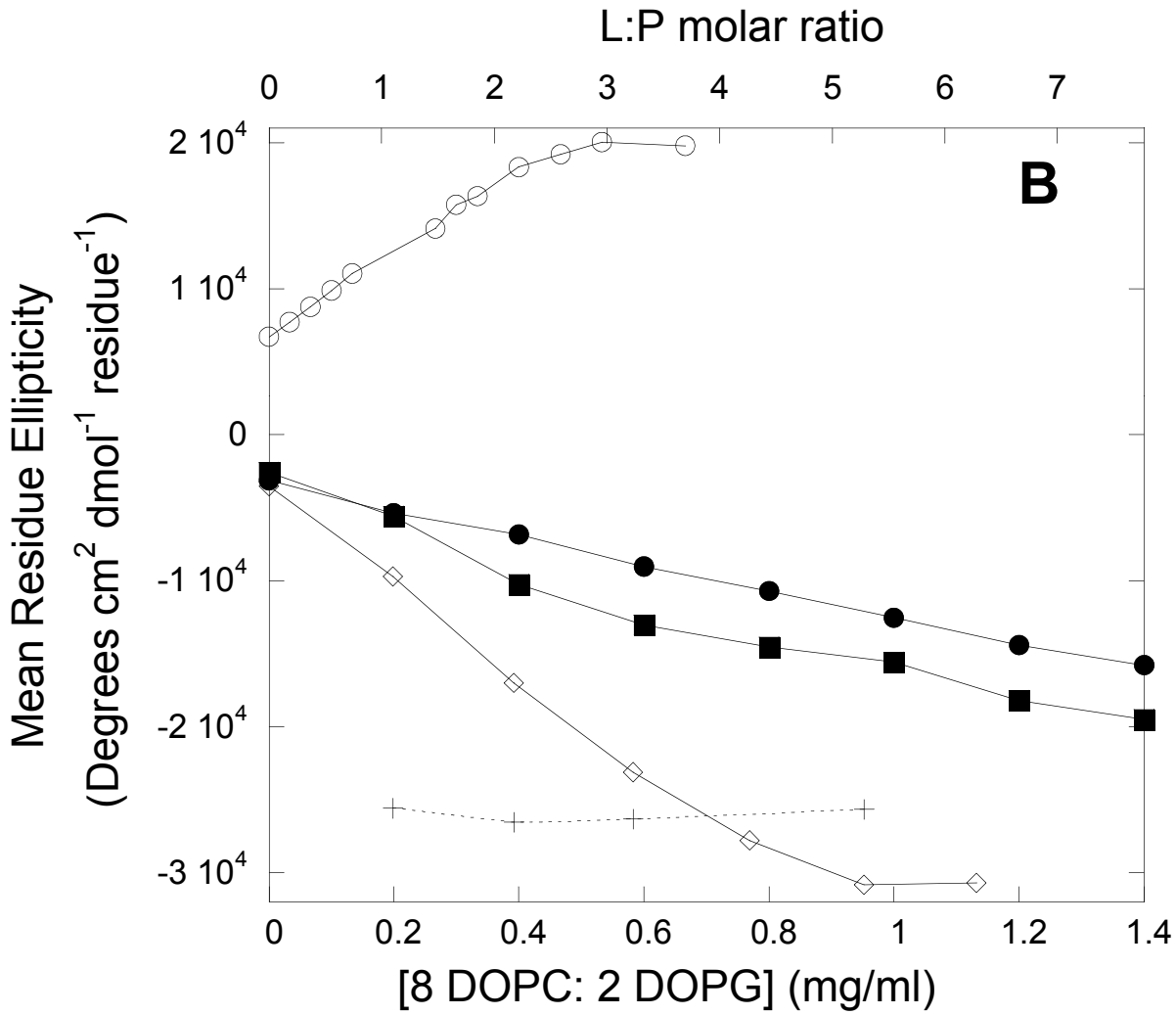

Vad et al. Fig. 3A

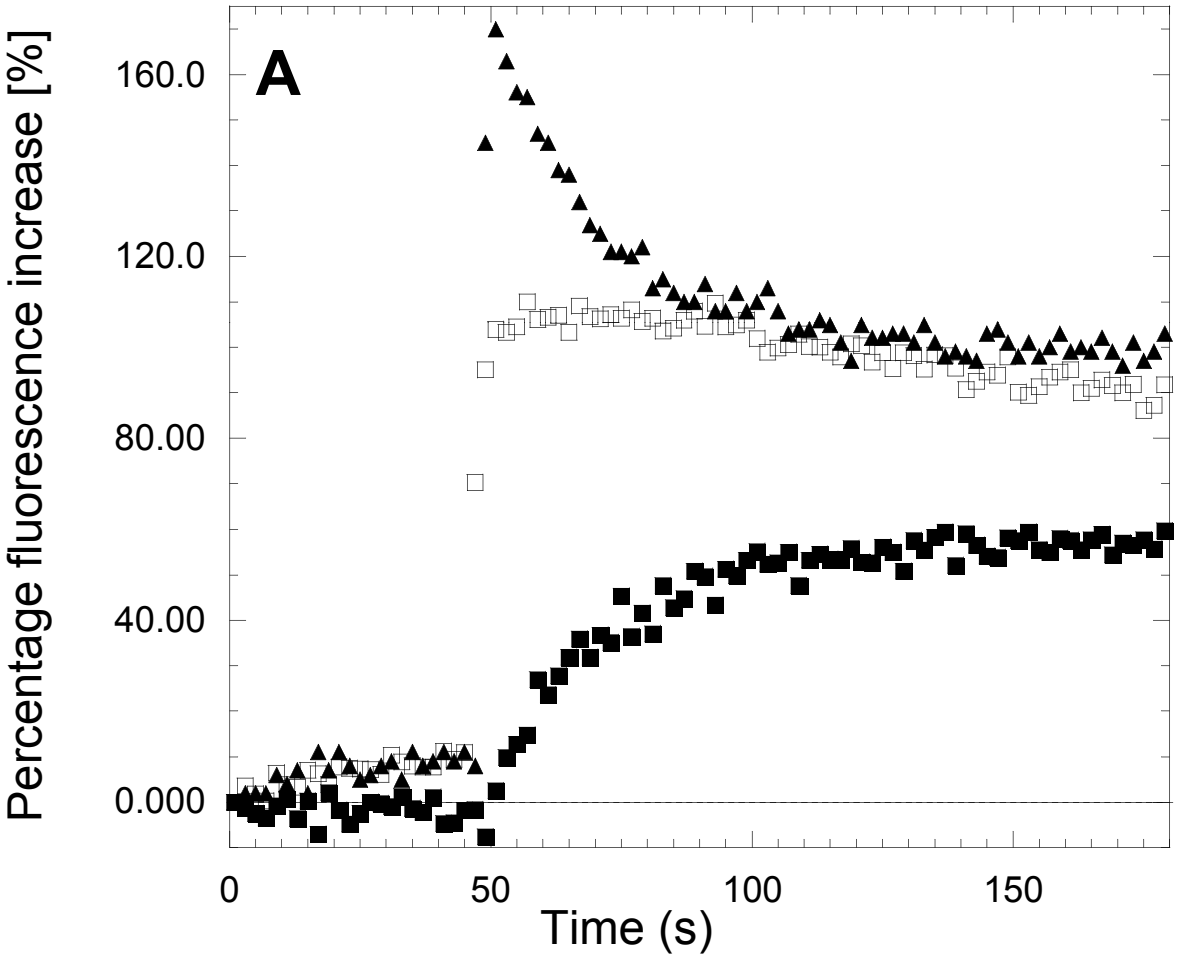

Vad et al. Fig. 3B

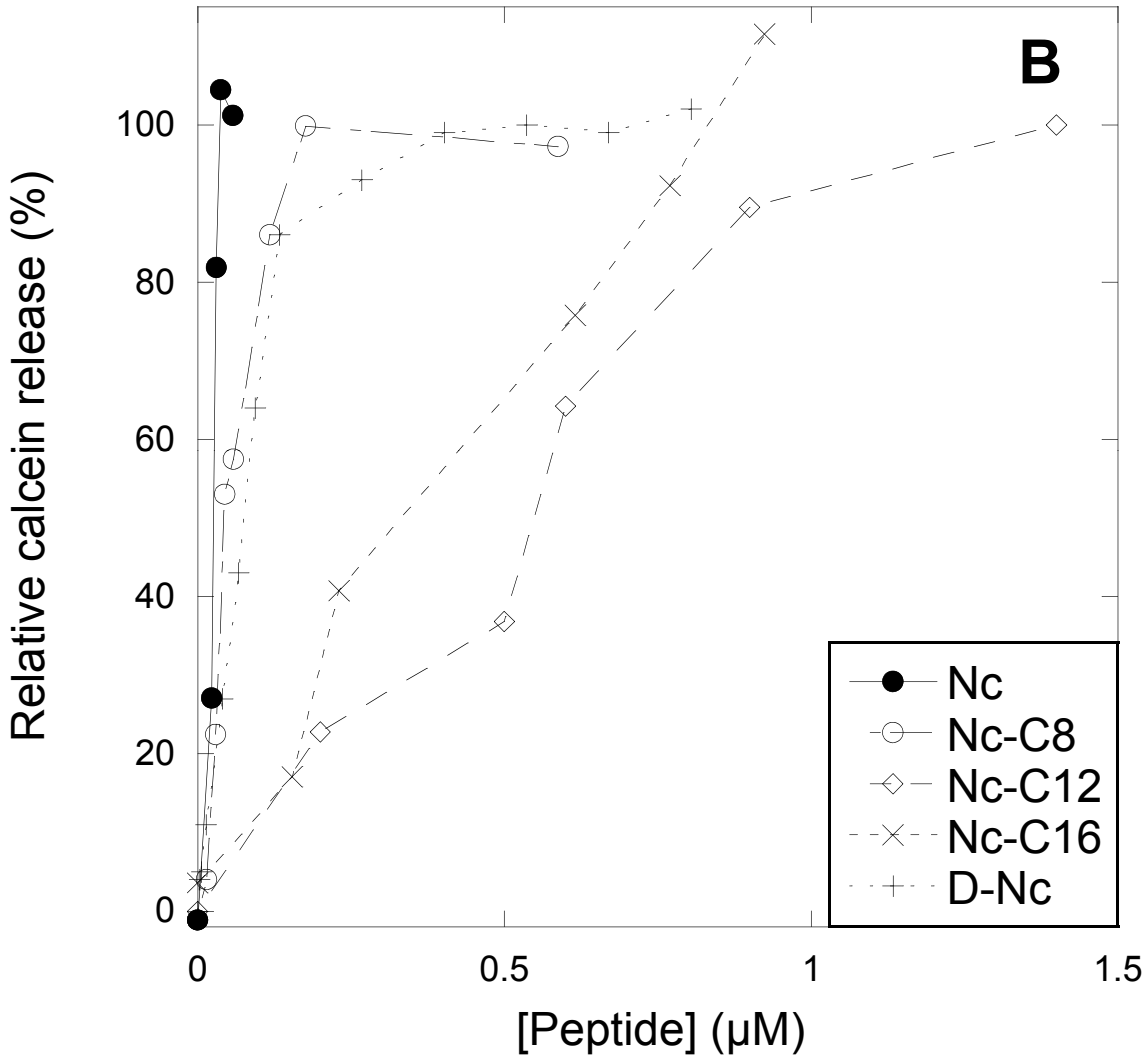

Vad et al. Fig. 3C

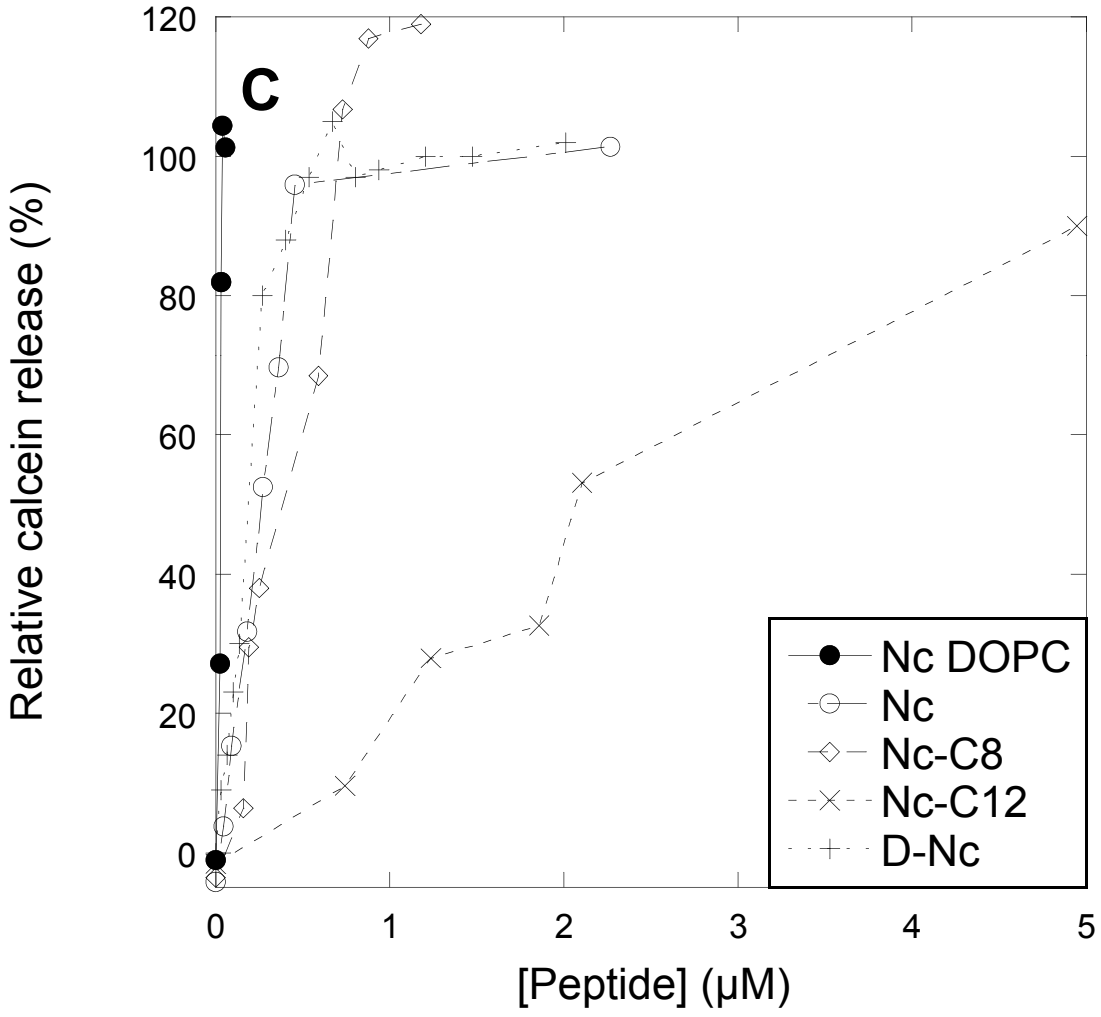

Vad et al. Fig. 3D

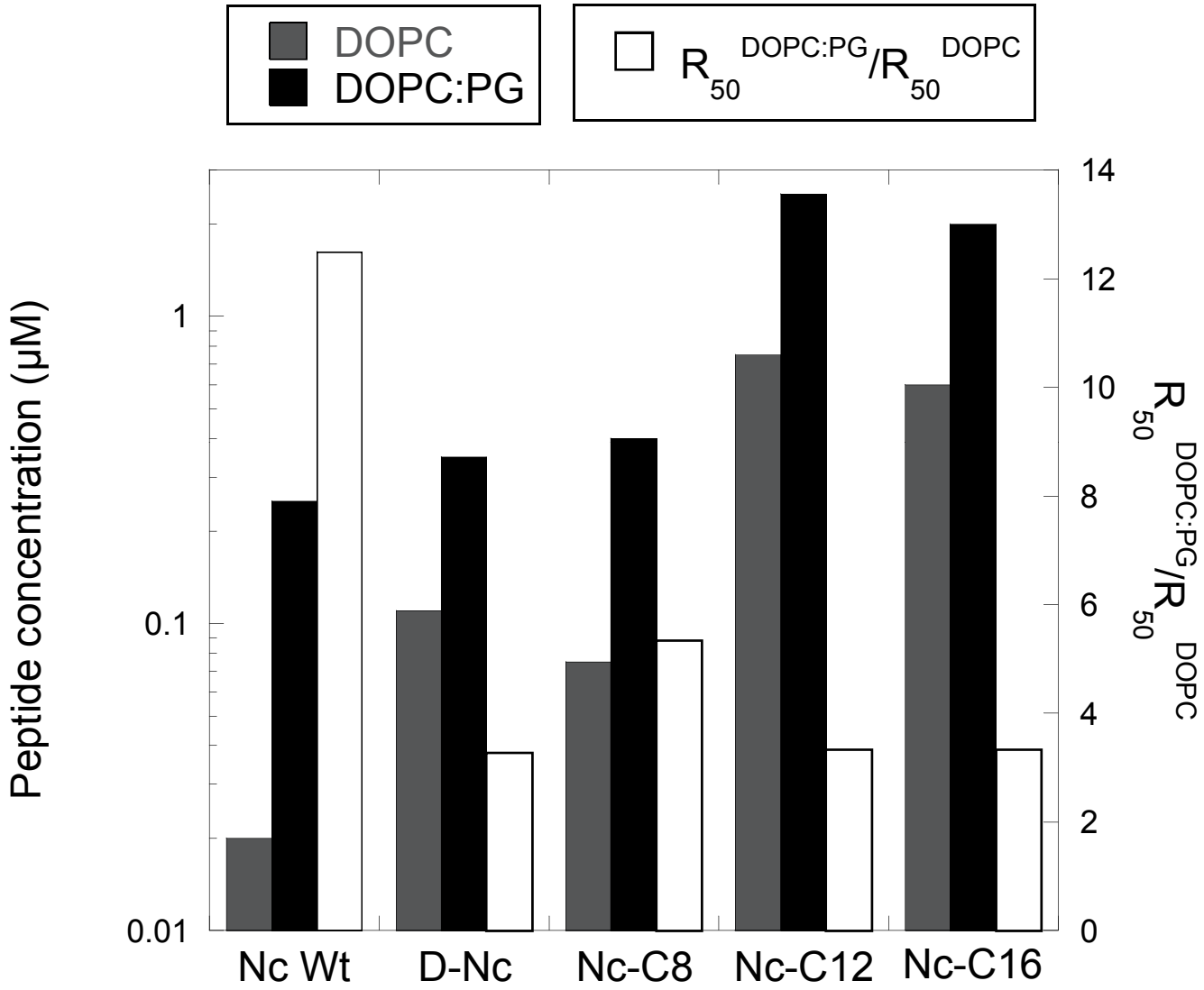

Vad et al. Fig. 4

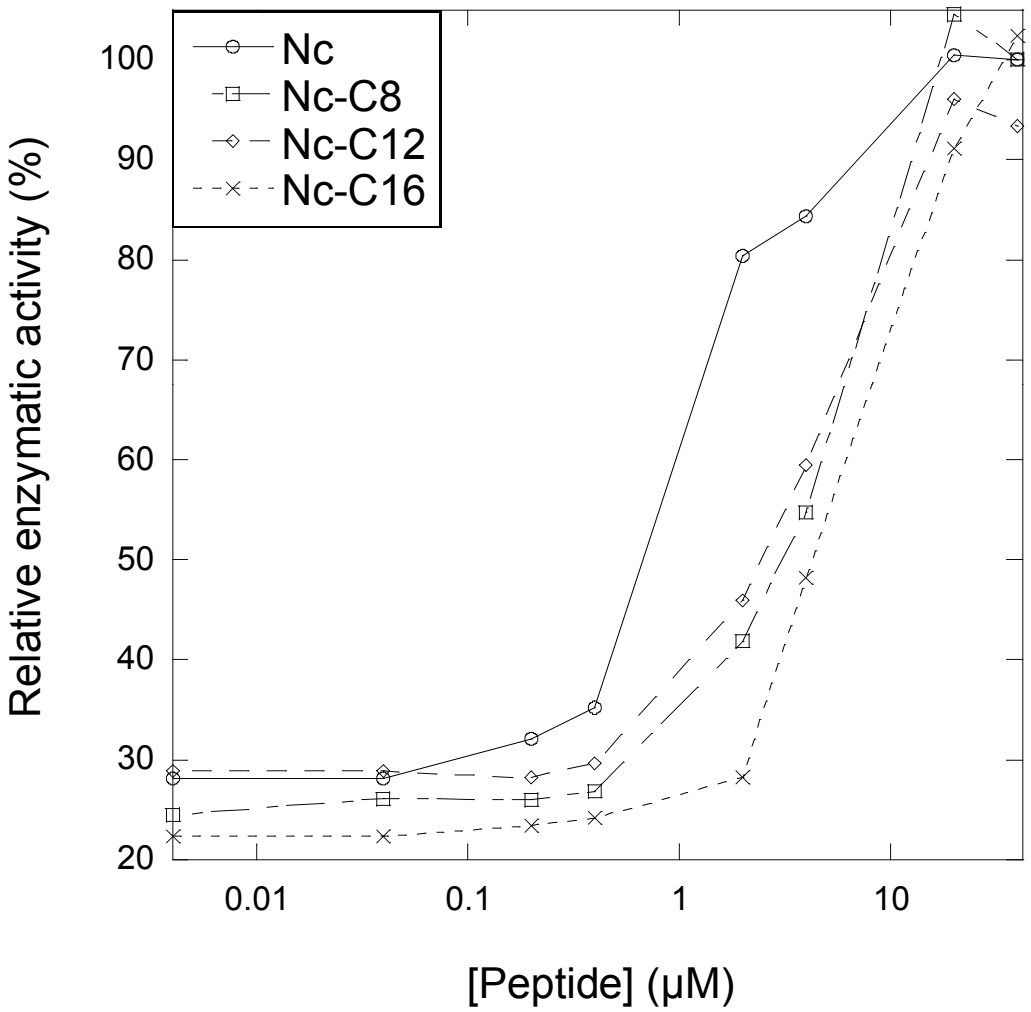

Vad et al. Fig. 5

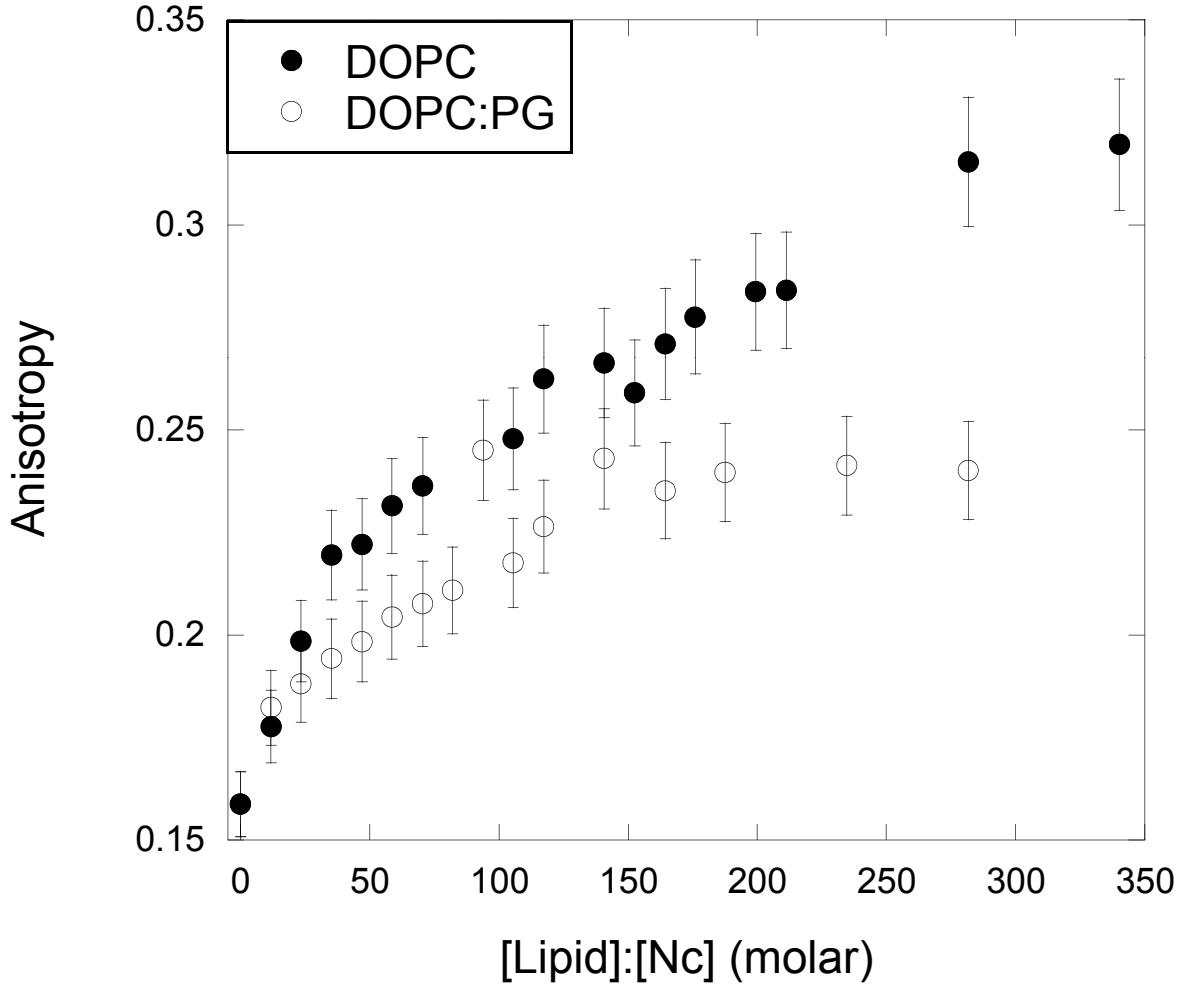

Vad et al. Fig. 6A

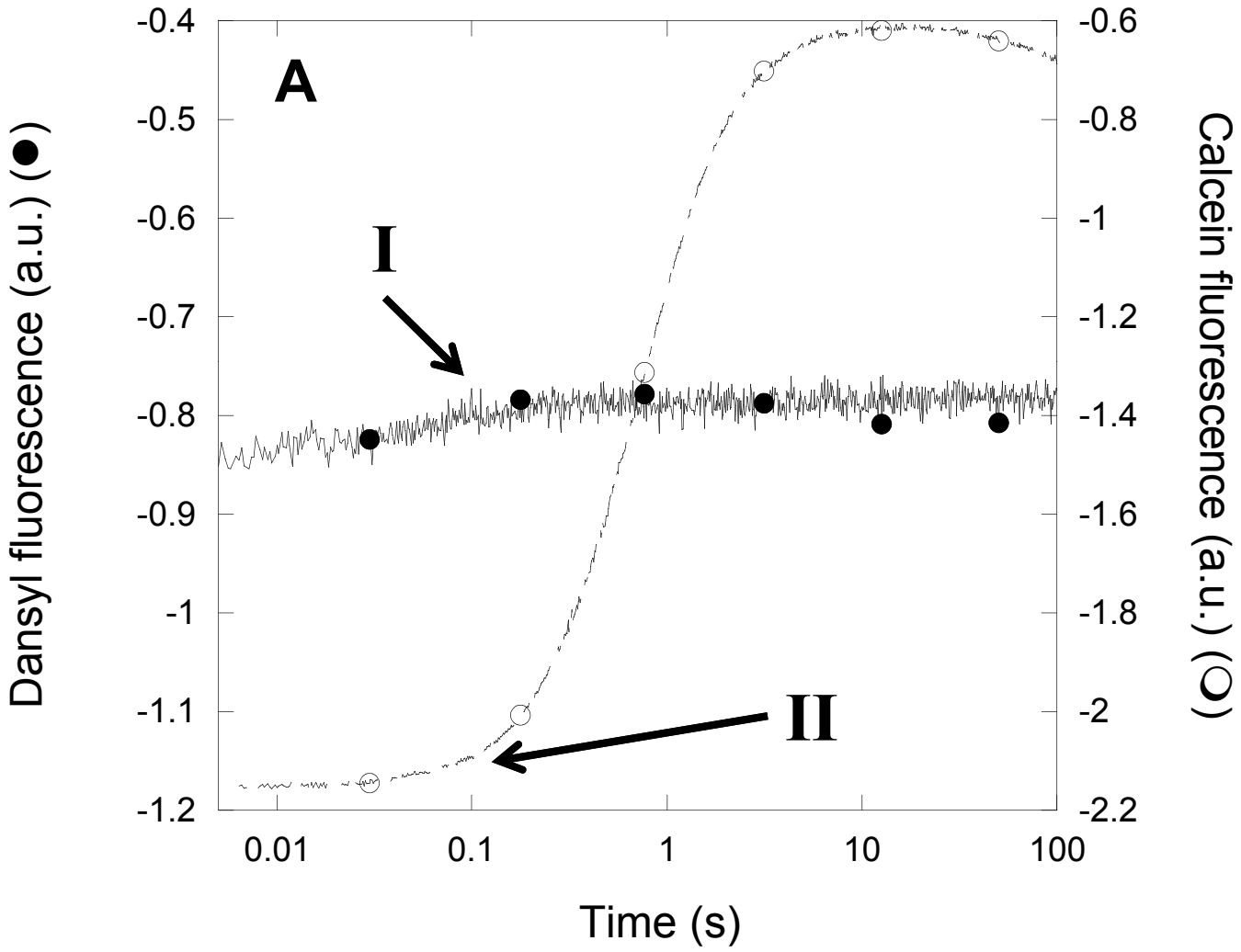

Vad et al. Fig. 6B

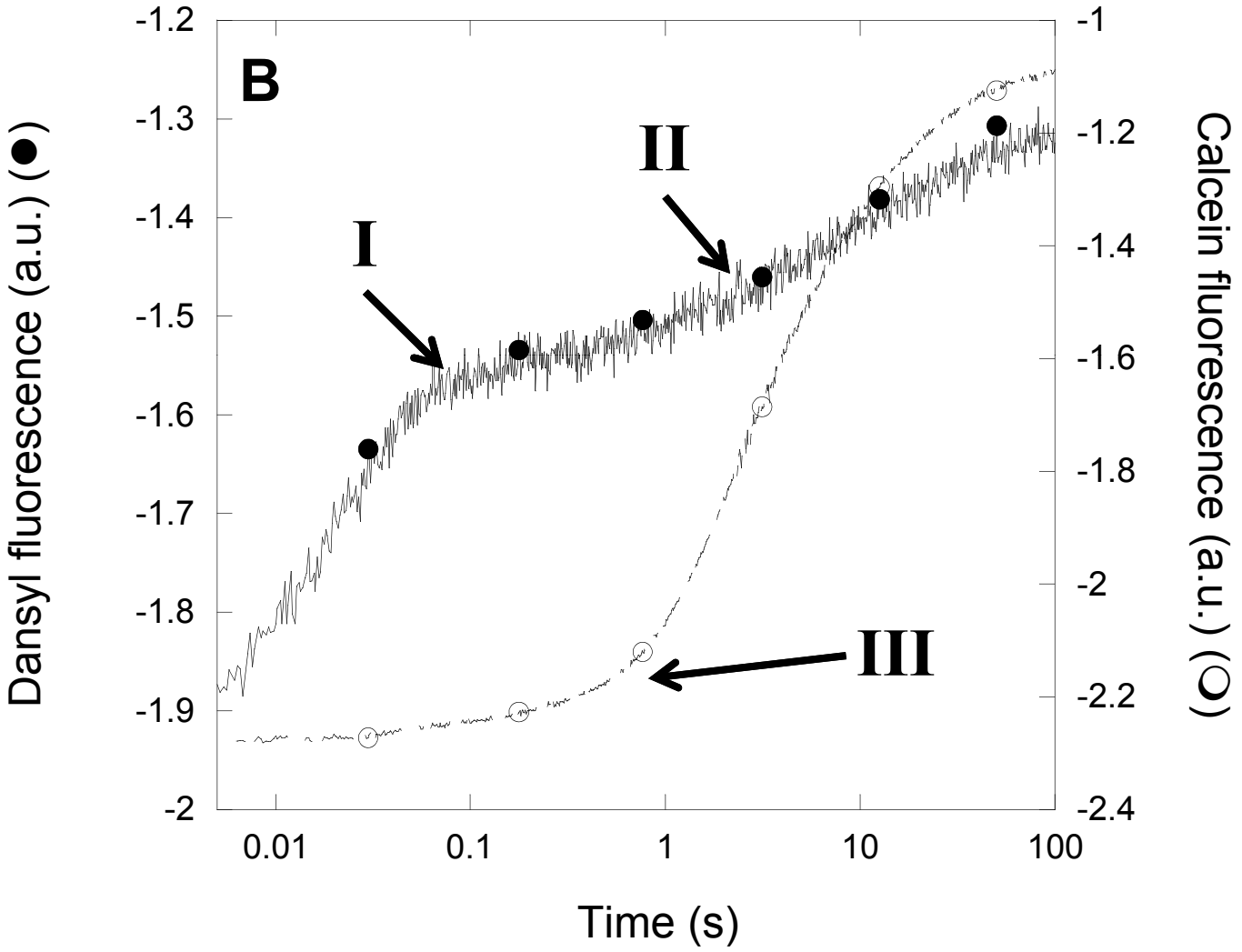

Vad et al. Fig. 7

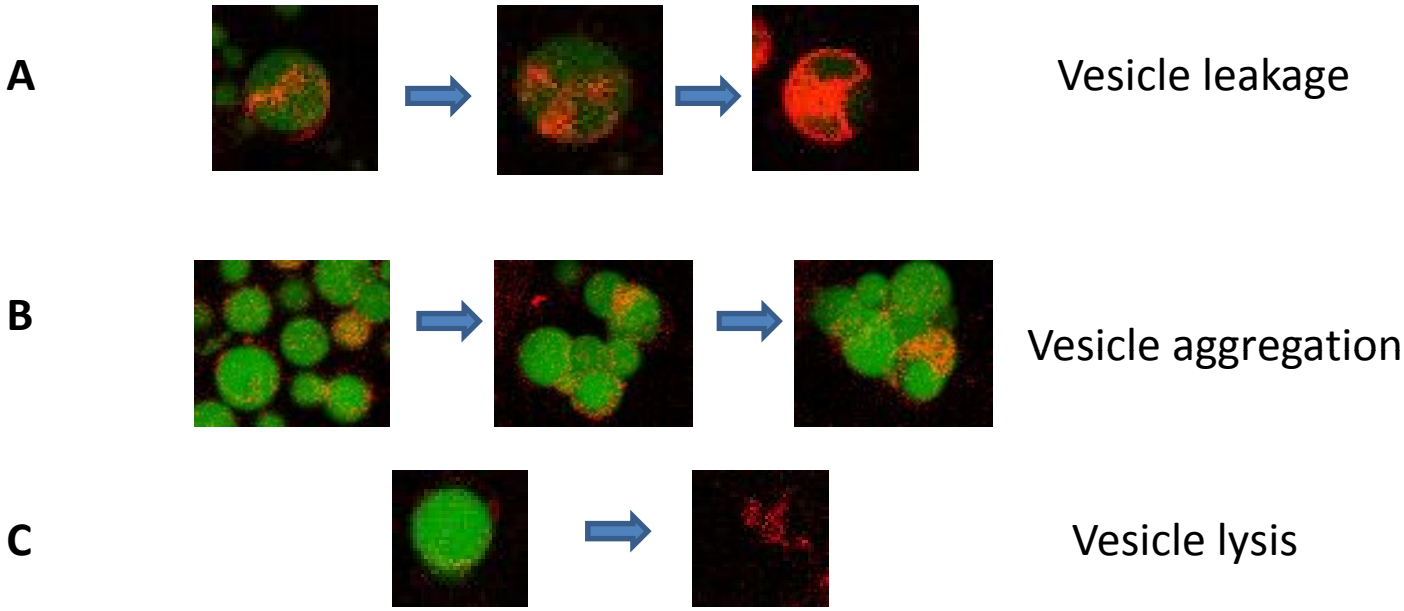

Vad et al. Fig. 8

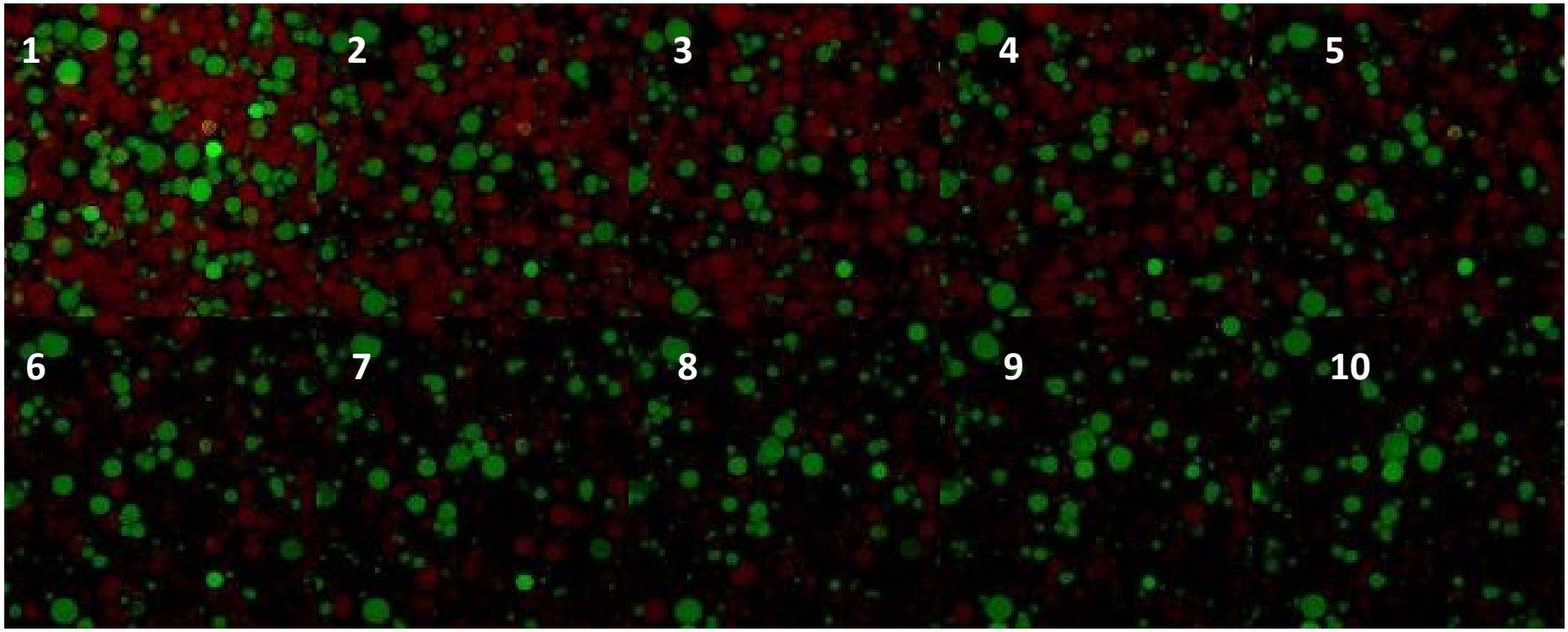

Vad et al. Fig. 9A

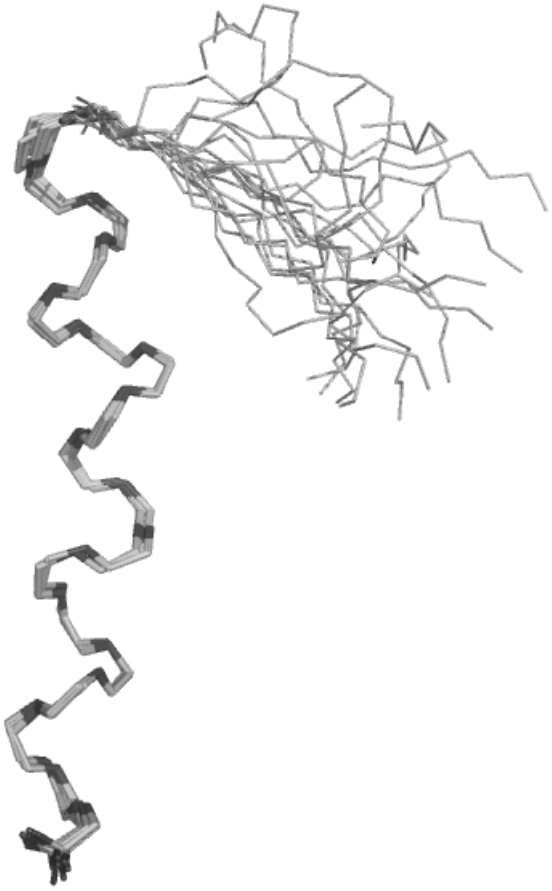

Vad et al. Fig. 9B

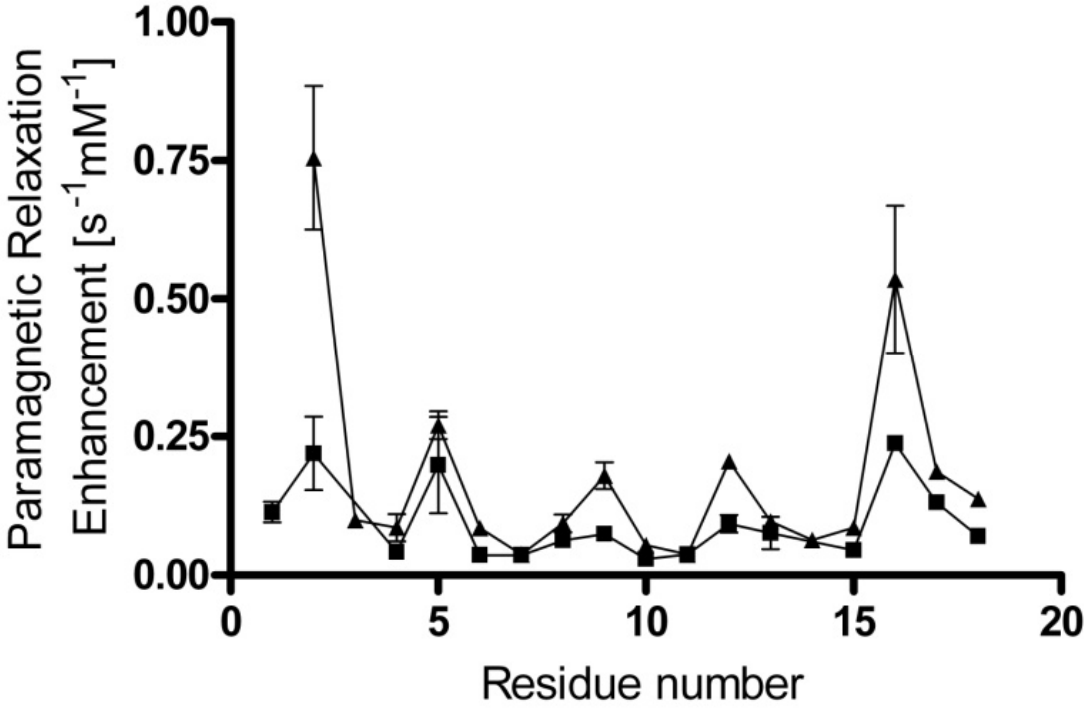

Vad et al. Fig. 10

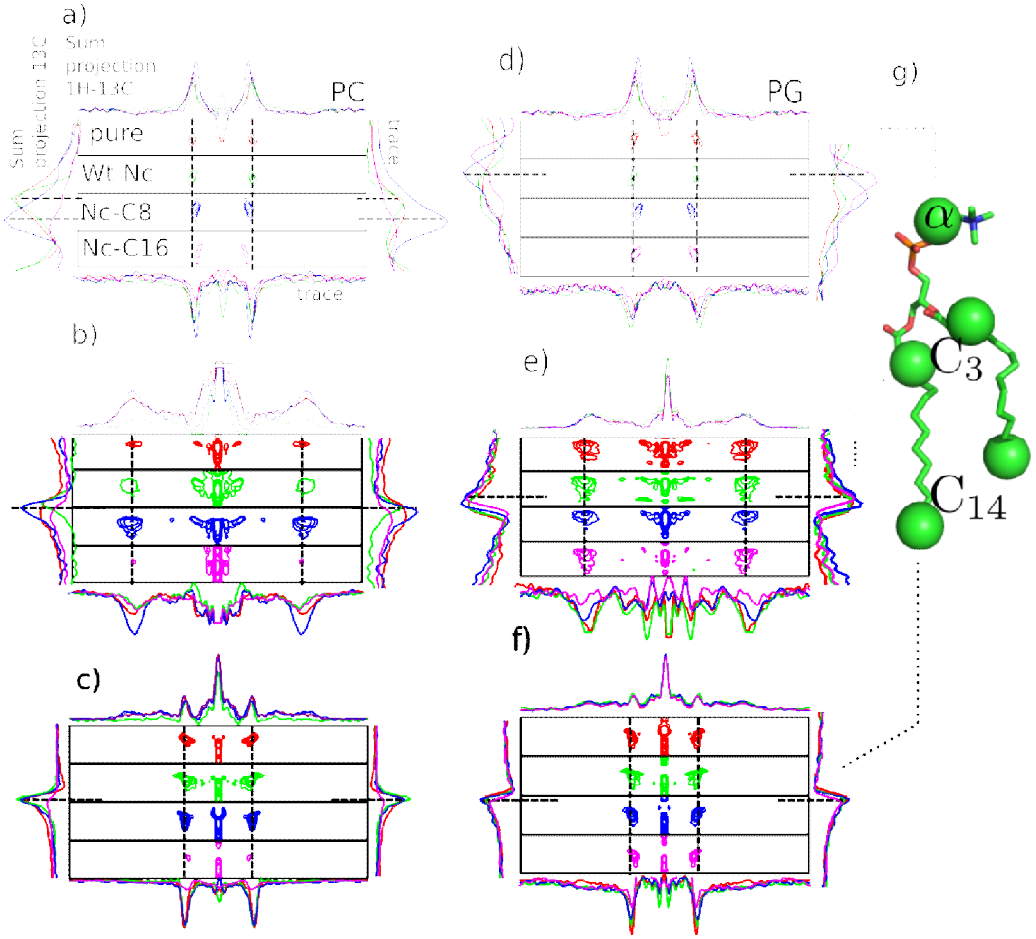

Vad et al. Fig. 11